UNIVERSITÀ
DEGLI STUDI
DI PADOVA

Head Office: Università degli Studi di Padova

Department of Biology

Ph.D. COURSE IN: Biosciences
CURRICULUM: Cell Biology and Physiology
SERIES XXXII

THE CONTRIBUTION OF CHLOROPLASTS AND ENDOPLASMIC RETICULUM TO THE PLANT CALCIUM SIGNALLING NETWORK

Coordinator: Prof. Ildikò Szabò
Supervisor: Prof. Lorella Navazio

Ph.D. student: Enrico Cortese

TABLE OF CONTENTS

SUMMARY

This thesis reports the results that I have obtained during my three-year Ph.D. course in Biosciences, *curriculum* Cell Biology and Physiology. The research activity that I carried out aimed to elucidate the contribution of chloroplasts and the endoplasmic reticulum to Ca^{2+} homeostasis and Ca^{2+}-based signal transduction events in response to environmental stimuli in the model plant *Arabidopsis thaliana*.

Calcium is a fundamental intracellular messenger involved in a wide range of different signalling pathways in all eukaryotes, and possibly prokaryotes as well. Since high concentrations of Ca^{2+} are toxic for the cell metabolism, due to the direct role of this ion in precipitating the phosphates into insoluble complexes, cells have evolved mechanisms to keep cytosolic Ca^{2+} concentration ($[Ca^{2+}]_{cyt}$) at a low level (about 100 nM). In eukaryotic cells the main strategy to achieve this tight regulation of $[Ca^{2+}]_{cyt}$ is represented by the export of Ca^{2+} in the extracellular space and sequestration of the ion in several intracellular Ca^{2+} storage compartments. The occurrence of a complex Ca^{2+} homeostatic apparatus has, in turn, allowed for the evolution of Ca^{2+}-based signalling pathways, based on the generation of finely controlled $[Ca^{2+}]_{cyt}$ changes.

In plants, Ca^{2+} is a signalling intermediate involved in the transduction of a large plethora of abiotic and biotic stimuli. The spatial and temporal characteristics of the elicited Ca^{2+} transients are connected with the nature and intensity of the inducing stimulus, enabling specific stimulus-response coupling. For a long time the scientific attention has mainly focused on the vacuole, because of its prominent role as major Ca^{2+} storage compartment of the plant cell. However, increasing evidence suggests that also additional organelles may play key roles in Ca^{2+} homeostasis and signalling in the plant cell, such as plastids and the endoplasmic reticulum (ER). Concerning plastids, recent evidence indicates that chloroplasts, as well as non-green chloroplasts, may indeed generate specific stromal Ca^{2+} signals and contribute to the fine tuning of cytoplasmic Ca^{2+} signalling in response to different environmental stimuli. However, information about intra-chloroplast Ca^{2+}

fluxes and Ca^{2+} transporters localized at chloroplast membranes (envelope and thylakoids) is still scarce. Likewise, the involvement of the ER in Ca^{2+} handling in plant cells has long been underappreciated, in contrast to animal cells, because of the lack of direct measurements of ER luminal [Ca^{2+}] and its potential variations during signal transduction. Both chloroplasts and ER seem to be able not only to influence the Ca^{2+} signalling pathways of the cytoplasm, but also undergo Ca^{2+} regulation themselves. In chloroplasts, both light reactions and carbon reactions of photosynthesis are modulated by Ca^{2+}. Furthermore, Ca^{2+} plays some role also in the regulation of various chloroplast enzymes, the import of nuclear-encoded proteins and the plastid division. Similarly, protein folding and quality control in the ER are known to be regulated by Ca^{2+}.

Analysis of the potential ER-chloroplast crosstalk in Ca^{2+} homeostasis and signalling is noteworthy also in consideration the structural interactions between these two organelles, mediated by plastid envelope protrusions, called stromules, that continuously extend and retract in an ER-aided manner. The occurrence of specific contact sites through which chloroplast and ER may exchange not only lipids, but also ions such as Ca^{2+}, opens up the possibility of an even more complex and finely-tuned Ca^{2+} regulation.

The work presented in this thesis was hence aimed at the investigation of how these organelles – chloroplasts and the ER – are integrated in the Ca^{2+} signalling networks of the plant cell. Three distinct major points were thus addressed: the first one concerned the elucidation of the role of thylakoids in Ca^{2+} homeostasis and modulation of chloroplast Ca^{2+} signals; the second one focused on the characterization of Ca^{2+}-permeable channels localized at chloroplast membranes and their role in shaping organellar and cytosolic Ca^{2+} signals; finally, the third one regarded the monitoring of Ca^{2+} dynamics in the ER, with an initial attempt towards the elucidation of potential crosstalk between the ER and chloroplasts in terms of Ca^{2+} handling.

As described in **Chapter 2**, the generation of new toolkit of aequorin-based Ca^{2+} indicators targeted to the thylakoid membrane and the thylakoid lumen was successfully achieved, thus increasing the number of subcellular

localizations for which organelle-targeted genetically encoded Ca^{2+} indicators (GECIs) are available. Moreover, these newly developed aequorin chimeras allowed for the monitoring of Ca^{2+} concentrations inside the thylakoid lumen and just outside the thylakoid membrane surface, providing evidence for the involvement of the thylakoid system in the Ca^{2+} homeostasis and signalling network in Arabidopsis. In particular, [Ca^{2+}] variations in the thylakoid lumen were found to be triggered in response to some abiotic stimuli (such as oxidative and salt stress), as well as in the transition from light to dark.

Chapter 3 deals with the identification and the functional characterization of one of the six Arabidopsis homologues of the mammalian mitochondrial calcium uniporter (MCU). The protein encoded by the gene At5g66650, displaying a strong predicted consensus targeting motif for chloroplasts, was demonstrated to localize to the chloroplast envelope, and was therefore named cMCU. Its functioning as an ion channel mediating Ca^{2+} fluxes was assessed both *in* vitro and *in vivo*, and insights into its structural features were provided, highlighting a spontaneous assembly into a tetrameric conformation. The involvement of cMCU in chloroplast-specific osmotic stress-triggered responses was also found to link the observed organellar [Ca^{2+}] transients to chloroplast-to-nucleus signalling, that in turn led to an increased plant tolerance to drought, as well as an improved recovery after rewatering.

In **Chapter 4** a research line (still ongoing in the laboratory) regarding other putative Ca^{2+}-permeable channels located at chloroplast envelope membranes is briefly presented. In order to investigate the role of the glutamate receptor-like channels GLR3.4 and GLR3.5 in the whole cell Ca^{2+} handling, knockout lines for these channels were transformed to stably express a stromal aequorin and then used in Ca^{2+} measurements assays. The preliminary data collected showed a potential involvement of GLR3.5 in the transduction of cold stress, whereas GLR3.4 knockout plants exhibited instead a differential response to salinity compared to the wild-type. Additional experiments will be required in order to support the hypothesis that different Ca^{2+}-permeable channels may be involved in the transduction of specific environmental stimuli.

Chapter 5 focuses on the procedures required to establish both photosynthetic and heterotrophic cell suspension cultures of *Arabidopsis thaliana*. Suspension-cultured cells are widely employed in plant sciences as experimental systems that can be used *e.g.* for signalling investigations, but their generation often require time-consuming protocols. In this manuscript, the detailed workflow description of how to establish and maintain Arabidopsis suspension-cultured cells, containing either chloroplasts or amyloplasts, is presented, together with an additional section of experience-based tips that should facilitate beginners in the generation of *in vitro* cell cultures.

The work described in **Chapter 6** deals with the targeting of a newly generated aequorin-based Ca^{2+} indicator to the ER. The successful development of this ER-targeted Ca^{2+} reporter, as well as the set up of a proper reconstitution protocol, allowed the first accurate *in vivo* measurements of the basal free [Ca^{2+}] in this compartment. Data collected in response to several environmental stimuli revealed stimulus-specific ER [Ca^{2+}] transients, each displaying distinct kinetics. Moreover, the use of cyclopiazonic acid (CPA), specific inhibitor of plant ER-type IIA Ca^{2+} pumps, suggested the involvement of an active transport mediated by ECA1 in the observed ER Ca^{2+} fluxes. The comparison of the ER Ca^{2+} traces with cytosolic and chloroplast Ca^{2+} dynamics suggests that the ER is potentially involved in the dissipation of cytosolic Ca^{2+} signatures, whereas a more complex interplay in terms of Ca^{2+} handling possibly underlies the functional interactions between ER and chloroplasts.

Chapter 7 summarizes the results of a side project performed during my Ph.D. activity, concerning the elucidation of the Ca^{2+} signalling pathway triggered in the model legume *Lotus japonicus* by HYTLO1, the major hydrophobin of the biocontrol fungus *Thricoderma longibrachiatum*. By using aequorin-expressing *L. japonicus* cell suspension cultures, the fungal hydrophobin was shown to trigger a rapid cytosolic Ca^{2+} increase, followed by the activation of some defence-related genes. The abolishment of HYTLO1-induced cytosolic Ca^{2+} transient by pharmacological approaches combining EGTA and Ned-19 (a NAADP receptor blocker) indicated a role of both the extracellular milieu and an internal store sensitive to NAADP, most likely the ER, in this Ca^{2+}

mobilization. These findings highlight the Ca^{2+}-related perception by plant cells of a fungal metabolite that may be considered as a mild elicitor, involved in the priming of plant defence responses against subsequent pathogen infections.

In conclusion, the research work that I have carried out during my Ph.D. has addressed the highly-solicited demand for new tools of investigation in the plant organellar Ca^{2+} signalling field, by providing novel aequorin-based Ca^{2+} sensors targeted to subcompartments of the chloroplast (the thylakoid lumen and the thylakoid membrane) and the endoplasmic reticulum. Ca^{2+} measurement assays carried out in entire seedlings of *Arabidopsis thaliana*, as well as in cell suspension cultures from them derived, allowed for the elucidation of subchloroplast Ca^{2+} dynamics in response to specific abiotic and biotic environmental cues. The putative molecular players mediating chloroplast Ca^{2+} fluxes were also investigated, by exploring the role of both cMCU and GLRs 3.4/3.5 as components of plant environmental sensing. Accurate measurements of $[Ca^{2+}]$ in the ER under both resting and stress-related conditions were provided, and the functional interaction of the ER and chloroplasts was inferred by the comparison of the kinetics of the Ca^{2+} traces recorded in the respective compartments. Additional analyses using Ca^{2+} chelators/specific inhibitors of organellar calcium transporters, as well as knockout mutant plants defective in these putative molecular players, will help to unravel the precise interplay of chloroplasts and ER in the plant Ca^{2+} signalling network.

CHAPTER 1

Introduction

INTRODUCTION

The early emergence of Ca^{2+} homeostasis and evolution of Ca^{2+} signalling

Calcium is the fifth most abundant element on earth. Initially it existed mostly as silicates in igneous rocks of the hot crust, unavailable to living cells. As the earth cooled and primitive life began, chemical and biological reactions caused leaching of ions, steadily raising the dissolved calcium load of sea water to the current 10 mM saturated solution. However, calcium *per se* is a dangerous element, which may display a high cytotoxicity if its intracellular concentration is not strictly controlled. Indeed, a sustained cytosolic calcium concentration ($[Ca^{2+}]$) at the submillimolar level or above would lead to several cellular damages, such as the precipitation of phosphate into insoluble salts, thus disrupting ATP-based reactions that occur in the cell. Also lipid membranes may be affected by an excessive Ca^{2+} concentration, which is deleterious for their integrity, as well as proteins and nucleic acids that in the presence of a continuous high $[Ca^{2+}]$ are subjected to aggregation (Stael *et al.*, 2012; Costa *et al.*, 2018). In this context, one of the compelling necessities that cells had to evolve was the ability to remove any excess of Ca^{2+} from their cytosol: indeed, Ca^{2+} resting levels in the cytosol of cells are required to be maintained as low as 100 nM.

Many biochemical reactions involved in the cell metabolic processes require a moderate range of $[Ca^{2+}]$ and thus, in order to maintain $[Ca^{2+}]_{cyt}$ levels compatible with life, biological systems developed two main strategies to keep free $[Ca^{2+}]$ in the cytosol at about 1:1000 ratio with respect to the extracellular concentrations (~1 mM). The first one already evolved in prokaryotes and is represented by active transport mechanisms aimed at the extrusion of Ca^{2+} in the extracellular space; the latter, instead, is relative to eukaryotic cells, that possess organelles into which further sequestrate any Ca^{2+} excess (Case *et al.*, 2007; Nomura and Shiina, 2014). In eukaryotes, overabundant Ca^{2+} is thereby compartmentalized and stored into internal membrane systems where the ion is generally bound to buffering proteins, free polyvalent inorganic and organic anions (such as phosphates, ADP and ATP) or other complexes

(mainly anionic heads of lipids and carboxyl residues of biopolimers) (Demidchik *et al.*, 2018). It has to be noted, however, that Ca^{2+} may play additional roles inside these compartments, such as the regulation of organelle-specific processes and/or enzymes that could require precise concentrations of the ion for their proper functioning (Berridge *et al.*, 2000; Rocha and Vothknecht, 2012). Sequestering and compartmentalization of Ca^{2+} outside the cytosol is also responsible for the generation of a steep electrochemical gradient across biological membranes: this is the case, in particular, for the plasma membrane, where the difference between the internal and the external [Ca^{2+}] is above 10000 times (Sanders *et al.*, 1999; Case *et al.*, 2007). Internal organelles typically show a more modest Ca^{2+} gradient across their membranes, with only a limited number of examples of high [Ca^{2+}] storage compartments represented by the ER and, in plants, by the vacuole.

The appearance of Ca^{2+} mobilization pathways – both from internal and external stores – is thereby linked to the emergence of Ca^{2+}-permeable channels as well as of active Ca^{2+} transporters. The former group can be further subdivided by classifying channels based on their activation requirements, if any: channels can thus be either freely permeable according to their selectivity filter or their activity may be gated by specific triggers, such as stretch (mechanosensitive channels) or a change in the polarization state (voltage-gated channels) of the hosting membrane as well as the binding of a specialized domain of the channel to a narrow group of molecules (ligand-gated channels) (Steinhorst and Kudla, 2014; Hamilton *et al.*, 2015; DeFalco *et al.*, 2016; Teardo *et al.*, 2017; Vincent *et al.*, 2017a; Demidchik *et al.*, 2018; Hedrich *et al.*, 2018). Concerning active Ca^{2+} transporters, instead, the major difference between the known subsets consists in on the origin of the energy required for the Ca^{2+} transport against the electrochemical gradient: direct ATP-consuming transporters are represented by Ca^{2+} ATPases, while indirect ones consist in Ca^{2+} exchangers in antiport with protons (CAXs) or other mono- or divalent cations (CCXs) (Bose *et al.*, 2011; Frei dit Frey *et al.*, 2012; Pittman and Hirschi, 2016; Costa *et al.*, 2017; Corso *et al.*, 2018; Demidchik *et al.*, 2018). Moreover, the presence of various homologues and isoforms for these

active and passive transporters, each defined by a unique combination of characteristics (stoichiometry, transport mechanism, ligand specificity, selectivity for Ca^{2+}, free Ca^{2+} affinity, sensitivity to inhibitors, other types of regulation) as well as their membrane localization, opens up for an extremely complex integration of the different internal and external compartments contribution to the modulation of the cytosolic Ca^{2+} concentration, thus setting the founding stone for the development of a finely-tuned Ca^{2+} homeostasis (Bonza *et al.*, 2011; Jammes *et al.*, 2011).

In a condition in which cells are actively maintaining an internal low [Ca^{2+}], the next step is the evolution of a signalling system based on Ca^{2+} fluxes, since each change (even feeble) in the concentration of this ion could be readily perceived and likewise immediately responded to (Kudla *et al.*, 2010). Considering in fact the low energy barrier that has to be overcome but also the lack of constraints about the formation of covalent bonds, the flux of Ca^{2+} through ion channels is actually one of the most rapid "elementary" processes affecting cell physiology, with kinetics in the range of nanoseconds (Kuyucak *et al.*, 2011). Conversely, the removal of Ca^{2+} by the means of active transport (and so against its electrochemical gradient) is much slower and estimated around microseconds, while buffering of the ion via high-affinity proteins and other compounds is thought to happen with an intermediate speed (Demidchik *et al.*, 2018). Indeed, changes in cytosolic [Ca^{2+}] are known to be triggered in response to the perception of a wide variety of signals, such as abiotic and biotic interactions in the external environment but also developmental stimuli coming from the inside of the cell or the organism itself (Sanders *et al.*, 2002; Stael *et al.*, 2012). In particular, the controlled occurrence of these finely-regulated cytosolic Ca^{2+} transients harbours a crucial feature that was vastly exploited by biological systems: the so-called calcium signatures represented by these $[Ca^{2+}]_{cyt}$ elevations are in fact defined by precise spatio-temporal kinetics as well as by dynamic characteristics such as amplitude, frequency and duration of the Ca^{2+} transient, and this allowed a straightforward coupling with communication functions (Trewavas *et al.*, 1996; Evans *et al.*, 2001; Xiong *et al.*, 2006; Monshausen, 2012; Whalley and Knight, 2013).

Ca^{2+} has long been known as a fundamental intracellular messenger that plays a key role in the transduction of a wide range of different environmental stimuli in all eukaryotes. Its universality along the whole life tree is mainly dependent on the great versatility that Ca^{2+} itself shows in the cell context: despite being an essential step through which most of the transduction pathways are processed, often simultaneously, Ca^{2+} signalling is able to retain the signal specificity, thus allowing an efficient coupling between signal perception and the opportune recruitment of cellular responses (McAinsh and Pittman, 2009). This is possible thanks to the high complexity degree that is obtainable by combining all the different components that are part of the signalling toolkit, ranging from active and passive Ca^{2+} transporters (**Fig. 1**) to proteins whose Ca^{2+}-dependent activity results in an extremely diversified array of cellular processes or regulations (Berridge *et al.*, 2000; Kudla *et al.*, 2010). Ca^{2+} signals triggered in the cell are thereby unique by means of stimulus-specific dynamics that allow a clear-cut recognition of the inducing stimulation, despite the occurrence of overlapping Ca^{2+}-mediated signals in response to concurrent perceptions. Emerging evidence thus points to the fact that Ca^{2+} signalling can be no longer considered as a sequence of linear pathways (as oversimplified in the past) but is rather a complex network of intersecting signal transduction pathways involving many interconnected nodes and hubs (Costa *et al.*, 2018).

By relying on high speed and rapid clearance, Ca^{2+}-based signalling thus offers a suitable way to specifically transduce perceived stimulations: this is achieved by linking changes in $[Ca^{2+}]_{cyt}$ to downstream transcriptional and metabolic responses through the action of Ca^{2+}-binding sensors (Dodd *et al.*, 2010). These proteins, which are part of a toolkit classically divided in two groups depending on their operative mechanism, owe their Ca^{2+}-sensitivity to EF-hand motifs characterized by domains in which helix-loop-helix structures can bind Ca^{2+} with high affinity. Sensor relays, such as calmodulins (CaMs), calmodulin-like proteins (CMLs) and calcineurin B-like proteins (CBLs), derive their name from the absence of any enzymatic activity and are so limited to the conveyance of the encrypted message to other elements of the signalling pathway, primarily through protein-protein interactions; sensor responders

(represented in plants by Ca^{2+}-dependent protein kinases (CDPKs) and CBL interacting protein kinases (CIPKs)) are instead endowed with kinase domains and can directly act by phosphorylating target proteins, thus translating the information encoded in the Ca^{2+} signals by triggering a subsequential signalling cascade (DeFalco *et al.*, 2009; Zhu, 2016; Tang and Luan, 2017). Ultimately, the conformational changes to which both these types of protein sensors undergo upon Ca^{2+} binding lead to the specific activation of transcription factors controlling gene and protein expression, as well as to the regulation of the metabolic activity through enzymes recruitment or to the interplay with other membrane transporters involved in different cellular pathways, hence inducing complex and concerted phenomena like development or acclimatation that allow plants to actively face the current situation (McAinsh and Pittman, 2009; Ranty *et al.*, 2016; Simeunovic *et al.*, 2016; Kudla *et al.*, 2018).

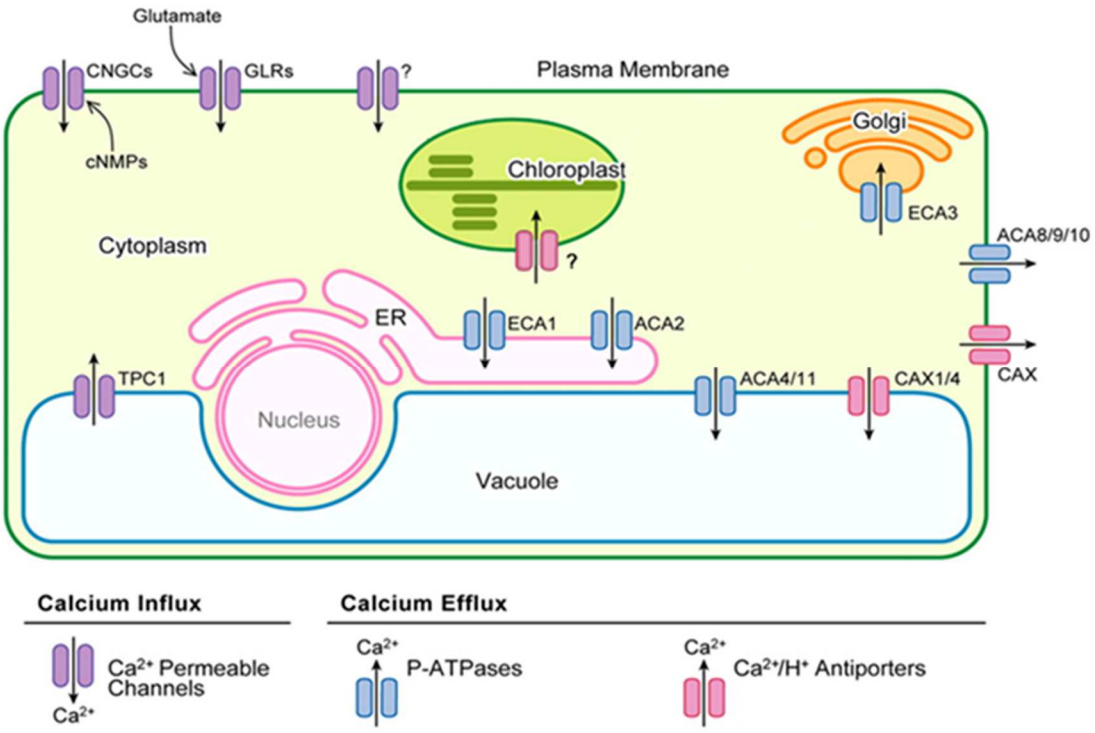

Fig. 1. Subcellular localization of some plant cell Ca^{2+} mobilization pathways. Both active transporters and Ca^{2+}-permeable channels are indicated. Recent advances in the field have added further insights with respect to the scenario illustrated in this figure (modified from Kudla *et al.*, 2010).

Plant organellar Ca^{2+} homeostasis and signalling

The generation of cytosolic Ca^{2+} signatures may stem from the influx of the ion from the external milieu but also from the release from intracellular Ca^{2+} storage compartments. Moreover, Ca^{2+} stores may be involved in the following sequestration of the ion in order to restore the physiological $[Ca^{2+}]_{cyt}$ (Dodd *et al.*, 2010; Kudla *et al.*, 2010). In this context, investigations about the contribution of each organelle to the whole cell Ca^{2+} signalling network has emerged as a crucial research field. Many efforts have been devoted (and are still ongoing) to the establishment of Ca^{2+} reporters targeted to different subcellular localizations, in order to unravel the potential interplay of the various compartments in terms of Ca^{2+} handling. However, so far the overall picture is rather incomplete, with only a partial elucidation of the precise role of each organelle in Ca^{2+} mobilization during signal transduction events (Stael *et al.*, 2012; Nomura and Shiina, 2014; Costa *et al.*, 2018) (**Fig. 2**).

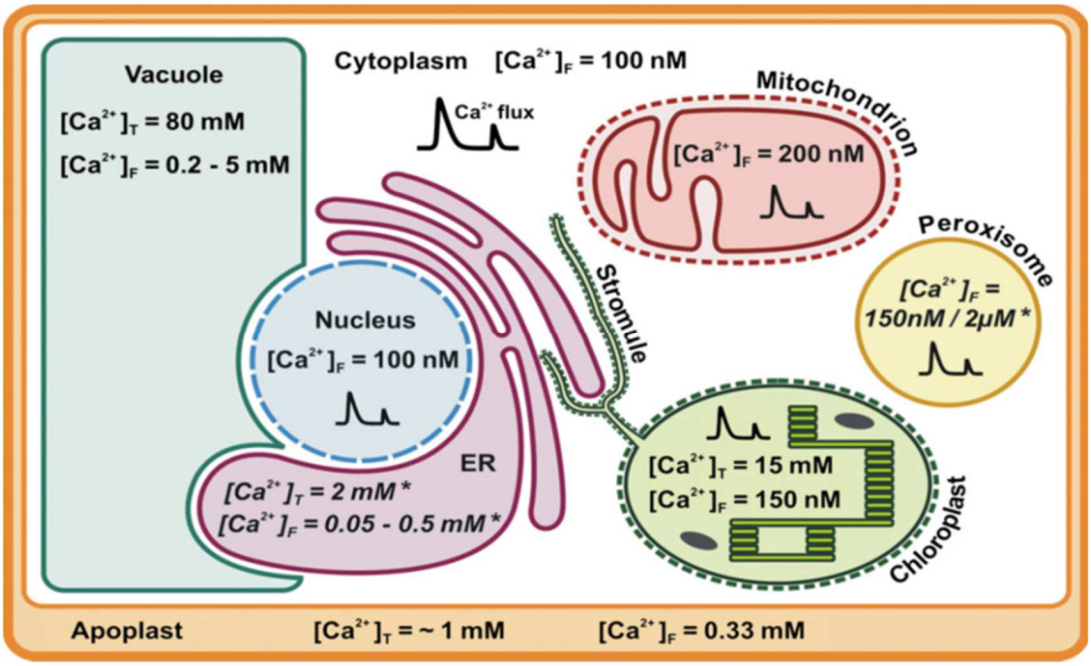

Fig. 2. Ca^{2+} concentrations in the intracellular compartments of the plant cell. $[Ca^{2+}]_T$ and $[Ca^{2+}]_F$ report total and free Ca^{2+} content, respectively. Values may vary according to cell types and species considered. Asterisks mark $[Ca^{2+}]$ recorded in animal cells, due to the absence of $[Ca^{2+}]$ measurements in the plant counterpart (from Stael *et al.*, 2012).

Concerning plant organellar Ca^{2+} signalling, the first compartment on which the scientific attention has focused is certainly the vacuole, mainly because of its prominent volume (up to 80% in mature plant cells) as well as for its high free Ca^{2+} concentration and widely recognized role in Ca^{2+} sequestration and complexation with organic anions (Costa *et al.*, 2018). Nonetheless, also other players were taken into account, in particular the plant cell wall (which can be defined as an intracellular, but extracytoplasmic compartment of the plant cell), the nucleus, the endoplasmic reticulum (ER), the Golgi apparatus, peroxisomes as well as bioenergetic organelles, *i.e.* mitochondria and chloroplasts.

Understanding the integration of the different plant organellar contributions in intracellular Ca^{2+} homeostasis and signalling represents an exciting challenge that requires detailed analyses also based on the future availability of proper methodological tools suitable to investigate Ca^{2+} dynamics in each intracellular compartment.

The vacuole

The vacuole in plant cells is considered as the major Ca^{2+} store, with a free concentration for this ion that ranges around the low millimolar level (0.2-1.5 mM) (Felle, 1989). However, the total calcium content of the vacuole is estimated to reach values up to 50-80 mM, although most of it is not readily available, since it is present in a bound form with chelating agents such as malate, citrate and isocitrate or Ca^{2+} buffering proteins (Conn and Gilliham, 2010). Due to their highly acidic internal environment, plant vacuoles are sometimes described as the plant counterpart to animal lysosomes, and indeed their similarity in ion handling is extended also to Na^{+} (Costa *et al.*, 2018). Nevertheless, vacuoles in plant cells are involved in a plethora of different other functions, especially the temporary accumulation of primary metabolites and the permanent storage of secondary metabolites, including compounds that are toxic to the cell (Kruger and Schumacher 2018; Shimada *et al.*, 2018).

Concerning its contribution to the whole cell Ca^{2+} signalling, the vacuole is considered to be involved in ion regulation through two distinct mechanisms: the first one regards the influence that its high Ca^{2+} content may exert over the activity of ion transporters localized at the tonoplast level (Peiter, 2011); the second one depends on the mobilization of massive quantities of Ca^{2+} into the cytosol, on the basis of vacuolar Ca^{2+} fluxes recorded in response to cold stress or the application of inositol-tris/hexakis-phophates (Alexandre and Lassalles, 1990; Allen *et al.*, 1995; Knight *et al.*, 1996; Lemtiri-Chlieh *et al.*, 2003; Munnik and Nielsen, 2011). The putative role of the vacuole in the generation of cytosolic Ca^{2+} transients has been assessed in experiments regarding the two-pore cation channel TPC1, a voltage-gated channel (previously called the slow-vacuolar channel) located at the vacuolar membrane: in a wide set of studies its structure was solved and its function as a Ca^{2+}-activated non-selective Ca^{2+}- and K^{+}-permeable channel finally proven (Peiter *et al.*, 2005; Guo *et al.*, 2016; Carpaneto and Gradogna, 2018). The ability of TPC1 to conduct Ca^{2+} has long been debated because experiments using mutant plants either lacking or overexpressing TPC1 indicated that cytosolic Ca^{2+} signals evoked by some abiotic and biotic environmental stimuli were unaltered (Ranf *et al.*, 2008). On the other hand, recent evidence has clearly demonstrated the involvement of TPC1 in the generation and propagation of Ca^{2+} waves triggered by either salt stress or wounding and herbivory signals (Choi *et al.*, 2014; Kiep *et al.*, 2015; Vincent *et al.*, 2017a). Conversely, other reports showed an opposite activity for TPC1 that should be linked to an influx of Ca^{2+} from the cytosol to the vacuole lumen, as in external Ca^{2+}-induced stomatal closure movements or in the *fou2* mutant which carries a hyperactive TPC1 variant (Beyhl *et al.*, 2009; Rienmüller *et al.*, 2010).

Concerning active transporters localized at the vacuolar membrane (Martinoia *et al.*, 2012; Xu *et al.*, 2015), P-type Ca^{2+} pumps as well as Ca^{2+}/proton exchangers (CAXs) were molecularly identified in *Arabidopsis thaliana*, with the isolation of two members for CaM-regulated autoinhibited Ca^{2+} ATPases (ACAs, namely AtACA4 and AtACA11) and four CAXs (AtCAX1-4), respectively (Cheng *et al.*, 2002; Pittman *et al.*, 2005; Lee *et al.*, 2007; Edel *et al.*, 2017) that are all thought to be responsible for the Ca^{2+} entry in the vacuole.

The former group was found to be involved in the control of a programmed cell death (PCD) pathway triggered by defence-related hormone salycilic acid (SA) (Boursiac *et al.*, 2010), while the use of knockout plants for the latter one showed altered phenotypes at the level of whole plant development, mainly due to perturbed hormone sensitivity, disrupted stomatal closure as well as impaired root growth in the presence of heavy metal stress conditions (Cheng *et al.*, 2003; Mei *et al.*, 2009; Cho *et al.*, 2012).

To date, the lack of a Ca^{2+} reporter targeted to the vacuole lumen (due to extremely low pH values that hamper the proper functioning of the protein-based Ca^{2+} indicators so far available) is thereby one of the greatest obstacles that prevents further investigations inside this compartment. Pioneering studies have targeted aequorin to the cytosolic surface of the tonoplast (Knight *et al.*, 1996); however, the information obtainable with such an approach are not sufficient to completely describe Ca^{2+} homeostasis as well as Ca^{2+} signalling events occurring in the vacuole (Krebs *et al.*, 2012). The recent generation of new pH-resistant Ca^{2+} sensors (either based on pH-resistant GFPs or not) and their targeting to lysosomes in animal cells (Albrecht *et al.*, 2015; Horikawa, 2015; Shinoda *et al.*, 2018) should pave the way to the development of similar probes that could be employed in the vacuole of plant cells. Nevertheless, since these probes are not totally insensitive to pH, calibration of the emitted signal and thus interpretation of the obtained data have to be performed with special care in order to avoid the risk of detection artifacts.

The apoplast

Together with the vacuole, the apoplastic space (formed by the continuity of plant cell walls between adjacent cells) is another relevant Ca^{2+} store from which plant cells take up the ion during signal transduction events, as well as for nutritional purposes (Demidchik *et al.*, 2018). Free Ca^{2+} concentration in this compartment is reported to vary around the submillimolar levels (reports indicate about 0.33 mM) while total Ca^{2+} is up to three times higher (Conn and

Gilliham, 2010; Stael *et al.*, 2012). Bound calcium in the plant cell wall is mostly complexed to negatively charged carboxyl groups of acidic pectines and oxalates, however this process needs to be strictly regulated because the crosslinking of pectines increases the rigidity of the plant cell wall, thus impairing its remodelling and related processes, such as stomatal closure operated via changes in the volume of guard cells (Hepler, 2005; Kim *et al.*, 2010). Interestingly, it has been reported that the lack of vacuolar CAX cation exchangers (which are tonoplast-located H^+/Ca^{2+} antiporters able to remove any excess of Ca^{2+} by pumping it into the vacuolar lumen) causes an overaccumulation of Ca^{2+} in the apoplast, leading to plant growth defects. The above observations suggest a potential communication between these two major Ca^{2+} stores (Conn *et al.*, 2011; Wang *et al.*, 2017).

The apoplast is considered as the first compartment of the plant that is subjected to environmental stimulation and indeed as an upstream node in the perception of external signals it well correlates with evidence suggesting that it serves also as the primary source for Ca^{2+} entry in the cell (Gao *et al.*, 2004; Costa *et al.*, 2018). This fact appeared evident by observing the conspicuous reduction, and sometimes even total abolishment, of stress-evoked $[Ca^{2+}]_{cyt}$ elevations either by removal of the free Ca^{2+} outside the cell (by using the chelating agents EGTA or BAPTA) or by inhibition of the non-selective voltage-gated cation channels located at the plasma membrane (via pre-treatment with La^{3+} or Gd^{3+}) (Knight *et al.*, 1996; Lamotte *et al.*, 2004; Ali *et al.*, 2007; Navazio *et al.*, 2007). Nonetheless, other Ca^{2+}-permeable channels were reported to be located at the plasma membrane (**Fig. 3**), *i.e.* several members belonging either to cyclic nucleotide-gated channels (CNGCs) or to glutamate receptor-like channels (GLRs) families, whose peculiar characteristics and specific activity are still under investigation (Ali *et al.*, 2007; Kaplan *et al.*, 2007; Jammes *et al.*, 2011; Stael *et al.*, 2012).

Considering that the cell wall harbours a situation, in terms of high $[Ca^{2+}]$ and low pH, that is somewhat similar to the vacuole, it is of no surprise that the same limitations concerning the inquiry of Ca^{2+} dynamics also apply (Costa *et al.*, 2018). Indeed, only few studies involving *in vivo* direct measurements of

[Ca^{2+}] have been carried out in the apoplast, despite its remarkable relevance in the generation of cytosolic Ca^{2+} signatures: by applying appropriate protocols, it was however possible to detect apoplastic [Ca^{2+}] variations that were found to be different from those observed in the cytosol (Gao *et al.*, 2004).

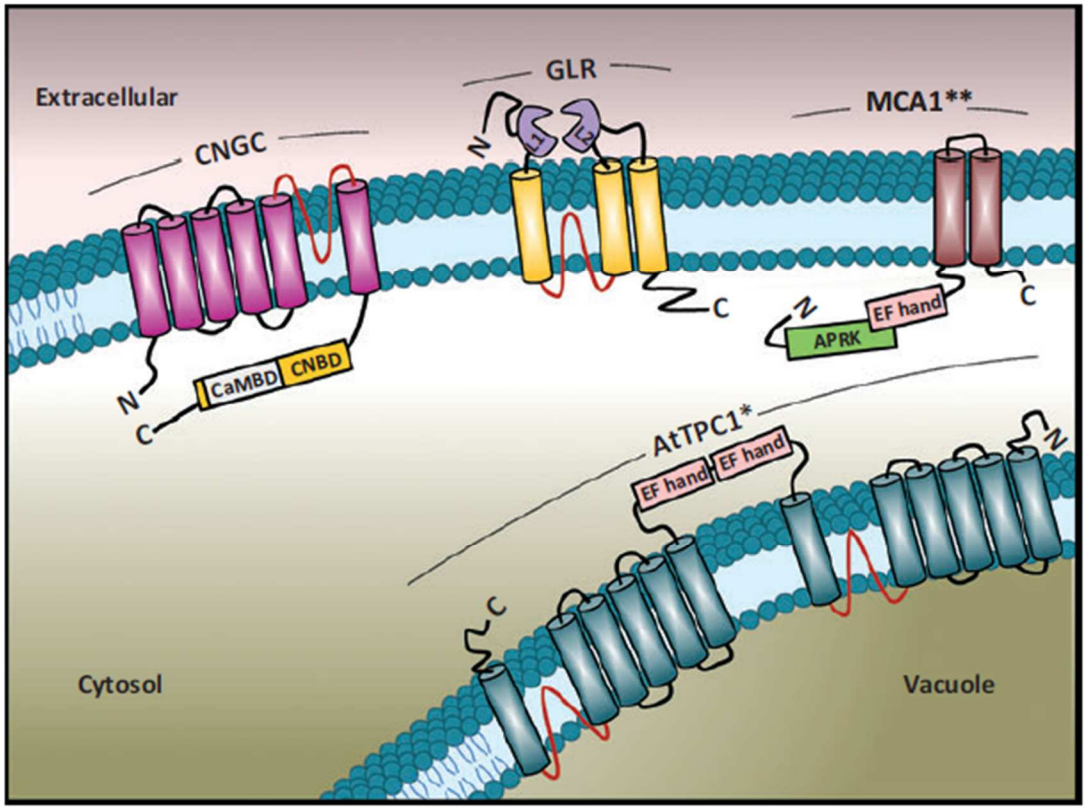

Fig. 3. Transmembrane topology of plasma membrane- and vacuolar membrane-located Ca^{2+}-permeable channels in plants. Pore regions are highlighted in red, whereas ligand-binding domains are represented in violet (from Jammes *et al.*, 2011).

The endoplasmic reticulum

Differently from animal cells, in which the endoplasmic reticulum (ER) has been widely investigated, thus assessing its role as a major Ca^{2+} store with free [Ca^{2+}] quantified at about 50-500 µM out of a total of 2 mM (Rossi and Dirksen, 2006; Coe and Michalak 2009; Rizzuto *et al.*, 2009; Sammels *et al.*, 2010; Raffaello *et al.*, 2016), very little is known about the Ca^{2+} handling properties of plant ER (Stael *et al.*, 2012). Third in order of importance after the vacuole and the apoplast, the plant ER is however thought to act in a

similar way by contributing to Ca^{2+}-mediated signal transduction with the mobilization of Ca^{2+} ions towards the cytosol upon perception of environmental stimulation. Despite the absence of direct measurements of its luminal [Ca^{2+}] ($[Ca^{2+}]_{ER}$), the ER continuity to the nuclear envelope has led to the suggestion that this compartment may serve as the source from which Ca^{2+} is taken prior to ion release in the nucleoplasm and perinuclear cytosol during symbiosis-related nuclear Ca^{2+} spiking events (Capoen *et al.*, 2011; Charpentier *et al.*, 2016). Similarly, in pollen tubes the ER is thought to be involved in the generation of the cytosolic Ca^{2+} gradient that regulates the growth of the pollen tube tip (Iwano *et al.*, 2009). The presence of calreticulin inside the ER is an additional piece of evidence pointing to submillimolar $[Ca^{2+}]_{ER}$: as a high-capacity (15-30 mol of Ca^{2+} per mol of protein) and low-affinity (K_d = 0.5 mM) ER luminal Ca^{2+}-binding protein, calreticulin actively participates in the modulation of ER Ca^{2+} homeostasis, carrying out also chaperone-like functions aimed at glycoprotein folding and quality control (in concert with calnexin) (Mariani *et al.*, 2003; Jia *et al.*, 2009; Jin *et al.*, 2009). When overexpressed, calreticulin was also proven to increase both plant survival in low Ca^{2+} medium and plant tolerance to high salinity (Persson *et al.*, 2001; Xiang *et al.*, 2015).

Concerning Ca^{2+} transporters, two Ca^{2+} pumps were found to be present and located at the ER membranes in Arabidopsis: one belongs to the ER-type Ca^{2+} ATPases (ECAs, specifically ECA1) while the other belongs instead to the Autoinhibited Ca^{2+} ATPases group (ACAs, in this case ACA2). Both are thought to be involved in the uptake of Ca^{2+} into the ER lumen, although with different kinetic properties and specificity (ECAs, for example, are not fully selective for Ca^{2+}, being able to transport also Mn^{2+}) (Costa *et al.*, 2018). Evidence suggest that the former mediates Ca^{2+} and Mn^{2+} uptake into the ER that is crucial for plant growth in either low Ca^{2+} of toxic-high Mn^{2+} environments, while the lack of the latter was linked to an alteration of intracellular Ca^{2+} signalling, leading to a faster PCD during innate immune responses (Wu *et al.*, 2002; Zhu *et al.*, 2010).

Ca^{2+}-permeable channels have not yet been identified at the molecular level in plants, mainly because genes encoding homologues of the animal inositol trisphosphate ($InsP_3$) and ryanodine receptors are absent in plant genomes (with the only exception being represented by genomes of several algal species – among which *Volvox* and *Chlamydomonas* – suggesting that the divergence from chlorophytic algae might have been followed by the loss of these receptor proteins) (Wheeler and Brownlee, 2008; Stael *et al.*, 2012). Nonetheless, early biochemical evidence reported the occurrence of Ca^{2+} fluxes from the inside of ER membrane vesicles upon administration of $InsP_3$, cyclic ADP-ribose (cADPR) and nicotine acid adenine dinucleotide phosphate (NAADP) (Muir and Sanders, 1997; Navazio *et al.*, 2000 and 2001). Moreover, ER membrane preparations obtained from *Bryonia dioica* and *Lepidium sativum* L. allowed to measure voltage-gated Ca^{2+} releases from the ER (Klusener *et al.*, 1995 and 1997; Klusener and Weiler, 1999). These data support the hypothesis that the ER may play a relevant, yet rather unexplored role, as Ca^{2+} source for the plant cell.

In recent times, the successful targeting of a Cameleon-based Ca^{2+} probe to the ER has allowed *in vivo* imaging of Ca^{2+} dynamics in this compartment in response to different environmental stimuli (salt stress, external ATP, glutamate). In particular, Ca^{2+} uptake in the ER was observed, rather than a Ca^{2+} release, pointing the attention to a role of this membrane system as a Ca^{2+} capacitor able to buffer transient cytosolic Ca^{2+} signals (Bonza *et al.*, 2013; Corso *et al.*, 2018). This hypothesis is further supported by the slower ER accumulation kinetics that seem to follow in time the cytosolic ones, as well as the demonstration that the use of cyclopiazonic acid (CPA) – a known blocker of the ECAs – was able to reduce luminal $[Ca^{2+}]_{ER}$ while increasing it in the cytosol (Zuppini *et al.*, 2004; Bonza *et al.*, 2013; De Vriese *et al.*, 2018). Another active transporter, the calcium/cation exchanger CCX2, was reported to be located at ER membranes and to be involved in the Ca^{2+} fluxes occurring between the cytosol and the ER, in particular showing a role in the ability of plants to cope with an osmotic stress (Corso *et al.*, 2018).

As a final note concerning this compartment, its peculiar structural architecture as well as its continuous dynamic remodelling are thought to allow the ER to establish physical interactions with other organelles, thus potentially forming highly interconnected intracellular communication networks. Microdomains involving a close relationship between the ER and the plasma membrane have reported not only in animal but also in plant cells, and have been proposed to function as signalling hubs directly integrated in the whole cell perception of external stimulations (Son *et al.*, 2016; Demaurex and Guido 2017; Bayer *et al.*, 2017). Moreover, the ER is known to interact both structurally and functionally with stroma-filled protrusions – called stromules – that extend and retract from plastid bodies in an ER-aided manner (**Fig. 4**). The occurrence of specific contact sites through which the two organelles exchange lipids leaves open the possibility that also ions are transferred and so this type of close interaction could be directly relevant in terms of Ca^{2+} homeostasis and signalling (Schattat *et al.*, 2011; Mehrshahi *et al.*, 2013). Conversely, the well-documented ER-mitochondria interplay that has been observed in mammalian cells is still uninvestigated in plants. It is tempting to speculate that the occurrence of contact sites between plant ER and mitochondria, if confirmed, would add an extra-level of intrinsic complexity to the integration of intracellular organelles in the overall cell Ca^{2+} handling (Rizzuto *et al.*, 2012; Brini *et al.*, 2017; Costa *et al.*, 2018).

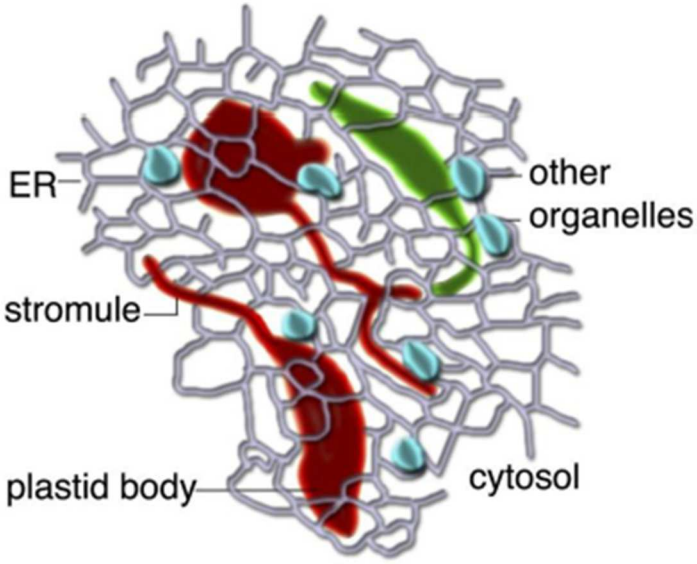

Fig. 4. Schematic representation of the physical interactions occurring between plastid stromules and the ER (from Mathur *et al.*, 2013).

The nucleus

Estimates obtained for the nucleus of both animal and plant cells set nuclear Ca^{2+} concentration ($[Ca^{2+}]_{nuc}$) at values similar to those recorded in the cytosol (Brini *et al.*, 1993; Mazars *et al.*, 2009). Indeed, nuclear free $[Ca^{2+}]$ keeps at around 100 nM, as if the large pores found at the nuclear envelope did not exert any type of control. Likewise, Ca^{2+} fluxes were measured in response to several environmental stimuli, both abiotic and biotic (Pauly *et al.*, 2000; Lecourieux *et al.*, 2005; Oldroyd and Downie, 2006; Sieberer *et al.*, 2009). Nevertheless, and despite a high degree of continuity between the nucleoplasm and the cytosol through the nuclear pores, the idea of a nucleus dependence on the cytosolic $[Ca^{2+}]$ variations was disproved, setting instead the hypothesis of an autonomous generation of nuclear $[Ca^{2+}]$ transients. Experiments carried out under different conditions proved in fact that nuclear and cytosolic Ca^{2+} responses to external stimuli are not synchronous. Moreover, the administration of a jasmonate derivative has been reported to trigger a nuclear Ca^{2+} flux without affecting the $[Ca^{2+}]_{cyt}$ in tobacco cells (Walter *et al.*, 2007; Stael *et al.*, 2012). Additional confirmation came from analyses

performed on isolated nuclei, which further demonstrated the autonomous behavior of nuclei (Xiong *et al.*, 2004 and 2008).

As mentioned above, the nucleus is also involved in the generation of repeated [Ca^{2+}] oscillations (a phenomenon called Ca^{2+} spiking) upon the perception of symbiotic signals from arbuscular mycorrhizal fungi or rhizobial bacteria (Sieberer *et al.*, 2009; Genre *et al.*, 2013). Extensive efforts spent on studies about these beneficial plant-microbe interactions allowed the identification of several active Ca^{2+} transporters and Ca^{2+}-permeable channels located at the nuclear envelope membranes involved in the modulation of the nuclear Ca^{2+} spiking, in particular a Ca^{2+} ATPase (Capoen *et al.*, 2011) and cyclic nucleotide-gated channels (Charpentier *et al.*, 2016).

Regarding the specific function that Ca^{2+} exerts in the nucleus – and besides its involvement in symbiosis-related signalling – the most straightforward hypothesis has proven incredibly difficult to be explored and required numerous inquiries in order to be properly addressed: in fact, nuclear [Ca^{2+}] changes were expected to regulate gene expression in order to accommodate plant responses to the perceived stimuli, thus allowing the plant to enact fitting strategies for survival (Ikura *et al.*, 2002; Kaplan *et al.*, 2006; Galon *et al.*, 2010; Reddy *et al.*, 2011). However, genes exhibiting Ca^{2+}-dependent expression are only a recent discovery, mainly because it has been difficult to discriminate the role of Ca^{2+} from that of different elements belonging to other signaling pathways, also activated by stress conditions (Finkler *et al.*, 2007; Wurzinger *et al.*, 2011). For example, most of the Ca^{2+}-regulated genes are also sensitive to abscisic acid (AB) through AB-responsive elements (Hirayama and Shinozaki, 2010). The identification of Ca^{2+}-binding transcription factors, CaM-binding transcription activators as well as a conspicuous number of nuclear CDPKs, which are involved in the phosphorylation of transcription factors, finally confirmed the direct role of this ion in the modulation of downstream transcriptional responses (Dammann *et al.*, 2003; Choi *et al.*, 2005; Zhu *et al.*, 2007; Boudsocq *et al.*, 2010; Mehlmer *et al.*, 2010).

The Golgi apparatus

Not much is known about the Ca^{2+} handling properties of the Golgi apparatus in plants: in parallel with its unique structure (discrete stacks dispersed throughout the cytoplasm and moving at high speed along the ER surface via actin filaments (Robinson *et al.*, 2015)) which differs from the animal counterpart, also the free [Ca^{2+}] levels seem to diverge between the two eurakyotic branches, with reports for submillimolar concentrations in animal cells (ranging from about 250 µM in the *cis*-Golgi to 130 µM in the *trans*-Golgi, (Pizzo *et al.*, 2011)) while submicromolar levels were estimated for plants (with a steady state at around 0.7 µM, (Ordenes *et al.*, 2012)). This could be due to plant-specific Ca^{2+}-buffering phenomena, possibly linked to the presence of calreticulin in the plant Golgi (Navazio *et al.*, 2002; Nardi *et al.*, 2006). This apparatus was also found to respond to abiotic stimuli such as a cold shock, hyperosmotic stress or mechanical stimulation by increasing its luminal [Ca^{2+}], in contrast to a slow reduction observed when the synthetic auxin 2,4-dichlorophenoxyc acetic acid (2,4-D) was administrated (Ordenes *et al.*, 2012).

Concerning Ca^{2+} decoding mechanisms, the calmodulin-like proteins CML4 and CML5 were identified in the Golgi-to-endosomes intermediate vesicles in Arabidopsis; however, their CaM domain was found to be exposed to the cytosolic side, thus suggesting a role in the decodification of cytosolic Ca^{2+} signals rather than Golgi-related ones (Ruge *et al.*, 2016). Concerning mechanisms of active Ca^{2+} uptake into the Golgi, ECA3 – a homologue of the ER-specific Ca^{2+} ATPase – is known to reside in the Golgi membranes with a proposed role in the transport of Ca^{2+} and/or Mn^{2+} towards the organelle lumen (Mills *et al.*, 2008).

In addition to classical functions exerted in all eukaryotic cells, plant Golgi plays additional roles in the synthesis of cell wall matrix polysaccharides. Interestingly, the architecture of hemicelluloses and pectines at the cell wall, as well as endo- and exocytotic events at the plasma membrane, were reported to be modulated by Ca^{2+} (Vitale and Galili 2001; Cucu *et al.*, 2017; Mravec *et al.*, 2017).

Peroxisomes

Like the Golgi apparatus, also peroxisomes are quite elusive organelles when Ca^{2+} homeostasis and signalling are considered. With few reports of their free [Ca^{2+}] available only for mammalian cells (namely 150 nM or 2 µM, (Drago *et al.*, 2008), but Ca^{2+} dynamics imaged also in plants, the peroxisomal contribution to the whole cell Ca^{2+} signalling network seems to be limited to equilibration of cytosolic variations, as highlighted by stimulus-evoked dynamics that are in fact reminiscent of cytosolic Ca^{2+} signatures (Costa *et al.*, 2010 and 2013). Furthermore, no Ca^{2+} transporters have been identified so far on peroxisomes: the membranes of these organelles are thought to lack any sort of electrochemical gradient or electron transport chain and indeed – despite their impermeability to molecules with MW >1 kDa, thus requiring specific carriers for metabolite transport – Ca^{2+} fluxes detected in peroxisomes of animal cells required no ATP, H^+ gradient or membrane potential at all (Drago *et al.*, 2008; Linka and Weber, 2010; Linka and Esser, 2012; Costa *et al.*, 2018). Nonetheless, considering that the activity of a peroxisomal catalase isoform (CAT3) controlling H_2O_2 levels in epidermal guard cells is dependent on Ca^{2+} (either at the level of peroxisomes via CaM o in the cytosol via the Ca^{2+}-dependent protein kinase CPK8), [Ca^{2+}] variations in these organelles could implement a second level of regulation for this enzyme other than the one already occurring in the cytosol (Yang and Poovaiah, 2002; Zhou *et al.*, 2014). Likewise, evidence suggests that Ca^{2+} in peroxisomes is required for the import of resident enzymes (either with antioxidant, photorespiratory or nitric oxide production functions) through a CaM-dependent mechanism (Corpas and Barroso, 2017), while another CPK (CPK1) – which in Arabidopsis mediates pathogen resistance – also localizes to the external surface of these organelles (Coca and San Segundo, 2010).

Mitochondria

In animal cells, mitochondrial Ca^{2+} dynamics have been extensively studied and are still a central point in order to understand the role of this bioenergetic

organelle in the entire cell Ca^{2+} handling, mainly because of its involvement in the regulation of crucial Krebs cycle enzymes, as well as by mediating the release of apoptotic signals (McCormack *et al.*, 1990; Giacomello *et al.*, 2007; Szabadkai and Duchen, 2008). In contrast, plant mitochondrial Ca^{2+} signalling is still lacking unambiguous evidence that could clarify the precise contribution of mitochondria to the whole framework (Costa *et al.*, 2018). Nevertheless, the general idea is that plant mitochondria act in a similar way to the animal counterpart, thus participating to intracellular Ca^{2+} homeostasis by modulating cytosolic Ca^{2+} signatures. Indeed, whereas free [Ca^{2+}] inside plant mitochondria was found to range between 100 nm and 600 nM depending on cell types and plant species (Zottini and Zannoni, 1993; Logan and Knight, 2003; Wagner *et al.*, 2015a), the administration of stimuli of environmental nature triggered mitochondrial Ca^{2+} responses that strictly mimicked cytosolic one (and were likewise dependent on them) with only few exceptions, such as H_2O_2 and touch-related stimulations (Logan and Knight, 2003; Loro *et al.*, 2012; Manzoor *et al.*, 2012; Teardo *et al.*, 2015; Wagner *et al.*, 2015b). Moreover, the slow rate of Ca^{2+} accumulation into (or release from) mitochondria, with respect to faster cytosolic [Ca^{2+}] variations, has suggested that this organelle may actually act as a Ca^{2+} capacitor (McAinsh and Pittman, 2009).

Ca^{2+} fluxes across mitochondrial membranes are made possible by the activity of two distinct classes of transporters, with either low or high Ca^{2+} affinity, respectively (Costa *et al.*, 2018). The former is represented by Ca^{2+}-permeable channels that are either homologues of the mammalian mitochondrial calcium uniporter (MCU) or members of the glutamate receptor-like family, while the latter consist in Ca^{2+} exchangers, the putative Ca^{2+}/H^+ antiporters LETM1/2 and a Na^+/Ca^{2+} one named NCLX. Moreover, these plant mitochondrial Ca^{2+} transporters have been however investigated only recently: concerning MCU homologues, the identification of six MCU members in Arabidopsis led to the actual confirmation of their localization and ability to transport Ca^{2+} at least for some members (MCU1 and 2), while the absence of striking differences in the single knockout *mcu1* mutant led to the consideration of a potential functional redundancy with other homologues (despite each MCU isoform is predicted to

have tissue-specific distribution) (Stael *et al.*, 2012; Tsai *et al.*, 2016; Teardo *et al.*, 2017; Selles *et al.*, 2018). Also the involvement of MICU1 – short for mitochondrial Ca^{2+} uptake regulator protein – was evaluated observing that its absence is intimately linked to an overaccumulation of Ca^{2+} inside mitochondria, causing altered stress-related mitochondrial Ca^{2+} dynamics in root tip cells but not in the cytosol (as if the two events were not dependent on each other) (Wagner *et al.*, 2015b). GLRs channels, instead, belong to a wide family whose members show numerous intracellular localizations: GLR3.5, in particular, displays a double targeting, either to plastids or to mitochondria, this latter one resulting from a splicing variant. Its Ca^{2+} transport activity was confirmed by experiments employing the knockout mutant which allowed the observation of a reduced mitochondrial Ca^{2+} accumulation with respect to the wild-type (Teardo *et al.*, 2015). At last, with regards to LETM1/2, early reports indicate that these Ca^{2+}/H^{+} antiporter reside in the inner mitochondrial membrane and could be implied in the high-affinity Ca^{2+} influx from the cytosol as well as in its efflux from mitochondria when the channel activity is reversed (also stating that the double knockout is not even viable) (Zhang *et al.*, 2012; Shao *et al.*, 2016; Austin *et al.*, 2017). However, more recent investigations have raised a debate about the actual ion species transported by these proteins, supported also by the lack of any Ca^{2+} dynamics measurement either in the cytosol or in mitochondria of single LETM knockout mutants (Costa *et al.*, 2018). Similarly, NCLX was found to be targeted to mitochondria but details about is activity and functioning specifics are still missing (Palty *et al.*, 2010).

To conclude this brief overview on the contribution of mitochondria to the plant Ca^{2+} signalling network, it has to be noted that only one single study has addressed so far the presence of CaM inside mitochondria, revealing in particular the presence for this high-affinity Ca^{2+} binding protein in the intermembrane space (Biro *et al.*, 1984). However, additional inquiries highlighted a Ca^{2+}/CaM-related promotion of protein import into mitochondria in a similar fashion to chloroplasts, claiming that it represents a plant-specific trait since no parallelism was found in yeast mitochondria (Kuhn *et al.*, 2009). The presented data – together with other indications on the importance of mitochondrial Ca^{2+} in the regulation of the organelle metabolic and energetic

functions – thus point to a required crucial regulation of mitochondrial [Ca^{2+}] in order to maintain a proper homeostatic state of both the organelle and the whole cytosol.

Chloroplasts

As crucial organelles that define the uniqueness of the plant cell, in the last decades the scientific community has spent extensive effort in the study of chloroplasts – and plastids in general. As the site of photosynthetic reactions, chloroplasts were also vastly investigated under several aspects, among which Ca^{2+} signalling has rapidly emerged only in recent times (Rocha and Vothknecht, 2012; Nomura and Shiina, 2014; Kmiecik *et al.*, 2016). Free [Ca^{2+}] in the stroma of this organelle was quantified revealing a slightly increased level with respect to the cytosol, namely 150 nM: however, total [Ca^{2+}] in the chloroplast is known to be much higher (at around 15 mM), being most of it bound to stromal Ca^{2+} buffering proteins or to the negatively-charged membranes of thylakoids (Stael *et al.*, 2012; Hochmal *et al.*, 2015). Indeed, despite evidence for a chloroplast role in acting as a cytosolic Ca^{2+} capacitor able to accumulate high quantities of this ion and thus being implied in shaping cytosolic Ca^{2+} signatures. Ca^{2+} also exerts other fundamental functions that are essential for the homeostasis of the organelle itself. Hence stromal [Ca^{2+}] ($[Ca^{2+}]_{str}$) must be kept at low levels and its variations finely regulated (Rocha and Vothknecht, 2012; Loro *et al.*, 2016; Sello *et al.*, 2016; Costa *et al.*, 2018). The light-dependent phosphorylation of the photosynthetic complexes by thylakoid membrane protein kinases STN7 and 8 (State Transition 7 and 8) was suggested to potentially contribute in buffering Ca^{2+} inside this organelle (Depege *et al.*, 2003). Moreover, stromal [Ca^{2+}] transients were linked to the activation of plant immunity responses (Nomura *et al.*, 2012) and non-green plastids showed differential Ca^{2+} levels (both in resting conditions and in response to various stimulations), possibly underlying a regulatory role in plastid development (Stael *et al.*, 2015; Sello *et al.*, 2016). Asynchronous Ca^{2+} spiking events were also recorded in chloroplasts belonging to guard cells, strongly suggesting that Ca^{2+} signals are modulated independently in each

organelle even though the cytosolic source to which they are exposed is the same (Loro *et al.*, 2016).

In a similar fashion, inquiries about Ca^{2+} transporters located at chloroplast membranes are also a matter of recent times: the general idea, however, is that due to the negative electrochemical gradient found across the chloroplast envelope (-110 mV at the inner envelope membrane) the influx of Ca^{2+} could be simply driven into the organelle by the stimulus-induced opening of Ca^{2+} channels, without the need for active transporters (Wu *et al.*, 1991; Finazzi *et al.*, 2015; Carraretto *et al.*, 2016; Pottosin and Shabala, 2016). Likewise, the outer membrane of the envelope is generally considered permeable to Ca^{2+}, thanks to porin-like proteins, thus pointing additional investigation towards the identification of Ca^{2+}-permeable channels located at the level of the inner envelope membrane (Szabo and Zoratti, 2014; Carraretto *et al.*, 2016). Nonetheless, the potential presence of Ca^{2+} ATPases and/or Ca^{2+} exchangers involved in the active maintenance of the organelle proper Ca^{2+} levels (as mentioned above) is not discarded.

Accordingly, the best candidates for passive Ca^{2+}-influx into chloroplasts were hence represented by plastid-located members of the GLR family (in particular the GLR3.4, also targeted to plasma membrane (Teardo *et al.*, 2010 and 2011), and the already described GLR3.5, with a second localization in mitochondria (Teardo *et al.*, 2015)) or the mechanosensitive channels MSL2 and 3 (Haswell and Meyerowitz, 2006). However, no actual identification of their role in Ca^{2+} transport and chloroplast Ca^{2+} dynamics have so far been provided, except for a GLR-related glutamate- and glutamine-induced ion current that was found to be inhibited by the administration of non-selective cation channels blockers, typically considered as inhibitors of animal ionotropic glutamate receptors (such as La^{3+}, the 6,7-dinitroquinoxaline-2,3-dione (DNQX) or the 6-cyano-7-nitroquinoxaline-2,3-dione (CNQX)) (De Vriese *et al.*, 2018). Interestingly, one of the six MCU homologues (At5g66650) encoded by the Arabidopsis genome was equally predicted to be targeted either to mitochondria or chloroplasts, but again a characterization of its activity as Ca^{2+} channel as well as its localization were lacking (Stael *et al.*, 2012; Costa *et al.*,

2018). On the other hand, presence and/or actual selectivity of putative chloroplast ACA1 and HMA1 Ca^{2+} ATPases (the latter standing for Heavy Metal P-type ATPase) are highly debated (Huang *et al.*, 1993; Ferro *et al.*, 2010; Hochmal *et al.*, 2015). Conversely, the identified PAM71 and PAM71-HL exchangers (located to thylakoid membranes and the chloroplast envelope, respectively, and whose name is derived from the so-called PHOTOSYNTHESIS AFFECTED MUTANT71 knockout mutant) were initially linked to Mn^{2+} mobilization and only more recently they were renamed BICAT1 and 2 for their role in both Ca^{2+} and Mn^{2+} transport against protons (Schneider *et al.*, 2016; Eisenhut *et al.*, 2018; Frank *et al.*, 2019). These bivalent cations antiporters are of crucial importance for the regulation of both pH as well as Ca^{2+} and Mn^{2+} homeostasis in chloroplasts, and specifically inside thylakoids, where both the ions are required for proper assembly of the photosystem II (PSII) (Wang *et al.*, 2016; Frank *et al.*, 2019). In this sense, also other ions could exert fundamental roles inside chloroplasts and their regulation might be related to that of Ca^{2+} through still uninvestigated mobilization pathways: the case for potassium shows indeed that the envelope-located K^+/H^+ antiporters KEA1 and 2 are actually of equal importance since their double knockout was responsible for a reduced cytosolic Ca^{2+} level in response to a sorbitol-induced hyperosmotic stress (Stephan *et al.*, 2016).

Concerning Ca^{2+}-binding proteins present inside the chloroplast, the thylakoid-localized Ca^{2+} sensor CAS was found to modulate intracellular Ca^{2+} signals during stomatal closure by controlling cytosolic Ca^{2+} transients induced by external Ca^{2+} uptake (Nomura *et al.*, 2008; Weinl *et al.*, 2008). Its knockout proved in fact impaired in both stomatal movements and plant growth, while it also failed to evoke the production of salicylic acid in response to pathogen infections (in agreement with transcriptome analyses showing that CAS was involved in PAMP-triggered nuclear reprogramming of plant defense genes in a chloroplast-mediated way) (Nomura *et al.*, 2012; Wang *et al.*, 2012 and 2016; Fu *et al.*, 2013). Moreover, being involved in plastid-to-nucleus retrograde signalling, CAS was reported to regulate mitogen-activated protein kinases (MAPK) activity in the framework of a close Ca^{2+}-related interorganellar communication in response to several stimuli such as salt and drought

stresses (Zhao *et al.*, 2015; Guo *et al.*, 2016; Leister *et al.*, 2017; Zheng *et al.*, 2017). Similarly, also the glycosyltransferase QUASIMODO1 (QUA1) was recently demonstrated to act as a regulator of cytosolic [Ca^{2+}] changes in response to these two last-mentioned stress conditions (Zheng *et al.*, 2017).

Overall, Ca^{2+} in chloroplasts has to be tightly regulated, since low concentration of this ion are necessary for the correct functioning of limiting CO_2 fixation enzymes in the Calvin-Benson-Bassham cycle (the fructose-1,6-bisphosphatase and the sedoheptulose bisphosphatase), while an uncontrolled increase of chloroplast [Ca^{2+}] would instead lead to inactivation of the same enzymes (Rocha and Vothknecht, 2012). Likewise, the requirement for Ca^{2+} at the oxygen evolving complex level as well as its binding to the 8 kDa subunit of the thylakoid-targeted ATP synthase highlight the role of this ion in controlling both the photosynthetic proton flow and the consequent ATP production (Zakharov *et al.*, 1993; Ifuku *et al.*, 2010). Furthermore, in addition to being a basic component for the above-mentioned retrograde signalling to the nucleus, Ca^{2+} is also required for the import into chloroplasts of nuclear-encoded proteins, mediated by the Ca^{2+}/CaM regulated TOC and TIC complexes (translocons at the outer/inner envelope) (Chigri *et al.*, 2005 and 2006; Balsera *et al.*, 2009). However, CaM and CaM-like proteins as well as Ca^{2+}-regulated kinases and their targets inside chloroplasts have not yet been identified (Stael *et al.*, 2012).

From Ca^{2+}-sensitive dyes to genetically encoded Ca^{2+} indicators: the ever-increasing toolkit of Ca^{2+} reporters

Ca^{2+} probes are necessarily required in order to measure [Ca^{2+}] values and to monitor Ca^{2+} dynamics during signal transduction events: most – if not all – of our knowledge in the field has in fact been obtained in this manner. However, molecules which bind Ca^{2+} with high affinity may be suitable to carry out this purpose only if their free and bound physicochemical characteristics are sufficiently different to enable precise recognition of the probe state (Rudolf *et al.*, 2003). Indeed, actual quantification of the Ca^{2+}-complexed indicator with

respect to the non-bound one is the founding stone in order to effectively measure Ca^{2+} content in the selected intracellular compartment. This is achieved mainly by the detection of either luminescence or fluorescence changes in the Ca^{2+} probe upon Ca^{2+}-binding, thus discriminating two major classes of Ca^{2+} indicators based on the origin of the emitted light signal. Moreover, owing to different intrinsic characteristics, available Ca^{2+} reporters were also initially subdivided between Ca^{2+}-sensitive dyes and genetically encoded Ca^{2+} indicators (GECIs), with the former ones representing the historical starting point in cell [Ca^{2+}] investigations in contrast to the latter ones, stemming instead as the expression of more modern and efficient ways to fulfill the same task (Pérez Koldenkova and Nagai, 2013).

Ca^{2+}-sensitive dyes are fluorescent derivatives of the Ca^{2+} chelator EGTA, whose conformational change caused by binding to Ca^{2+} ions leads to an alteration of excitation/emission properties of the associated fluorophore. However, many dyes such as fluo-4, rhod-2 and Oregon Green BAPTA are non-ratiometric, meaning that the [Ca^{2+}] values detected are based uniquely on the relative increase in fluorescence intensity: this condition is clearly dependent on the actual quantity of the Ca^{2+} dye loaded into the cell, as well as it appears prone to artifacts linked to sample bleaching, differential illumination intensity or unequal optical path length. The subsequential development of ratiometric fluorescent dyes such as fura-2 and indo-1 – characterized by either dual excitation or dual emission spectra in which one of the two wavelength signal is insensitive to Ca^{2+} binding – allowed to determine in a more precise way the actual cell [Ca^{2+}], but still resulted limited in the type of spatial information they could provide for the monitoring of Ca^{2+} dynamics. Indeed – and in parallel with their difficult loading in some cell types, *e.g.* plant cells due to the presence of a thick cell wall – injected Ca^{2+}-sensitive dyes diffuse in the whole cytosol, thus making impossible to target them to subcellular compartments of interest (Brownlee, 1986; Sanders *et al.*, 1999; Goddard *et al.*, 2000; Rudolf *et al.*, 2003; Wheeler and Brownlee, 2008; Costa *et al.*, 2018).

For these reasons, GECIs development represented a revolutionary advance in the field by providing Ca^{2+} signalling studies with a powerful toolkit of differently-targeted Ca^{2+} indicators that permitted non-invasive monitoring of *in vivo* free Ca^{2+} levels. The possibility to perform real-time Ca^{2+} recording in various cell types and organisms with a high spatial and temporal resolution is thus a key feature that guided the progressive transition from the employment of dyes to the well-established use of GECIs, on the basis of which extensive efforts are still ongoing in order to broaden the number of intracellular localization for which these Ca^{2+} indicators are available to date. GECIs – both luminescent and fluorescent ones – are based on the high-affinity binding of Ca^{2+} ions to 3-to-4 EF-hand motifs of the protein and on its subsequent conformational change (Pérez Koldenkova and Nagai, 2013; Costa and Kudla, 2015; Costa *et al.*, 2018).

Concerning luminescent GECIs, the most relevant one is represented by aequorin, a Ca^{2+}-sensitive photoprotein widely employed in organellar Ca^{2+} measurements. It consists in an apoprotein (apoequorin) that has to be reconstituted with its prosthetic group coelenterazine. Upon Ca^{2+} binding, the resulting conformational change of the photoprotein drives the oxidation of coelenterazine to coelenteramide with a concurrent emission of a single photon of blue light (**Fig. 5**) that, once detected by a proper apparatus, is easily converted into [Ca^{2+}] values by using a reliable calibration procedure (**Fig. 6**). Many advantages can be ascribed to this specific Ca^{2+} reporter, such as a nearly insensitiveness to variations of pH and [Mg^{2+}], a great dynamic range (spanning from 10^{-7} to 10^{-3} M and extendable even further via suitable low Ca^{2+}-affinity mutants and coelenterazine variants (**Fig. 7**)), a high signal-to-noise ratio, as well as the lack of any damaging excitation light (which allows prolonged measurements even in organelles containing chlorophylls) (Brini *et al.*, 1995; Brini, 2008; Martí *et al.*, 2013; Ottolini *et al.*, 2014; Costa *et al.*, 2018). Although the use of recombinant aequorin still remains the method of choice to accurately quantify Ca^{2+} concentrations, the low amount of emitted light per single aequorin molecule is not compatible with single-cell imaging studies (*i.e.* cell populations or entire seedlings are required). In this context, the development of novel bioluminescence resonance energy transfer (BRET)-

based green fluorescent protein (GFP)-aequorin probes has overcome the problem, allowing the visualization of Ca^{2+} signals that spread systemically in intact plants (Baubet *et al.*, 2000; Rogers *et al.*, 2005; Xiong *et al.*, 2014). Aequorin-based reporters have been extensively used for plant Ca^{2+} signalling studies: indeed they were targeted not only to the cytosol but also to intracellular compartments such as the vacuolar membrane facing the cytosol (Knight *et al.*, 1996), the nucleus (van Der Luit *et al.*, 1999), mitochondria (Logan and Knight, 2003), and the Golgi apparatus (Ordenes *et al.*, 2012), in addition to the apoplast (Gao *et al.*, 2004). Obviously, chloroplasts were not left uninvestigated, with aequorin chimeras targeted to the stroma (Johnson *et al.*, 1995; Sai and Johnson, 2002) and more recently even to the outer and inner membrane of the envelope (Mehlmer *et al.*, 2012; Sello *et al.*, 2016).

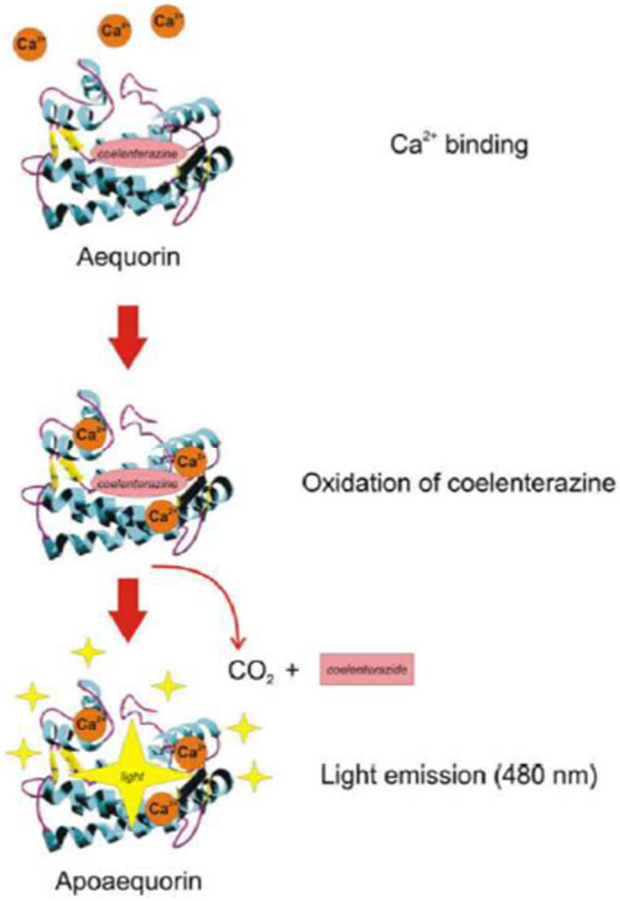

Fig. 5. Schematic representation of the Ca^{2+}-dependent bioluminescence of aequorin. Upon binding to 3 Ca^{2+} ions, the holoprotein undergoes a conformational change that leads to oxidation of the prosthetic group coelenterazine to coelenteramide and to the emission of a single photon of blue light (from Brini, 2008).

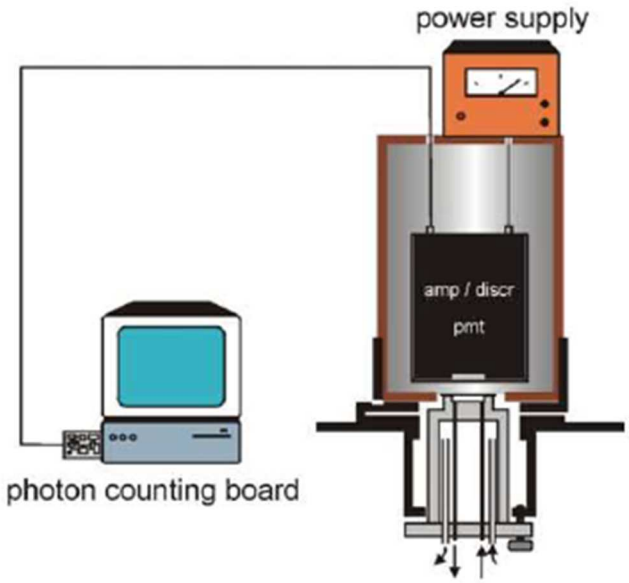

Fig. 6. Schematic representation of the aequorin-based Ca^{2+}-measuring apparatus, consisting in a luminometer plus a software that converts the recorded luminescence data into $[Ca^{2+}]$ values (from Brini, 2008).

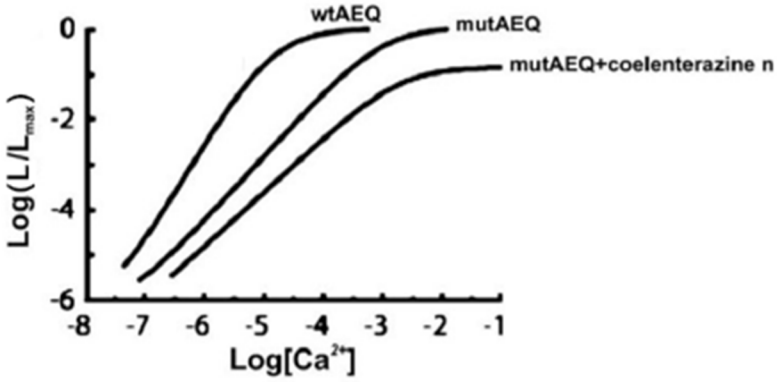

Fig. 7. Ca^{2+} response curves for wild-type and mutated aequorin, correlating luminescence and $[Ca^{2+}]$ (modified from Brini, 2008).

Fluorescent Ca^{2+} reporters are instead classified according to the number of GFP variants interacting with the Ca^{2+}-binding protein CaM and the CaM-binding peptide M13. Single-fluorescent protein (FP) Ca^{2+} probes are represented by GECOs, Camgaroos, Pericams and GCaMPs and are able to increase their fluorescence emission in conjunction with the binding of Ca^{2+} (**Fig. 8**). Conversely, Cameleons are based on the Förster Resonance Energy Transfer (FRET) occurring between two GFP variants (typically cyan and

yellow, CFY and YFP) when they come in close vicinity to each other as a consequence of the Ca^{2+}-binding-induced conformation change of the probe (Miyawaki *et al.*, 1997; Pérez Koldenkova and Nagai, 2013; Costa and Kudla, 2015) (**Fig. 9**). The simultaneous use of Cameleon indicators – as well as of GECOs – built from different spectral variants FPs also allowed the parallel measurement of Ca^{2+} dynamics in distinct subcellular compartments (Krebs *et al.*, 2012; Costa and Kudla, 2015; Kelner *et al.*, 2018). Whereas Cameleons have been targeted to many different subcellular localizations, *i.e.* mitochondria (Loro *et al.*, 2012 and 2013), chloroplasts (Loro *et al.*, 2016), peroxisomes (Palmer *et al.*, 2006; Costa *et al.*, 2010), the endoplasmic reticulum (Iwano *et al.*, 2009; Bonza *et al.*, 2013), the plasma membrane (Krebs *et al.*, 2012; Iwano *et al.*, 2015) and the vacuolar membrane (Krebs *et al.*, 2012) the targeting of GECO and GCaMP reporters is so far limited to the cytosol and the nucleus only (Ngo *et al.*, 2014; Zhu *et al.*, 2014; Keinath *et al.*, 2015; Liu *et al.*, 2017; Vincent *et al.*, 2017a and 2017b; Waadt *et al.*, 2017; Kelner *et al.*, 2018).

It has to be noted that, since each of the above-mentioned classes of GECIs displays its own advantages and limitations, a joint use of both luminescent and fluorescent GECIs would be advisable, in order to obtain a precise photograph of the complex Ca^{2+} signalling and homeostatic network of the plant cell. Indeed, the comparative use of both aequorin-based and GFP-based Ca^{2+} reporters has provided in recent times a solid knowledge in terms of organellar Ca^{2+} handling, which can be further advanced by tackling new challenges aimed at a deeper investigation of the relative contribution of the different plant intracellular compartments to Ca^{2+}-mediated signal transduction (Costa *et al.*, 2018).

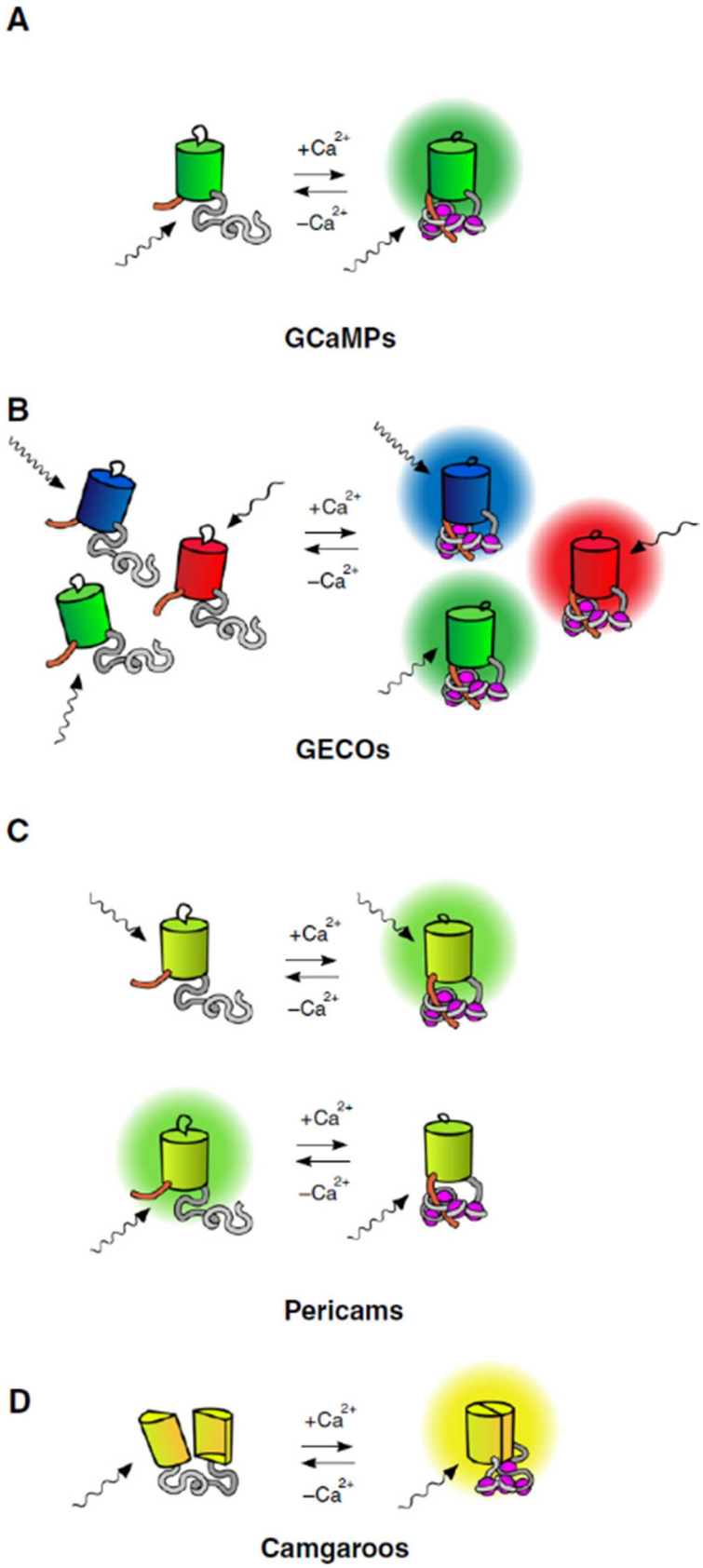

Fig. 8. Single-fluorescent protein GECIs. **A**, GCaMPs; **B**, GECOs; **C**, Pericams; **D**, Camgaroos. Different wavy arrows indicate different light frequencies required for the excitation of the fluorescent proteins (modified from Pérez Koldenkova and Nagai, 2013).

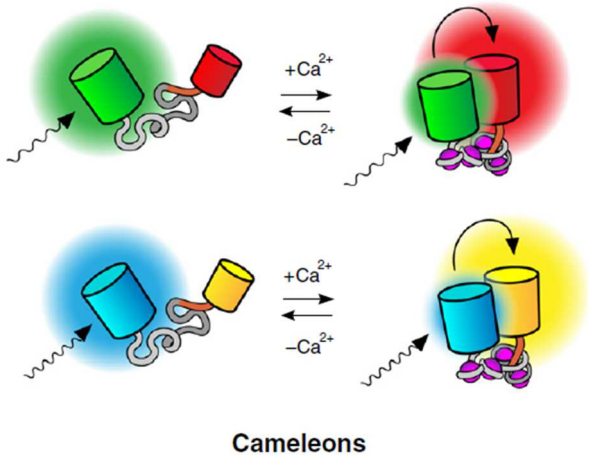

Fig. 9. FRET-based two-fluorescent protein GECIs (Cameleons). Different wavy arrows indicate different light frequencies required for the excitation of the fluorescent proteins (modified from Pérez Koldenkova and Nagai, 2013).

REFERENCES

Albrecht T, Zhao Y, Nguyen TH, Campbell RE, Johnson JD (2015) Fluorescent biosensors illuminate calcium levels within defined beta-cell endosome subpopulations. Cell Calcium **57:** 263-274

Alexandre J, Lassalles JP (1990) Effect of d-myo-inositol 1,4,5-trisphosphate on the electrical properties of the red beet vacuole membrane. Plant Physiol **93:** 837-840

Ali R, Ma W, Lemtiri-Chlieh F, Tsaltas D, Leng Q, von Bodman S, Berkowitz GA (2007) Death don't have no mercy and neither does calcium: *Arabidopsis* CYCLIC NUCLEOTIDE GATED CHANNEL2 and innate immunity. Plant Cell **19:** 1081-1095

Allen GJ, Muir SR, Sanders D (1995) Release of Ca^{2+} from individual plant vacuoles by both InsP3 and cyclic ADP-ribose. Science **268:** 735-737

Austin S, Tavakoli M, Pfeiffer C, Seifert J, Mattarei A, De Stefani D, Zoratti M, Nowikovsky K (2017) LETM1-mediated K^+ and Na^+ homeostasis regulates mitochondrial Ca^{2+} efflux. Front Physiol **8:** 839

Balsera M, Goetze TA, Kovacs-Bogdan E, Schurmann P, Wagner R, Buchanan BB, Soll J, Bolter B (2009) Characterization of Tic110, a channel-forming protein at the inner envelope membrane of chloroplasts, unveils a response to Ca^{2+} and a stromal regulatory disulfide bridge. J Biol Chem **284:** 2603-2616

Baubet V, Le Mouellic H, Campbell AK, Lucas-Meunier E, Fossier P, Brulet P (2000) Chimeric green fluorescent protein-aequorin as bioluminescent Ca^{2+} reporters at the single-cell level. Proc Natl Acad Sci U S A **97:** 7260-7265

Bayer EM, Sparkes I, Vanneste S, Rosado A (2017) From shaping organelles to signalling platforms: the emerging functions of plant ER-PM contact sites. Curr Opin Plant Biol **40:** 89-96

Berridge MJ, Lipp P, Bootman MD (2000) The versatility and universality of calcium signalling. Nat Rev Mol Cell Biol **1:** 11-21

Beyhl D, Hortensteiner S, Martinoia E, Farmer EE, Fromm J, Marten I, Hedrich R (2009) The *fou2* mutation in the major vacuolar cation channel TPC1 confers tolerance to inhibitory luminal calcium. Plant J **58:** 715-723

Biro RL, Daye S, Serlin BS, Terry ME, Datta N, Sopory SK, Roux SJ (1984) Characterization of oat calmodulin and radioimmunoassay of its subcellular distribution. Plant Physiol **75:** 382-386

Bonza MC, De Michelis MI (2011) The plant Ca^{2+}-ATPase repertoire: biochemical features and physiological functions. Plant Biol (Stuttg) **13:** 421-430

Bonza MC, Loro G, Behera S, Wong A, Kudla J, Costa A (2013) Analyses of Ca^{2+} accumulation and dynamics in the endoplasmic reticulum of Arabidopsis root cells using a genetically encoded Cameleon sensor. Plant Physiol **163:** 1230-1241

Bose J, Pottosin, II, Shabala SS, Palmgren MG, Shabala S (2011) Calcium efflux systems in stress signaling and adaptation in plants. Front Plant Sci **2:** 85

Boudsocq M, Willmann MR, McCormack M, Lee H, Shan L, He P, Bush J, Cheng SH, Sheen J (2010) Differential innate immune signalling via Ca^{2+} sensor protein kinases. Nature **464:** 418-422

Boursiac Y, Lee SM, Romanowsky S, Blank R, Sladek C, Chung WS, Harper JF (2010) Disruption of the vacuolar calcium-ATPases in *Arabidopsis* results in the activation of a salicylic acid-dependent programmed cell death pathway. Plant Physiol **154:** 1158-1171

Brini M, Murgia M, Pasti L, Picard D, Pozzan T, Rizzuto R (1993) Nuclear Ca^{2+} concentration measured with specifically targeted recombinant aequorin. EMBO J **12:** 4813-4819

Brini M, Marsault R, Bastianutto C, Alvarez J, Pozzan T, Rizzuto R (1995) Transfected aequorin in the measurement of cytosolic Ca^{2+} concentration ($[Ca^{2+}]_c$). A critical evaluation. J Biol Chem **270:** 9896-9903

Brini M (2008) Calcium-sensitive photoproteins. Methods **46:** 160-166

Brini M, Leanza L, Szabo I (2017) Lipid-mediated modulation of intracellular ion channels and redox state: physiopathological implications. Antioxid Redox Signal

Brownlee C (1986) Cytoplasmic free calcium in growing rhizoids of *Fucus serratus*. Prog Clin Biol Res **210:** 71-78

Capoen W, Sun J, Wysham D, Otegui MS, Venkateshwaran M, Hirsch S, Miwa H, Downie JA, Morris RJ, Ane JM, Oldroyd GE (2011) Nuclear membranes control symbiotic calcium signaling of legumes. Proc Natl Acad Sci U S A **108:** 14348-14353

Carpaneto A, Gradogna A (2018) Modulation of calcium and potassium permeation in plant TPC channels. Biophys Chem **236:** 1-7

Carraretto L, Teardo E, Checchetto V, Finazzi G, Uozumi N, Szabo I (2016) Ion channels in plant bioenergetic organelles, chloroplasts and mitochondria: from molecular identification to function. Mol Plant **9:** 371-395

Case RM, Eisner D, Gurney A, Jones O, Muallem S, Verkhratsky A (2007) Evolution of calcium homeostasis: from birth of the first cell to an omnipresent signalling system. Cell Calcium **42:** 345-350

Charpentier M, Sun J, Vaz Martins T, Radhakrishnan GV, Findlay K, Soumpourou E, Thouin J, Very AA, Sanders D, Morris RJ, Oldroyd GE (2016) Nuclear-localized cyclic nucleotide-gated channels mediate symbiotic calcium oscillations. Science **352:** 1102-1105

Cheng NH, Pittman JK, Shigaki T, Hirschi KD (2002) Characterization of CAX4, an *Arabidopsis* H^+/cation antiporter. Plant Physiol **128:** 1245-1254

Cheng NH, Pittman JK, Barkla BJ, Shigaki T, Hirschi KD (2003) The *Arabidopsis cax1* mutant exhibits impaired ion homeostasis, development, and hormonal responses and reveals interplay among vacuolar transporters. Plant Cell **15:** 347-364

Chigri F, Soll J, Vothknecht UC (2005) Calcium regulation of chloroplast protein import. Plant J **42:** 821-831

Chigri F, Hormann F, Stamp A, Stammers DK, Bolter B, Soll J, Vothknecht UC (2006) Calcium regulation of chloroplast protein translocation is mediated by calmodulin binding to Tic32. Proc Natl Acad Sci U S A **103:** 16051-16056

Cho D, Villiers F, Kroniewicz L, Lee S, Seo YJ, Hirschi KD, Leonhardt N, Kwak JM (2012) Vacuolar CAX1 and CAX3 influence auxin transport in guard cells via regulation of apoplastic pH. Plant Physiol **160:** 1293-1302

Choi HI, Park HJ, Park JH, Kim S, Im MY, Seo HH, Kim YW, Hwang I, Kim SY (2005) *Arabidopsis* calcium-dependent protein kinase *AtCPK32* interacts with ABF4, a transcriptional regulator of abscisic acid-responsive gene expression, and modulates its activity. Plant Physiol **139:** 1750-1761

Choi WG, Toyota M, Kim SH, Hilleary R, Gilroy S (2014) Salt stress-induced Ca^{2+} waves are associated with rapid, long-distance root-to-shoot signaling in plants. Proc Natl Acad Sci U S A **111:** 6497-6502

Coca M, San Segundo B (2010) *AtCPK1* calcium-dependent protein kinase mediates pathogen resistance in *Arabidopsis*. Plant J **63:** 526-540

Coe H, Michalak M (2009) Calcium binding chaperones of the endoplasmic reticulum. Gen Physiol Biophys **28 Spec No Focus:** F96-F103

Conn S, Gilliham M (2010) Comparative physiology of elemental distributions in plants. Ann Bot **105:** 1081-1102

Conn SJ, Gilliham M, Athman A, Schreiber AW, Baumann U, Moller I, Cheng NH, Stancombe MA, Hirschi KD, Webb AA, Burton R, Kaiser BN, Tyerman SD, Leigh RA (2011) Cell-specific vacuolar calcium storage mediated by CAX1 regulates apoplastic calcium concentration, gas exchange, and plant productivity in *Arabidopsis*. Plant Cell **23:** 240-257

Corpas FJ, Barroso JB (2017) Nitric oxide synthase-like activity in higher plants. Nitric Oxide **68:** 5-6

Corso M, Doccula FG, de Melo JRF, Costa A, Verbruggen N (2018) Endoplasmic reticulum-localized CCX2 is required for osmotolerance by regulating ER and cytosolic Ca^{2+} dynamics in *Arabidopsis*. Proc Natl Acad Sci U S A **115:** 3966-3971

Costa A, Drago I, Behera S, Zottini M, Pizzo P, Schroeder JI, Pozzan T, Lo Schiavo F (2010) H_2O_2 in plant peroxisomes: an in vivo analysis uncovers a Ca^{2+}-dependent scavenging system. Plant J **62:** 760-772

Costa A, Drago I, Zottini M, Pizzo P, Pozzan T (2013) Peroxisome Ca^{2+} homeostasis in animal and plant cells. Subcell Biochem **69:** 111-133

Costa A, Kudla J (2015) Colorful insights: advances in imaging drive novel breakthroughs in Ca^{2+} signaling. Mol Plant **8:** 352-355

Costa A, Luoni L, Marrano CA, Hashimoto K, Koster P, Giacometti S, De Michelis MI, Kudla J, Bonza MC (2017) Ca^{2+}-dependent phosphoregulation of the plasma membrane Ca^{2+}-ATPase ACA8 modulates stimulus-induced calcium signatures. J Exp Bot **68:** 3215-3230

Costa A, Navazio L, Szabo I (2018) The contribution of organelles to plant intracellular Calcium signalling. J Exp Bot **69:** 4175-4193

Cucu B, Degreif D, Bertl A, Thiel G (2017) Vesicle fusion and fission in plants and yeast. Cell Calcium **67:** 40-45

Dammann C, Ichida A, Hong B, Romanowsky SM, Hrabak EM, Harmon AC, Pickard BG, Harper JF (2003) Subcellular targeting of nine calcium-dependent protein kinase isoforms from *Arabidopsis*. Plant Physiol **132:** 1840-1848

De Vriese K, Costa A, Beeckman T, Vanneste S (2018) Pharmacological strategies for manipulating plant Ca^{2+} signalling. Int J Mol Sci **19:** 1506

DeFalco TA, Bender KW, Snedden WA (2009) Breaking the code: Ca^{2+} sensors in plant signalling. Biochem J **425:** 27-40

DeFalco TA, Moeder W, Yoshioka K (2016) Opening the gates: insights into cyclic nucleotide-gated channel-mediated signaling. Trends Plant Sci **21:** 903-906

Demaurex N, Guido D (2017) The role of mitochondria in the activation/maintenance of SOCE: membrane contact sites as signaling hubs sustaining store-operated Ca^{2+} entry. Adv Exp Med Biol **993:** 277-296

Demidchik V, Shabala S, Isayenkov S, Cuin TA, Pottosin I (2018) Calcium transport across plant membranes: mechanisms and functions. New Phytol **220:** 49-69

Depege N, Bellafiore S, Rochaix JD (2003) Role of chloroplast protein kinase Stt7 in LHCII phosphorylation and state transition in *Chlamydomonas*. Science **299:** 1572-1575

Dodd AN, Kudla J, Sanders D (2010) The language of calcium signaling. Annu Rev Plant Biol **61:** 593-620

Drago I, Giacomello M, Pizzo P, Pozzan T (2008) Calcium dynamics in the peroxisomal lumen of living cells. J Biol Chem **283:** 14384-14390

Edel KH, Marchadier E, Brownlee C, Kudla J, Hetherington AM (2017) The evolution of calcium-based signalling in plants. Curr Biol **27:** R667-R679

Eisenhut M, Hoecker N, Schmidt SB, Basgaran RM, Flachbart S, Jahns P, Eser T, Geimer S, Husted S, Weber APM, Leister D, Schneider A (2018) The plastid envelope CHLOROPLAST MANGANESE TRANSPORTER1 is essential for manganese homeostasis in *Arabidopsis*. Mol Plant **11:** 955-969

Evans NH, McAinsh MR, Hetherington AM (2001) Calcium oscillations in higher plants. Curr Opin Plant Biol **4:** 415-420

Felle H (1989) Ca^{2+}-selective microelectrodes and their application to plant cells and tissues. Plant Physiol **91:** 1239-1242

Ferro M, Brugiere S, Salvi D, Seigneurin-Berny D, Court M, Moyet L, Ramus C, Miras S, Mellal M, Le Gall S, Kieffer-Jaquinod S, Bruley C, Garin J, Joyard J, Masselon C, Rolland N (2010) AT_CHLORO, a comprehensive chloroplast proteome database with subplastidial localization and curated information on envelope proteins. Mol Cell Proteomics **9:** 1063-1084

Finazzi G, Petroutsos D, Tomizioli M, Flori S, Sautron E, Villanova V, Rolland N, Seigneurin-Berny D (2015) Ions channels/transporters and chloroplast regulation. Cell Calcium **58:** 86-97

Finkler A, Kaplan B, Fromm H (2007) Ca^{2+}-responsive cis-elements in plants. Plant Signal Behav **2:** 17-19

Frank J, Happeck R, Meier B, Hoang MTT, Stribny J, Hause G, Ding H, Morsomme P, Baginsky S, Peiter E (2019) Chloroplast-localized BICAT proteins shape stromal calcium signals and are required for efficient photosynthesis. New Phytol **221:** 866-880

Frei dit Frey N, Mbengue M, Kwaaitaal M, Nitsch L, Altenbach D, Haweker H, Lozano-Duran R, Njo MF, Beeckman T, Huettel B, Borst JW, Panstruga R, Robatzek S (2012) Plasma membrane calcium ATPases are important components of receptor-mediated signaling in plant immune responses and development. Plant Physiol **159:** 798-809

Fu YL, Zhang GB, Lv XF, Guan Y, Yi HY, Gong JM (2013) *Arabidopsis* histone methylase CAU1/PRMT5/SKB1 acts as an epigenetic suppressor of the calcium signaling gene CAS to mediate stomatal closure in response to extracellular calcium. Plant Cell **25:** 2878-2891

Galon Y, Finkler A, Fromm H (2010) Calcium-regulated transcription in plants. Mol Plant **3:** 653-669

Gao D, Knight MR, Trewavas AJ, Sattelmacher B, Plieth C (2004) Self-reporting *Arabidopsis* expressing pH and [Ca^{2+}] indicators unveil ion dynamics in the cytoplasm and in the apoplast under abiotic stress. Plant Physiol **134:** 898-908

Genre A, Chabaud M, Balzergue C, Puech-Pages V, Novero M, Rey T, Fournier J, Rochange S, Becard G, Bonfante P, Barker DG (2013) Short-chain chitin oligomers from arbuscular mycorrhizal fungi trigger nuclear Ca^{2+} spiking in *Medicago truncatula* roots and their production is enhanced by strigolactone. New Phytol **198:** 190-202

Giacomello M, Drago I, Pizzo P, Pozzan T (2007) Mitochondrial Ca^{2+} as a key regulator of cell life and death. Cell Death Differ **14:** 1267-1274

Goddard H, Manison NF, Tomos D, Brownlee C (2000) Elemental propagation of calcium signals in response-specific patterns determined by environmental stimulus strength. Proc Natl Acad Sci U S A **97:** 1932-1937

Guo J, Zeng W, Chen Q, Lee C, Chen L, Yang Y, Cang C, Ren D, Jiang Y (2016) Structure of the voltage-gated two-pore channel TPC1 from *Arabidopsis thaliana*. Nature **531:** 196-201

Hamilton ES, Schlegel AM, Haswell ES (2015) United in diversity: mechanosensitive ion channels in plants. Annu Rev Plant Biol **66:** 113-137

Haswell ES, Meyerowitz EM (2006) MscS-like proteins control plastid size and shape in *Arabidopsis thaliana*. Curr Biol **16:** 1-11

Hedrich R, Mueller TD, Becker D, Marten I (2018) Structure and function of TPC1 vacuole SV channel gains shape. Mol Plant **11:** 764-775

Hepler PK (2005) Calcium: a central regulator of plant growth and development. Plant Cell **17:** 2142-2155

Hirayama T, Shinozaki K (2010) Research on plant abiotic stress responses in the post-genome era: past, present and future. Plant J **61:** 1041-1052

Hochmal AK, Schulze S, Trompelt K, Hippler M (2015) Calcium-dependent regulation of photosynthesis. Biochim Biophys Acta **1847:** 993-1003

Horikawa K (2015) Recent progress in the development of genetically encoded Ca^{2+} indicators. J Med Invest **62:** 24-28

Huang L, Berkelman T, Franklin AE, Hoffman NE (1993) Characterization of a gene encoding a Ca^{2+}-ATPase-like protein in the plastid envelope. Proc Natl Acad Sci U S A **90:** 10066-10070

Ifuku K, Ishihara S, Sato F (2010) Molecular functions of oxygen-evolving complex family proteins in photosynthetic electron flow. J Integr Plant Biol **52:** 723-734

Ikura M, Osawa M, Ames JB (2002) The role of calcium-binding proteins in the control of transcription: structure to function. Bioessays **24:** 625-636

Iwano M, Entani T, Shiba H, Kakita M, Nagai T, Mizuno H, Miyawaki A, Shoji T, Kubo K, Isogai A, Takayama S (2009) Fine-tuning of the cytoplasmic Ca^{2+} concentration is essential for pollen tube growth. Plant Physiol **150:** 1322-1334

Iwano M, Ito K, Fujii S, Kakita M, Asano-Shimosato H, Igarashi M, Kaothien-Nakayama P, Entani T, Kanatani A, Takehisa M, Tanaka M, Komatsu K, Shiba H, Nagai T, Miyawaki A, Isogai A, Takayama S (2015) Calcium signalling mediates self-incompatibility response in the Brassicaceae. Nat Plants **1:** 15128

Jammes F, Hu HC, Villiers F, Bouten R, Kwak JM (2011) Calcium-permeable channels in plant cells. FEBS J **278:** 4262-4276

Jia XY, He LH, Jing RL, Li RZ (2009) Calreticulin: conserved protein and diverse functions in plants. Physiol Plant **136:** 127-138

Jin H, Hong Z, Su W, Li J (2009) A plant-specific calreticulin is a key retention factor for a defective brassinosteroid receptor in the endoplasmic reticulum. Proc Natl Acad Sci U S A **106:** 13612-13617

Johnson CH, Knight MR, Kondo T, Masson P, Sedbrook J, Haley A, Trewavas A (1995) Circadian oscillations of cytosolic and chloroplastic free calcium in plants. Science **269:** 1863-1865

Kaplan B, Davydov O, Knight H, Galon Y, Knight MR, Fluhr R, Fromm H (2006) Rapid transcriptome changes induced by cytosolic Ca^{2+} transients reveal ABRE-related sequences as Ca^{2+}-responsive cis elements in *Arabidopsis*. Plant Cell **18:** 2733-2748

Kaplan B, Sherman T, Fromm H (2007) Cyclic nucleotide-gated channels in plants. FEBS Lett **581:** 2237-2246

Keinath NF, Waadt R, Brugman R, Schroeder JI, Grossmann G, Schumacher K, Krebs M (2015) Live cell imaging with R-GECO1 sheds light on flg22- and chitin-induced transient $[Ca^{2+}]_{cyt}$ patterns in *Arabidopsis*. Mol Plant **8:** 1188-1200

Kelner A, Leitao N, Chabaud M, Charpentier M, de Carvalho-Niebel F (2018) Dual color sensors for simultaneous analysis of calcium signal dynamics in the nuclear and cytoplasmic compartments of plant cells. Front Plant Sci **9:** 245

Kiep V, Vadassery J, Lattke J, Maass JP, Boland W, Peiter E, Mithofer A (2015) Systemic cytosolic Ca^{2+} elevation is activated upon wounding and herbivory in *Arabidopsis*. New Phytol **207:** 996-1004

Kim TH, Bohmer M, Hu H, Nishimura N, Schroeder JI (2010) Guard cell signal transduction network: advances in understanding abscisic acid, CO_2, and Ca^{2+} signaling. Annu Rev Plant Biol **61:** 561-591

Klusener B, Boheim G, Liss H, Engelberth J, Weiler EW (1995) Gadolinium-sensitive, voltage-dependent calcium release channels in the endoplasmic reticulum of a higher plant mechanoreceptor organ. EMBO J **14:** 2708-2714

Klusener B, Boheim G, Weiler EW (1997) Modulation of the ER Ca^{2+} channel BCC1 from tendrils of *Bryonia dioica* by divalent cations, protons and H_2O_2. FEBS Lett **407:** 230-234

Klusener B, Weiler EW (1999) A calcium-selective channel from root-tip endomembranes of garden cress. Plant Physiol **119:** 1399-1406

Kmiecik P, Leonardelli M, Teige M (2016) Novel connections in plant organellar signalling link different stress responses and signalling pathways. J Exp Bot **67:** 3793-3807

Knight H, Trewavas AJ, Knight MR (1996) Cold calcium signaling in *Arabidopsis* involves two cellular pools and a change in calcium signature after acclimation. Plant Cell **8:** 489-503

Krebs M, Held K, Binder A, Hashimoto K, Den Herder G, Parniske M, Kudla J, Schumacher K (2012) FRET-based genetically encoded sensors allow high-resolution live cell imaging of Ca^{2+} dynamics. Plant J **69:** 181-192

Kruger F, Schumacher K (2018) Pumping up the volume - vacuole biogenesis in *Arabidopsis thaliana*. Semin Cell Dev Biol **80:** 106-112

Kudla J, Batistic O, Hashimoto K (2010) Calcium signals: the lead currency of plant information processing. Plant Cell **22:** 541-563

Kudla J, Becker D, Grill E, Hedrich R, Hippler M, Kummer U, Parniske M, Romeis T, Schumacher K (2018) Advances and current challenges in calcium signaling. New Phytol **218:** 414-431

Kuhn S, Bussemer J, Chigri F, Vothknecht UC (2009) Calcium depletion and calmodulin inhibition affect the import of nuclear-encoded proteins into plant mitochondria. Plant J **58:** 694-705

Kuyucak S, Andersen O, Chung S (2001) Models of permeation in ion channels. Rep Prog Phys **64:** 1427-1472

Lamotte O, Gould K, Lecourieux D, Sequeira-Legrand A, Lebrun-Garcia A, Durner J, Pugin A, Wendehenne D (2004) Analysis of nitric oxide signaling functions in tobacco cells challenged by the elicitor cryptogein. Plant Physiol **135:** 516-529

Lecourieux D, Lamotte O, Bourque S, Wendehenne D, Mazars C, Ranjeva R, Pugin A (2005) Proteinaceous and oligosaccharidic elicitors induce different calcium signatures in the nucleus of tobacco cells. Cell Calcium **38:** 527-538

Lee SM, Kim HS, Han HJ, Moon BC, Kim CY, Harper JF, Chung WS (2007) Identification of a calmodulin-regulated autoinhibited Ca^{2+}-ATPase (ACA11) that is localized to vacuole membranes in *Arabidopsis*. FEBS Lett **581:** 3943-3949

Leister D, Wang L, Kleine T (2017) Organellar gene expression and acclimation of plants to environmental stress. Front Plant Sci **8:** 387

Lemtiri-Chlieh F, MacRobbie EA, Webb AA, Manison NF, Brownlee C, Skepper JN, Chen J, Prestwich GD, Brearley CA (2003) Inositol hexakisphosphate mobilizes an endomembrane store of calcium in guard cells. Proc Natl Acad Sci U S A **100:** 10091-10095

Linka N, Weber AP (2010) Intracellular metabolite transporters in plants. Mol Plant **3:** 21-53

Linka N, Esser C (2012) Transport proteins regulate the flux of metabolites and cofactors across the membrane of plant peroxisomes. Front Plant Sci **3:** 3

Liu KH, Niu Y, Konishi M, Wu Y, Du H, Sun Chung H, Li L, Boudsocq M, McCormack M, Maekawa S, Ishida T, Zhang C, Shokat K, Yanagisawa S, Sheen J (2017) Discovery of nitrate-CPK-NLP signalling in central nutrient-growth networks. Nature **545:** 311-316

Logan DC, Knight MR (2003) Mitochondrial and cytosolic calcium dynamics are differentially regulated in plants. Plant Physiol **133:** 21-24

Loro G, Drago I, Pozzan T, Schiavo FL, Zottini M, Costa A (2012) Targeting of Cameleons to various subcellular compartments reveals a strict cytoplasmic/mitochondrial Ca^{2+} handling relationship in plant cells. Plant J **71:** 1-13

Loro G, Ruberti C, Zottini M, Costa A (2013) The D3cpv Cameleon reports Ca^{2+} dynamics in plant mitochondria with similar kinetics of the YC3.6 Cameleon, but with a lower sensitivity. J Microsc **249:** 8-12

Loro G, Wagner S, Doccula FG, Behera S, Weinl S, Kudla J, Schwarzlander M, Costa A, Zottini M (2016) Chloroplast-specific *in vivo* Ca^{2+} imaging using yellow cameleon fluorescent protein sensors reveals organelle-autonomous Ca^{2+} signatures in the stroma. Plant Physiol **171:** 2317-2330

Manzoor H, Chiltz A, Madani S, Vatsa P, Schoefs B, Pugin A, Garcia-Brugger A (2012) Calcium signatures and signaling in cytosol and organelles of tobacco cells induced by plant defense elicitors. Cell Calcium **51:** 434-444

Mariani P, Navazio L, Zuppini A (2003) Calreticulin and the endoplasmic reticulum in plant cell biology. *In* P Eggleton, M Michalak, eds, Calreticulin: Second Edition. Springer US, Boston, MA, pp 94-104

Marti MC, Stancombe MA, Webb AA (2013) Cell- and stimulus type-specific intracellular free Ca^{2+} signals in *Arabidopsis*. Plant Physiol **163:** 625-634

Martinoia E, Meyer S, De Angeli A, Nagy R (2012) Vacuolar transporters in their physiological context. Annu Rev Plant Biol **63:** 183-213

Mathur J, Barton KA, Schattat MH (2013) Fluorescent protein flow within stromules. Plant Cell **25:** 2771-2772

Mazars C, Bourque S, Mithofer A, Pugin A, Ranjeva R (2009) Calcium homeostasis in plant cell nuclei. New Phytol **181:** 261-274

McAinsh MR, Pittman JK (2009) Shaping the calcium signature. New Phytol **181:** 275-294

McCormack JG, Halestrap AP, Denton RM (1990) Role of calcium ions in regulation of mammalian intramitochondrial metabolism. Physiol Rev **70:** 391-425

Mehlmer N, Wurzinger B, Stael S, Hofmann-Rodrigues D, Csaszar E, Pfister B, Bayer R, Teige M (2010) The Ca^{2+}-dependent protein kinase CPK3 is required for MAPK-independent salt-stress acclimation in *Arabidopsis*. Plant J **63:** 484-498

Mehlmer N, Parvin N, Hurst CH, Knight MR, Teige M, Vothknecht UC (2012) A toolset of aequorin expression vectors for in planta studies of subcellular calcium concentrations in *Arabidopsis thaliana*. J Exp Bot **63:** 1751-1761

Mehrshahi P, Stefano G, Andaloro JM, Brandizzi F, Froehlich JE, DellaPenna D (2013) Transorganellar complementation redefines the biochemical continuity of endoplasmic reticulum and chloroplasts. Proc Natl Acad Sci U S A **110:** 12126-12131

Mei H, Cheng NH, Zhao J, Park S, Escareno RA, Pittman JK, Hirschi KD (2009) Root development under metal stress in *Arabidopsis thaliana* requires the H^+/cation antiporter CAX4. New Phytol **183:** 95-105

Mills RF, Doherty ML, Lopez-Marques RL, Weimar T, Dupree P, Palmgren MG, Pittman JK, Williams LE (2008) ECA3, a Golgi-localized P2A-type ATPase, plays a crucial role in manganese nutrition in *Arabidopsis*. Plant Physiol **146:** 116-128

Miyawaki A, Llopis J, Heim R, McCaffery JM, Adams JA, Ikura M, Tsien RY (1997) Fluorescent indicators for Ca^{2+} based on green fluorescent proteins and calmodulin. Nature **388:** 882-887

Monshausen GB (2012) Visualizing Ca^{2+} signatures in plants. Curr Opin Plant Biol **15:** 677-682

Mravec J, Kracun SK, Rydahl MG, Westereng B, Pontiggia D, De Lorenzo G, Domozych DS, Willats WGT (2017) An oligogalacturonide-derived molecular probe demonstrates the dynamics of calcium-mediated pectin complexation in cell walls of tip-growing structures. Plant J **91:** 534-546

Muir SR, Sanders D (1997) Inositol 1,4,5-trisphosphate-sensitive Ca^{2+} release across nonvacuolar membranes in cauliflower. Plant Physiol **114:** 1511-1521

Munnik T, Nielsen E (2011) Green light for polyphosphoinositide signals in plants. Curr Opin Plant Biol **14:** 489-497

Nardi MC, Feron R, Navazio L, Mariani P, Pierson E, Wolters-Arts M, Knuiman B, Mariani C, Derksen J (2006) Expression and localization of calreticulin in tobacco anthers and pollen tubes. Planta **223:** 1263-1271

Navazio L, Bewell MA, Siddiqua A, Dickinson GD, Galione A, Sanders D (2000) Calcium release from the endoplasmic reticulum of higher plants elicited by the NADP metabolite nicotinic acid adenine dinucleotide phosphate. Proc Natl Acad Sci U S A **97:** 8693-8698

Navazio L, Mariani P, Sanders D (2001) Mobilization of Ca^{2+} by cyclic ADP-ribose from the endoplasmic reticulum of cauliflower florets. Plant Physiol **125:** 2129-2138

Navazio L, Miuzzo M, Royle L, Baldan B, Varotto S, Merry AH, Harvey DJ, Dwek RA, Rudd PM, Mariani P (2002) Monitoring endoplasmic reticulum-to-Golgi traffic of a plant calreticulin by protein glycosylation analysis. Biochemistry **41:** 14141-14149

Navazio L, Baldan B, Moscatiello R, Zuppini A, Woo SL, Mariani P, Lorito M (2007) Calcium-mediated perception and defense responses activated in plant cells by metabolite mixtures secreted by the biocontrol fungus *Trichoderma atroviride*. BMC Plant Biol **7:** 41

Ngo QA, Vogler H, Lituiev DS, Nestorova A, Grossniklaus U (2014) A calcium dialog mediated by the FERONIA signal transduction pathway controls plant sperm delivery. Dev Cell **29:** 491-500

Nomura H, Komori T, Kobori M, Nakahira Y, Shiina T (2008) Evidence for chloroplast control of external Ca^{2+}-induced cytosolic Ca^{2+} transients and stomatal closure. Plant J **53:** 988-998

Nomura H, Komori T, Uemura S, Kanda Y, Shimotani K, Nakai K, Furuichi T, Takebayashi K, Sugimoto T, Sano S, Suwastika IN, Fukusaki E, Yoshioka H, Nakahira Y, Shiina T (2012) Chloroplast-mediated activation of plant immune signalling in *Arabidopsis*. Nat Commun **3:** 926

Nomura H, Shiina T (2014) Calcium signaling in plant endosymbiotic organelles: mechanism and role in physiology. Mol Plant **7:** 1094-1104

Oldroyd GE, Downie JA (2006) Nuclear calcium changes at the core of symbiosis signalling. Curr Opin Plant Biol **9:** 351-357

Ordenes VR, Moreno I, Maturana D, Norambuena L, Trewavas AJ, Orellana A (2012) *In vivo* analysis of the calcium signature in the plant Golgi apparatus reveals unique dynamics. Cell Calcium **52:** 397-404

Ottolini D, Cali T, Brini M (2014) Methods to measure intracellular Ca^{2+} fluxes with organelle-targeted aequorin-based probes. Methods Enzymol **543:** 21-45

Palmer AE, Giacomello M, Kortemme T, Hires SA, Lev-Ram V, Baker D, Tsien RY (2006) Ca^{2+} indicators based on computationally redesigned calmodulin-peptide pairs. Chem Biol **13:** 521-530

Palty R, Silverman WF, Hershfinkel M, Caporale T, Sensi SL, Parnis J, Nolte C, Fishman D, Shoshan-Barmatz V, Herrmann S, Khananshvili D, Sekler I (2010) NCLX is an essential component of mitochondrial Na^+/Ca^{2+} exchange. Proc Natl Acad Sci U S A **107:** 436-441

Pauly N, Knight MR, Thuleau P, van der Luit AH, Moreau M, Trewavas AJ, Ranjeva R, Mazars C (2000) Control of free calcium in plant cell nuclei. Nature **405:** 754-755

Peiter E, Maathuis FJ, Mills LN, Knight H, Pelloux J, Hetherington AM, Sanders D (2005) The vacuolar Ca^{2+}-activated channel TPC1 regulates germination and stomatal movement. Nature **434:** 404-408

Peiter E (2011) The plant vacuole: emitter and receiver of calcium signals. Cell Calcium **50:** 120-128

Perez Koldenkova V, Nagai T (2013) Genetically encoded Ca^{2+} indicators: properties and evaluation. Biochim Biophys Acta **1833:** 1787-1797

Persson S, Wyatt SE, Love J, Thompson WF, Robertson D, Boss WF (2001) The Ca^{2+} status of the endoplasmic reticulum is altered by induction of calreticulin expression in transgenic plants. Plant Physiol **126:** 1092-1104

Pittman JK, Shigaki T, Hirschi KD (2005) Evidence of differential pH regulation of the *Arabidopsis* vacuolar Ca^{2+}/H^+ antiporters CAX1 and CAX2. FEBS Lett **579:** 2648-2656

Pittman JK, Hirschi KD (2016) CAX-ing a wide net: Cation/H^+ transporters in metal remediation and abiotic stress signalling. Plant Biol (Stuttg) **18:** 741-749

Pizzo P, Lissandron V, Capitanio P, Pozzan T (2011) Ca^{2+} signalling in the Golgi apparatus. Cell Calcium **50:** 184-192

Pottosin I, Shabala S (2016) Transport across chloroplast membranes: optimizing photosynthesis for adverse environmental conditions. Mol Plant **9:** 356-370

Raffaello A, Mammucari C, Gherardi G, Rizzuto R (2016) Calcium at the center of cell signaling: interplay between endoplasmic reticulum, mitochondria, and lysosomes. Trends Biochem Sci **41:** 1035-1049

Ranf S, Wunnenberg P, Lee J, Becker D, Dunkel M, Hedrich R, Scheel D, Dietrich P (2008) Loss of the vacuolar cation channel, AtTPC1, does not impair Ca^{2+} signals induced by abiotic and biotic stresses. Plant J **53:** 287-299

Ranty B, Aldon D, Cotelle V, Galaud JP, Thuleau P, Mazars C (2016) Calcium sensors as key hubs in plant responses to biotic and abiotic stresses. Front Plant Sci **7:** 327

Reddy AS, Ali GS, Celesnik H, Day IS (2011) Coping with stresses: roles of calcium- and calcium/calmodulin-regulated gene expression. Plant Cell **23:** 2010-2032

Rienmuller F, Beyhl D, Lautner S, Fromm J, Al-Rasheid KA, Ache P, Farmer EE, Marten I, Hedrich R (2010) Guard cell-specific calcium sensitivity of high density and activity SV/TPC1 channels. Plant Cell Physiol **51:** 1548-1554

Rizzuto R, Marchi S, Bonora M, Aguiari P, Bononi A, De Stefani D, Giorgi C, Leo S, Rimessi A, Siviero R, Zecchini E, Pinton P (2009) Ca^{2+} transfer from the ER to mitochondria: when, how and why. Biochim Biophys Acta **1787:** 1342-1351

Rizzuto R, De Stefani D, Raffaello A, Mammucari C (2012) Mitochondria as sensors and regulators of calcium signalling. Nat Rev Mol Cell Biol **13:** 566-578

Robinson DG, Brandizzi F, Hawes C, Nakano A (2015) Vesicles versus tubes: Is endoplasmic reticulum-Golgi transport in plants fundamentally different from other eukaryotes? Plant Physiol **168:** 393-406

Rocha AG, Vothknecht UC (2012) The role of calcium in chloroplasts–an intriguing and unresolved puzzle. Protoplasma **249:** 957-966

Rogers KL, Stinnakre J, Agulhon C, Jublot D, Shorte SL, Kremer EJ, Brulet P (2005) Visualization of local Ca^{2+} dynamics with genetically encoded bioluminescent reporters. Eur J Neurosci **21:** 597-610

Rossi AE, Dirksen RT (2006) Sarcoplasmic reticulum: the dynamic calcium governor of muscle. Muscle Nerve **33:** 715-731

Rudolf R, Mongillo M, Rizzuto R, Pozzan T (2003) Looking forward to seeing calcium. Nat Rev Mol Cell Biol **4:** 579-586

Ruge H, Flosdorff S, Ebersberger I, Chigri F, Vothknecht UC (2016) The calmodulin-like proteins *AtCML4* and *AtCML5* are single-pass membrane proteins targeted to the endomembrane system by an N-terminal signal anchor sequence. J Exp Bot **67:** 3985-3996

Sai J, Johnson CH (2002) Dark-stimulated calcium ion fluxes in the chloroplast stroma and cytosol. Plant Cell **14:** 1279-1291

Sammels E, Parys JB, Missiaen L, De Smedt H, Bultynck G (2010) Intracellular Ca^{2+} storage in health and disease: a dynamic equilibrium. Cell Calcium **47:** 297-314

Sanders D, Brownlee C, Harper JF (1999) Communicating with calcium. Plant Cell **11:** 691-706

Sanders D, Pelloux J, Brownlee C, Harper JF (2002) Calcium at the crossroads of signaling. Plant Cell **14 Suppl:** S401-417

Schattat M, Barton K, Baudisch B, Klosgen RB, Mathur J (2011) Plastid stromule branching coincides with contiguous endoplasmic reticulum dynamics. Plant Physiol **155:** 1667-1677

Schneider A, Steinberger I, Herdean A, Gandini C, Eisenhut M, Kurz S, Morper A, Hoecker N, Ruhle T, Labs M, Flugge UI, Geimer S, Schmidt SB, Husted S, Weber AP, Spetea C, Leister D (2016) The evolutionarily conserved protein PHOTOSYNTHESIS AFFECTED MUTANT71 is required for efficient manganese uptake at the thylakoid membrane in *Arabidopsis*. Plant Cell **28:** 892-910

Selles B, Michaud C, Xiong TC, Leblanc O, Ingouff M (2018) *Arabidopsis* pollen tube germination and growth depend on the mitochondrial calcium uniporter complex. New Phytol **219:** 58-65

Sello S, Perotto J, Carraretto L, Szabo I, Vothknecht UC, Navazio L (2016) Dissecting stimulus-specific Ca^{2+} signals in amyloplasts and chloroplasts of *Arabidopsis thaliana* cell suspension cultures. J Exp Bot **67:** 3965-3974

Shao J, Fu Z, Ji Y, Guan X, Guo S, Ding Z, Yang X, Cong Y, Shen Y (2016) Leucine zipper-EF-hand containing transmembrane protein 1 (LETM1) forms a Ca^{2+}/H^{+} antiporter. Sci Rep **6:** 34174

Shimada T, Takagi J, Ichino T, Shirakawa M, Hara-Nishimura I (2018) Plant vacuoles. Annu Rev Plant Biol **69:** 123-145

Shinoda H, Ma Y, Nakashima R, Sakurai K, Matsuda T, Nagai T (2018) Acid-tolerant monomeric GFP from *Olindias formosa*. Cell Chem Biol **25:** 330-338 e337

Sieberer BJ, Chabaud M, Timmers AC, Monin A, Fournier J, Barker DG (2009) A nuclear-targeted cameleon demonstrates intranuclear Ca^{2+} spiking in *Medicago truncatula* root hairs in response to rhizobial nodulation factors. Plant Physiol **151:** 1197-1206

Simeunovic A, Mair A, Wurzinger B, Teige M (2016) Know where your clients are: subcellular localization and targets of calcium-dependent protein kinases. J Exp Bot **67:** 3855-3872

Son A, Park S, Shin DM, Muallem S (2016) Orai1 and STIM1 in ER/PM junctions: roles in pancreatic cell function and dysfunction. Am J Physiol Cell Physiol **310:** C414-422

Stael S, Wurzinger B, Mair A, Mehlmer N, Vothknecht UC, Teige M (2012) Plant organellar calcium signalling: an emerging field. J Exp Bot **63:** 1525-1542

Stael S, Kmiecik P, Willems P, Van Der Kelen K, Coll NS, Teige M, Van Breusegem F (2015) Plant innate immunity–sunny side up? Trends Plant Sci **20:** 3-11

Steinhorst L, Kudla J (2014) Signaling in cells and organisms - calcium holds the line. Curr Opin Plant Biol **22:** 14-21

Stephan AB, Kunz HH, Yang E, Schroeder JI (2016) Rapid hyperosmotic-induced Ca^{2+} responses in *Arabidopsis thaliana* exhibit sensory potentiation and involvement of plastidial KEA transporters. Proc Natl Acad Sci U S A **113:** E5242-5249

Szabadkai G, Duchen MR (2008) Mitochondria: the hub of cellular Ca^{2+} signaling. Physiology (Bethesda) **23:** 84-94

Szabo I, Zoratti M (2014) Mitochondrial channels: ion fluxes and more. Physiol Rev **94:** 519-608

Tang RJ, Luan S (2017) Regulation of calcium and magnesium homeostasis in plants: from transporters to signaling network. Curr Opin Plant Biol **39:** 97-105

Teardo E, Segalla A, Formentin E, Zanetti M, Marin O, Giacometti GM, Lo Schiavo F, Zoratti M, Szabo I (2010) Characterization of a plant glutamate receptor activity. Cell Physiol Biochem **26:** 253-262

Teardo E, Formentin E, Segalla A, Giacometti GM, Marin O, Zanetti M, Lo Schiavo F, Zoratti M, Szabo I (2011) Dual localization of plant glutamate receptor AtGLR3.4 to plastids and plasmamembrane. Biochim Biophys Acta **1807:** 359-367

Teardo E, Carraretto L, De Bortoli S, Costa A, Behera S, Wagner R, Lo Schiavo F, Formentin E, Szabo I (2015) Alternative splicing-mediated targeting of the Arabidopsis GLUTAMATE RECEPTOR3.5 to mitochondria affects organelle morphology. Plant Physiol **167:** 216-227

Teardo E, Carraretto L, Wagner S, Formentin E, Behera S, De Bortoli S, Larosa V, Fuchs P, Lo Schiavo F, Raffaello A, Rizzuto R, Costa A, Schwarzlander M, Szabo I (2017) Physiological characterization of a plant mitochondrial calcium uniporter *in vitro* and *in vivo*. Plant Physiol **173:** 1355-1370

Trewavas A, Read N, Campbell AK, Knight M (1996) Transduction of Ca^{2+} signals in plant cells and compartmentalization of the Ca^{2+} signal. Biochem Soc Trans **24:** 971-974

Tsai MF, Phillips CB, Ranaghan M, Tsai CW, Wu Y, Willliams C, Miller C (2016) Dual functions of a small regulatory subunit in the mitochondrial calcium uniporter complex. Elife **5**

van Der Luit AH, Olivari C, Haley A, Knight MR, Trewavas AJ (1999) Distinct calcium signaling pathways regulate calmodulin gene expression in tobacco. Plant Physiol **121:** 705-714

Vincent TR, Avramova M, Canham J, Higgins P, Bilkey N, Mugford ST, Pitino M, Toyota M, Gilroy S, Miller AJ, Hogenhout SA, Sanders D (2017a) Interplay of plasma membrane and vacuolar ion channels, together with BAK1, elicits rapid cytosolic calcium elevations in *Arabidopsis* during aphid feeding. Plant Cell **29:** 1460-1479

Vincent TR, Canham J, Toyota M, Avramova M, Mugford ST, Gilroy S, Miller AJ, Hogenhout S, Sanders D (2017b) Real-time *in vivo* recording of *Arabidopsis* calcium signals during insect feeding using a fluorescent biosensor. J Vis Exp

Vitale A, Galili G (2001) The endomembrane system and the problem of protein sorting. Plant Physiol **125:** 115-118

Waadt R, Krebs M, Kudla J, Schumacher K (2017) Multiparameter imaging of calcium and abscisic acid and high-resolution quantitative calcium measurements using R-GECO1-mTurquoise in *Arabidopsis*. New Phytol **216:** 303-320

Wagner S, Nietzel T, Aller I, Costa A, Fricker MD, Meyer AJ, Schwarzlander M (2015a) Analysis of plant mitochondrial function using fluorescent protein sensors. Methods Mol Biol **1305:** 241-252

Wagner S, Behera S, De Bortoli S, Logan DC, Fuchs P, Carraretto L, Teardo E, Cendron L, Nietzel T, Fussl M, Doccula FG, Navazio L, Fricker MD, Van Aken O, Finkemeier I, Meyer AJ, Szabo I, Costa A, Schwarzlander M (2015b) The EF-hand Ca^{2+} binding protein MICU choreographs mitochondrial Ca^{2+} dynamics in *Arabidopsis*. Plant Cell **27:** 3190-3212

Walter A, Mazars C, Maitrejean M, Hopke J, Ranjeva R, Boland W, Mithofer A (2007) Structural requirements of jasmonates and synthetic analogues as inducers of Ca^{2+} signals in the nucleus and the cytosol of plant cells. Angew Chem Int Ed Engl **46:** 4783-4785

Wang WH, Yi XQ, Han AD, Liu TW, Chen J, Wu FH, Dong XJ, He JX, Pei ZM, Zheng HL (2012) Calcium-sensing receptor regulates stomatal closure through hydrogen peroxide and nitric oxide in response to extracellular calcium in *Arabidopsis*. J Exp Bot **63:** 177-190

Wang WH, He EM, Chen J, Guo Y, Chen J, Liu X, Zheng HL (2016) The reduced state of the plastoquinone pool is required for chloroplast-mediated stomatal closure in response to calcium stimulation. Plant J **86:** 132-144

Wang Y, Kang Y, Ma C, Miao R, Wu C, Long Y, Ge T, Wu Z, Hou X, Zhang J, Qi Z (2017) CNGC2 is a Ca^{2+} influx channel that prevents accumulation of apoplastic Ca^{2+} in the leaf. Plant Physiol **173:** 1342-1354

Weinl S, Held K, Schlucking K, Steinhorst L, Kuhlgert S, Hippler M, Kudla J (2008) A plastid protein crucial for Ca^{2+}-regulated stomatal responses. New Phytol **179:** 675-686

Whalley HJ, Knight MR (2013) Calcium signatures are decoded by plants to give specific gene responses. New Phytol **197:** 690-693

Wheeler GL, Brownlee C (2008) Ca^{2+} signalling in plants and green algae–changing channels. Trends Plant Sci **13:** 506-514

Wu W, Peters J, Berkowitz GA (1991) Surface charge-mediated effects of Mg^{2+} on K^{+} flux across the chloroplast envelope are associated with regulation of stromal pH and photosynthesis. Plant Physiol **97:** 580-587

Wu Z, Liang F, Hong B, Young JC, Sussman MR, Harper JF, Sze H (2002) An endoplasmic reticulum-bound Ca^{2+}/Mn^{2+} pump, ECA1, supports plant growth and confers tolerance to Mn^{2+} stress. Plant Physiol **130:** 128-137

Wurzinger B, Mair A, Pfister B, Teige M (2011) Cross-talk of calcium-dependent protein kinase and MAP kinase signaling. Plant Signal Behav **6:** 8-12

Xiang Y, Lu YH, Song M, Wang Y, Xu W, Wu L, Wang H, Ma Z (2015) Overexpression of a *Triticum aestivum* calreticulin gene (*TaCRT1*) improves salinity tolerance in tobacco. PLoS One **10:** e0140591

Xiong TC, Jauneau A, Ranjeva R, Mazars C (2004) Isolated plant nuclei as mechanical and thermal sensors involved in calcium signalling. Plant J **40:** 12-21

Xiong TC, Bourque S, Lecourieux D, Amelot N, Grat S, Briere C, Mazars C, Pugin A, Ranjeva R (2006) Calcium signaling in plant cell organelles delimited by a double membrane. Biochim Biophys Acta **1763:** 1209-1215

Xiong TC, Coursol S, Grat S, Ranjeva R, Mazars C (2008) Sphingolipid metabolites selectively elicit increases in nuclear calcium concentration in cell suspension cultures and in isolated nuclei of tobacco. Cell Calcium **43:** 29-37

Xiong TC, Ronzier E, Sanchez F, Corratge-Faillie C, Mazars C, Thibaud JB (2014) Imaging long distance propagating calcium signals in intact plant leaves with the BRET-based GFP-aequorin reporter. Front Plant Sci **5:** 43

Xu H, Martinoia E, Szabo I (2015) Organellar channels and transporters. Cell Calcium **58:** 1-10

Yang T, Poovaiah BW (2002) A calmodulin-binding/CGCG box DNA-binding protein family involved in multiple signaling pathways in plants. J Biol Chem **277:** 45049-45058

Zakharov SD, Ewy RG, Dilley RA (1993) Subunit III of the chloroplast ATP-synthase can form a Ca^{2+}-binding site on the lumenal side of the thylakoid membrane. FEBS Lett **336:** 95-99

Zhang B, Carrie C, Ivanova A, Narsai R, Murcha MW, Duncan O, Wang Y, Law SR, Albrecht V, Pogson B, Giraud E, Van Aken O, Whelan J (2012) LETM proteins play a role in the accumulation of mitochondrially encoded proteins in *Arabidopsis thaliana* and AtLETM2 displays parent of origin effects. J Biol Chem **287:** 41757-41773

Zhao X, Xu M, Wei R, Liu Y (2015) Expression of *OsCAS* (calcium-sensing receptor) in an *Arabidopsis* mutant increases drought tolerance. PLoS One **10:** e0131272

Zheng Y, Liao C, Zhao S, Wang C, Guo Y (2017) The glycosyltransferase QUA1 regulates chloroplast-associated calcium signaling during salt and drought stress in *Arabidopsis*. Plant Cell Physiol **58:** 329-341

Zhou L, Lan W, Jiang Y, Fang W, Luan S (2014) A calcium-dependent protein kinase interacts with and activates a calcium channel to regulate pollen tube growth. Mol Plant **7:** 369-376

Zhu SY, Yu XC, Wang XJ, Zhao R, Li Y, Fan RC, Shang Y, Du SY, Wang XF, Wu FQ, Xu YH, Zhang XY, Zhang DP (2007) Two calcium-dependent protein kinases, CPK4 and CPK11, regulate abscisic acid signal transduction in *Arabidopsis*. Plant Cell **19:** 3019-3036

Zhu X, Caplan J, Mamillapalli P, Czymmek K, Dinesh-Kumar SP (2010) Function of endoplasmic reticulum calcium ATPase in innate immunity-mediated programmed cell death. EMBO J **29:** 1007-1018

Zhu X, Taylor A, Zhang S, Zhang D, Feng Y, Liang G, Zhu JK (2014) Measuring spatial and temporal Ca^{2+} signals in *Arabidopsis* plants. J Vis Exp**:** e51945

Zhu JK (2016) Abiotic stress signaling and responses in plants. Cell **167:** 313-324

Zottini M, Zannoni D (1993) The use of fura-2 fluorescence to monitor the movement of free calcium ions into the matrix of plant mitochondria (*Pisum sativum* and *Helianthus tuberosus*). Plant Physiol **102:** 573-578

Zuppini A, Navazio L, Mariani P (2004) Endoplasmic reticulum stress-induced programmed cell death in soybean cells. J Cell Sci **117:** 2591-2598

AIM OF THE WORK

The main goal of my Ph.D. project was the investigation of the relative contribution and potential functional interactions between chloroplasts and the endoplasmic reticulum (ER) in terms of calcium homeostasis and signalling in the plant cell. Ca^{2+} is known to play a crucial role in the transduction of a large plethora of environmental stimuli of both abiotic and biotic nature in all plant lineages. Although the participation of organelles to plant intracellular Ca^{2+} signalling is increasingly emerging, the relative contribution of the different intracellular compartments in shaping Ca^{2+} signatures awaits further investigation. Moreover, detailed information about the pathways mediating Ca^{2+} fluxes across plant intracellular membranes is still scarce. For example, the involvement of the plant ER in Ca^{2+} handling has long been overlooked, because of the lack of direct measurements of [Ca^{2+}] in the lumen of this compartment and Ca^{2+} transporters localized at chloroplast have just started to be identified.

In order to fulfill the proposed tasks, transgenic lines of the model plant *Arabidopsis thaliana* stably expressing the bioluminescent Ca^{2+} reporter aequorin targeted the cytosol, to the chloroplast stroma and to the outer membrane of the chloroplast envelope were used. In addition to these lines, already available in our laboratory, a new toolkit of aequorin-based Ca^{2+} indicators targeted to thylakoids, in particular the thylakoid lumen and the thylakoid membrane, was generated, thus allowing the monitoring of Ca^{2+} dynamics in subchloroplast compartments. Ca^{2+} measurement assays were performed in transgenic seedlings and cell cultures from them derived to get a better understanding of how this Ca^{2+} capacitor-acting organelle is involved in Ca^{2+} storage and signal transduction in the plant cell. The results were published in Plant Physiology in 2018 and are presented in **Chapter 2** of this thesis.

My research activity also focused on the characterization of Ca^{2+}-permeable channels localized at chloroplast membranes, as well as their role in shaping organellar and cytosolic Ca^{2+} signals, in particular a chloroplast homologue of the mitochondrial calcium uniporter (cMCU) and plant glutamate receptor-like

homologues (GLRs). The obtained data suggest a likely involvement for each Ca^{2+}-permeable channel in transducing given stresses in Arabidopsis, thus adding an extra-dimension to specificity in stimulus-response coupling. The results about cMCU were published in Nature Plants in 2019 and are presented in **Chapter 3**. Preliminary results obtained for GLR3.4 and 3.5 are presented in **Chapter 4**.

During my research activity I made wide use of suspension-cultured cells as a simplified experimental system useful to dissect the otherwise complex integration of organelles in the whole cell Ca^{2+} signalling network. A detailed description of the experimental procedures used in our laboratory to set up and maintain *A. thaliana* photosynthetic and heterotrophic cell suspension cultures is the subject of an invited review, currently under revision, in Methods in Molecular Biology and is presented in **Chapter 5**.

Concerning the potential involvement of the ER in the Ca^{2+} signalling network, the design of a specifically targeted aequorin probe allowed for the monitoring of ER Ca^{2+} dynamics in a quantitative and reliable way. Analyses of $[Ca^{2+}]_{ER}$ and its variations during signal transduction events in Arabidopsis demonstrated the occurrence of stimulus-specific $[Ca^{2+}]_{ER}$ elevations in response to environmental stimuli as well as their putative integration with Ca^{2+} signatures evoked in the cytosol and the chloroplast stroma. The results of this research line are the subject of a manuscript in preparation and are presented in **Chapter 6**.

Finally, during my Ph.D. activity I have also participated, as a side project, to a study aimed at the elucidation of the Ca^{2+}-mediated signalling pathway evoked in *Lotus japonicus* in response to a fungal hydrophobin released by antagonistic fungi, used as biocontrol agents and plant biostimulants. Ca^{2+}-dependent upregulation of plant defence-related genes indicated a role of the fungal hydrophobin in priming the plant responses against subsequent pathogen infections. Moreover, the use of pharmacological approaches suggested the occurrence of an ER-mediated Ca^{2+} release into the cytosol during a beneficial plant-fungus interaction. The results were published in

International Journal of Molecular Sciences in 2018 and are presented in **Chapter 7**.

CHAPTER 2

Integration of thylakoids into chloroplast Ca^{2+} storage and signal transduction

PROLOGUE

Chloroplasts and plastids in general are one of the major cellular distinctive features of plants among Eukarya (Jarvis and López-Juez, 2013). In the last few years considerable effort has been spent to unravel how plastids are integrated in the cellular regulatory circuits that coordinate plant development and functions (Rocha and Vothknecht, 2012), since these organelles not only are the site for the photosynthetic process but also host (at least in part) many other fundamental metabolic pathways of the plant cell (Rocha and Vothknecht, 2012) as well as biological processes related to plant defences in response to pathogen attack (Lu and Yao, 2018). It is well-established that calcium plays both regulatory and structural roles in the chloroplast (Rocha and Vothknecht, 2012) and its concentration is finely-tuned to prevent inhibition of photosynthesis as well as the impairment of other chloroplast-localized processes (Stael *et al*., 2012).

Concerning Ca^{2+} dynamics taking place in these organelles, it has long been known that chloroplasts act as calcium capacitors, since they possess a high concentration of this ion (estimates are around 15 mM) most of which, however, is buffered by Ca^{2+}-binding proteins or bound to the negatively charged thylakoid membranes, leaving in ultimate analysis only a small fraction (about 150 nM) as free stromal [Ca^{2+}] eligible for rapid mobilization (Costa *et al*., 2018). Their impact over the whole cell Ca^{2+}-based signalling network – and in particular in shaping cytosolic Ca^{2+} signals – has been recently demonstrated in response to various abiotic stimuli such as salinity, drought, oxidative stress and cold shock, as well as a biotic one, represented by a cell wall-derived elicitor of plant defence responses (Sello *et al*., 2016). Moreover, chloroplasts has also been shown to have the ability to generate their own unique Ca^{2+} signals under peculiar stimulation. Light-to-dark transition (Johnson *et al*., 1995; Sai and Johnson, 2002; Loro *et al*., 2016; Sello *et al*., 2016) as well as heat stress (Lenzoni and Knight, 2019) were shown to trigger chloroplast-specific Ca^{2+} responses, since Ca^{2+} increases are evoked in the chloroplast stroma, but no corresponding Ca^{2+} changes are detected in

the cytosol. The origin of these organelle-autonomous Ca^{2+} signatures is still unclear (Loro *et al.*, 2016).

The research work described in this chapter was performed to analyze the involvement of thylakoids, the chloroplast-specific internal membrane system, in terms of Ca^{2+} handling and signalling within chloroplasts and plant cells. The analysis of thylakoid Ca^{2+} dynamics was addressed by engineering two new aequorin-based Ca^{2+} sensors targeted to the thylakoid lumen (TL-YA) and the stromal surface of the thylakoid membrane (TM-YA). This was achieved by fusing the cDNA for YFP-aequorin to nucleotide sequences encoding domains of organellar proteins known to reside in the two different chloroplast locations (the thylakoid lumen protein (TLP18.3) and the state transition kinase 7 (STN7), respectively). The transformation of Arabidopsis seedlings was carried via the floral dip method (Clough and Bent, 1998) and photosynthetic cell suspension cultures were subsequently set up from the obtained transgenic lines. Both the TL-YA and TM-YA lines showed unaltered phenotype, chloroplast ultrastructure and photosynthetic activity compared to the wild-type. RT-PCR and immunoblot analyses confirmed aequorin expression in both the Arabidopsis transgenic lines. The subcellular localization of the YFP-aequorin chimeras was then checked by confocal microscopy analyses of seedling leaves, together with immunogold labelling with an anti-aequorin antibody and biochemical analyses carried out on isolated thylakoids using the proteolytic enzyme thermolysin, hence revealing the correct targeting of the aequorin chimeras. Ca^{2+} assays were performed in these lines, along with a stroma-targeted aequorin one, by using both entire seedlings and photosynthetic cell cultures: this latter approach was pursued in order to avoid the detection of Ca^{2+} signals stemming from the stroma of non-green plastids that do not contain thylakoids (*i.e.* root amyloplasts). The intra-chloroplast Ca^{2+} fluxes detected were found to be characterized by specific dynamics and to be triggered in response to some abiotic stimuli (such as an oxidative and salt stress), whereas a biotic one (oligogalacturonides, pectic fragments of the plant cell wall released during pathogen attack) was found to evoke a response only in the chloroplast stroma of cell cultures, possibly due to an amplification of the signal in homogeneous cell populations. The

temporal comparison of the Ca^{2+} traces recorded in the three subcloroplast compartments (*i.e.* stroma, thylakoid membrane and lumen) indicated that, at least in some cases, the thylakoid lumen may be involved in the dissipation of Ca^{2+} gradients across the thylakoid membrane, thereby shaping stromal Ca^{2+} signals.

The effect of light-to-dark transition on chloroplast Ca^{2+} dynamics was also evaluated, since the lights-off stimulus is known to trigger a transient increase in stromal Ca^{2+} that is intimately linked with the regulation of some enzymes of the Calvin-Benson-Bassham cycle. No detectable Ca^{2+} changes were measured in either the bulk cytosol or at the outer envelope level, suggesting that the cytosol does not participate in the generation of the stromal Ca^{2+} change. On the contrary, the thylakoid lumen – and to a minor extent also the thylakoid membrane microdomain – both showed a gradual increase in Ca^{2+} that was found to be abolished by the administration of nigericin, a ionophore able to dissipate the thylakoid proton gradient, thus pointing to a likely involvement in this Ca^{2+} uptake of a Ca^{2+}/H^{+} antiporter (Wang *et al.*, 2016; Frank *et al.*, 2019).

My contribution to this work, which was initiated by a previous Ph.D. student (Simone Sello) in the laboratory, mainly consisted in aequorin-based Ca^{2+} measurement assays carried out in plants *in toto* and suspension-cultured cells. Moreover, I carried out the pharmacological approach to the analysis of the origin of dark-induced Ca^{2+} fluxes.

Taken together, the data collected in this work clearly demonstrate that thylakoids have an active role in the modulation of chloroplast Ca^{2+} responses upon perception of environmental stimuli. The newly developed thylakoid-targeted aequorin-based Ca^{2+} reporters may represent a useful tool to carry out further studies about the role of chloroplast Ca^{2+} signals in thylakoid-specific processes (Finazzi *et al.*, 2015; Hochmal *et al.*, 2015), as well in the modulation of intracellular Ca^{2+} signalling networks. This novel toolkit of subchloroplast Ca^{2+} reporters improves the current understanding of Ca^{2+} homeostasis and signal transduction in chloroplasts and provides new insights into plant organellar Ca^{2+} signalling.

REFERENCES

Clough SJ, Bent AF (1998) Floral dip: a simplified method for *Agrobacterium*-mediated transformation of *Arabidopsis thaliana*. Plant J **16:** 735-743

Costa A, Navazio L, Szabo I (2018) The contribution of organelles to plant intracellular Calcium signalling. J Exp Bot **69:** 4175-4193

Finazzi G, Petroutsos D, Tomizioli M, Flori S, Sautron E, Villanova V, Rolland N, Seigneurin-Berny D (2015) Ions channels/transporters and chloroplast regulation. Cell Calcium **58:** 86-97

Frank J, Happeck R, Meier B, Hoang MTT, Stribny J, Hause G, Ding H, Morsomme P, Baginsky S, Peiter E (2019) Chloroplast-localized BICAT proteins shape stromal calcium signals and are required for efficient photosynthesis. New Phytol **221:** 866-880

Hochmal AK, Schulze S, Trompelt K, Hippler M (2015) Calcium-dependent regulation of photosynthesis. Biochim Biophys Acta **1847:** 993-1003

Jarvis P, Lopez-Juez E (2013) Biogenesis and homeostasis of chloroplasts and other plastids. Nat Rev Mol Cell Biol **14:** 787-802

Johnson CH, Knight MR, Kondo T, Masson P, Sedbrook J, Haley A, Trewavas A (1995) Circadian oscillations of cytosolic and chloroplastic free calcium in plants. Science **269:** 1863-1865

Lenzoni G, Knight MR (2019) Increases in absolute temperature stimulate free calcium concentration elevations in the chloroplast. Plant Cell Physiol **60:** 538-548

Loro G, Wagner S, Doccula FG, Behera S, Weinl S, Kudla J, Schwarzlander M, Costa A, Zottini M (2016) Chloroplast-specific in vivo Ca^{2+} imaging using yellow Cameleon fluorescent protein sensors reveals organelle-autonomous Ca^{2+} signatures in the stroma. Plant Physiol **171:** 2317-2330

Lu Y, Yao J (2018) Chloroplasts at the crossroad of photosynthesis, pathogen infection and plant defense. Int J Mol Sci **19:** 3900

Rocha AG, Vothknecht UC (2012) The role of calcium in chloroplasts–an intriguing and unresolved puzzle. Protoplasma **249:** 957-966

Sai J, Johnson CH (2002) Dark-stimulated calcium ion fluxes in the chloroplast stroma and cytosol. Plant Cell **14:** 1279-1291

Sello S, Perotto J, Carraretto L, Szabo I, Vothknecht UC, Navazio L (2016) Dissecting stimulus-specific Ca^{2+} signals in amyloplasts and chloroplasts of *Arabidopsis thaliana* cell suspension cultures. J Exp Bot **67:** 3965-3974

Stael S, Wurzinger B, Mair A, Mehlmer N, Vothknecht UC, Teige M (2012) Plant organellar calcium signalling: an emerging field. J Exp Bot **63:** 1525-1542

Wang C, Xu W, Jin H, Zhang T, Lai J, Zhou X, Zhang S, Liu S, Duan X, Wang H, Peng C, Yang C (2016) A putative chloroplast-localized Ca^{2+}/H^{+} antiporter CCHA1 is involved in calcium and pH homeostasis and required for PSII function in *Arabidopsis*. Mol Plant **9:** 1183-1196

This work was published as:

Chloroplast Ca^{2+} Fluxes into and across Thylakoids Revealed by Thylakoid-Targeted Aequorin Probes

Simone Sello[1], Roberto Moscatiello[1], Norbert Mehlmer[2], Manuela Leonardelli[1,2], Luca Carraretto[1], Enrico Cortese[1], Filippo G. Zanella[1], Barbara Baldan[1,3], Ildikò Szabò[1,3], Ute C. Vothknecht[2,4], and Lorella Navazio[1,3]

[1]Department of Biology, University of Padova, 35131 Padova, Italy

[2]Department of Biology I, Faculty of Biology, LMU Munich, D-82152 Munich, Germany

[3]Botanical Garden, University of Padova, 35123 Padova, Italy

[4]Plant Cell Biology, Institute of Cellular and Molecular Botany, University of Bonn, Kirschallee 1, D-53115 Bonn, Germany

in Plant Physiology, May 2018, vol. 177, issue 1, pages 38-51.

Chloroplast Ca^{2+} Fluxes into and across Thylakoids Revealed by Thylakoid-Targeted Aequorin Probes[1]

Simone Sello,[a,2] Roberto Moscatiello,[a,2] Norbert Mehlmer,[b,3] Manuela Leonardelli,[a,b,4] Luca Carraretto,[a] Enrico Cortese,[a] Filippo G. Zanella,[a] Barbara Baldan,[a,c] Ildikò Szabò,[a,c] Ute C. Vothknecht,[b,d,5] and Lorella Navazio[a,c,5]

[a]Department of Biology, University of Padova, 35131 Padova, Italy
[b]Department of Biology I, Faculty of Biology, LMU Munich, D-82152 Munich, Germany
[c]Botanical Garden, University of Padova, 35123 Padova, Italy
[d]Plant Cell Biology, Institute of Cellular and Molecular Botany, University of Bonn, Kirschallee 1, D-53115 Bonn, Germany

ORCID IDs: 0000-0001-5335-6295 (S.S.); 0000-0003-4829-5744 (R.M.); 0000-0002-6854-4341 (N.M.); 0000-0001-6215-1478 (M.L.); 0000-0002-3307-8774 (L.C.); 0000-0001-8242-6803 (E.C.); 0000-0003-1240-5147 (F.G.Z.); 0000-0002-5564-1214 (B.B.); 0000-0002-3637-3947 (I.S.); 0000-0002-8930-0127 (U.C.V.); 0000-0001-5640-108X (L.N.).

Chloroplasts require a fine-tuned control of their internal Ca^{2+} concentration, which is crucial for many aspects of photosynthesis and for other chloroplast-localized processes. Increasing evidence suggests that calcium regulation within chloroplasts also may influence Ca^{2+} signaling pathways in the cytosol. To investigate the involvement of thylakoids in Ca^{2+} homeostasis and in the modulation of chloroplast Ca^{2+} signals in vivo, we targeted the bioluminescent Ca^{2+} reporter aequorin as a YFP fusion to the lumen and the stromal surface of thylakoids in Arabidopsis (*Arabidopsis thaliana*). Thylakoid localization of aequorin-based probes in stably transformed lines was confirmed by confocal microscopy, immunogold labeling, and biochemical analyses. In resting conditions in the dark, free Ca^{2+} levels in the thylakoid lumen were maintained at about 0.5 μM, which was a 3- to 5-fold higher concentration than in the stroma. Monitoring of chloroplast Ca^{2+} dynamics in different intrachloroplast subcompartments (stroma, thylakoid membrane, and thylakoid lumen) revealed the occurrence of stimulus-specific Ca^{2+} signals, characterized by unique kinetic parameters. Oxidative and salt stresses initiated pronounced free Ca^{2+} changes in the thylakoid lumen. Localized Ca^{2+} increases also were observed on the thylakoid membrane surface, mirroring transient Ca^{2+} changes observed for the bulk stroma, but with specific Ca^{2+} dynamics. Moreover, evidence was obtained for dark-stimulated intrathylakoid Ca^{2+} changes, suggesting a new scenario for light-to-dark-induced Ca^{2+} fluxes inside chloroplasts. Hence, thylakoid-targeted aequorin reporters can provide new insights into chloroplast Ca^{2+} storage and signal transduction. These probes represent novel tools with which to investigate the role of thylakoids in Ca^{2+} signaling networks within chloroplasts and plant cells.

Intracellular calcium signaling is universal among eukaryotes, mediating a wide range of physiological processes. Plant Ca^{2+} homeostasis and signaling reflect both structures and organelles unique to the plant cell as well as differences in the growth and development of plants compared with eukaryotes that lack plastids. In plants, Ca^{2+} is involved in environmental sensing, and a wide variety of abiotic and biotic stimuli (such as osmotic stress, oxidative stress, and pathogen attack) can induce transient changes in intracellular free Ca^{2+} concentration ($[Ca^{2+}]$) with unique spatiotemporal patterns, thus enabling specific stimulus-response coupling (Dodd et al., 2010). Several intracellular compartments of the plant cell participate in Ca^{2+} homeostasis, including the vacuole, endoplasmic reticulum, mitochondria, and plastids. However, the mobilization of Ca^{2+} from the different organelles and their potential interplay in plant Ca^{2+} signaling networks are still under investigation (Stael et al., 2012).

The vacuole is the main intracellular Ca^{2+} reservoir in plant cells, in terms of both function and volume, with a prominent role in overall ion homeostasis in mature cells. It is a major intracellular stimulus-releasable Ca^{2+} store in the signal transduction pathways triggered by cold shock (Knight et al., 1996) as well as drought and salinity (Knight et al., 1997). The vacuolar cation channel TPC1 (Peiter et al., 2005), the structure of which was reported recently (Guo et al., 2016; Kintzer and Stroud, 2016), was shown to be involved in mediating systemic Ca^{2+} signaling upon salt stress (Choi et al., 2014), wounding, and herbivory (Kiep et al., 2015) and in the generation of highly localized cytosolic Ca^{2+} elevations during aphid feeding (Vincent et al., 2017).

Chloroplasts also have been shown to participate in Ca^{2+} homeostasis and signaling. Numerous studies indicate that chloroplasts require a fine-tuned control of the organellar Ca^{2+} concentration. It is known that free Ca^{2+} modulates crucial aspects of photosynthesis, including the assembly and function of PSII, the regulation of stromal enzymes of the Calvin cycle, as well as other plastid-localized processes such as the import of nucleus-encoded proteins and organelle division (Rocha and Vothknecht, 2012; Nomura and Shiina, 2014; Hochmal et al., 2015). However, little is known about the mechanisms that underlie the generation and dissipation of Ca^{2+} transients and the

transduction of environmental signals within plastids or their localization inside the organelle.

To better understand how chloroplasts are integrated into the plant Ca^{2+} signaling network, specific high-resolution tools are required to monitor and quantify plastid Ca^{2+} dynamics. In early studies, the bioluminescent Ca^{2+} reporter aequorin was targeted to the chloroplast stroma, highlighting the induction of stromal Ca^{2+} fluxes upon light-to-dark transition (Johnson et al., 1995; Sai and Johnson, 2002). Studies on the thylakoid-localized Ca^{2+}-sensing receptor CAS showed that chloroplasts modulate intracellular Ca^{2+} signals by controlling external Ca^{2+}-induced cytosolic Ca^{2+} transients during stomatal closure (Nomura et al., 2008; Weinl et al., 2008). Stromal Ca^{2+} signals also have been implicated in the activation of plant immunity (Nomura et al., 2012; Stael et al., 2015). Constructs encoding YFP-aequorin chimeras targeted to the stroma as well as outer and inner membranes of the chloroplast envelope are available to investigate Ca^{2+} dynamics in these compartments (Mehlmer et al., 2012). Plastid-targeted aequorin probes also were used recently to determine differential stimulus-specific Ca^{2+} responses between amyloplasts and chloroplasts (Sello et al., 2016). However, information about free Ca^{2+} levels and their changes during signal transduction on thylakoid membranes and inside the thylakoid lumen is lacking.

Here, we present the targeting of YFP-fused aequorin probes to the thylakoid lumen and the stromal surface of the thylakoid membrane. Arabidopsis (*Arabidopsis thaliana*) lines stably expressing these aequorin chimeras were used in Ca^{2+} measurement assays in response to different abiotic and biotic stimuli, revealing the occurrence of stimulus-specific thylakoid Ca^{2+} signals. This novel toolkit of thylakoid-targeted Ca^{2+} reporters advances the current understanding of Ca^{2+} regulation in chloroplasts and paves the way for future investigations on plant organellar Ca^{2+} signaling.

RESULTS

Generation of Arabidopsis Transgenic Lines Stably Expressing YFP-Aequorin Chimeras Targeted to Thylakoids

To monitor Ca^{2+} dynamics in Arabidopsis thylakoids, we expressed YFP-aequorin (YA) chimeras targeted to the thylakoid lumen (TL-YA) and the stromal surface of the thylakoid membrane (TM-YA). YA was fused to the first 92 amino acids of the thylakoid lumen protein TLP18.3 (Sirpiö et al., 2007; Wu et al., 2011) to obtain TL-YA and to the N-terminal transmembrane domain of the thylakoid protein kinase STN7 to obtain TM-YA (Supplemental Table S1). In the latter, the transmembrane domain anchors the protein in an orientation that exposes the C-terminal tag to the stroma (Bellafiore et al., 2005; Tikkanen et al., 2012). Aequorin expression was confirmed with reverse transcription (RT)-PCR and immunoblot analyses on transgenic Arabidopsis plants expressing these constructs under the control of the UBI10 promoter (Fig. 1). Aequorin activity was measured in the T2 generation by screening five independent TL-YA and TM-YA sublines for aequorin-based total luminescence. In vivo discharge gave positive results for all sublines, with luminescence levels ranging from 10^5 to 2×10^6 counts per seedling. The established thylakoid-targeted aequorin sensor lines (T3 generation) did not exhibit any significant difference in either phenotype or photosynthetic activity when compared with wild-type plants. Moreover, the ultrastructural organization of chloroplasts was well preserved (Fig. 2).

Subcellular Localization of YA Fusion Proteins

Confocal microscopy observations of leaves from the TL-YA and TM-YA lines showed that the fluorescent signal of YFP overlapped perfectly with the red chlorophyll fluorescence of mesophyll cells, indicating that the recombinant proteins indeed reside inside chloroplasts (Fig. 3A). Fluorescence was not detected in roots, except a faint signal in the external cell layers. This was likely due to the light exposure of roots growing on the surface of the agar-containing medium for confocal microscopy experiments (Supplemental Fig. S1A). Conversely, roots of dark-grown seedlings from both TL-YA and TM-YA lines exhibited no fluorescence (Supplemental Fig. S1B).

TEM after immunogold labeling with an anti-aequorin antibody showed the presence of electron-dense gold particles on thylakoids in both the TL-YA

[1] This work was supported by Progetti di Ricerca di Ateneo (prot. CPDA127210) and Dotazione Ordinaria della Ricerca Dipartimentale 2016-2017 to L.N., the EU within the Marie-Curie ITN CALIPSO (FP7) (project no. 607607) to U.C.V., and the Human Frontier Science Program (HFSP0052) to I.S.

[2] These authors contributed equally to the article.

[3] Current address: Department of Chemistry, Technische Universität München, Lichtenberg Strasse 4, 85748 Garching bei Muenchen, Germany.

[4] Current address: Department of Ecogenomics and Systems Biology, University of Vienna, Althanstrasse 14, A-1090 Vienna, Austria.

[5] Address correspondence to vothknecht@uni-bonn.de or lorella.navazio@unipd.it.

The author responsible for distribution of materials integral to the findings presented in this article in accordance with the policy described in the Instructions for Authors (www.plantphysiol.org) is: Ute C. Vothknecht (vothknecht@uni-bonn.de).

S.S., R.M., E.C., and F.G.Z. carried out Ca^{2+} measurement assays; N.M. and M.L. designed the expression plasmids and performed Arabidopsis transformation; L.C. performed confocal microscopy and pulse amplitude modulation imaging analyses; R.M. and L.N. carried out data analyses; B.B. and F.G.Z. performed TEM analyses; I.S. contributed to discussion of the results, designed some experiments, and assisted in article editing; U.C.V. and L.N. conceived the research and designed the experiments; S.S., U.C.V., and L.N. wrote the article.

www.plantphysiol.org/cgi/doi/10.1104/pp.18.00027

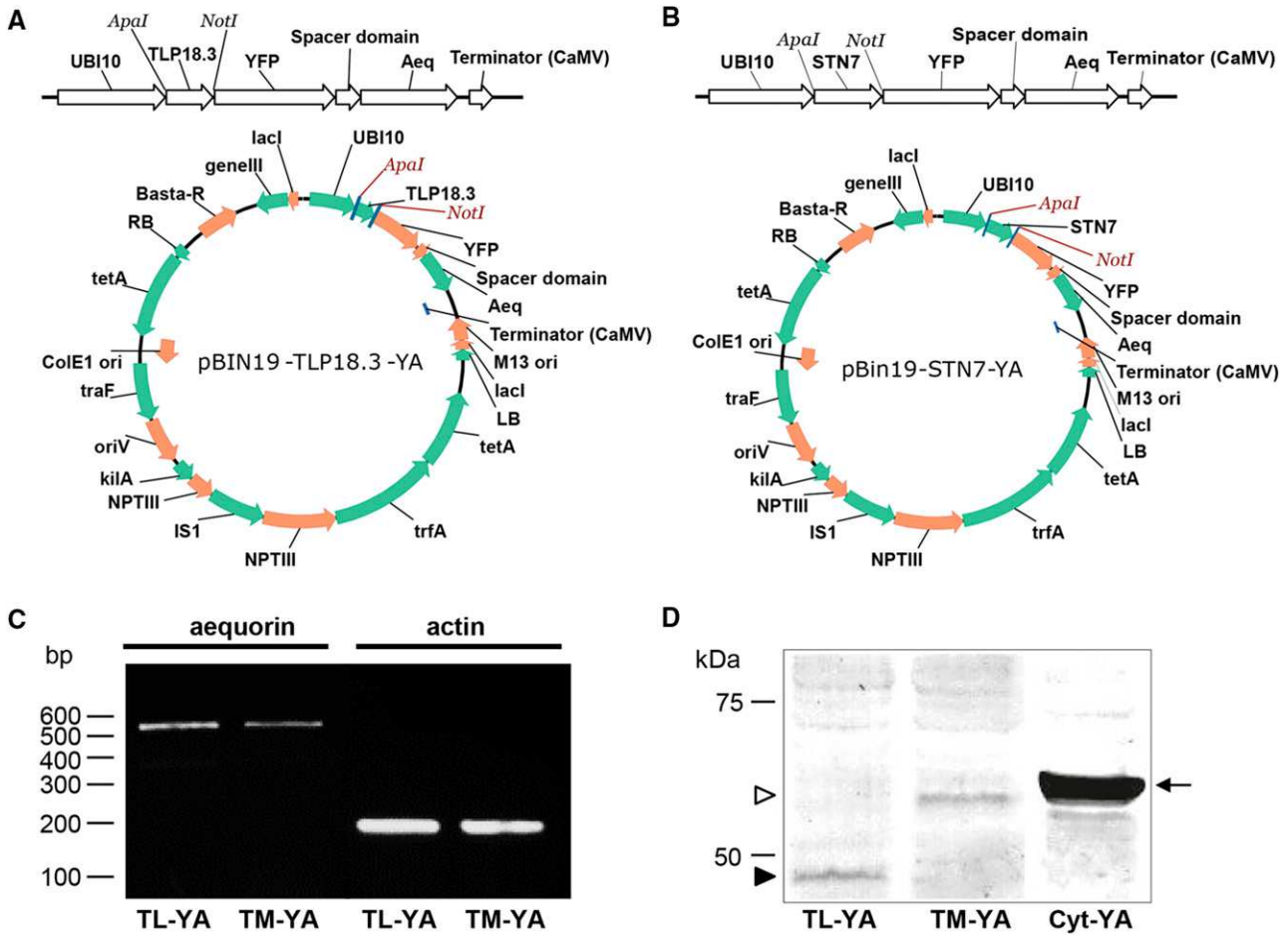

Figure 1. Overview of the cloning strategy for the creation of expression vectors targeting YA to the thylakoid lumen and thylakoid membrane, and analysis of aequorin expression in Arabidopsis transgenic lines. A and B, The targeting sequences for the thylakoid lumen (A) and for the thylakoid membrane (B) were cloned into an expression cassette in front of YA using the restriction enzymes *Apa*I and *Not*I. The complete expression cassettes were transferred subsequently into the binary vector pBIN19 carrying Basta resistance. C and D, Analysis of aequorin expression by RT-PCR (C) and immunoblotting (D) in Arabidopsis transgenic lines stably transformed with the constructs encoding TL-YA and TM-YA. For RT-PCR analyses, actin was used as a housekeeping gene. For immunoblot analyses, total protein extracts (50 μg) were separated by 10% SDS-PAGE, transferred to PVDF, and incubated with an anti-aequorin antibody (diluted 1:10,000). Black and white arrowheads indicate the YA chimeras targeted to the thylakoid lumen and the thylakoid membrane, respectively. The black arrow indicates the YA targeted to the cytosol, excluding the nucleus, in the Arabidopsis line $CPK17_{G2A}$-NES-YA (Cyt-YA), used here as a positive control.

and TM-YA lines (Fig. 3, B and C). The wild-type negative control lacked labeling anywhere in the cell. As a positive control, the Str-YA line (Mehlmer et al., 2012) was used, revealing gold particles in the chloroplast stroma (Fig. 3, B and C). Furthermore, intact thylakoids were isolated from Arabidopsis leaves of the TL-YA and TM-YA transgenic lines, with half of the preparation incubated for 20 min with the proteolytic enzyme thermolysin (0.1 μg μL^{-1}) to remove all proteins exposed on the membrane surface. Immunoblot analyses showed that aequorin targeted to the thylakoid lumen was protected from proteolysis, indicating that the chimeric TL-YA protein resides inside the thylakoid lumen. For the TM-YA line, the signal from chimeric protein targeted to the thylakoid membrane was removed by the proteolytic treatment, indicating its expected exposure on the stromal thylakoid surface (Fig. 3D). Together, these data document the correct subcellular localization and topology of the thylakoid lumen- and thylakoid membrane surface-targeted YA fusion proteins for the subsequent Ca^{2+} signaling study.

Stimulus-Specific Ca^{2+} Signals Are Triggered in the Thylakoid Lumen and at the Thylakoid External Surface by Different Environmental Stimuli

Arabidopsis photosynthetic cell lines expressing the thylakoid-targeted YA probes were established (Supplemental Fig. S2, A–C) by using a recently developed procedure (Sello et al., 2017) and assayed in Ca^{2+} measurement experiments to elucidate potential changes in free [Ca^{2+}] in thylakoids. The Str-YA line also was used for comparison (Sello et al., 2016). In this first

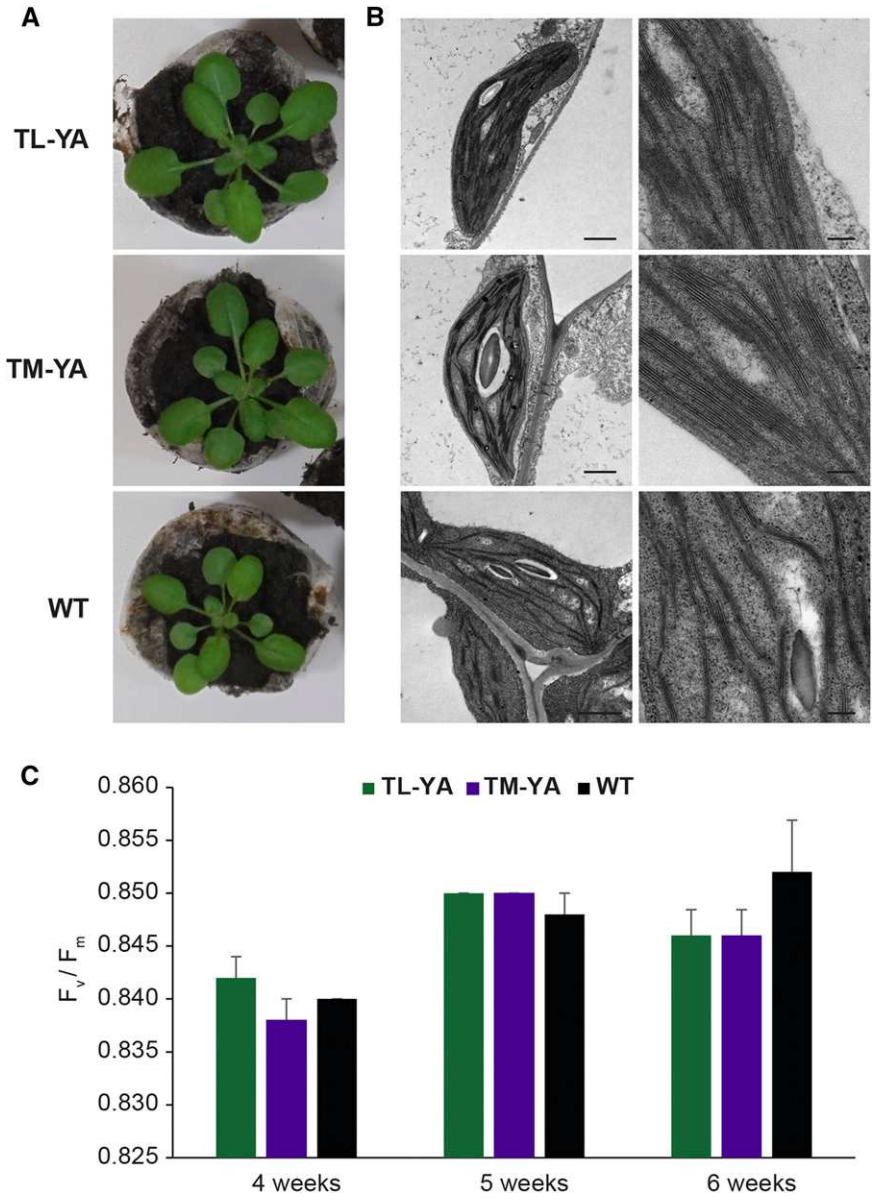

Figure 2. Phenotype, chloroplast ultrastructure, and photosynthetic activity of Arabidopsis transgenic lines stably expressing TL-YA and TM-YA. A, Representative photographs of 4-week-old seedlings of TL-YA, TM-YA, and wild-type (WT) lines. B, Transmission electron microscopy (TEM) observations of chloroplast ultrastructure, showing good preservation of thylakoids. Bars = 1 μm (left column) and 250 nm (right column). C, Pulse amplitude modulation imaging analyses of Arabidopsis seedlings at 4, 5, and 6 weeks. Data are means ± SE of five independent experiments. No significant differences were observed (Student's *t* test).

validation stage, photosynthetic cell suspension cultures were used instead of seedlings to avoid the detection of Ca^{2+} signals originating from the stroma of nongreen plastids that lack thylakoids, such as amyloplasts in roots (Sello et al., 2016). Aequorin protein levels in the TL-YA and TM-YA lines were suitable to perform reliable Ca^{2+} assays, even though these levels were lower than in the Str-YA lines (Supplemental Fig. S2D). This was expected based on the level of aequorin-derived total luminescence observed in Ca^{2+} assays after the discharge step. In resting conditions in the dark, free [Ca^{2+}] in the thylakoid lumen was maintained around 0.5 μM. This concentration is 3- to 5-fold higher than the level recorded in the bulk stroma (~0.1–0.15 μM) as well as in the stromal region just outside the thylakoid membrane (Fig. 4, A–C). Next, suspension-cultured cells were exposed to different environmental cues, which were demonstrated previously to induce both cytosolic and stromal Ca^{2+} signals (Sello et al., 2016). In particular, 10 mM H_2O_2 and 0.3 M NaCl were applied as abiotic stimuli simulating oxidative and salt stress, respectively (Price et al., 1994; Knight et al., 1997; Ranf et al., 2008; Martí et al., 2013; Abdul-Awal et al., 2016). Plus, 20 μg mL^{-1} oligogalacturonides (OGs) with degree of polymerization 10 to 15 were applied as elicitors that mimicked a pathogen attack (Navazio et al., 2002; Moscatiello et al., 2006). These treatment doses did not affect cell viability, as demonstrated by Evans blue-based assays (Supplemental Fig. S3), and touch-control experiments ruled out that the stress application itself caused remarkable changes in [Ca^{2+}] within the chloroplasts (Supplemental Fig. S4).

Oxidative stress triggered a gradual [Ca^{2+}] increase to well over 1.5 μM at the external surface of the thylakoid membrane that followed the trend recorded in the bulk

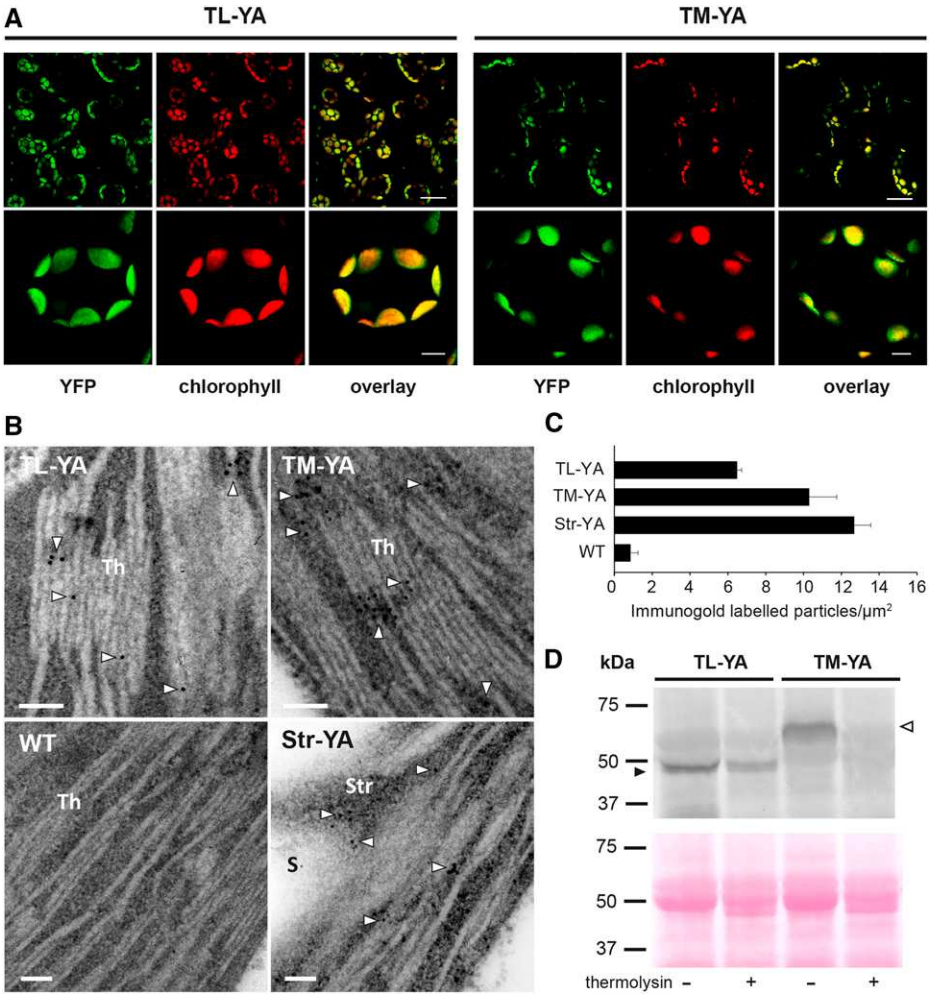

Figure 3. Confocal microscopy analyses, immunogold labeling, and biochemical analyses of Arabidopsis seedlings of the TL-YA and TM-YA lines. A, Fluorescence microscopy images of mesophyll cells of Arabidopsis seedling leaves with a YFP filter and a chlorophyll filter. An overlay of the two channels also is shown. Bars = 25 μm (top row) and 5 μm (bottom row). B, Immunocytochemical analyses of aequorin subcellular localization. The wild-type (WT) line and a line expressing YA in the stroma (Str-YA) were used as negative and positive controls, respectively. White arrowheads indicate gold particles. Bars = 100 nm. S, Starch granule; Str, stroma; Th, thylakoids. C, Quantitative analyses of immunogold-labeled particles. Data are means ± SE of 40 different fields from three biological replicates. D, Immunoblot analyses of isolated thylakoids, incubated in the absence (−) or presence (+) of 0.1 μg μL^{-1} thermolysin, as indicated. Isolated thylakoids corresponding to 50 μg of protein were probed with an anti-aequorin antibody (top gel). Equal loading was confirmed by Ponceau Red staining of the blot membrane (bottom gel). Black and white arrowheads indicate YA chimeras targeted to the thylakoid lumen and the thylakoid membrane, respectively.

stroma, although characterized by a higher magnitude. Ca^{2+} dynamics in the thylakoid lumen started from a higher resting level and quickly reached a plateau at an intermediate level of about 1 μM (Fig. 4, D–F). In the case of salt stress, NaCl triggered a very rapid and transient [Ca^{2+}] increase in all three chloroplast subcompartments. However, distinct differences in the amplitude and shape of the transient could be observed. Notably, a microdomain of high [Ca^{2+}] was found to be transiently established in proximity to the thylakoid membrane surface, whose dissipation temporally coincided with the sustained [Ca^{2+}] increase in the thylakoid lumen (Fig. 4, G–I). These data suggest that the thylakoid lumen may be involved in dissipating Ca^{2+} gradients across the thylakoid membrane and, thus, shaping stromal Ca^{2+} signals. By contrast, OGs induced a transient and relatively small Ca^{2+} change in the bulk stroma and on the thylakoid surface, although characterized by slower dynamics. However, no detectable Ca^{2+} changes were triggered in the thylakoid lumen (Fig. 4, J–L). Altogether, these data strongly indicate that the intrachloroplast [Ca^{2+}] changes measured by the TL-YA and TM-YA lines are specific, stimulus-induced responses.

Aequorin-based Ca^{2+} assays in response to the same stimuli were conducted subsequently in entire seedlings (Fig. 5; Supplemental Fig. S4), reinforcing the involvement of thylakoids in Ca^{2+}-mediated responses to environmental stimuli. Resting Ca^{2+} levels and Ca^{2+} responses to oxidative stress were found to be very similar in seedlings (Fig. 5, A–F) and cultured cells (Fig. 4, A–F). The sustained chloroplast Ca^{2+} changes induced by 10 mM H_2O_2 did not dissipate within 1 h (Supplemental Fig. S5, A–C), indicating a prolonged organellar Ca^{2+} response. However, a direct effect of H_2O_2 on coelenterazine oxidation to coelenteramide independent of aequorin was ruled out by comparing luminescence levels in seedlings of the TL-YA, TM-YA, and Str-YA lines with those in wild-type (nontransformed) seedlings preincubated with coelenterazine (Supplemental Fig. S5, D–F).

For the salt stress treatment, the magnitude of chloroplast [Ca^{2+}] change was found to be higher in entire seedlings (Fig. 5, G–I) than in cultured cells (Fig. 4, G–I), possibly as a consequence of systemic Ca^{2+} signaling in plants in toto (Choi et al., 2014). The different Ca^{2+} dynamics observed in the three intrachloroplast subcompartments suggested a role of thylakoids in

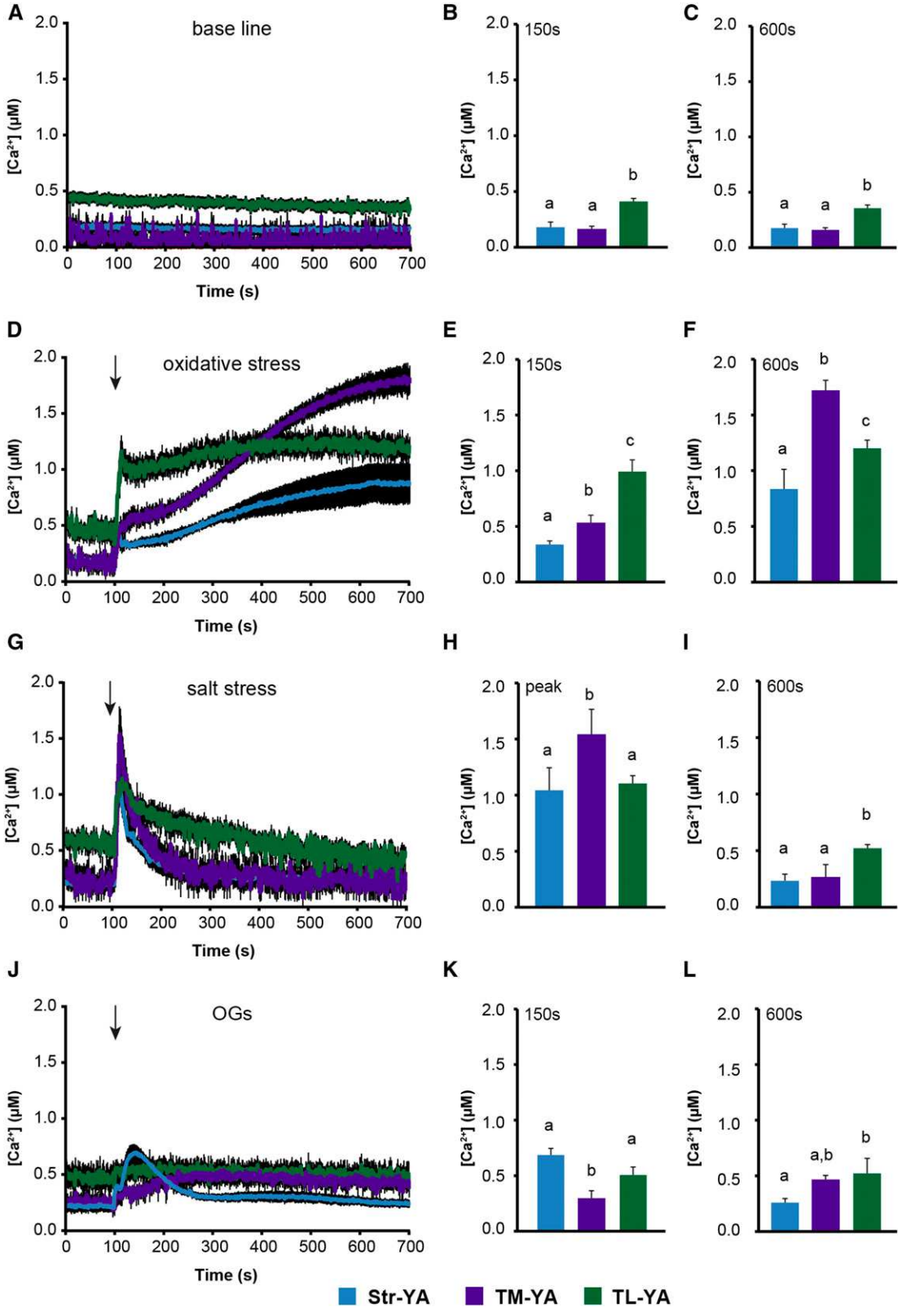

Figure 4. Monitoring of subchloroplast free $[Ca^{2+}]$ in Arabidopsis cell suspension cultures in response to environmental stimuli. Ca^{2+} measurements were conducted in Str-YA (blue traces), TM-YA (violet traces), and TL-YA (green traces) lines. A to C, In resting conditions. D to F, In response to 10 mM H_2O_2. G to I, In response to 0.3 M NaCl. J to L, In response to 20 μg mL^{-1} OGs. In A, D, G, and J, data are presented as means ± SE (black shading) of 15 traces obtained from 15 aliquots of suspension-cultured cells derived from five independent

switching off stromal Ca^{2+} signals (Fig. 5G, inset), as observed previously in cultured cells (Fig. 4G). On the other hand, exposing the seedlings to OG elicitors caused only modest and transient chloroplast Ca^{2+} changes (Fig. 5, J–L). These data indicate that subtle chloroplast Ca^{2+} signals, such as those triggered by OGs, may be amplified in homogenous cell populations (i.e. suspension cell cultures) compared with the in vivo situation, where Ca^{2+} signals may be limited only to a particular tissue or cell type (Moscatiello et al., 2013). These findings demonstrate that the thylakoid lumen- and thylakoid membrane surface-targeted Ca^{2+} probes can effectively monitor Ca^{2+} changes elicited by specific stimuli in the respective chloroplast subcompartments.

Unique Ca^{2+} Dynamics in the Thylakoid Lumen Are Induced by the Transition from Light to Dark

Light is one of the most important factors for plant growth and development. Therefore, Arabidopsis lines stably expressing the thylakoid-targeted bioluminescent Ca^{2+} reporter were used to evaluate the effect of light-to-dark transition on chloroplast Ca^{2+} dynamics. In this set of experiments, whole seedlings were used (instead of plant cell suspension cultures), since previous studies had shown a transient stromal Ca^{2+} signal increase in response to the light-to-dark transition in chloroplasts but not in amyloplasts (Sello et al., 2016). Hence, the presence of roots should not affect the readout. Moreover, analyses of the organism in toto may more closely mimic the actual in vivo situation, especially if the overall Ca^{2+}-mediated response entails systemic integration (Gilroy et al., 2014). In agreement with previous reports (Nomura et al., 2012), the lights-off stimulus was found to trigger a transient $[Ca^{2+}]$ increase in the stroma, which peaked at about 0.35 μM after 15 min and slowly decayed to the basal level within 3 h (Fig. 6A). Concurrently in the thylakoid lumen, $[Ca^{2+}]$ was found to increase gradually from a basal level of about 0.25 μM to about 0.45 μM (Fig. 6B). The Ca^{2+} trace recorded at the thylakoid membrane exposed to the stroma differed from the Ca^{2+} dynamics recorded in the whole stroma, being characterized by a gradual, moderate Ca^{2+} increase; this suggests that the stromal Ca^{2+} increase likely occurred in microdomain(s) far from the thylakoid surface (Fig. 6C). In addition to Str-YA, TL-YA, and TM-YA, Ca^{2+} measurement assays in response to light-to-dark transition were performed in previously established Arabidopsis lines with aequorin localized in the cytosol (Cyt-YA) and on the cytosolic surface of the outer membrane of the plastid envelope (OE-YA; Mehlmer et al., 2012). Lights-off-induced Ca^{2+} transients were not observed in the cytosol or at the cytosolic surface of the plastid envelope (Fig. 6, D and E), confirming that the cytosol does not seem to be involved in Ca^{2+} changes in response to light-to-dark transition, as suggested previously (Nomura et al., 2012). Control measurements of luminescence values in either aequorin-expressing lines that were not reconstituted with coelenterazine or wild-type (nontransformed) seedlings incubated with coelenterazine (Supplemental Fig. S6) suggested that the initial decrease of $[Ca^{2+}]$ commonly observed upon light-to-dark transition (Fig. 6) is actually due to chlorophyll fluorescence emission.

Ca^{2+} assays in seedlings that had been exposed to 6 h of light and then moved rapidly to darkness confirmed that $[Ca^{2+}]$ is maintained around 0.2 μM in the thylakoid lumen during the light phase and that the lights-off stimulus induces a gradual increase in thylakoid $[Ca^{2+}]$ (Supplemental Fig. S7A). Moreover, at the end of the dark transition, lumen $[Ca^{2+}]$ persisted at high levels (~0.5 μM), and this concentration remained unchanged when plants were kept in the dark at the beginning of the following day (Supplemental Fig. S7B). The high level of Ca^{2+} recorded in the thylakoid lumen at the end of light-to-dark experiments (Fig. 6B; Supplemental Fig. S7) corresponded to the thylakoid luminal $[Ca^{2+}]$ detected in resting conditions in the dark (Figs. 4A and 5A).

To test if the activity of a putative H^+/Ca^{2+} antiporter localized at the thylakoid membrane could be involved in the dark-induced Ca^{2+} fluxes into the thylakoid lumen, Arabidopsis seedlings were pretreated with 5 μM nigericin (an H^+/K^+ ionophore able to dissipate ΔpH without affecting the $\Delta\psi$ component of the proton motive force). Upon disruption of the H^+ gradient across the thylakoid membrane, the gradual increase of luminal $[Ca^{2+}]$ was abolished, suggesting that the slow dark-induced Ca^{2+} uptake into the thylakoid lumen requires a pH gradient across the membrane (Supplemental Fig. S8, A–C). Notably, in the presence of nigericin, a rapid and transient Ca^{2+} rise was recorded in the lumen, peaking at about 1 μM after ~3 min and dissipating promptly within 30 min (Supplemental Fig. S8, A–C). A luminal Ca^{2+} increase was observed at a smaller amplitude when nigericin was added 45 min after the onset of darkness, when the relaxation of the Ca^{2+} signal in the stroma had already begun (Supplemental Fig. S8A, inset). The transient $[Ca^{2+}]$ increase, activated in response to dark in the bulk stroma, displayed a higher amplitude in the presence of 5 μM nigericin and maintained a higher steady-state level at the end of light-to-dark experiments without falling to the basal level observed in control conditions (Supplemental Fig. S8, D–F). A similar Ca^{2+} signature, although characterized by a slightly higher and delayed

Figure 4. (*Continued.*)
growth replicates. Arrows indicate the time of stimulation (100 s). B, C, E, F, H, I, K, and L show statistical analyses of Ca^{2+} levels recorded in the different transgenic lines at two different time points: after 150 s (B, E, and K) and 600 s (C, F, I, and L). In H, the maximum $[Ca^{2+}]$ (at the peak) is reported. Bars labeled with different letters differ significantly ($P < 0.05$, Student's *t* test).

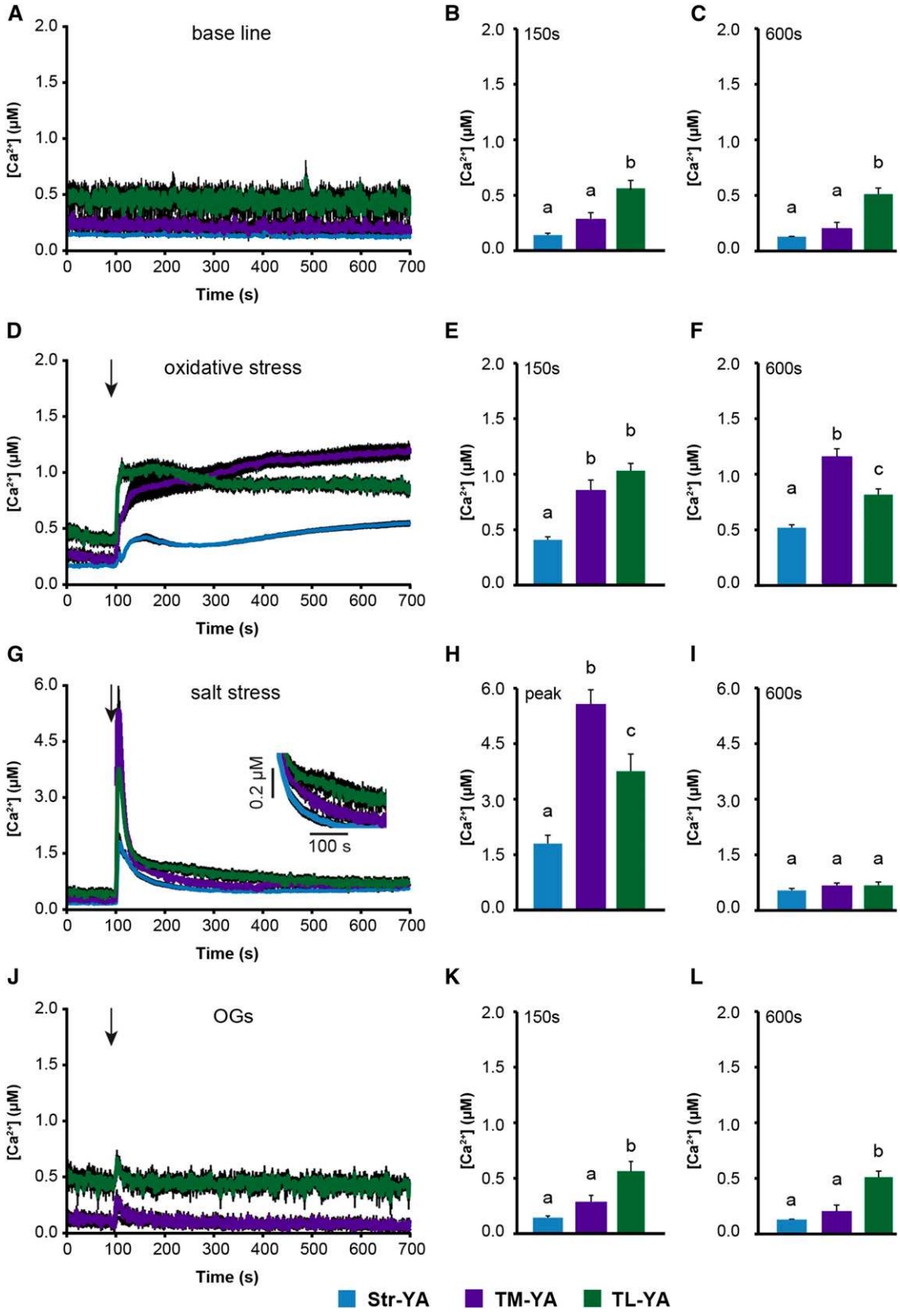

Figure 5. Monitoring of subchloroplast free [Ca^{2+}] in Arabidopsis seedlings in response to environmental stimuli. Ca^{2+} measurements were conducted in Str-YA (blue traces), TM-YA (violet traces), and TL-YA (green traces) lines. A to C, In resting conditions. D to F, In response to 10 mM H_2O_2. G to I, In response to 0.3 M NaCl. J to L, In response to 20 μg mL^{-1} OGs. In A, D, G, and

Ca^{2+} peak, was observed at the stromal surface of the thylakoid membrane (Supplemental Fig. S8, G–I). These data suggest that the rise in dark-induced stromal Ca^{2+} may be amplified as a consequence of the inhibition of Ca^{2+} uptake in the thylakoid lumen, indirectly triggered by the proton-translocating uncoupler nigericin.

DISCUSSION

The participation of chloroplasts, and plastids in general, in the cellular Ca^{2+} response and their ability to generate their own Ca^{2+} transients have long been debated. Previous studies of chloroplast Ca^{2+} dynamics provided information only on stromal [Ca^{2+}] (Johnson et al., 1995; Sai and Johnson, 2002; Manzoor et al., 2012; Nomura et al., 2012; Loro et al., 2016; Sello et al., 2016; Stephan et al., 2016). A novel set of YA chimeras were targeted recently to the outer and inner surfaces of the chloroplast envelope membranes as well as the stroma (Mehlmer et al., 2012). However, information on thylakoid lumen [Ca^{2+}] was lacking.

In this work, TL-YA and TM-YA chimeras were engineered, and Arabidopsis lines stably transformed with the above constructs were generated for in vivo Ca^{2+} measurements. The thylakoid lumen and outer thylakoid surface localizations of TL-YA and TM-YA were confirmed by laser scanning confocal microscopy, plus immunocytochemical and biochemical analyses. Since aequorin is largely insensitive to pH (Brini, 2008), it was used as a reliable probe to monitor thylakoid lumen [Ca^{2+}], where the pH can drop to 5.5 (Szabó et al., 2005). Its bioluminescent properties, high signal-to-noise ratio, and lack of damaging excitation light permit Ca^{2+} measurement in chlorophyll-containing tissues for long time intervals, an advantage over fluorescent Ca^{2+} reporters (Martí et al., 2013; Xiong et al., 2014).

Monitoring of [Ca^{2+}] in transgenic Arabidopsis lines resulted in [Ca^{2+}] values measured just outside the thylakoid surface and within the thylakoid lumen. Thylakoid-targeted aequorin revealed that lumen Ca^{2+} levels in the dark are 3- to 5-fold higher than in the stroma. Oxidative and salt stresses triggered chloroplast Ca^{2+} signals in both the chloroplast stroma and inside the thylakoid lumen, characterized by specific kinetic parameters. On the other hand, exposure to OGs elicited a moderate Ca^{2+} increase only in the stroma and only when suspension-cultured cells were used (i.e. homogenous cell populations), compared with entire seedlings. Because the basal [Ca^{2+}] in the thylakoid lumen in the dark is high, it is possible that the extent of the transient stromal [Ca^{2+}] increase was not sufficient to induce elevated [Ca^{2+}] in the lumen, potentially mediated by passive Ca^{2+} transporters located at the thylakoid membrane. Further work will be required to clarify whether the thylakoid lumen may have a role in Ca^{2+} responses to other biotic stresses.

The proteins mediating Ca^{2+} flux into and out of the thylakoid lumen are not known. Although a Ca^{2+}-permeable ion channel was detected in the thylakoid membrane by patch clamp (Enz et al., 1993) and compelling evidence for the presence of Ca^{2+}/H^+ exchange activity has been provided (Ettinger et al., 1999), genes encoding these proteins are still unidentified (Carraretto et al., 2016). A putative chloroplast-localized Ca^{2+}/H^+ antiporter was identified recently in Arabidopsis (Wang et al., 2016). The same protein has been proposed to function instead as a transporter for Mn^{2+} and to be located in the thylakoid membrane (Schneider et al., 2016).

The effect of light on chloroplast [Ca^{2+}] is known to encompass a lights-off stimulus that induces a slow, long-lasting [Ca^{2+}] increase in the stroma (Sai and Johnson, 2002; Nomura et al., 2012). This dark-induced Ca^{2+} transient also was observed in our stroma-targeted aequorin line. The lack of any detectable [Ca^{2+}] variation in either the bulk cytosol or the cytosolic microdomain close to the chloroplast envelope is consistent with earlier reports indicating that the cytosol does not participate in the generation of the stromal [Ca^{2+}] change in response to light-to-dark transition (Nomura et al., 2012). However, [Ca^{2+}] measured in the thylakoid lumen revealed unexpected Ca^{2+} dynamics in response to darkness. In particular, the light-to-dark transition induced a long-lasting and sustained [Ca^{2+}] increase in the thylakoid lumen. After 16 h of light, thylakoid lumen [Ca^{2+}] was maintained at about 0.25 μM (a slightly higher concentration than in the stroma). After lights off, [Ca^{2+}] in the thylakoid lumen showed a progressive increase to about 0.5 μM after 3 h of darkness. This high [Ca^{2+}] remained unchanged during the night and correlates well with the dark resting level observed in both autotrophic cell cultures and seedlings. Due to the lack of any detectable [Ca^{2+}] changes either in the cytosol or on the chloroplast surface, the dark-induced intrachloroplast Ca^{2+} fluxes likely originate from inside the organelle. Since the lights-off stimulus was found to induce increases of [Ca^{2+}] in both stroma and thylakoid lumen, a possibility for the origin of these Ca^{2+} fluxes is the release of the ion from thylakoid membrane proteins. Since there was a lack of evident high-[Ca^{2+}] microdomains close to the thylakoid

Figure 5. (*Continued.*)
J, data are presented as means ± SE (black shading) of 15 traces obtained from 15 different plants derived from five independent growth replicates. Arrows indicate the time of stimulation (100 s). In the inset in G, a magnification of the region between 150 and 400 s is shown. B, C, E, F, H, I, K, and L show statistical analyses of Ca^{2+} levels recorded after 150 s (B, E, and K), after 600 s (C, F, I, and L), and at the peak (H). Bars labeled with different letters differ significantly ($P < 0.05$, Student's *t* test).

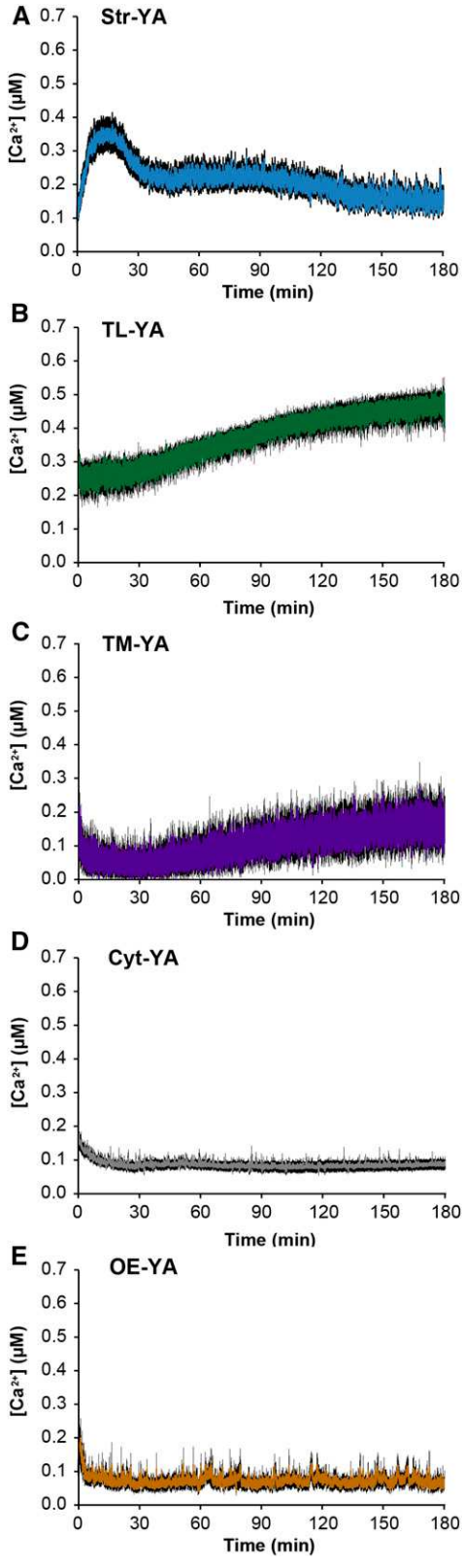

Figure 6. Measurement of Ca^{2+} fluxes in response to light-to-dark transition. Ca^{2+} assays were conducted in Arabidopsis seedlings stably expressing YA chimeras in different subcellular locations: stroma (A; blue trace), thylakoid lumen (B; green trace), thylakoid membrane (C; violet trace), cytosol (D; gray trace), and cytosolic surface of the plastid outer envelope (E; brown trace). Data are presented as means ± SE (black shading) of 15 traces obtained from 15 different plants derived from five independent growth replicates. In all graphs, the lights-off stimulus starts at time 0.

membrane, the involvement of soluble Ca^{2+}-binding/buffering proteins potentially located in the chloroplast stroma cannot be ruled out. At later time points, the $[Ca^{2+}]$ peak in the stroma seemed to dissipate by the continuous Ca^{2+} uptake into the thylakoid lumen. This was responsible for the generation of the high intraluminal $[Ca^{2+}]$ established progressively during the dark phase. The finding that transient stromal Ca^{2+} signals in response to light-to-dark transition occurred only in chloroplasts (but not in nongreen plastids of Arabidopsis cell cultures [Sello et al., 2016], as confirmed recently by in vivo Ca^{2+} imaging based on stroma-targeted cameleon [Loro et al., 2016]) is consistent with our current data suggesting a modulation of the lights-off-induced stromal Ca^{2+} transient by thylakoids.

As mentioned above, nigericin was reported to dissipate ΔpH without affecting the $\Delta\psi$ component of the proton motive force in higher plants (Joliot and Johnson, 2011). Abolishment of the dark-induced Ca^{2+} uptake into the thylakoid lumen observed after nigericin addition suggests that the ΔpH built up during illumination is necessary for the dark-phase return of stromal Ca^{2+} to the lumen. In the presence of nigericin, a sustained increase in thylakoid luminal Ca^{2+} was not observed. Instead, stromal Ca^{2+} was significantly higher over prolonged time scales. The presence of a residual ΔpH maintained across the thylakoid membrane in the dark (Bailleul et al., 2015) may provide a driving force for the uptake of Ca^{2+} into the lumen via a Ca^{2+}/H^{+} antiporter suggested previously to be localized at thylakoid membranes (Ettinger et al., 1999). Interestingly, in the presence of nigericin during the light phase (30 min before the shift to dark), aequorin-based Ca^{2+} measurements revealed an immediate, fast, and unexpected Ca^{2+} increase in the thylakoid lumen upon transition to dark, which then dissipated just as quickly. These rapid changes may be mediated by still unidentified channel proteins that would allow the flux of calcium ions according to the actual electrochemical gradient, depending on both the concentration gradient for Ca^{2+} and the membrane potential. One hypothesis is that indirect inhibition of a Ca^{2+}/H^{+} exchange activity might cause a transient microdomain of high $[Ca^{2+}]$ just outside the thylakoid membrane, leading to a rapid and transient opening of a still unidentified Ca^{2+}-permeable thylakoid channel. This is supported by the nigericin experiments conducted with the TM-YA line. However, the identities of Ca^{2+}-permeable channels/transporters in the plastid envelope and thylakoid membranes remain unknown (Pottosin and Dobrovinskaya, 2015; Xu et al., 2015; Carraretto et al., 2016). Unless the molecules

responsible for intraplastidial Ca^{2+} transport and their ion specificity are clarified, only a tentative interpretation of these results can be provided. Moreover, we cannot exclude that nigericin also may affect H^+ gradients across the inner envelope membrane (Checchetto et al., 2016), thus participating in the observed increase in stromal [Ca^{2+}] upon addition of the K^+/H^+ ionophore. Furthermore, proton gradients in additional intracellular membranes (such as the inner membrane of mitochondria and the tonoplast) could be affected by nigericin, and these changes might a priori contribute indirectly to the observed intrachloroplast Ca^{2+} transients. In summary, the determination of the exact role of transmembrane pH gradients in the regulation of chloroplast Ca^{2+} fluxes requires further exploration. Unfortunately, neither aequorin (a bioluminescent probe) nor cameleon (a fluorescent probe) can be used for direct [Ca^{2+}] measurements under white light conditions, such that the luminal [Ca^{2+}] response to lights-on stimuli cannot be easily measured.

In conclusion, the new toolkit of aequorin reporters targeted to thylakoids has provided estimates of the thylakoid luminal [Ca^{2+}] and has shown that thylakoids have an active role in the modulation of chloroplast Ca^{2+} responses to environmental cues. The involvement of chloroplasts in switching off stromal Ca^{2+} signals, such as those triggered by salt stress, may be essential to quickly restore low basal stromal [Ca^{2+}] after a Ca^{2+} signaling event that traverses into the organelle from the cytosol without prolonging the transient in that compartment via a back flux. For the light-to-dark transition, thylakoids may play a key role in shaping the stroma-located transient Ca^{2+} increase. This latter change in stromal [Ca^{2+}] has been suggested to regulate the activity of some Calvin cycle enzymes, resulting in a further inhibition of CO_2 fixation during the night (Sai and Johnson, 2002; Johnson et al., 2006) in addition to that provided by the well-studied, light-driven thioredoxin system.

Thylakoid-targeted aequorin probes provide new tools to analyze the role of thylakoid Ca^{2+} signals in modulating the many processes specific to the thylakoid lumen (for review, see e.g. Finazzi et al., 2015; Hochmal et al., 2015). This toolkit should initiate the identification and elucidation of the functions of protein(s) that may mediate Ca^{2+} fluxes across thylakoids (e.g. the $Ca^{2+}[Mn^{2+}]/H^+$ transporter) under different light and stress conditions.

MATERIALS AND METHODS

Molecular Cloning and Construction of Expression Plasmids

The nucleotide sequences encoding the first 92 amino acids of TLP18.3 (At1G54780.1) and the first 137 amino acids (including the transmembrane domain) of the thylakoid protein kinase STN7 (At1G68830) were used as targeting sequences for the thylakoid lumen and the stromal surface of the thylakoid membrane, respectively. These were cloned into vectors carrying the coding sequence for YA to create expression cassettes driven by the UBI10 promoter (Supplemental Table S1). Afterward, expression cassettes were cloned into pBIN19 vectors carrying Basta resistance via the *Apa*I and *Not*I restriction sites as described previously (Mehlmer et al., 2012), creating the final constructs pBIN19-TLP18.3-YA and pBIN19-STN7-YA (Fig. 1). For cloning of TLP18.3, the primers 5′-AATAACCATGGAGACCCTTCTCTCCCCTCG-3′ and 5′-ATTATTAGCGGCCGCCATCGTTGAGGATATTGAAC-3′ were used. For cloning of STN7, the primers 5′-TTATAAGGGCCCATGGCTACAATATCTCCGGG-3′ and 5′-TAATTATGCGGCCGCTCCCAACAACAAAATCATCC-3′ were used.

Generation of Transgenic Arabidopsis Lines

Arabidopsis (*Arabidopsis thaliana*) ecotype Columbia plants were transformed with the floral dip method (Clough and Bent, 1998) with the constructs pBIN19-TLP18.3-YA and pBIN19-STN7-YA to generate lines called TL-YA and TM-YA, respectively. Primary T1 transformants were identified by Basta (0.25%, w/v) spraying on soil. Successful transformation and expression of the constructs were confirmed by the analysis of YFP fluorescence. Selected plants were transferred into single pots, and the T2 generation was assayed for aequorin expression and activity.

Analysis of Aequorin Expression

RT-PCR analyses were carried out using Arabidopsis leaves from 1-month-old Basta-resistant plants. Total RNA was extracted using the RNeasy Plant Mini Kit (Qiagen) and reverse transcribed with SuperScript III (Thermo Fisher Scientific) according to the manufacturer's instructions. Primers designed on the cDNA sequence of aequorin (forward, 5′-TCGACAACCCAAGATGGATTGGA-3′; reverse, 5′-TGATAGCATGCGAATTCATCAGTGTTTTAT-3′) were used to analyze aequorin gene expression. The coding sequence of actin was used as a control (forward, 5′-GGTTGCACCGCCAGAGAGAAAATAC-3′; reverse, 5′-AACAAACTCACCACCACGAACCAGA-3′). Immunoblot analyses were carried out on total protein extracts obtained from leaves of 1-month-old Arabidopsis plants as described previously (Zonin et al., 2011). Aequorin fusion proteins were decorated with a polyclonal anti-aequorin antibody (Abcam) diluted 1:10,000. An Arabidopsis line stably expressing aequorin in the cytosol ($CPK17_{G2A}$-NES-YA; Mehlmer et al., 2012) was used as a positive control.

Analysis of Aequorin Activity

For the initial screening of the T2 generation of Arabidopsis TL-YA and TM-YA lines, luminescence levels were monitored in planta with a custom-built luminometer (Electron Tubes) containing a 9893/350A photomultiplier (Thorn EMI). Arabidopsis seeds were surface sterilized for 60 s in a 70% (v/v) ethanol and 0.05% (v/v) Triton X-100 solution, 60 s in 100% (v/v) ethanol, and then dried on an autoclaved Whatman paper disc for at least 10 min. Seeds were subsequently plated on one-half-strength Murashige and Skoog (MS) medium (Duchefa Biochemie) containing 0.8% (w/v) plant agar supplemented with 1.5% (w/v) Suc and 50 μM Basta. After 48 h of stratification in darkness at 4°C, MS plates were incubated in a growth chamber at 21°C with a 16-h/8-h light/dark cycle. Five 11- to 14-d-old seedlings from all sublines were reconstituted overnight with 5 μM coelenterazine (Prolume) and kept in the dark. The next day, seedlings were placed singly in the luminometer chamber containing 300 μL of water, and total aequorin was discharged by injection of an equal volume of the discharge solution (30% [v/v] ethanol and 1 M $CaCl_2$). Total luminescence values from every plant line were pooled, and the average luminescence was calculated. All subsequent analyses were carried out in the T3 generation.

Setup of Autotrophic Cell Suspension Cultures from the Transformed Arabidopsis Lines

Arabidopsis seeds (T3 generation) from the TL-YA and TM-YA sublines that revealed the highest aequorin activity were used to establish photosynthetic cell cultures, as described recently (Sello et al., 2017). Briefly, surface-sterilized seeds were plated on MS medium containing 3% (w/v) Suc, 0.8% (w/v) agar, pH 5.5, 0.5 μg mL^{-1} 2,4-dichlorophenoxyacetic acid, 0.25 μg mL^{-1} 6-benzylaminopurine, and 50 μM Basta. After exactly 3 weeks, well-developed green calli formed at the hypocotyl. Those showing the highest YFP fluorescence were separated from roots and cotyledons, cut in small pieces with a sterilized scalpel, and transferred into liquid MS medium containing 2% (w/v) Suc with the same concentrations of phytohormones and herbicide as described above. Cell suspension cultures were maintained at 24°C with a 16-h/8-h light/dark cycle under an illumination rate of 110 μmol photons m^{-2} s^{-1} on a rotary shaker at 80 rpm. They were subcultured every week by transferring 1 packed

cell volume of cell culture in 20 mL of fresh medium containing decreasing Suc concentration (up to 0.5%, w/v) to stimulate photosynthetic activity (Hampp et al., 2012). The expression of thylakoid-targeted aequorin in the cell cultures was confirmed by western-blot analyses of total protein extracts from mid-exponential phase cultured cells. Densitometric analysis was carried out using Quantity One software (Bio-Rad). Aequorin protein levels were normalized against calreticulin (by using an anti-spinach calreticulin antibody diluted 1:2,000; Navazio et al., 1995) and compared with a cell line stably expressing aequorin in the stroma (Sello et al., 2016).

Fluorescence and Confocal Microscopy Analyses

Developing calli were observed with a Leica MZ16F fluorescence stereomicroscope equipped with a GFP filter (excitation at 450/490 nm and emission at 500/550 nm) and a chlorophyll filter (excitation at 460/500 nm and emission above 605 nm). Images were acquired with a Leica DFC480 digital camera using the Leica Application Suite software. Arabidopsis seedlings (14-d-old) grown either under a 16-h-light/8-h-dark cycle or in the dark (etiolated seedlings) in vertical square petri dishes (100 × 100 × 20 mm) and suspension-cultured cells (4-d-old) were observed with a Leica TCS SP5 II confocal laser scanning system mounted on a Leica DMI6000 inverted microscope. Excitation with the argon laser was carried out at 488 nm, and the emitted fluorescence was detected at 505 to 530 nm for YFP and at 680 to 720 nm for chlorophyll.

Pulse Amplitude Modulation Analyses

Arabidopsis seedlings and exponentially growing cell suspension cultures were placed in a Closed FluorCam 800 MF (Photon Systems Instruments), and the photosynthetic activity was measured as F_v/F_m (where F_v is the difference between the maximal [F_m] and the basal [F_0] fluorescence of chlorophyll). Chlorophyll fluorescence images were recorded using a CCD camera, and data analysis was conducted using the FluorCam 7 software (Photon Systems Instruments).

Immunocytochemistry and TEM Analyses

Leaf fragments from 2-week-old Arabidopsis plants were fixed overnight at 4°C in 4% (v/v) paraformaldehyde and 0.5% (v/v) glutaraldehyde in 0.1 M cacodylate buffer, pH 7. After three washes in cacodylate buffer, dehydration in a graded ethanol series was performed. Samples were then embedded progressively in medium-grade London Resin White (PolySciences). Ultrathin sections (500 Å) were obtained on a Reichert-Jung ultramicrotome and mounted on uncoated nickel grids. For immunogold labeling, grids were incubated for 45 min in 0.1% (v/v) Tween 20, 1% (w/v) BSA in TBS, and then for 1 h with rabbit anti-aequorin antibody at a 1:1,000 dilution. After three washes with 0.1% (v/v) Tween 20 in TBS, samples were incubated for 1 h with an anti-rabbit secondary antibody conjugated with colloidal gold particles of 10 nm diameter (Sigma-Aldrich) diluted 1:100. After two washes as above and one wash in distilled water, samples were exposed to osmium tetroxide vapors overnight. After extensive washing with distilled water, samples were counterstained with uranyl acetate and lead citrate and observed using a Tecnai 12-BT transmission electron microscope (FEI) operating at 120 kV and equipped with a Tietz camera. Arabidopsis wild-type plants and plants stably expressing aequorin in the chloroplast stroma (Mehlmer et al., 2012) were used as negative and positive controls, respectively. TEM analyses of chloroplast ultrastructure were carried out as described by Zuppini et al. (2004).

Chloroplast Isolation and Thermolysin Treatment

Chloroplasts were isolated from leaves of 1-month-old Arabidopsis plants using the procedure described by Aronsson and Jarvis (2011). Chloroplasts were resuspended in wash buffer (0.3 M sorbitol, 50 mM HEPES/KOH, 3 mM $MgCl_2$, and 1 mM $CaCl_2$, pH 7.6), vigorously diluted with 10 volumes of osmotic shock buffer (50 mM HEPES/KOH, 3 mM $MgCl_2$, and 1 mM $CaCl_2$, pH 7.6), and then centrifuged at 48,000*g* for 10 min at 4°C to isolate thylakoids. The thylakoid-containing pellet was then resuspended in wash buffer. Treatment with the proteolytic enzyme thermolysin was carried out as described by Mehlmer et al. (2012). Briefly, the thylakoid suspension (50 μg of protein) was incubated with 0.1 $\mu g\ \mu L^{-1}$ thermolysin (Sigma-Aldrich) for 20 min on ice, and the reaction was stopped by the addition of 5 mM EDTA. Immunoblot analyses were conducted as described above.

Aequorin-Based Ca^{2+} Measurement Assays

For Ca^{2+} measurement assays in the Arabidopsis cell lines stably expressing aequorin targeted to the thylakoid system, exponentially growing (4-d-old) autotrophic cell suspension cultures were reconstituted overnight with 5 μM coelenterazine. On the following day, after extensive washing, 50 μL of cells was placed in the luminometer chamber and exposed to different environmental stimuli, as described by Sello et al. (2016). Oxidative stress (10 mM H_2O_2), salt stress (0.3 M NaCl), and pathogen attack (20 $\mu g\ mL^{-1}$ OGs with degree of polymerization from 10 to 15; Moscatiello et al., 2006) were simulated by injection into the cell suspension culture of an equal volume of a 2-fold-concentrated stimulant dissolved in plant cell culture medium. Touch controls were performed by injecting an equal volume of plant cell culture medium. Ca^{2+} dynamics were recorded for a total of 700 s before the injection of 100 μL of the discharge solution (30% v/v ethanol and 1 M $CaCl_2$). The light signal was collected and converted offline into Ca^{2+} concentration values using a computer algorithm based on the Ca^{2+} response curve of aequorin (Brini et al., 1995). In parallel experiments, an Arabidopsis autotrophic cell line stably expressing aequorin in the chloroplast stroma (Sello et al., 2016) was used. Cell viability was determined, after 1 h of treatment with the above stimuli, by the Evans blue method (Baker and Mock, 1994).

To perform Ca^{2+} measurements in aequorin-expressing seedlings in toto, seeds (T3 generation) were surface sterilized and sown on agarized (0.8% [w/v] plant agar) one-half-strength MS medium supplemented with 1.5% (w/v) Suc to germinate under a 16-h/8-h light/dark cycle at 21°C. After overnight reconstitution with 5 μM coelenterazine, 7- to 14-d-old seedlings were exposed to the same stimuli used for the in vitro cell cultures, as described above. For the monitoring of Ca^{2+} dynamics in response to light-to-dark transition, Arabidopsis lines stably expressing aequorin targeted to the cytosol and outer surface of the plastid envelope (Mehlmer et al., 2012) also were used. At the beginning of the dark phase, reconstituted seedlings were quickly transferred into the luminometer chamber containing 300 μL of water, and Ca^{2+} dynamics were monitored for a total of 3 h. In some experiments, seedlings were pretreated with 5 μM nigericin (Sigma-Aldrich) for 30 min before the end of the light phase or for 45 min after the onset of darkness. The final concentration of ethanol was 0.1% (v/v).

Accession Numbers

Sequence data from this article can be found in the GenBank/EMBL data libraries under the following accession numbers: NP_564667 (Arabidopsis TLP18.3, At1G54780.1), NP_564946 (Arabidopsis STN7, At1G68830), NP_565954 (Arabidopsis NTRC, At2G41680), NP_190810 (Arabidopsis OEP7, At3G52420) and NP_196779 (Arabidopsis CPK17, At5G12180).

Supplemental Data

The following supplemental materials are available.

Supplemental Figure S1. Confocal microscopy analyses of roots of Arabidopsis seedlings of the TL-YA and TM-YA lines.

Supplemental Figure S2. Setup of Arabidopsis photosynthetic cell suspension cultures from the TL-YA and TM-YA lines.

Supplemental Figure S3. Effect of the treatment with different stimuli on Arabidopsis cell viability.

Supplemental Figure S4. Monitoring of subchloroplast free [Ca^{2+}] in Arabidopsis transgenic lines in response to touch.

Supplemental Figure S5. Monitoring of subchloroplast free [Ca^{2+}] in Arabidopsis transgenic lines in response to oxidative stress over 1 h, and comparison of luminescence levels in aequorin-expressing seedlings versus wild-type seedlings.

Supplemental Figure S6. Control measurements of luminescence levels upon light-to-dark transition in Arabidopsis seedlings.

Supplemental Figure S7. Monitoring of thylakoid luminal [Ca^{2+}] in Arabidopsis seedlings that were transferred to the luminometer chamber after 6 h of dark or at the end of the dark phase.

Supplemental Figure S8. Effect of the H^+-translocating uncoupler nigericin on dark-induced Ca^{2+} dynamics in the thylakoid lumen, stroma, and stromal surface of thylakoids.

Supplemental Table S1. Amino acid and corresponding nucleotide sequences used for the targeting of the YA fusion proteins to the thylakoid lumen and thylakoid membrane.

ACKNOWLEDGMENTS

We thank M. Brini (University of Padova, Italy) for fruitful discussion on aequorin-based measurements of organellar Ca^{2+} dynamics and W. Martin (University of Düsseldorf, Germany) for critical comments on an earlier version of the article. We also thank the Electron Microscopy Service of the Department of Biology, University of Padova, for skillful technical assistance.

Received January 9, 2018; accepted March 5, 2018; published March 20, 2018.

LITERATURE CITED

Abdul-Awal SM, Hotta CT, Davey MP, Dodd AN, Smith AG, Webb AA (2016) NO-mediated $[Ca^{2+}]_{cyt}$ increases depend on ADP-ribosyl cyclase activity in Arabidopsis. Plant Physiol **171:** 623–631

Aronsson H, Jarvis RP (2011) Rapid isolation of Arabidopsis chloroplasts and their use for in vitro protein import assays. Methods Mol Biol **774:** 281–305

Bailleul B, Berne N, Murik O, Petroutsos D, Prihoda J, Tanaka A, Villanova V, Bligny R, Flori S, Falconet D, et al (2015) Energetic coupling between plastids and mitochondria drives CO_2 assimilation in diatoms. Nature **524:** 366–369

Baker CJ, Mock NM (1994) An improved method for monitoring cell death in cell suspension and leaf disk assays using Evans blue. Plant Cell Tissue Organ Cult **39:** 7–12

Bellafiore S, Barneche F, Peltier G, Rochaix JD (2005) State transitions and light adaptation require chloroplast thylakoid protein kinase STN7. Nature **433:** 892–895

Brini M (2008) Calcium-sensitive photoproteins. Methods **46:** 160–166

Brini M, Marsault R, Bastianutto C, Alvarez J, Pozzan T, Rizzuto R (1995) Transfected aequorin in the measurement of cytosolic Ca^{2+} concentration ($[Ca^{2+}]c$): a critical evaluation. J Biol Chem **270:** 9896–9903

Carraretto L, Teardo E, Checchetto V, Finazzi G, Uozumi N, Szabo I (2016) Ion channels in plant bioenergetic organelles, chloroplasts and mitochondria: from molecular identification to function. Mol Plant **9:** 371–395

Checchetto V, Teardo E, Carraretto L, Leanza L, Szabo I (2016) Physiology of intracellular potassium channels: a unifying role as mediators of counterion fluxes? Biochim Biophys Acta **1857:** 1258–1266

Choi WG, Toyota M, Kim SH, Hilleary R, Gilroy S (2014) Salt stress-induced Ca^{2+} waves are associated with rapid, long-distance root-to-shoot signaling in plants. Proc Natl Acad Sci USA **111:** 6497–6502

Clough SJ, Bent AF (1998) Floral dip: a simplified method for *Agrobacterium*-mediated transformation of *Arabidopsis thaliana*. Plant J **16:** 735–743

Dodd AN, Kudla J, Sanders D (2010) The language of calcium signaling. Annu Rev Plant Biol **61:** 593–620

Enz C, Steinkamp T, Wagner R (1993) Ion channels in the thylakoid membrane (a patch-clamp study). Biochim Biophys Acta **1143:** 67–76

Ettinger WF, Clear AM, Fanning KJ, Peck ML (1999) Identification of a Ca^{2+}/H^{+} antiport in the plant chloroplast thylakoid membrane. Plant Physiol **119:** 1379–1386

Finazzi G, Petroutsos D, Tomizioli M, Flori S, Sautron E, Villanova V, Rolland N, Seigneurin-Berny D (2015) Ions channels/transporters and chloroplast regulation. Cell Calcium **58:** 86–97

Gilroy S, Suzuki N, Miller G, Choi WG, Toyota M, Devireddy AR, Mittler R (2014) A tidal wave of signals: calcium and ROS at the forefront of rapid systemic signaling. Trends Plant Sci **19:** 623–630

Guo J, Zeng W, Chen Q, Lee C, Chen L, Yang Y, Cang C, Ren D, Jiang Y (2016) Structure of the voltage-gated two-pore channel TPC1 from *Arabidopsis thaliana*. Nature **531:** 196–201

Hampp C, Richter A, Osorio S, Zellnig G, Sinha AK, Jammer A, Fernie AR, Grimm B, Roitsch T (2012) Establishment of a photoautotrophic cell suspension culture of *Arabidopsis thaliana* for photosynthetic, metabolic, and signaling studies. Mol Plant **5:** 524–527

Hochmal AK, Schulze S, Trompelt K, Hippler M (2015) Calcium-dependent regulation of photosynthesis. Biochim Biophys Acta **1847:** 993–1003

Johnson CH, Knight MR, Kondo T, Masson P, Sedbrook J, Haley A, Trewavas A (1995) Circadian oscillations of cytosolic and chloroplastic free calcium in plants. Science **269:** 1863–1865

Johnson CH, Shingles R, Ettinger W (2006) Regulation and role of calcium fluxes in the chloroplast. *In* RR Wise, JK Hoober, eds, The Structure and Function of Plastids. Springer, Dordrecht, The Netherlands, pp 403–416

Joliot P, Johnson GN (2011) Regulation of cyclic and linear electron flow in higher plants. Proc Natl Acad Sci USA **108:** 13317–13322

Kiep V, Vadassery J, Lattke J, Maaß JP, Boland W, Peiter E, Mithöfer A (2015) Systemic cytosolic Ca^{2+} elevation is activated upon wounding and herbivory in *Arabidopsis*. New Phytol **207:** 996–1004

Kintzer AF, Stroud RM (2016) Structure, inhibition and regulation of two-pore channel TPC1 from *Arabidopsis thaliana*. Nature **531:** 258–262

Knight H, Trewavas AJ, Knight MR (1996) Cold calcium signaling in *Arabidopsis* involves two cellular pools and a change in calcium signature after acclimation. Plant Cell **8:** 489–503

Knight H, Trewavas AJ, Knight MR (1997) Calcium signalling in *Arabidopsis thaliana* responding to drought and salinity. Plant J **12:** 1067–1078

Loro G, Wagner S, Doccula FG, Behera S, Weinl S, Kudla J, Schwarzländer M, Costa A, Zottini M (2016) Chloroplast-specific in vivo Ca^{2+} imaging using Yellow Cameleon fluorescent protein sensors reveals organelle-autonomous Ca^{2+} signatures in the stroma. Plant Physiol **171:** 2317–2330

Manzoor H, Chiltz A, Madani S, Vatsa P, Schoefs B, Pugin A, Garcia-Brugger A (2012) Calcium signatures and signaling in cytosol and organelles of tobacco cells induced by plant defense elicitors. Cell Calcium **51:** 434–444

Martí MC, Stancombe MA, Webb AAR (2013) Cell- and stimulus type-specific intracellular free Ca^{2+} signals in Arabidopsis. Plant Physiol **163:** 625–634

Mehlmer N, Parvin N, Hurst CH, Knight MR, Teige M, Vothknecht UC (2012) A toolset of aequorin expression vectors for in planta studies of subcellular calcium concentrations in *Arabidopsis thaliana*. J Exp Bot **63:** 1751–1761

Moscatiello R, Baldan B, Navazio L (2013) Plant cell suspension cultures. Methods Mol Biol **953:** 77–93

Moscatiello R, Mariani P, Sanders D, Maathuis FJM (2006) Transcriptional analysis of calcium-dependent and calcium-independent signalling pathways induced by oligogalacturonides. J Exp Bot **57:** 2847–2865

Navazio L, Baldan B, Dainese P, James P, Damiani E, Margreth A, Mariani P (1995) Evidence that spinach leaves express calreticulin but not calsequestrin. Plant Physiol **109:** 983–990

Navazio L, Moscatiello R, Bellincampi D, Baldan B, Meggio F, Brini M, Bowler C, Mariani P (2002) The role of calcium in oligogalacturonide-activated signalling in soybean cells. Planta **215:** 596–605

Nomura H, Komori T, Kobori M, Nakahira Y, Shiina T (2008) Evidence for chloroplast control of external Ca^{2+}-induced cytosolic Ca^{2+} transients and stomatal closure. Plant J **53:** 988–998

Nomura H, Komori T, Uemura S, Kanda Y, Shimotani K, Nakai K, Furuichi T, Takebayashi K, Sugimoto T, Sano S, et al (2012) Chloroplast-mediated activation of plant immune signalling in *Arabidopsis*. Nat Commun **3:** 926

Nomura H, Shiina T (2014) Calcium signaling in plant endosymbiotic organelles: mechanism and role in physiology. Mol Plant **7:** 1094–1104

Peiter E, Maathuis FJM, Mills LN, Knight H, Pelloux J, Hetherington AM, Sanders D (2005) The vacuolar Ca^{2+}-activated channel TPC1 regulates germination and stomatal movement. Nature **434:** 404–408

Pottosin I, Dobrovinskaya O (2015) Ion channels in native chloroplast membranes: challenges and potential for direct patch-clamp studies. Front Physiol **6:** 396

Price AH, Taylor A, Ripley SJ, Griffiths A, Trewavas AJ, Knight MR (1994) Oxidative signals in tobacco increase cytosolic calcium. Plant Cell **6:** 1301–1310

Ranf S, Wünnenberg P, Lee J, Becker D, Dunkel M, Hedrich R, Scheel D, Dietrich P (2008) Loss of the vacuolar cation channel, AtTPC1, does not impair Ca^{2+} signals induced by abiotic and biotic stresses. Plant J **53:** 287–299

Rocha AG, Vothknecht UC (2012) The role of calcium in chloroplasts: an intriguing and unresolved puzzle. Protoplasma **249:** 957–966

Sai J, Johnson CH (2002) Dark-stimulated calcium ion fluxes in the chloroplast stroma and cytosol. Plant Cell **14:** 1279–1291

Schneider A, Steinberger I, Herdean A, Gandini C, Eisenhut M, Kurz S, Morper A, Hoecker N, Rühle T, Labs M, et al (2016) The evolutionarily conserved protein PHOTOSYNTHESIS AFFECTED MUTANT71 is

required for efficient manganese uptake at the thylakoid membrane in *Arabidopsis*. Plant Cell **28:** 892–910

Sello S, Moscatiello R, La Rocca N, Baldan B, Navazio L (2017) A rapid and efficient method to obtain photosynthetic cell suspension cultures of *Arabidopsis thaliana*. Front Plant Sci **8:** 1444

Sello S, Perotto J, Carraretto L, Szabò I, Vothknecht UC, Navazio L (2016) Dissecting stimulus-specific Ca^{2+} signals in amyloplasts and chloroplasts of *Arabidopsis thaliana* cell suspension cultures. J Exp Bot **67:** 3965–3974

Sirpiö S, Allahverdiyeva Y, Suorsa M, Paakkarinen V, Vainonen J, Battchikova N, Aro EM (2007) TLP18.3, a novel thylakoid lumen protein regulating photosystem II repair cycle. Biochem J **406:** 415–425

Stael S, Kmiecik P, Willems P, Van Der Kelen K, Coll NS, Teige M, Van Breusegem F (2015) Plant innate immunity: sunny side up? Trends Plant Sci **20:** 3–11

Stael S, Wurzinger B, Mair A, Mehlmer N, Vothknecht UC, Teige M (2012) Plant organellar calcium signalling: an emerging field. J Exp Bot **63:** 1525–1542

Stephan AB, Kunz HH, Yang E, Schroeder JI (2016) Rapid hyperosmotic-induced Ca^{2+} responses in *Arabidopsis thaliana* exhibit sensory potentiation and involvement of plastidial KEA transporters. Proc Natl Acad Sci USA **113:** E5242–E5249

Szabó I, Bergantino E, Giacometti GM (2005) Light and oxygenic photosynthesis: energy dissipation as a protection mechanism against photooxidation. EMBO Rep **6:** 629–634

Tikkanen M, Gollan PJ, Suorsa M, Kangasjärvi S, Aro EM (2012) STN7 operates in retrograde signaling through controlling redox balance in the electron transfer chain. Front Plant Sci **3:** 277

Vincent TR, Avramova M, Canham J, Higgins P, Bilkey N, Mugford ST, Pitino M, Toyota M, Gilroy S, Miller AJ, et al (2017) Interplay of plasma membrane and vacuolar ion channels, together with BAK1, elicits rapid cytosolic calcium elevations in *Arabidopsis* during aphid feeding. Plant Cell **29:** 1460–1479

Wang C, Xu W, Jin H, Zhang T, Lai J, Zhou X, Zhang S, Liu S, Duan X, Wang H, et al (2016) A putative chloroplast-localized Ca^{2+}/H^{+} antiporter CCHA1 is involved in calcium and pH homeostasis and required for PSII function in *Arabidopsis*. Mol Plant **9:** 1183–1196

Weinl S, Held K, Schlücking K, Steinhorst L, Kuhlgert S, Hippler M, Kudla J (2008) A plastid protein crucial for Ca^{2+}-regulated stomatal responses. New Phytol **179:** 675–686

Wu HY, Liu MS, Lin TP, Cheng YS (2011) Structural and functional assays of AtTLP18.3 identify its novel acid phosphatase activity in thylakoid lumen. Plant Physiol **157:** 1015–1025

Xiong TC, Ronzier E, Sanchez F, Corratgé-Faillie C, Mazars C, Thibaud JB (2014) Imaging long distance propagating calcium signals in intact plant leaves with the BRET-based GFP-aequorin reporter. Front Plant Sci **5:** 43

Xu H, Martinoia E, Szabo I (2015) Organellar channels and transporters. Cell Calcium **58:** 1–10

Zonin E, Moscatiello R, Miuzzo M, Cavallarin N, Di Paolo ML, Sandonà D, Marin O, Brini M, Negro A, Navazio L (2011) TAT-mediated aequorin transduction: an alternative approach for effective calcium measurements in plant cells. Plant Cell Physiol **52:** 2225–2235

Zuppini A, Baldan B, Millioni R, Favaron F, Navazio L, Mariani P (2004) Chitosan induces Ca^{2+}-mediated programmed cell death in soybean cells. New Phytol **161:** 557–568

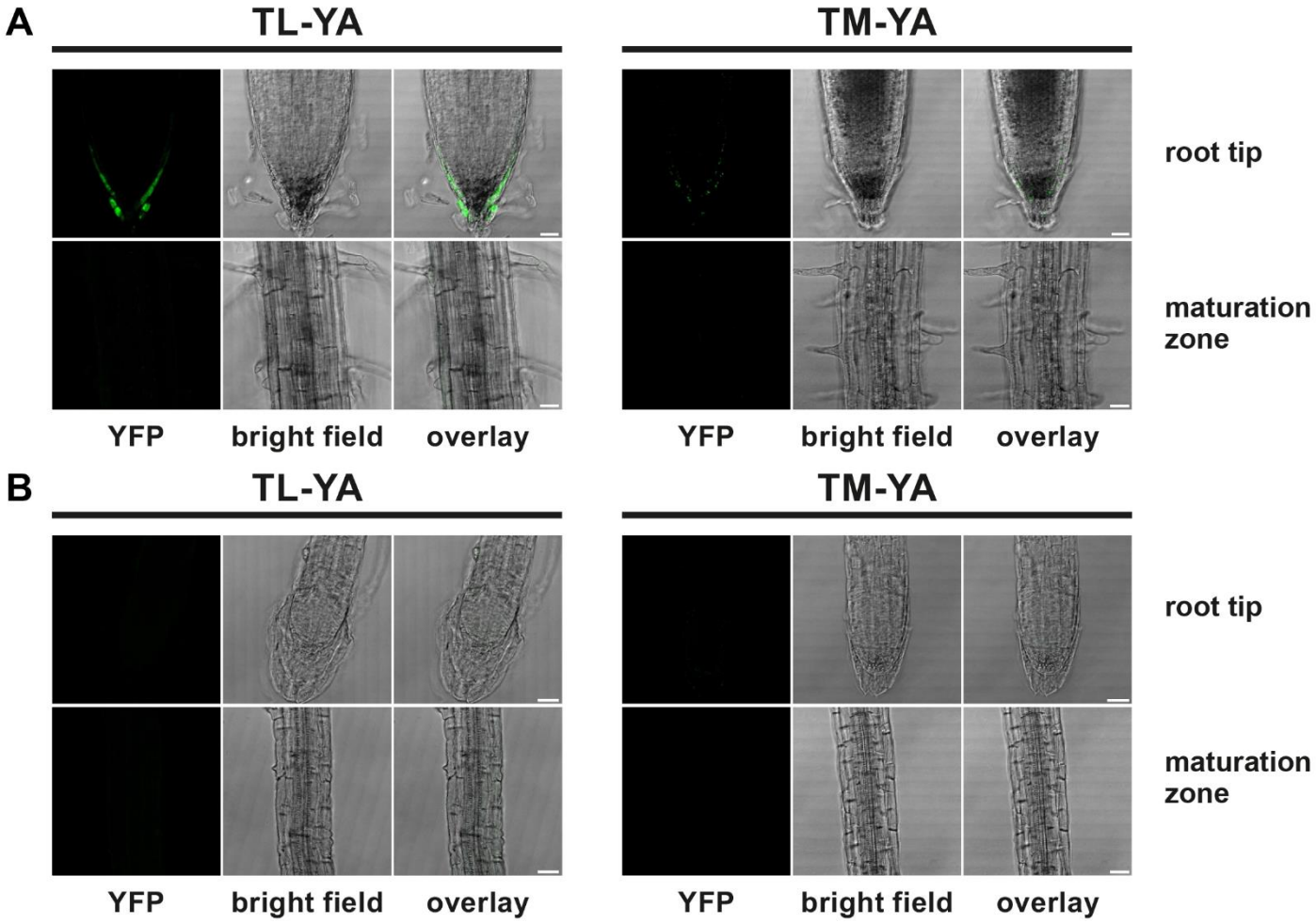

Supplemental Figure S1. Confocal microscopy analyses of roots of Arabidopsis seedlings of the TL-YA and TM-YA lines. Seedlings were grown under a 16h/8h light/dark photoperiod (panel A) or in the darkness (panel B). Bars, 25 µm.

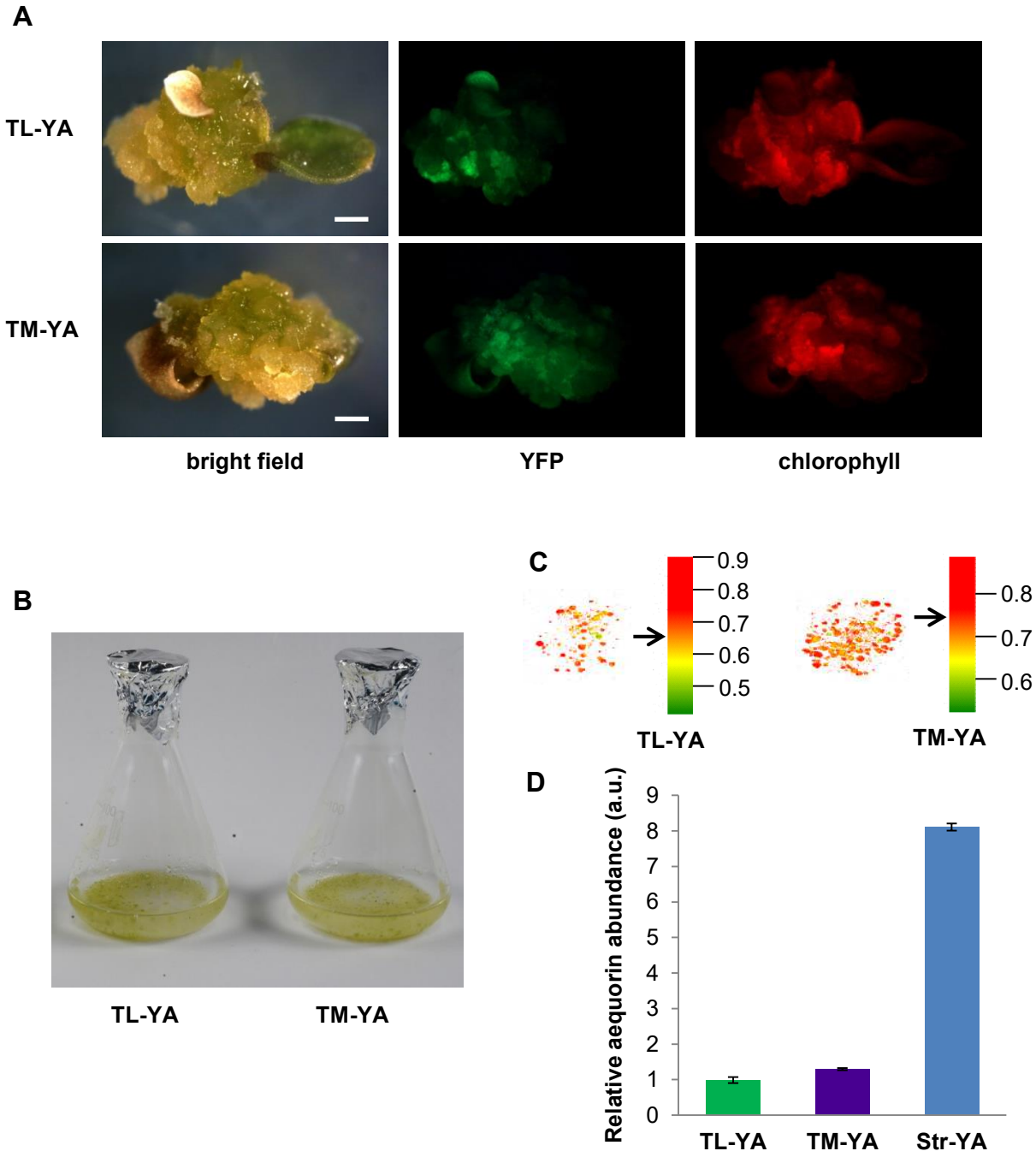

Supplemental Figure S2. Set up of Arabidopsis photosynthetic cell suspension cultures from the TL-YA and TM-YA lines. A, Observations at the fluorescence stereomicroscope of green calli derived from dedifferentiation of hypocotyls from Arabidopsis seeds germinated on hormone-enriched MS solid medium. Bar, 1 mm. B, Photosynthetic cell suspension cultures obtained after the transfer of green calli from solid to liquid medium containing a progressively reduced sucrose concentration (from 2% to 0.5%). C, PAM imaging analyses of TL-YA (F_v/F_m = 0.67) and TM-YA (F_v/F_m = 0.72) suspension-cultured cells. D, Analysis of aequorin protein levels in TL-YA and TM-YA cell cultures, in comparison with a cell line expressing stroma-targeted aequorin (Str-YA). Densitometric analysis of Western blots. Relative abundance of aequorin was normalized against calreticulin. Data are the means ± SD (n = 3).

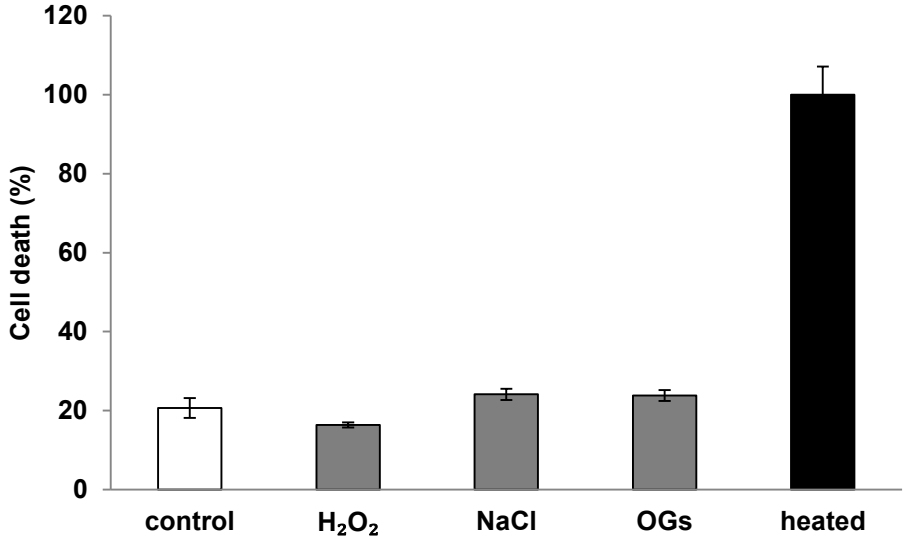

Supplemental Figure S3. Effect of the treatment with different stimuli on Arabidopsis cell viability. Exponentially growing cells were incubated for 1 h with 10 mM H_2O_2, 0.3 M NaCl, or 20 µg/ml OGs (grey columns). Control cells (white column) were incubated with cell culture medium only. The 100% value corresponds to cells treated for 10 min at 100°C (black column). Data are the means ± SE (n=5).

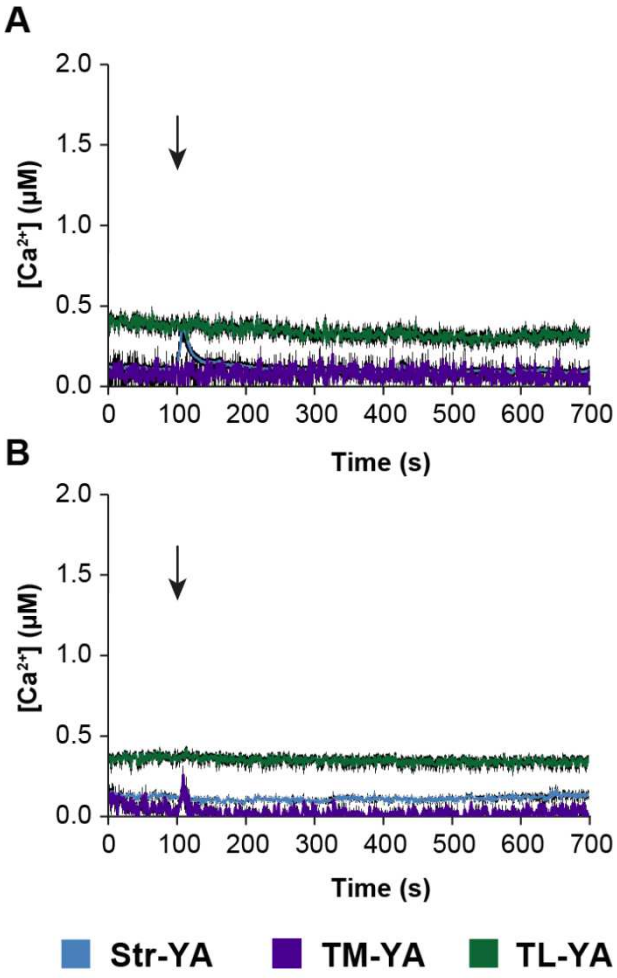

Supplemental Figure S4. Monitoring of subchloroplast free [Ca^{2+}] in Arabidopsis transgenic lines in response to touch. Ca^{2+} measurements were carried out in Arabidopsis cell suspension cultures (A) and seedlings (B) of the lines stably expressing YFP-aequorin in the stroma (Str-YA, blue trace), thylakoid membrane (TM-YA, violet trace) and thylakoid lumen (TL-YA, green trace). Arrows indicate the timing of injection of one volume of plant cell culture medium (A) or distilled H_2O (B), respectively. Data are presented as means ± SE (black shading) of n ≥ 8 experiments.

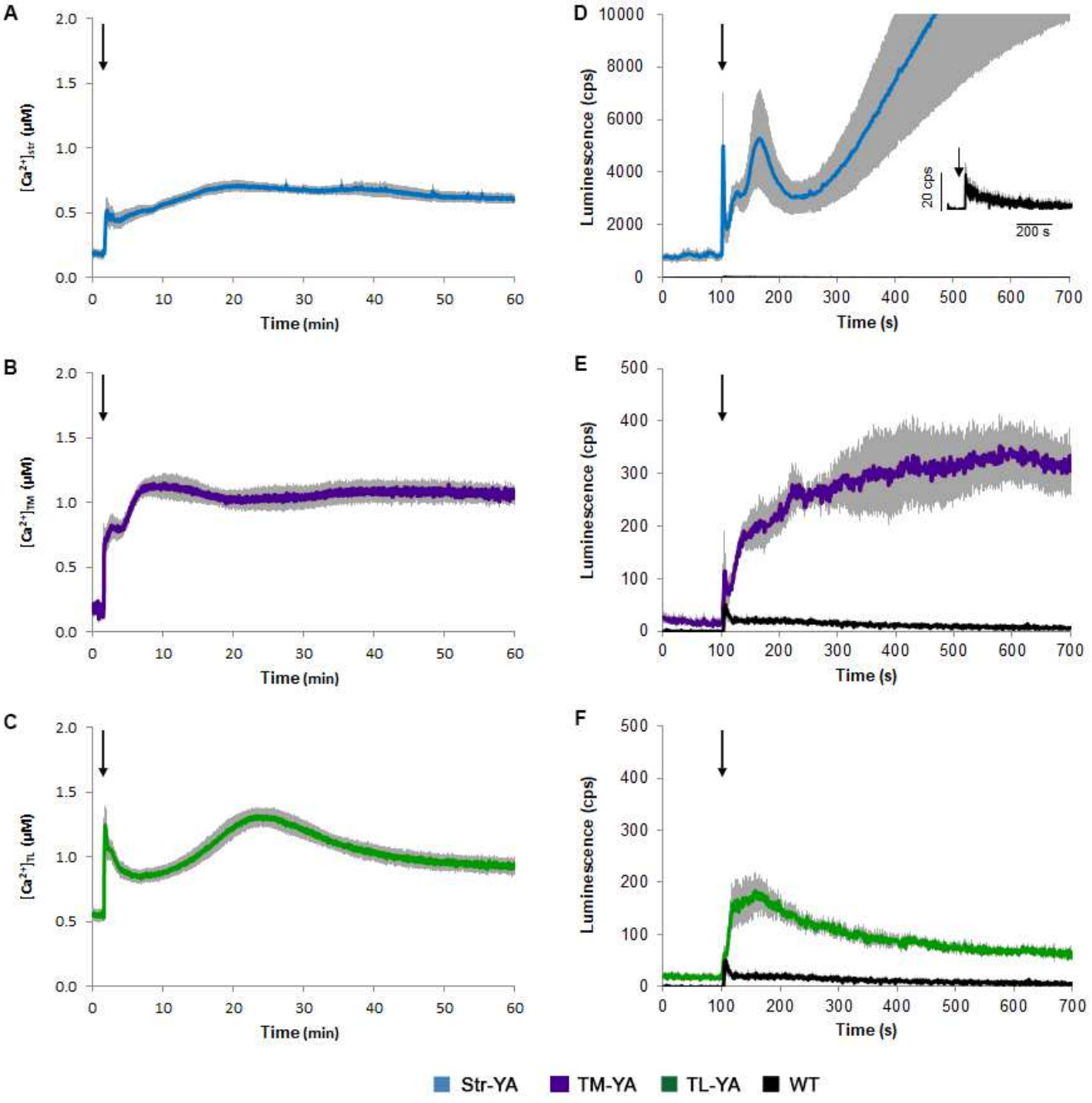

Supplemental Figure S5. Monitoring of subchloroplast free [Ca^{2+}] in Arabidopsis transgenic lines of the Str-YA, TM-YA and TL-YA in response to oxidative stress (10 mM H_2O_2) over 1 h (A-C) and comparison of luminescence levels in aequorin-expressing seedlings *versus* wild-type seedlings (D-F). Arrows indicate the time of stimulation (100 s). Data are presented as means ± SE (grey shading) of n ≥ 6 experiments.

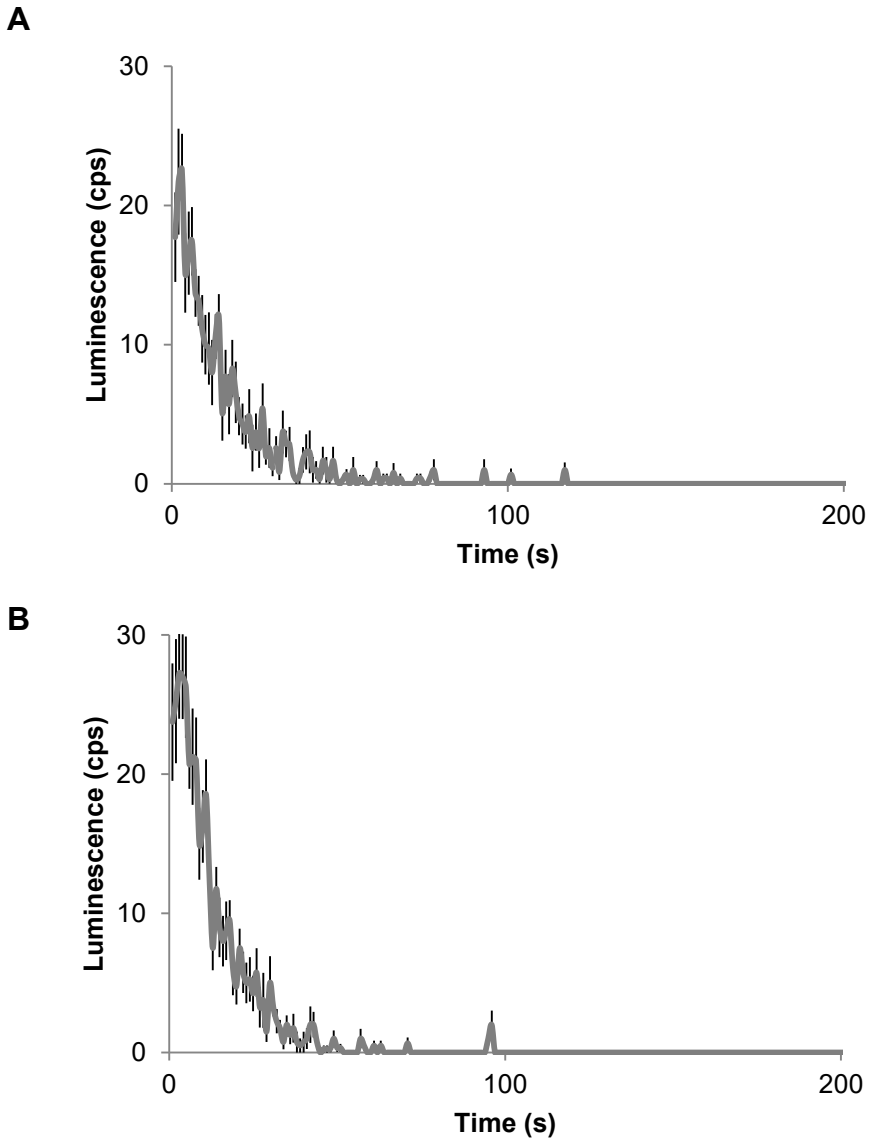

Supplemental Figure S6. Control measurements of luminescence levels upon light-to-dark transition in Arabidopsis aequorin-expressing seedlings that were not reconstituted with coelenterazine (A) *versus* wild-type (non-transformed) seedlings incubated with coelenterazine (B). Data are presented as means ± SE of 8 experiments.

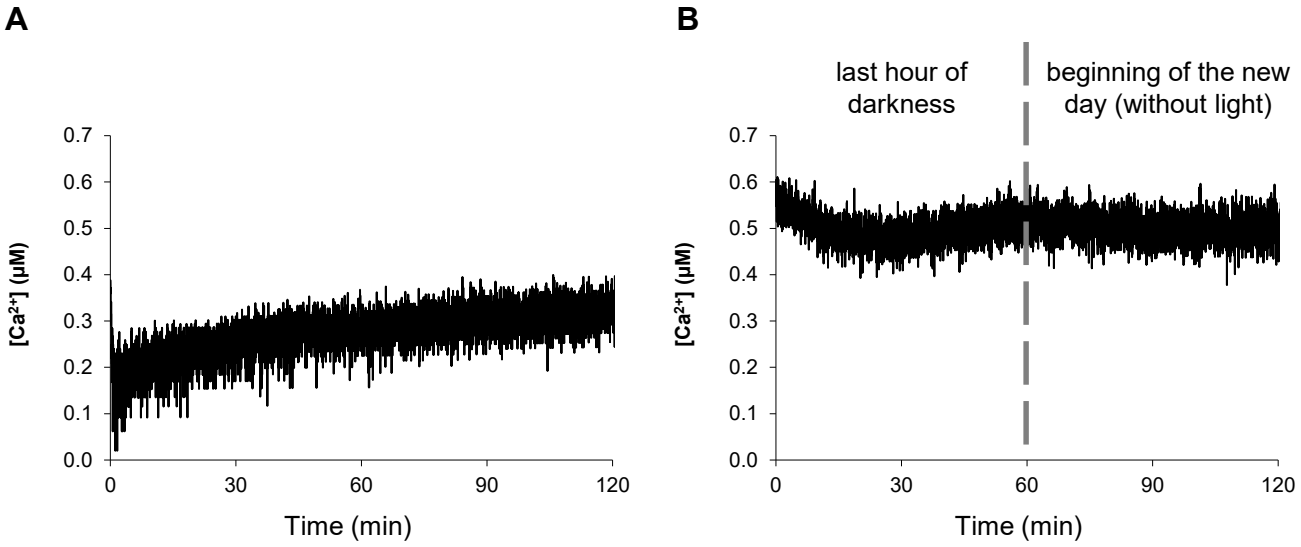

Supplemental Figure S7. Monitoring of thylakoid luminal [Ca^{2+}] in Arabidopsis seedlings (TL-YA) that were transferred to the luminometer chamber after 6 h of light (A) or at the end of the dark phase (B). Traces are representative of three independent experiments.

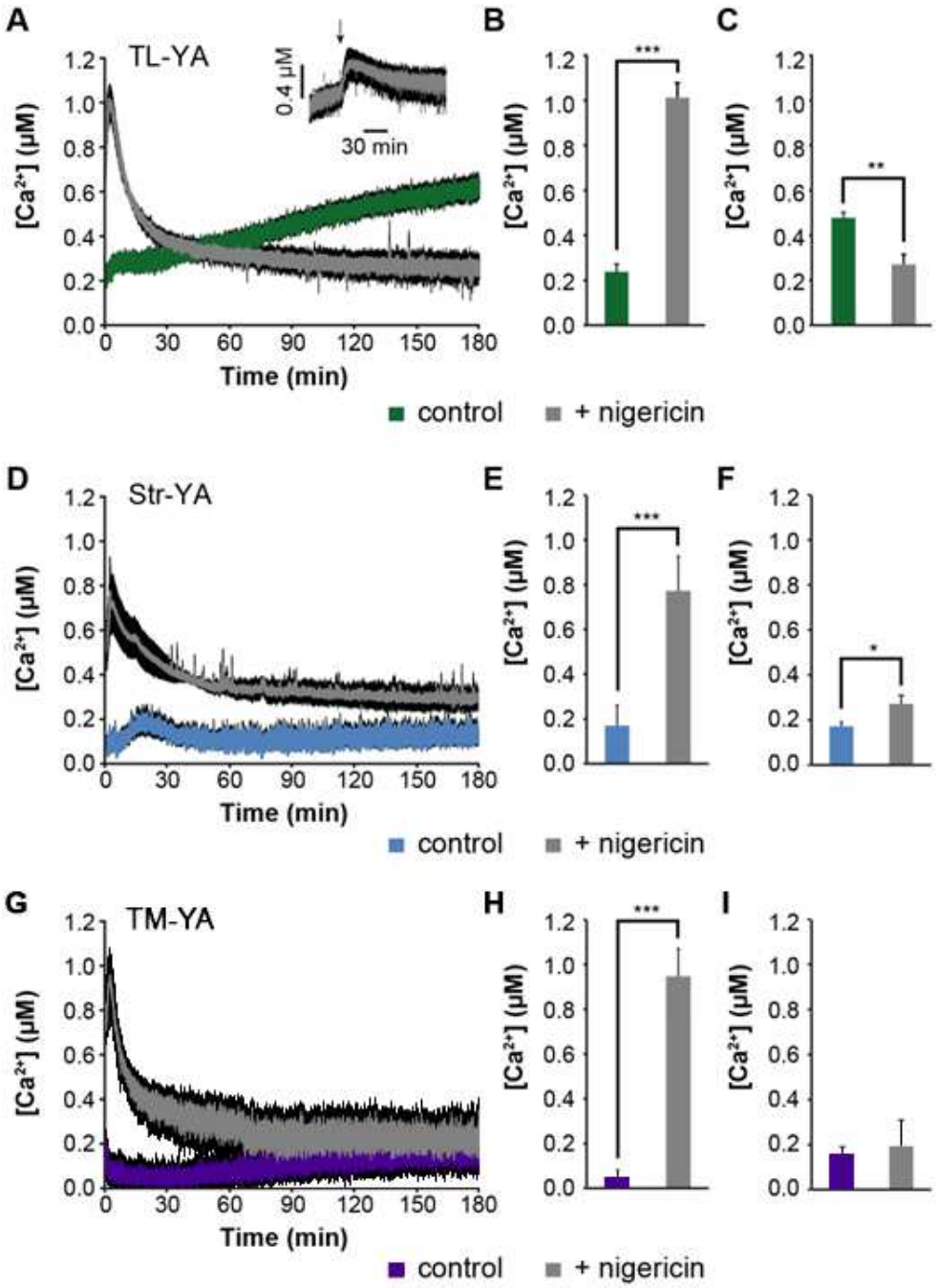

Supplemental Figure S8. Effect of the H^+-translocating uncoupler nigericin on dark-induced Ca^{2+} dynamics in the thylakoid lumen, stroma and stromal surface of thylakoids. Arabidopsis seedlings stably expressing YFP-aequorin in the thylakoid lumen (TL-YA, A-C), stroma (Str-YA, D-F) or stromal side of the thylakoid membrane (TM-YA, G-I) were subjected to light-to-dark transition in control conditions (A, green trace; D, blue trace; G, violet trace) or after 30 min pre-treatment with 5 µM nigericin (A, D, G, grey trace). In the insert of panel A, nigericin was added (arrow) 45 min after darkness. Traces represent average $[Ca^{2+}]$ responses ± SE (black shading) of at least four independent experiments. B-C, E-F, H-I, Statistical analysis of $[Ca^{2+}]$ levels measured at the time point of the nigericin-induced peak (B, E, H) and after 150 min of darkness (C, F, I). * P<0.05; ** P<0.01; *** P<0.001 (Student's t-test).

Supplemental Table S1. Amino acid and corresponding nucleotide sequences used for the targeting of the YA fusion proteins to the thylakoid lumen and thylakoid membrane.

TLP18.3 – thylakoid lumen

METLLSPRALSPPLNPKPLSLHQTKPTSHSLSLSKPTTFSGPKHLSTRFTKPESRN
WLIDAKQGLAALALSLTLTFSPVGTALASEFNILND

atggagacccttctctcccctcgtgcgctctctcctcctctcaatcccaaacctttgtcccttcaccagaccaaacccacttcacat
tcattgtctctctcaaaacccaccaccttctccggtcctaaacacctctccacccggttcactaaaccggaatcaagaaactggtt
aatagatgcaaagcaaggactagctgctttagctttatctctaactctcactttctcacctgttggcactgctttagcctctgagttc
aatatcctcaacgat

STN7 – thylakoid membrane

MATISPGGAYIGTPSPFLGKKLKPFSLTSPILSFKPTVKLNSSCRAQLIDTVHNLFI
GVGVGLPCTVMECGDMIYRSTLPKSNGLTITAPGVALALTALSYLWATPGVAPGF
FDMFVLAFVERLFRPTFRKDDFVVG

atggctacaatatctccgggaggagcttacatcggaactccctcaccgtttctcggcaaaaaactcaaacctttctctctaacttc
accgattttgagttttaaaccaacggttaagctcaattccagttgtcgcgctcaattgatcgatacggttcacaatctcttcatcgga
gttggagttggacttccatgtacggttatggagtgtggtgatatgatatatcgaagtactttgccgaaatctaatggtttaacgatc
actgctcctggagtagctttagctctcactgctctttcgtatctatgggcaacacctggtgttgctcctgggtttttcgatatgtttgtt
cttgcttttgttgagagattgtttcgacctacttttagaaaggatgattttgttgttggg

CHAPTER 3

Identification of a chloroplast-localized MCU in Arabidopsis

PROLOGUE

Although increasing knowledge supports the integration of chloroplasts in the overall cell Ca^{2+} homeostasis and signalling, very little is known to date about the molecular players that regulate Ca^{2+} fluxes across chloroplast membranes. Concerning active transporters that may mediate Ca^{2+} mobilization in chloroplasts, a few reports have suggested the presence of the Ca^{2+} ATPase ACA1 (Huang *et al.*, 1993) and the P-type ATPase HMA1 (Ferro *et al.*, 2010) on chloroplast envelope, but their intracellular localization is still under debate. Moreover, early biochemical evidence provided compelling evidence for the presence of a Ca^{2+}/H^{+} antiporter at the thylakoid membrane (Ettinger *et al.*, 1999). More recently, PAM71 and PAM71-HL (also called BICAT1 and 2) were demonstrated to act as divalent cation/proton exchangers able to transport either Mn^{2+} or Ca^{2+} in exchange with H^{+} (Schneider *et al.*, 2016; Frank *et al.*, 2019). The Ca^{2+}/H^{+} antiporters, which were suggested to play a key role in Ca^{2+} and pH homeostasis (Wang *et al.*, 2016), are localized at the thylakoid membrane and inner membrane of the chloroplast envelope, respectively. Interestingly, a reduced cytosolic Ca^{2+} transient upon treatment with a hyperosmotic stress was observed in knockout mutants lacking the envelope-located K^{+}/H^{+} antiporters KEA1 and KEA2, suggesting a specific but still elusive link between these K^{+} transporters and Ca^{2+} mobilization pathways at chloroplast membranes (Stephan *et al.*, 2016).

Concerning Ca^{2+}-permeable channels located at plastidial membranes, the most promising candidates were a chloroplast-targeted homologue of the mitochondrial calcium uniporter (cMCU) (De Stefani *et al.*, 2011) as well as two members (GLR3.4 and GLR3.5) of the glutamate receptor-like family, a group of ligand-gated cation channels mainly activated by glutamate (Wudick *et al.*, 2018a and 2018b). This chapter deals with the identification and functional characterization of cMCU in *Arabidopsis thaliana*, whereas **Chapter 4** focuses on preliminary analyses carried out in Arabidopsis mutant lines defective in either GLR3.4 or GLR3.5, respectively.

The research study regarding cMCU has involved the collaborative work of several laboratory teams, mainly located at the Department of Biology,

University of Padova. Among the six Arabidopsis homologues of MCU, only one (encoded by At5g66650 gene) displays an N-terminal signal sequence that is predicted to target the protein to chloroplasts (Stael *et al*., 2012). In the work presented in this chapter evidence was provided that this chloroplast-localized MCU homologue serves as an ion channel mediating Ca^{2+} fluxes into the organelle *in vivo*. Indeed, Western blot analyses as well as confocal microscopy analyses of Arabidopsis seedlings and protoplasts (derived from photosynthetic and heterotrophic suspension-cultured cells) transformed with a cMCU-GFP construct confirmed the localization of the protein at the chloroplast envelope. The ability of cMCU to conduct Ca^{2+} was investigated using electrophysiology and the channel was found to be inhibited by Gd^{3+} and ruthenium red, two classical blockers of MCU in animal cells. Functional characterization of this chloroplast Ca^{2+}-permeable channel was performed by heterologous expression in *E. coli* of both cMCU and its mutated version cMCU(QQ) (in which crucial acidic residues of the selectivity filter had been replaced by two glutamine residues). Ca^{2+} assays performed in *E. coli* strains expressing aequorin as a cytosolic Ca^{2+} probe demonstrated the induction of robust Ca^{2+} transients in response to external Ca^{2+} pulses only in the bacterial line expressing wild-type cMCU. Moreover, ruthenium red was found to inhibit the bacterial Ca^{2+} uptake in a dose-dependent manner. Functional and structural aspects of the cMCU channel were further investigated on the purified recombinant cMCU N-terminal domain (NTD) by conducting native polyacrilamide gel electrophoresis (PAGE), crosslinking experiments, size-exclusion chromatography and $^{45}Ca^{2+}$-overlay studies. All these *in vitro* biochemical assays confirmed the cMCU NTD tendency to oligomerize into tetramers and to weakly bind Ca^{2+}; nevertheless, Ca^{2+} does not interfere with the oligomerization state of NTD.

In addition to the functional characterization of cMCU, my contribution to this work mainly focused on Ca^{2+} measurement assays performed on two independent Arabidopsis knockout lines and respective wild-type lines (Col-0 and Col-4 genetic backgrounds), that were stably transformed with a construct encoding YFP-aequorin targeted to the plastid stroma. Among the different environmental stimuli that were tested on these lines, acute oxidative stress

and osmotic stress were found to trigger Ca^{2+} transients characterized by a significantly lower amplitude in the knockout lines with respect to wild-type ones. Interestingly, wild-type and cMCU knockout plants expressing cytosolic aequorin exhibited similar Ca^{2+} signatures in response to osmotic stress, suggesting that drought may affect only stromal Ca^{2+} concentrations in a cMCU-dependent manner, without altering the bulk $[Ca^{2+}]_{cyt}$. Plants lacking cMCU did not display constitutive growth defects, impaired photosynthetic efficiency or altered chloroplast ultrastructure; on the contrary, prolonged water starvation (up to 18 days) resulted in an improved drought tolerance of *cmcu* lines compared to wild-type one (both at the phenotypic and at the photosynthesis efficiency level). Moreover, in contrast to wild-type plants, *cmcu* knockout plants were able to fully recover leaf turgor and photosynthetic activity after irrigation for 1 day. The key components of the Ca^{2+}-related signalling pathway underlying this improved tolerance of *cmcu* mutants to drought were also investigated. Osmotic stress was found to increase MAPK3/6 phosphorylation in leaves of both cMCU ko lines compared with wild-type leaves, together with an altered expression of the ERF6 and MYB60 transcript factors, which in turn are responsible for the modulation of stomata closure.

In summary, in this work the first *bone fide* Ca^{2+}-permeable channel targeted to chloroplasts was identified and functionally characterized. Moreover, it was demonstrated to be involved in the plant cell response to osmotic stress via a Ca^{2+}-dependent signalling pathway that involves MAPK3/6, ERF6 and MYB60. These data indicate that cMCU is involved in the regulation of chloroplast-to-nucleus signalling evoked by osmotic stress and demonstrate that a chloroplast-located Ca^{2+} channel acts as a component of environmental sensing. The increased resistance of cMCU knockout plants to long-term H_2O deficit and improved recovery on rewatering suggest a possible biotechnological exploitation for the development of new strategies to mitigate the negative impact of climate change on plant productivity.

This work, that was published in Nature Plants (Teardo *et al.*, 2019), was also commented in the “news and views” section of the journal issue (Stael, 2019).

In that commentary, relevance was given to the new insights provided by our findings into the impact of chloroplast Ca^{2+}-signalling on drought tolerance and plant physiology in general (**Fig. 1**).

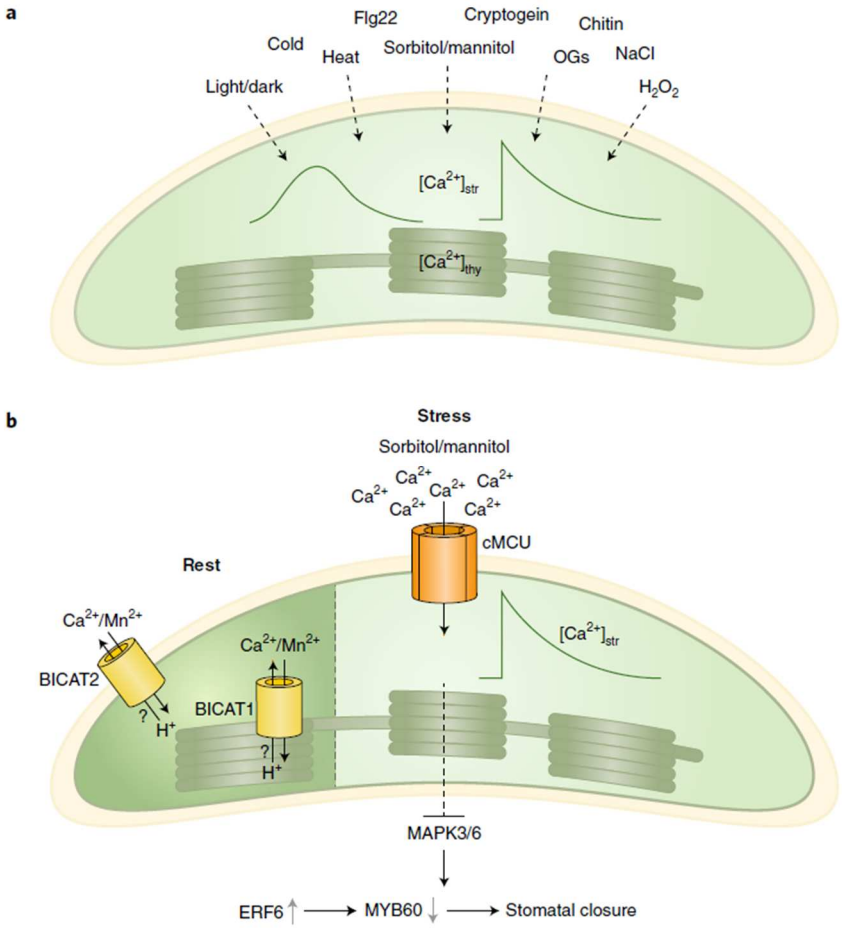

Fig. 1. cMCU-mediated chloroplast calcium signals modulate stomata closure and tolerance to drought in Arabidopsis. **a**, Environmental stress conditions of both abiotic and biotic nature trigger [Ca^{2+}] transient elevations in the chloroplast stroma. **b**, Identification of cMCU as the first chloroplast-located Ca^{2+}-permeable channel involved in Ca^{2+}-mediated signal transduction in response to osmotic stress. Compared to the recently identified potential Ca^{2+}/H^+ antiporters BICAT1 and 2, cMCU was shown to transport Ca^{2+} from the cytosol into the chloroplast stroma during specific osmotic stress-induced events. These chloroplast-specific Ca^{2+} signatures were also linked to downstream activation of a MAPK3/6-mediated signalling pathway (from Stael, 2019).

The study about cMCU, published in Nature Plants (Teardo *et al.*, 2019), has also attracted a great deal of interest from the local and national press, as attested by several articles that appeared either online or in printed versions in newspapers/magazines sections such as:

- ANSA (http://www.ansa.it/canale_scienza_tecnica/notizie/biotech/2019/06/12/scoperto-il-segreto-che-fa-resistere-le-piante-alla-siccita-_7c0a6f30-12bc-46bf-806a-8ac45b7e9be3.html);
- Il Bo Live (https://ilbolive.unipd.it/it/news/piante-proteina-resistenza-siccita);
- Le Scienze (https://www.lescienze.it/news/2019/06/11/news/piante_scoperta_proteina_che_genera_resistenza_alla_siccita_-4442934/);
- BBC Scienze (vol. Sept./Oct. 2019);
- Treccani Atlante (http://www.treccani.it/magazine/atlante/scienze/La_proteina_della_siccita.html);
- la Repubblica (https://www.repubblica.it/scienze/2019/06/11/news/scoperto_il_segreto_che_fa_resistere_le_piante_alla_siccita_-228501105/);
- Corriere del Veneto (Moranduzzo S. "Equipe padovana scopre il segreto che fa resistere le piante alla siccità" *Corriere del Veneto*. Ed. Venezia. (2019): Pagina 6. Stampato il 12 giugno 2019).

This work was also the subject of an interview on Rai Radio3 Scienza (https://media.mimesi.com/cacheServer/servlet/CNcacheCopy?file=pdf/201906/18/24777_binpage1932145619.pdf&authCookie=-1056898719&trc=pMailCN-t20190618-a443568106-h43663-c2784-f8274-n24777-u7474).

REFERENCES

De Stefani D, Raffaello A, Teardo E, Szabo I, Rizzuto R (2011) A forty-kilodalton protein of the inner membrane is the mitochondrial calcium uniporter. Nature **476:** 336-340

Ettinger WF, Clear AM, Fanning KJ, Peck ML (1999) Identification of a Ca^{2+}/H^{+} antiport in the plant chloroplast thylakoid membrane. Plant Physiol **119:** 1379-1386

Ferro M, Brugiere S, Salvi D, Seigneurin-Berny D, Court M, Moyet L, Ramus C, Miras S, Mellal M, Le Gall S, Kieffer-Jaquinod S, Bruley C, Garin J, Joyard J, Masselon C, Rolland N (2010) AT_CHLORO, a comprehensive chloroplast proteome database with subplastidial localization and curated information on envelope proteins. Mol Cell Proteomics **9:** 1063-1084

Frank J, Happeck R, Meier B, Hoang MTT, Stribny J, Hause G, Ding H, Morsomme P, Baginsky S, Peiter E (2019) Chloroplast-localized BICAT proteins shape stromal calcium signals and are required for efficient photosynthesis. New Phytol **221:** 866-880

Huang L, Berkelman T, Franklin AE, Hoffman NE (1993) Characterization of a gene encoding a Ca^{2+}-ATPase-like protein in the plastid envelope. Proc Natl Acad Sci U S A **90:** 10066-10070

Schneider A, Steinberger I, Herdean A, Gandini C, Eisenhut M, Kurz S, Morper A, Hoecker N, Ruhle T, Labs M, Flugge UI, Geimer S, Schmidt SB, Husted S, Weber AP, Spetea C, Leister D (2016) The evolutionarily conserved protein PHOTOSYNTHESIS AFFECTED MUTANT71 is required for efficient manganese uptake at the thylakoid membrane in Arabidopsis. Plant Cell **28:** 892-910

Stael S, Wurzinger B, Mair A, Mehlmer N, Vothknecht UC, Teige M (2012) Plant organellar calcium signalling: an emerging field. J Exp Bot **63:** 1525-1542

Stael S (2019) Chloroplast calcium signalling quenches a thirst. Nat Plants **5:** 559-560

Stephan AB, Kunz HH, Yang E, Schroeder JI (2016) Rapid hyperosmotic-induced Ca^{2+} responses in *Arabidopsis thaliana* exhibit sensory potentiation and involvement of plastidial KEA transporters. Proc Natl Acad Sci U S A **113:** E5242-5249

Teardo E, Carraretto L, Moscatiello R, Cortese E, Vicario M, Festa M, Maso L, De Bortoli S, Cali T, Vothknecht UC, Formentin E, Cendron L, Navazio L, Szabo I (2019) A chloroplast-localized mitochondrial calcium uniporter transduces osmotic stress in *Arabidopsis*. Nat Plants **5:** 581-588

Wang C, Xu W, Jin H, Zhang T, Lai J, Zhou X, Zhang S, Liu S, Duan X, Wang H, Peng C, Yang C (2016) A putative chloroplast-localized Ca^{2+}/H^{+} antiporter CCHA1 is involved in calcium and pH homeostasis and required for PSII function in *Arabidopsis*. Mol Plant **9:** 1183-1196

Wudick MM, Michard E, Oliveira Nunes C, Feijo JA (2018a) Comparing plant and animal glutamate receptors: common traits but different fates? J Exp Bot **69:** 4151-4163

Wudick MM, Portes MT, Michard E, Rosas-Santiago P, Lizzio MA, Nunes CO, Campos C, Santa Cruz Damineli D, Carvalho JC, Lima PT, Pantoja O, Feijo JA (2018b) CORNICHON sorting and regulation of GLR channels underlie pollen tube Ca^{2+} homeostasis. Science **360:** 533-536

This work was published as:

A chloroplast-localized mitochondrial calcium uniporter transduces osmotic stress in *Arabidopsis*

Enrico Teardo[1], Luca Carraretto[1], Roberto Moscatiello[1], Enrico Cortese[1], Mattia Vicario[1], Margherita Festa[1], Lorenzo Maso[1], Sara De Bortoli[1], Tito Calì[2], Ute C. Vothknecht[3], Elide Formentin[1,4], Laura Cendron[1], Lorella Navazio[1,4] and Ildiko Szabo[1,4]

[1]Department of Biology, University of Padova, Padova, Italy

[2]Department of Biomedical Sciences, University of Padova, Padova, Italy

[3]IZMB – Plant Cell Biology, University of Bonn, Bonn, Germany

[4]Botanical Garden, University of Padova, Padova, Italy

in Nature Plants, June 2019, vol. 5, pages 581-588.

nature plants

LETTERS

https://doi.org/10.1038/s41477-019-0434-8

A chloroplast-localized mitochondrial calcium uniporter transduces osmotic stress in *Arabidopsis*

Enrico Teardo[1,5], Luca Carraretto[1,5], Roberto Moscatiello[1], Enrico Cortese[1], Mattia Vicario[1], Margherita Festa[1], Lorenzo Maso[1], Sara De Bortoli[1], Tito Calì[2], Ute C. Vothknecht[3], Elide Formentin[1,4*], Laura Cendron[1], Lorella Navazio[1,4*] and Ildiko Szabo[1,4*]

Chloroplasts are integral to sensing biotic and abiotic stress in plants, but their role in transducing Ca^{2+}-mediated stress signals remains poorly understood[1,2]. Here we identify cMCU, a member of the mitochondrial calcium uniporter (MCU) family, as an ion channel mediating Ca^{2+} flux into chloroplasts in vivo. Using a toolkit of aequorin reporters targeted to chloroplast stroma and the cytosol in cMCU wild-type and knockout lines, we provide evidence that stress-stimulus-specific Ca^{2+} dynamics in the chloroplast stroma correlate with expression of the channel. Fast downstream signalling events triggered by osmotic stress, involving activation of the mitogen-activated protein kinases (MAPK) MAPK3 and MAPK6, and the transcription factors MYB60 and ethylene-response factor 6 (ERF6), are influenced by cMCU activity. Relative to wild-type plants, cMCU knockouts display increased resistance to long-term water deficit and improved recovery on rewatering. Modulation of stromal Ca^{2+} in specific processing of stress signals identifies cMCU as a component of plant environmental sensing.

Plants have evolved a complex suite of responses that are exquisitely fine-tuned to enable them to cope with abiotic and biotic stresses. Chloroplasts sense environmental conditions and chloroplast-specific responses are indispensable for the survival of plants following abiotic and biotic stress (for example, in ref. [3]). Although Ca^{2+} is a ubiquitous intracellular messenger involved in physiological and stress responses of plants[4], recent data indicate that chloroplasts respond to environmental stimuli with specific Ca^{2+} signals[5–10]. Chloroplasts contain high concentrations of Ca^{2+}, although most of it is present in bound form and may serve as intracellular cytosolic 'Ca^{2+} capacitors' for plant cells, thereby shaping cytoplasmic Ca^{2+} transients[11–13]. However, the molecular entities that mediate negative-voltage-driven (−100 mV) Ca^{2+} uptake across the inner envelope membrane remain elusive[14,15].

To fully understand the impact of chloroplast Ca^{2+} dynamics on plant physiology, it is necessary to identify the Ca^{2+} transporters involved. Among the six homologues of mitochondrial calcium uniporter (MCU)[9] in *Arabidopsis thaliana*, At5g66650, named here cMCU, displays a strong predicted consensus targeting motif for chloroplasts and a lower probability sequence for mitochondria (scores of 18.5 and 8.8, respectively) (http://aramemnon.uni-koeln.de). To experimentally test its localization, protoplasts isolated from wild-type plant mesophyll cells (Fig. 1a) and from cultured autotrophic (Supplementary Fig. 1a) or heterotrophic (Supplementary Fig. 1b) cells were transformed with cMCU::EGFP::35S construct for expression of a cMCU fusion with green fluorescent protein (GFP). Localization of the protein to the chloroplast envelope was observed, similar to that of the envelope marker 'outer envelope membrane protein 7' (OEP7) (Supplementary Fig. 1c) and in contrast to the thylakoid-located potassium channel TPK3[16] (Supplementary Fig. 1d). This localization was also observed in protoplasts from mesophyll cells of cMCU knockout *Arabidopsis* plants (Supplementary Fig. 2a) either transiently transformed (Supplementary Fig. 2b–d) or stably transfected with cMCU–GFP under the control of the endogenous promoter (Fig. 1b and Supplementary Fig. 2e). In addition, when protoplasts from plants were transformed with both OEP7::GFP::35S and cMCU::tdTomato::35S constructs, a clear co-localization of the two signals was observed, further indicating envelope localization of cMCU (Fig. 1c and Supplementary Fig. 3a,b). In intact plants stably expressing mitochondrial β-F1-ATPase–EGFP that were transformed with cMCU::tdTomato, the channel localized predominantly to chloroplasts (Supplementary Fig. 3c and Supplementary Video 1). In accordance with chloroplast localization—further confirmed by western blot using chloroplasts from plants stably expressing cMCU–GFP (Fig. 1d and Supplementary Fig. 3d)—quantitative PCR (qPCR) analysis showed prevalent expression of cMCU in fully expanded leaves (Fig. 1e). In leaf epidermal cells (Supplementary Fig. 4a–c and Supplementary Videos 2 and 3) and in the root (Supplementary Fig. 4d), cMCU was preferentially targeted to mitochondria. In guard cells harbouring green chloroplasts, cMCU was observable in chloroplasts but not in mitochondria, as shown by tetramethylrhodamine staining of mitochondria (Supplementary Fig. 4e,f and Supplementary Video 4), suggesting that the predicted dual localization is cell type-dependent and that in the absence of mature plastids or chloroplasts, cMCU can be targeted to mitochondria.

Next, we investigated the ability of cMCU to conduct Ca^{2+} using electrophysiology. Similarly to the mammalian MCU[17] and to *A. thaliana* MCU1[18], in vitro-expressed cMCU (Supplementary Fig. 5a) can conduct sodium when divalent cations are not present (Fig. 2a) and forms channels with low conductance (8 ± 2 pS) in Ca^{2+}-gluconate solution. cMCU is inhibited by gadolinium (Gd^{3+}) and ruthenium red (RR), two classical inhibitors of MCU (Fig. 2a,b and Supplementary Fig. 5b). In a previous study, uptake of Ca^{2+} into isolated chloroplasts was proposed to be mediated by a ruthenium red-sensitive uniport-type carrier in the envelope membrane[19].

To functionally characterize cMCU in vivo, we first established a heterologous system using *Escherichia coli* cells expressing the Ca^{2+}-sensitive photoprotein aequorin as a cytosolic Ca^{2+} reporter.

[1]Department of Biology, University of Padova, Padova, Italy. [2]Department of Biomedical Sciences, University of Padova, Padova, Italy. [3]IZMB - Plant Cell Biology, University of Bonn, Bonn, Germany. [4]Botanical Garden, University of Padova, Padova, Italy. [5]These authors contributed equally: Enrico Teardo, Luca Carraretto. *e-mail: elide.formentin@unipd.it; lorella.navazio@unipd.it; ildiko.szabo@unipd.it

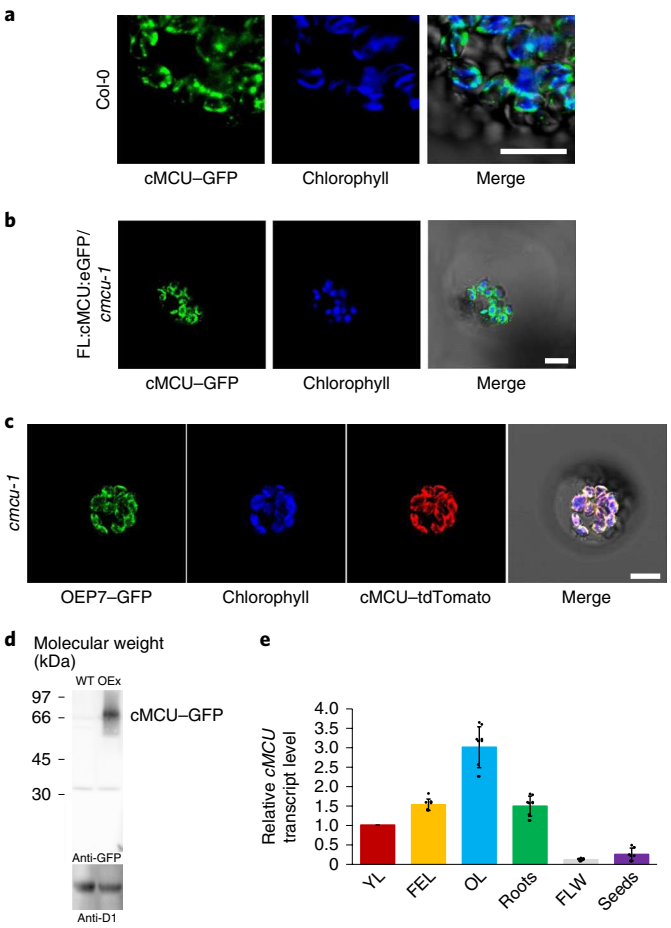

Fig. 1 | cMCU localizes to chloroplasts in *Arabidopsis* mesophyll cells. **a**,**b**, Mesophyll protoplasts isolated from mesophyll cells of wild-type (WT) *Arabidopsis* plants transiently transformed with cMCU:GFP:35S construct (**a**) or from cMCU knockout plants stably transfected with plasmid encoding cMCU–GFP under the control of the endogenous promoter (**b**), showing localization of cMCU to chloroplasts in protoplasts. **c**, Protoplasts from plants expressing OEP7–GFP and cMCU–tdTomato. cMCU clearly localizes to the chloroplast envelope. Scale bars in **a**–**c**, 10 µm. **d**, Western blot of lysate from purified chloroplasts from wild-type *Arabidopsis* plants and from plants expressing cMCU–GFP under the control of two 35S promoters (OEx) (100 µg total protein per lane). cMCU–GFP was detected with GFP antibody; the predicted molecular weight of cMCU–GFP is 67 kDa. The loading control is D1 core protein of photosystem II. Contamination by mitochondria is negligible (see Supplementary Fig. 3d). Localization studies in **a**–**d** are representative of 3–5 biological replicates with independent plants giving the same results. **e**, *cMCU* expression in different plant tissues ($n = 3$; data are mean ± s.d.). Transcript levels relative to the young leaf (YL) sample are shown. *ACTIN 2* was used as the reference gene. FEL, fully expanded leaves; OL, old leaves (external leaves from four-week-old rosette); FLW, flowers; Seeds, imbibed seeds.

E. coli cells were transformed with constructs encoding either the full-length wild-type cMCU homologue or a mutated version, in which crucial acidic residues of the selectivity filter (WDVMEP) had been replaced by two glutamine residues (cMCUQQ)[17] (Supplementary Fig. 6a). Potent Ca^{2+} transients were detected in the bacterial cells expressing wild-type cMCU in response to external Ca^{2+} pulses in a dose-dependent manner, whereas in cMCUQQ-harbouring cells, such transients were as low as in the *E. coli* control (Fig. 2c,d). Moreover, ruthenium red effectively inhibited the Ca^{2+} uptake in a dose-dependent manner (Fig. 2e and Supplementary Fig. 6b). Altogether, these results confirmed that cMCU is a pore-forming unit defining the minimal element sufficient for the Ca^{2+} uniporter activity.

MCU homologues are detectable in most branches of eukaryotic life from protists to metazoan. The recently reported cryo-electron microscopy (cryo-EM) and X-ray structures of MCU proteins[20–22] have enabled reconstruction of a reliable model for the highly conserved pore- and vestibule-forming cMCU tetramer by homology modelling (Supplementary Fig. 7a). The N-terminal subdomain (NTD) sequences of all the *Arabidopsis* cMCU isoforms do not share sequence homology with any of the MCU structures determined so far (Supplementary Fig. 6a). Multiple independent prediction servers identified similarities of cMCU NTD to the C-terminal of Roc (COR) dimerization device of Ras of complex proteins–C-terminal of Roc (RocCOR) GTPase from *Chlorobium tepidum* and to calmodulin-like structures such as red fluorescent genetically encoded Ca^{2+} indicator for optical imaging (RGECO). The similarity to RocCOR supports the intrinsic tendency of cMCU NTD to oligomerize, whereas the similarity to RGECO leads to the hypothesis of Ca^{2+} binding by the NTD (Supplementary Fig. 6a).

Next, structural and functional aspects of cMCU were investigated in vitro: recombinant NTD domain (Supplementary Fig. 7b) clearly showed a tendency to oligomerize into tetramers in cross-linking experiments (Fig. 2h), native polyacrylamide gel electrophoresis (PAGE) (Supplementary Fig. 7c) and in size-exclusion chromatography (Supplementary Fig. 8a). $^{45}Ca^{2+}$-overlay studies indicated the ability of NTD to bind Ca^{2+}, albeit more weakly than well-characterized Ca^{2+}-binding proteins (Supplementary Fig. 8b). However, size-exclusion chromatography in the presence of a large excess of Ca^{2+} or the chelating agent EGTA suggested that Ca^{2+} does not interfere with the oligomerization state of NTD (Supplementary Fig. 8a). cMCU primary sequence analysis and a homology model built using Phyre2[23] enabled us to identify three segments reminiscent of EF-hand motifs (107–118, 159–172 and 194–205), with only the first showing a conserved pattern (Fig. 2g and Supplementary Fig. 6a). Mutation of the 107–118 EF-hand-like motif (Supplementary Fig. 8c)) resulted in a significant reduction in Ca^{2+} uptake (Fig. 2f and Supplementary Fig. 8d). Together, these results support the hypothesis that NTD may play a role in both the tetramerization of cMCU channel and the regulation of Ca^{2+}-transporting efficiency, possibly through conformational dynamics or changes involving the EF-hand-like motif.

Various stress stimuli including osmotic stress and oxidative stress can cause increases in the cytosolic free-Ca^{2+} concentration in plants (for example, in refs. [2,24]), and these transient Ca^{2+} changes may trigger, in turn, the uptake of Ca^{2+} into the chloroplast[12]. To analyse the involvement of cMCU in the organellar Ca^{2+} fluxes evoked by different environmental stimuli in vivo, two independent *Arabidopsis* knockout lines and respective wild-type lines (Col-0 and Col-4 genetic backgrounds) were stably transformed with a construct encoding yellow fluorescent protein–aequorin targeted to the plastid stroma[12,25,26]. Evidence for the correct subcellular localization of the Ca^{2+} probe was provided by laser-scanning confocal microscopy analysis (Supplementary Fig. 9). In accordance with the localization of cMCU in the chloroplast envelope membrane, we observed a clear difference in stromal Ca^{2+} levels between wild-type plants and those lacking cMCU on application of acute oxidative stress (Fig. 3a,b) or osmotic stress, triggered by application of either mannitol[27] (Fig. 3c,d) or sorbitol[28] (Supplementary Fig. 10a,b). Such differences were not observable when seedlings were subjected to salt stress (Fig. 3e,f) or to the biotic stress elicitor flg22 (Supplementary Fig. 10c), indicating the involvement of this Ca^{2+} channel in the organellar response to specific environmental cues. In addition, wild-type and cMCU knockout plants displayed similar Ca^{2+} signatures in the thylakoid lumen, in accordance with the envelope localization of cMCU (Supplementary Fig. 11a–d). This is in agreement

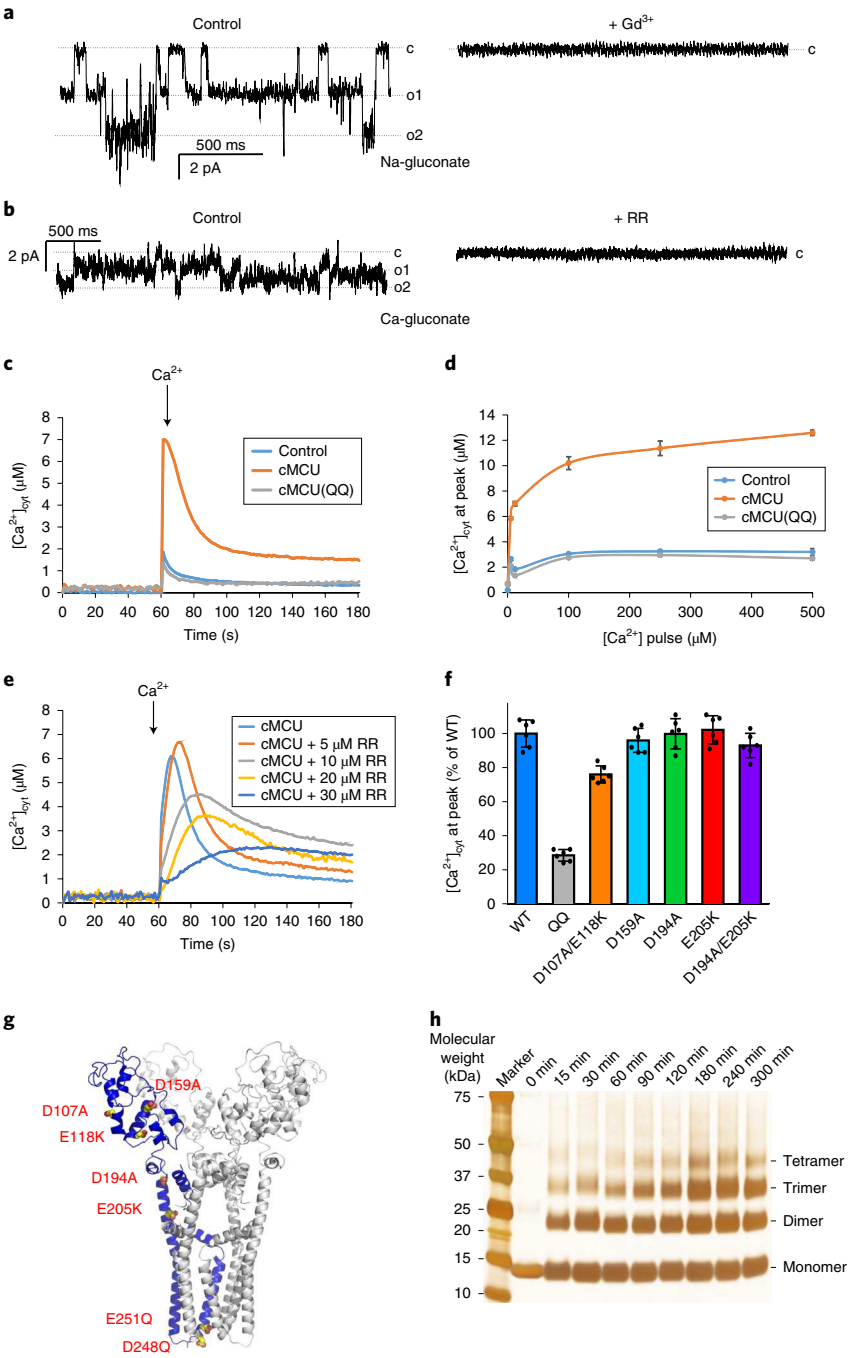

Fig. 2 | Recombinant cMCU mediates Ca^{2+} fluxes in electrophysiological experiments and in a heterologous expression system. a,**b**, Representative current traces recorded in a planar lipid bilayer using in-vitro-expressed and solubilized cMCU in 100 mM Na-gluconate solution ($n=12$) (**a**) and in 100 mM Ca-gluconate ($n=7$) (**b**) before (left) and after (right) addition of 100 μM gadolinium (Gd^{3+}) ($n=6$) or of 10 μM ruthenium red (RR) ($n=5$). Vcis (voltage applied on the *cis* side of the bilayer chamber): −60 mV (**a**) and −120 mV (**b**). Closed (c) and open (o1 and o2) states are indicated. Amplitude histograms from current traces of ≥30 s are shown in Supplementary Fig. 5b. **c**, Cytosolic Ca^{2+} concentration ($[Ca^{2+}]_{cyt}$) measured using cytosol-targeted aequorin in *E. coli* cells transformed with aequorin only, with aequorin and cMCU or with aequorin and inactive cMCU harbouring two single point mutations (from E/D to Q) in the pore region (cMCU QQ), and challenged with a single dose of 12 μM $CaCl_2$ added to the external medium. **d**, Peak cytosolic Ca^{2+} concentration measured as in **c** as a function of externally added Ca^{2+}. **e**, Dose-dependent inhibition of Ca^{2+} uptake by increasing doses of ruthenium red. **f**, Cytosolic Ca^{2+} peak measured in *E. coli* cells transformed with aequorin and wild-type cMCU or one of the following mutated variants: D107A/E118K, D159A, D194A, E205K, D194A/E205K (cMCUΔSP variants that harbour the specified single or double point mutations in the NTD in putative calcium binding motifs) and QQ mutant (D248Q/E251Q). The histogram shows the average cytosolic Ca^{2+} peaks, normalized to the wild-type cMCU ($n=6$ biological replicates; data are mean ± s.e.m.) following addition of maximal free Ca^{2+} to the cells. Statistically significant differences ($P < 0.001$, Student's *t*-test) were observed between the WT and QQ mutant, as well as the WT and the D107A/E118K mutant. **g**, Structural overview of the studied cMCU mutations. Grey and blue cartoon view of cMCU hypothetical tetrameric assembly built by homology modelling (Phyre2 server), adjusted with graphical software, crude molecular dynamics and geometry optimization (Phenix Interface). For clarity, mutated residues side chains are shown as spheres and labelled only on the blue monomer. **h**, Cross-linking studies with purified NTD using glutaraldehyde vapours, analysed by SDS–PAGE with silver staining.

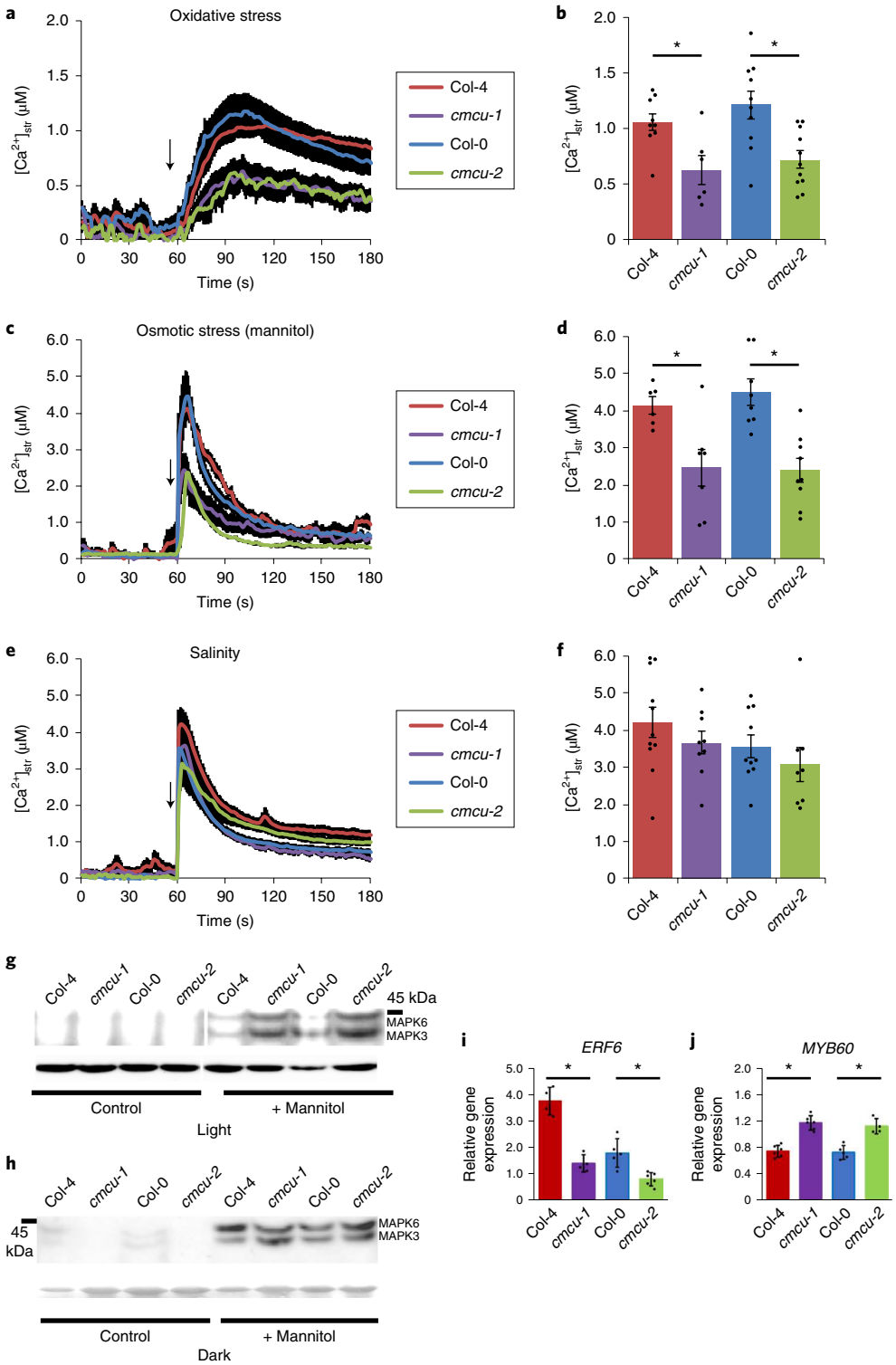

Fig. 3 | Monitoring of stromal Ca^{2+} concentration reveals differential calcium dynamics and signalling in wild-type versus cMCU knockout plants. **a**–**f**, Stromal calcium concentration ($[Ca^{2+}]_{str}$) in two *Arabidopsis* wild-type ecotypes (red and blue) and in two independent cMCU knockout (violet and green) lines. Traces represent average $[Ca^{2+}]$ responses ± s.e.m. (black shading) of $n \geq 6$ independent plants from three biological replicates. Stimuli (**a**,**b**, 10 mM H_2O_2; **c**,**d**, 600 mM mannitol; **e**,**f**, 300 mM NaCl) were applied (arrows) after 60 s. In **b**,**d**,**f**, statistical analysis of Ca^{2+} concentration at the peak: $^*P < 0.05$ (Student's *t*-test). **g**,**h**, MAPK3 and MAPK6 activation in leaves subjected to mannitol stress applied to plants kept in the light (**g**) or in the dark (**h**) for 24 h before stress. Total proteins were extracted after treatment for 10 min; phosphorylated MAPK6 and MAPK3 were detected using phospho-p44/42 MAPK (Erk1/2) antibody. Equal loading was indicated using VDAC antibody (**g**) or Ponceau red (**h**). Western blots are representative of five experiments giving similar results. **i**,**j**, Transcript level analysis of *ERF6* (**i**) and *MYB60* (**j**). Illuminated leaves were treated as in **g**,**h**, for 10 min and RT–qPCR was performed to compare transcript levels of *ERF6* and *MYB60*. Transcript levels are reported relative to mock-treated; *ACTIN 2* was used as a reference gene. $^*P < 0.05$, Student's *t*-test. Experiments were repeated four times for three leaves per plant in two different sets of *Arabidopsis* plants. Data are mean ± s.e.m.

with the recent evidence that Ca^{2+} signals might be independently regulated in the chloroplast stroma and thylakoid lumen[26]. A significant increase in the transient cytosolic Ca^{2+} elevation triggered by 10 mM H_2O_2 was observed in cMCU knockout plants compared with the wild type (Supplementary Fig. 12a), possibly as a consequence of the impaired Ca^{2+} uptake into the chloroplast stroma, since chloroplasts seem to be involved in the dissipation of cytosolic Ca^{2+} signals[12]. The cytosolic Ca^{2+} traces recorded in the cMCU-deficient and in the wild-type lines in response to mannitol and salt stress were found to be nearly superimposable (Supplementary Fig. 12b,c). This finding is not surprising as osmotic (mannitol or sorbitol) and salt stress trigger overlapping but distinct signals (for example, in ref. [29]).

Plants lacking cMCU did not display growth defects (Supplementary Fig. 13a,b), impaired photosynthetic efficiency (Supplementary Fig. 13c) or altered chloroplast ultrastructure (Supplementary Fig. 13d) under normal growth conditions. In *Arabidopsis*, the plastidial calcium sensor CAS shapes stress-related stromal Ca^{2+} transients[13] and is involved in the regulation of the pathogen response-linked ABI4 transcription factor by Ca^{2+}-modulated MAPK[7]. Thus, we investigated cMCU-dependent activation of MAPK3 and MAPK6 (collectively, MAPK3/6). MAPK cascades are activated by various endogenous and exogenous stimuli and participate in cellular functions ranging from developmental processes to biotic and abiotic stress responses (for example, in ref. [30]). Short-term exposure of plants to 20 mM H_2O_2 or to osmotic stress are known to activate MAPK6, resulting in phosphorylation of the kinase itself[31]. Some MAPKs can be activated in a Ca^{2+}-dependent manner[7]. Others, such as MAPK3/6, can be deactivated by dephoshorylation mediated by Ca^{2+}-dependent MAPK phosphatase 1 (MPK1)[32]. Here we focused on mannitol-induced osmotic stress, since it affected only stromal Ca^{2+} concentration in a cMCU-dependent manner but did not influence the bulk cytosolic Ca^{2+} concentration. Acute application of mannitol for 10 min increased MAPK3/6 phosphorylation in leaves of both cMCU knockout lines compared with wild-type leaves (Fig. 3g), suggesting that in wild-type plants, stromal Ca^{2+} transients are either required for activation of a phosphatase that downregulates MAPK3/6 or for modulating the production or release of metabolic factor(s) that regulate MAPK3/6 phosphorylation and thereby MAPK3/6-dependent signalling[33]. The mannitol-induced MAPK3/6 phosphorylation was instead comparable between wild-type and cMCU knockout lines in the dark and in the presence of the cell-permeable reactive oxygen species scavenger *N*-acetylcysteine (NAC) (Fig. 3h and Supplementary Fig. 13e), suggesting that changes induced by osmotic stress were strictly dependent on reactive oxygen species and/or photosynthesis-related chloroplast metabolism. Similarly, it should be noted that differences in chloroplast Ca^{2+} dynamics between wild-type and cMCU knockout lines (Fig. 3c,d) were observed only when Ca^{2+} measurement assays were performed after seedlings were exposed to light, but not when they were kept in the dark (Supplementary Fig. 14a–c). The importance of the photosynthetically active status of chloroplasts in enhancing the organellar Ca^{2+} response to environmental stimuli has been previously highlighted[12].

MAPK6 can be activated in fast retrograde signalling between chloroplast and nucleus[34], where it regulates gene expression of several key transcription factors, including ERF6[35]. On short-term exposure to mannitol, *ERF6* is significantly upregulated, suggesting that a transcriptional cascade involving *ERF6* initiates the early response to mannitol[36] that finally leads to stomata closure. Ca^{2+} signalling is required for expression of ERF6[37] that is among the few genes that are directly connected with *cMCU* in network analysis (http://atted.jp/cgi-bin/locus.cgi?loc=At5g66650). In our experiments, expression levels of *ERF6* remained low within 10 min after mannitol (Fig. 3i) or sorbitol (Supplementary Fig. 15a) treatment in both knockout lines compared with their respective wild-type lines, suggesting that reduced stromal Ca^{2+} transients prevent activation of *ERF6*. ERF6 acts as a master regulator of early mannitol-induced stress response by activating various transcription factors, including MYB factors[36]. Given the presence of cMCU in guard cells, we investigated by reverse transcription with qPCR (RT–qPCR) the expression of the stomata-related transcription factor myb domain protein 60 (MYB60) to gain further information about downstream cellular effects related to cMCU-mediated Ca^{2+} uptake into chloroplasts in response to acute osmotic stress in leaves using mannitol (Fig. 3j) or sorbitol (Supplementary Fig. 15b). The regulatory region of *MYB60* specifically drives gene expression in guard cells of *Arabidopsis* leaves, and levels of *MYB60* transcript increase or decrease under conditions that promote stomata opening (for example in light) or closure (for example in drought or dark), respectively[38]. Whereas *MYB60* transcript level decreased in wild-type leaves within 10 min following application of strong osmotic stress, it remained stable in the two independent cMCU knockout lines (Fig. 3j and Supplementary Fig. 15b). Thus, *MYB60* expression appears to be regulated in response to chloroplast Ca^{2+} concentration following osmotic stress (given the lack of cMCU-dependent changes in the bulk cytosolic Ca^{2+} concentration (Supplementary Fig. 12b)). Blocking photosynthesis with 3-(3,4-dichlorophenyl)-1,1-dimethylurea abolished differences in activation of *ERF6* and *MYB60* between wild-type and cMCU knockout plants (Supplementary Fig. 15c,d), in accordance with results in Fig. 3h and Supplementary Fig. 14a–c. In sum, these data indicate that in light conditions, cMCU is involved in the regulation of plastid-to-nucleus signalling following osmotic stress. In response to osmotic stress, stomata closure normally reduces transpiration and water loss. In contrast to both wild-type ecotypes, stomata pore area did not decrease following osmotic stress applied to detached *Arabidopsis* leaves in cMCU knockout lines (Fig. 4a and Supplementary Fig. 16a). Stomata opening on dark-to-light transition was not impaired in the knockout lines compared with wild-type (Supplementary Fig. 16b). To further investigate this aspect, whole four-week-old plants were cut-off and absolute water content was measured. In agreement with the results shown in Fig. 4a, deficiency of cMCU had a significant impact on normalized water loss (indicating transpiration rate of the plants) within 60 min (Fig. 4b). Both cMCU knockout lines were characterized by constitutive reduction in stomata opening (Fig. 4a), mirroring the behaviour of the MYB60 knockout, which exhibits increased long-term drought tolerance[38]. Both mannitol and sorbitol mimic drought stress. When we subjected intact plants to drought stress by long-term (18 d) water starvation, both cMCU knockout lines were more tolerant than wild-type plants (Fig. 4c–e and Supplementary Fig. 16c), suggesting that both short- and long-term drought responses are cMCU-dependent, but the underlying mechanisms may differ in the two cases. This is illustrated, for example, by changes in photosynthetic efficiency that occur only on the longer-term timescale (Supplementary Fig. 17a,b). Following irrigation for 1 d, cMCU knockouts were able to fully recover leaf turgor and photosynthetic activity, in contrast to wild-type plants (Fig. 4f and Supplementary Fig. 17c).

In summary, these results indicate that specific, osmotic-stress-induced, rapid cMCU-dependent downstream signalling involves MAPK3/6, ERF6 and MYB60, and affects stomata opening (Fig. 4g). Our results identify a bona fide Ca^{2+} channel of chloroplasts with a crucial role in intracellular stress signalling that is able to fine-tune the response of cells to osmotic stress. As the channel is not localized to mitochondria in mesophyll cells, a contribution of mitochondria to the observed signalling is unlikely, although it cannot be excluded. Our data are in line with the findings that mesophyll chloroplasts are key players in extracellular Ca^{2+}-induced stomatal closure[2] and that mutation of the putative chloroplastic Ca^{2+} sensor CAS leads to impaired stomatal movement (reviewed in

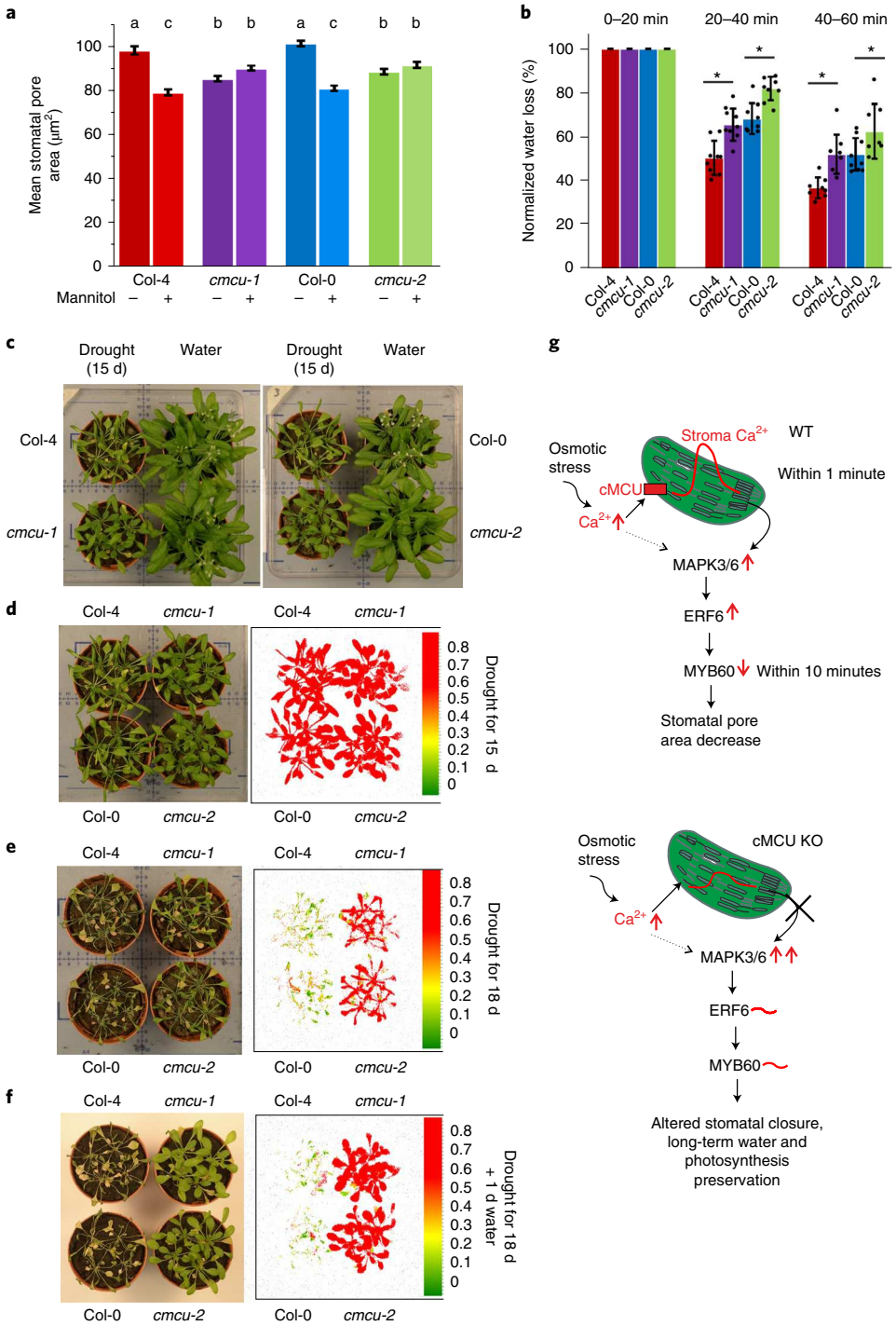

Fig. 4 | Plants lacking cMCU are drought resistant and recover quickly following rewatering. a, Mean stomata size was determined in epidermal strips 30 min following treatment with mannitol (600 mM). $n \geq 155$ for each sample. Statistically significant differences are marked by letters; one-way ANOVA($\alpha = 0.05$) followed by Student's *t*-test ($P < 0.01$). **b**, Four-week-old plants grown under the same conditions and in the same soil were subjected to drought stress. Transpiration rate was calculated as normalized percentage variation of absolute water content. The water content lost in the first 20 min was considered as 100%. $n \geq 10$ for each point. Statistically significant differences are marked by asterisks; one-way ANOVA ($\alpha = 0.05$) followed by Student's *t*-test (*$P < 0.01$). **c**–**e** Wild-type and cMCU knockout plants after 15 d (**c**,**d**) and 18 d (**e**) of water deprivation. **f**, One day of recovery following irrigation was sufficient to restore leaf turgidity and complete photosynthetic efficiency of cMCU mutants; wild-type plants never recovered. $n = 6$ for each genotype. In **d**–**f**, photosynthetic efficiency is indicated by PAM imaging; chlorophyll fluorescence (F_v/F_m) values are indicated on the right scale of the images. **g**, Hypothetical short-term signalling pathway following mannitol-induced osmotic stress in wild-type (top) and cMCU knockout (KO, bottom) plants. In this model, Ca^{2+} concentration changes in the chloroplast stroma fine-tune cytosolic MAPK3/6 phosphorylation. In the absence of cMCU, a plastid-derived factor (a photosynthesis-related metabolite) is either not released or is not active, thereby leading to excessive phosphorylation of MAPK3/6, which alters its kinase activity, leading to reduced stomata closure. This ultimately results in unchanged levels of transcription factors ERF6 and MYB60 (the latter transcription factor is specifically expressed in guard cells). In turn, this inefficient signalling in the cMCU knockout alters stomata closure and, in the longer term, leads to preservation of photosynthetic efficiency and water content in drought-stressed plants.

ref. [10]). Rapid changes in calcium concentration in the chloroplast stroma may directly regulate the production and/or release of different molecules known to be involved in chloroplast-to-nucleus signalling: Calvin cycle-related metabolite export through the triose phosphate–phosphate translocator has been shown to rapidly (within few minutes) activate MAPK6 in response to high light levels[35]. Several enzymes in this pathway, which is active in light (but not in the dark), are known to be inhibited by high stromal Ca^{2+} concentration[6,9]. Therefore, one possible explanation for our observations involves stromal Ca^{2+}-regulated production and/or export of Calvin-cycle metabolites to optimize MAPK3/6 phosphorylation (and to avoid over-phosphorylation)[33]. Alternatively, H_2O_2 may have a role: extracellular Ca^{2+}-induced stomatal closure did not occur in plants treated with NAC, due to the inhibition of chloroplast H_2O_2 synthesis in mesophyll, which has been shown to be dependent on phosphorylation of CAS and light-harvesting complex II[39]. Whether the above players and cMCU affect stomata closure solely by influencing the behaviour of guard cells or whether they also mediate a mesophyll chloroplast-driven guard-cell response is a question for future studies. Likewise, the relationship between CAS and cMCU and the recently described chloroplast Mn^{2+}/H^+ transporters[40,41] affecting Ca^{2+} dynamics remains to be understood. The observations reported here have the potential to be exploited for the biotechnological development of new strategies to alleviate the impact of climate change on agricultural productivity.

Methods

Plasmid construction. cMCU was cloned into the following vectors: (1) pGREAT::EGFP[16] or pGREAT::tdTomato for confocal microscopy; (2) pIVEX1.4 WG (Roche) for in vitro-expression[18]; (3) pET28a (Novagen) for *E. coli* expression[42]. Primers and restriction enzymes used are listed in Supplementary Table 1.

In vitro characterization of cMCU. Electrophysiological bilayer experiments using recombinant cMCU were performed as described in ref. [43]. The His-tagged N-terminal domain was expressed and purified from *E. coli* and cross-linking using glutaraldehyde[44] was performed as described in Supplementary Methods. $^{45}Ca^{2+}$- overlay assay with recombinant cMCU and other Ca^{2+}-binding proteins was carried out as described[45,46]. A molecular model of cMCU was obtained on the basis of recently solved metazoan MCU structures using the fold-recognition server Phyre2.0[23] and was refined with Phenix Interface[47]. See Supplementary Methods for further details.

Calcium uptake into *E. coli* cells expressing aequorin and cMCU. For Ca^{2+}-uptake measurements in *E. coli*, C41(DE3) *E. coli* competent cells were co-transformed with pACYCDuet-1(HA1-Aeq) and pET28a::cMCUΔSP or mutant forms and used as described in Supplementary Methods.

Subcellular localization of cMCU. The subcellular localization of cMCU was examined by confocal microscopy in plants stably expressing cMCU–eGFP or through the agroinfiltration of four-week-old *A. thaliana* leaves[16] and by transformation of protoplasts with pGREAT::cMCU::EGFP[16] or pGREAT::cMCU::tdTomato as described[12,48]. Chlorophyll and EGFP were excited at 488 nm, tdTomato was excited at 543 nm (this wavelength excites chlorophyll to a very low extent). Fluorescence emission was detected at 515–525 nm, 560–620 nm and 680–720 nm for EGFP, tdTomato and chlorophyll, respectively. See Supplementary Methods for further details. Percoll-purified chloroplasts were obtained from plants expressing cMCU–EGFP according to the protocol described in ref. [49] and tested for the presence of the fusion protein by western blot.

Plant material and characterization. Two independent transfer DNA insertion lines for the *At5g66650* locus were SK16605 (*cmcu-1*) and SALK_031408 (*cmcu-2*). Photosynthetic efficiency was measured by pulse amplitude modulator (PAM) as in ref. [18].

Aequorin-based Ca^{2+} measurements in intact plants. For Ca^{2+} measurements, wild-type and knockout *Arabidopsis* lines were transformed with constructs encoding yellow fluorescent protein–aequorin chimaeras targeted to the cytosol, chloroplast stroma[25] or thylakoid lumen[26]. Calibration and analysis was performed according to refs. [50,51].

Stress assessment. Intact plants were treated with 600 mM mannitol or sorbitol to induce osmotic stress. MAPK3/6 assay was performed using phospho-p44/42 MAPK (ERK1/2) (Thr202/Tyr204) antibody (Cell Signaling Technology)[52].

Determination of absolute water content and stomatal pore area is described in the Supplementary Methods. RT–qPCR was performed to assess expression of *cMCU* in different tissues and expression of *ERF6* and *MYB60* under different conditions. Data were analysed by the $\Delta\Delta C_t$ method[53] with respect to untreated samples. Further experimental details are given in the Supplementary Methods.

Reporting Summary. Further information on research design is available in the Nature Research Reporting Summary linked to this article.

Data availability

The data that support the findings of this study are available from the corresponding authors upon request.

Received: 9 July 2018; Accepted: 23 April 2019;
Published online: 10 June 2019

References

1. Kudla, J. et al. Advances and current challenges in calcium signaling. *New Phytol.* **218**, 414–431 (2018).
2. Zhu, J. K. Abiotic stress signaling and responses in plants. *Cell* **167**, 313–324 (2016).
3. Leister, D., Wang, L. & Kleine, T. Organellar gene expression and acclimation of plants to environmental stress. *Front. Plant Sci.* **8**, 387 (2017).
4. Dodd, A. N., Kudla, J. & Sanders, D. The language of calcium signaling. *Annu. Rev. Plant Biol.* **61**, 593–620 (2010).
5. Kmiecik, P., Leonardelli, M. & Teige, M. Novel connections in plant organellar signalling link different stress responses and signalling pathways. *J. Exp. Bot.* **67**, 3793–3807 (2016).
6. Nomura, H. & Shiina, T. Calcium signaling in plant endosymbiotic organelles: mechanism and role in physiology. *Mol. Plant* **7**, 1094–1104 (2014).
7. Guo, H. et al. Plastid–nucleus communication involves calcium-modulated MAPK signalling. *Nat. Commun.* **7**, 12173 (2016).
8. Sai, J. & Johnson, C. H. Dark-stimulated calcium ion fluxes in the chloroplast stroma and cytosol. *Plant Cell* **14**, 1279–1291 (2002).
9. Stael, S. et al. Plant organellar calcium signalling: an emerging field. *J. Exp. Bot.* **63**, 1525–1542 (2012).
10. Hochmal, A. K., Schulze, S., Trompelt, K. & Hippler, M. Calcium-dependent regulation of photosynthesis. *Biochim. Biophys. Acta* **1847**, 993–1003 (2015).
11. Loro, G. et al. Chloroplast-specific in vivo Ca^{2+} imaging using yellow cameleon fluorescent protein sensors reveals organelle-autonomous Ca^{2+} signatures in the stroma. *Plant Physiol.* **171**, 2317–2330 (2016).
12. Sello, S. et al. Dissecting stimulus-specific Ca^{2+} signals in amyloplasts and chloroplasts of *Arabidopsis thaliana* cell suspension cultures. *J. Exp. Bot.* **67**, 3965–3974 (2016).
13. Nomura, H. et al. Chloroplast-mediated activation of plant immune signalling in *Arabidopsis*. *Nat. Commun.* **3**, 926 (2012).
14. Costa, A., Navazio, L. & Szabo, I. The contribution of organelles to plant intracellular calcium signalling. *J. Exp. Bot.* **69**, 4175–4193 (2018).
15. Carraretto, L. et al. Ion channels in plant bioenergetic organelles chloroplast and mitochondria: from molecular identification to function. *Mol. Plant* **9**, 371–395 (2016).
16. Carraretto, L. et al. A thylakoid-located two-pore K^+ channel controls photosynthetic light utilization in plants. *Science* **342**, 114–118 (2013).
17. De Stefani, D., Raffaello, A., Teardo, E., Szabo, I. & Rizzuto, R. A forty-kilodalton protein of the inner membrane is the mitochondrial calcium uniporter. *Nature* **476**, 336–340 (2011).
18. Teardo, E. et al. Physiological characterization of a plant mitochondrial calcium uniporter in vitro and in vivo. *Plant Physiol.* **173**, 1355–1370 (2017).
19. Kreimer, G., Melkonian, M., Holtum, J. A. & Latzko, E. Characterization of calcium fluxes across the envelope of intact spinach chloroplasts. *Planta* **166**, 515–523 (1985).
20. Nguyen, N. X. et al. Cryo-EM structure of a fungal mitochondrial calcium uniporter. *Nature* **559**, 570–574 (2018).
21. Yoo, J. et al. Cryo-EM structure of a mitochondrial calcium uniporter. *Science* **361**, 506–511 (2018).
22. Baradaran, R., Wang, C., Siliciano, A. F. & Long, S. B. Cryo-EM structures of fungal and metazoan mitochondrial calcium uniporters. *Nature* **559**, 580–584 (2018).
23. Kelley, L. A., Mezulis, S., Yates, C. M., Wass, M. N. & Sternberg, M. J. The Phyre2 web portal for protein modeling, prediction and analysis. *Nat. Protoc.* **10**, 845–858 (2015).
24. McAinsh, M. R. & Pittman, J. K. Shaping the calcium signature. *New Phytol.* **181**, 275–294 (2009).
25. Mehlmer, N. et al. A toolset of aequorin expression vectors for in planta studies of subcellular calcium concentrations in *Arabidopsis thaliana*. *J. Exp. Bot.* **63**, 1751–1761 (2012).

26. Sello, S. et al. Chloroplast Ca^{2+} fluxes into and across thylakoids revealed by thylakoid-targeted aequorin probes. *Plant Physiol.* **177**, 38–51 (2018).
27. Kazama, D., Kurusu, T., Mitsuda, N., Ohme-Takagi, M. & Tada, Y. Involvement of elevated proline accumulation in enhanced osmotic stress tolerance in *Arabidopsis* conferred by chimeric repressor gene silencing technology. *Plant Signal. Behav.* **9**, e28211 (2014).
28. Shkolnik, D., Nuriel, R., Bonza, M. C., Costa, A. & Fromm, H. MIZ1 regulates ECA1 to generate a slow, long-distance phloem-transmitted Ca^{2+} signal essential for root water tracking in *Arabidopsis*. *Proc. Natl Acad. Sci. USA* **115**, 8031–8036 (2018).
29. Choudhury, F. K., Rivero, R. M., Blumwald, E. & Mittler, R. Reactive oxygen species, abiotic stress and stress combination. *Plant J.* **90**, 856–867 (2017).
30. de Zelicourt, A., Colcombet, J. & Hirt, H. The role of MAPK modules and ABA during abiotic stress signaling. *Trends Plant Sci.* **21**, 677–685 (2016).
31. Ichimura, K., Mizoguchi, T., Yoshida, R., Yuasa, T. & Shinozaki, K. Various abiotic stresses rapidly activate *Arabidopsis* MAP kinases ATMPK4 and ATMPK6. *Plant J.* **24**, 655–665 (2000).
32. Lee, K. et al. Regulation of MAPK phosphatase 1 (*At*MKP1) by calmodulin in *Arabidopsis*. *J. Biol. Chem.* **283**, 23581–23588 (2008).
33. Brock, A. K. et al. The *Arabidopsis* mitogen-activated protein kinase phosphatase PP2C5 affects seed germination, stomatal aperture, and abscisic acid-inducible gene expression. *Plant Physiol.* **153**, 1098–1111 (2010).
34. Meng, X. & Zhang, S. MAPK cascades in plant disease resistance signaling. *Annu Rev. Phytopathol.* **51**, 245–266 (2013).
35. Vogel, M. O. et al. Fast retrograde signaling in response to high light involves metabolite export, MITOGEN-ACTIVATED PROTEIN KINASE6, and AP2/ERF transcription factors in Arabidopsis. *Plant Cell* **26**, 1151–1165 (2014).
36. Dubois, M. et al. The ETHYLENE RESPONSE FACTORs ERF6 and ERF11 antagonistically regulate mannitol-induced growth inhibition in *Arabidopsis*. *Plant Physiol.* **169**, 166–179 (2015).
37. Sewelam, N. et al. Ethylene response factor 6 is a regulator of reactive oxygen species signaling in *Arabidopsis*. *PLoS ONE* **8**, e70289 (2013).
38. Cominelli, E. et al. A guard-cell-specific MYB transcription factor regulates stomatal movements and plant drought tolerance. *Curr. Biol.* **15**, 1196–1200 (2005).
39. Wang, W. H. et al. The reduced state of the plastoquinone pool is required for chloroplast-mediated stomatal closure in response to calcium stimulation. *Plant J.* **86**, 132–144 (2016).
40. Frank, J. et al. Chloroplast-localized BICAT proteins shape stromal calcium signals and are required for efficient photosynthesis. *New Phytol.* **221**, 866–880 (2019).
41. Schneider, A. et al. The evolutionarily conserved protein PHOTOSYNTHESIS AFFECTED MUTANT71 is required for efficient manganese uptake at the thylakoid membrane in *Arabidopsis*. *Plant Cell* **28**, 892–910 (2016).
42. Patron, M. et al. MICU1 and MICU2 finely tune the mitochondrial Ca^{2+} uniporter by exerting opposite effects on MCU activity. *Mol. Cell* **53**, 726–737 (2014).
43. Raffaello, A. et al. The mitochondrial calcium uniporter is a multimer that can include a dominant-negative pore-forming subunit. *EMBO J.* **32**, 2362–2376 (2013).
44. Fadouloglou, V. E., Kokkinidis, M. & Glykos, N. M. Determination of protein oligomerization state: two approaches based on glutaraldehyde crosslinking. *Anal. Biochem.* **373**, 404–406 (2008).
45. Maruyama, K., Mikawa, T. & Ebashi, S. Detection of calcium binding proteins by ^{45}Ca autoradiography on nitrocellulose membrane after sodium dodecyl sulfate gel electrophoresis. *J. Biochem.* **95**, 511–519 (1984).
46. Wagner, S. et al. The EF-hand Ca^{2+} binding protein MICU choreographs mitochondrial Ca^{2+} dynamics in *Arabidopsis*. *Plant cell* **27**, 3190–3212 (2015).
47. Adams, P. D. et al. PHENIX: a comprehensive Python-based system for macromolecular structure solution. *Acta Crystallogr. D* **66**, 213–221 (2010).
48. Yoo, S. D., Cho, Y. H. & Sheen, J. *Arabidopsis* mesophyll protoplasts: a versatile cell system for transient gene expression analysis. *Nat. Protoc.* **2**, 1565–1572 (2007).
49. Seigneurin-Berny, D., Salvi, D., Dorne, A. J., Joyard, J. & Rolland, N. Percoll-purified and photosynthetically active chloroplasts from *Arabidopsis thaliana* leaves. *Plant Physiol. Biochem.* **46**, 951–955 (2008).
50. Brini, M. et al. Transfected aequorin in the measurement of cytosolic Ca^{2+} concentration ($[Ca^{2+}]_c$). A critical evaluation. *J. Biol. Chem.* **270**, 9896–9903 (1995).
51. Ottolini, D., Cali, T. & Brini, M. Methods to measure intracellular Ca^{2+} fluxes with organelle-targeted aequorin-based probes. *Methods Enzymol.* **543**, 21–45 (2014).
52. Flury, P., Klauser, D., Schulze, B., Boller, T. & Bartels, S. The anticipation of danger: microbe-associated molecular pattern perception enhances AtPep-triggered oxidative burst. *Plant Physiol.* **161**, 2023–2035 (2013).
53. Livak, K. J. & Schmittgen, T. D. Analysis of relative gene expression data using real-time quantitative PCR and the $2-\Delta\Delta c_T$ method. *Methods* **25**, 402–408 (2001).

Acknowledgements

The authors thank A. Weber, D. Leister, A. Costa, G. Finazzi, W. Martin and F. Lo Schiavo for useful discussions. We thank Human Frontiers Science Program (HFSP RG0052 to I.S.), the University of Padova (PRID 2018 prot. BIRD180317 to L.N. and STARS (Supporting Talents in Research project) to L.Carraretto), the MIUR (FFABR 2017 to E.F.), the EU within the Marie-Curie ITN CALIPSO (FP7, Project no. 607607 to U.C.V.) for financial support.

Author contribution

I.S., L.N., L.Cendron, E.F. and E.T. designed experiments; E.T., L.Carraretto, R.M., E.C., M.V., M.F., L.M. and S.D.B. performed experiments; I.S., L.N., L.Cendron, L.Carraretto, E.F., E.T., T.C. and U.C.V. analysed data; I.S., L.N., L.Cendron, E.F. and E.T. wrote the manuscript. I.S., L.N., E.F., U.C.V. and L.Carraretto acquired funding.

Competing interests

The authors declare no competing interests.

Additional information

Supplementary information is available for this paper at https://doi.org/10.1038/s41477-019-0434-8.

Reprints and permissions information is available at www.nature.com/reprints.

Correspondence and requests for materials should be addressed to E.F., L.N. or I.S.

Journal peer review information: *Nature Plants* thanks Jose Feijo, Simon Stael and Tou Cheu Xiong for their contribution to the peer review of this work.

Publisher's note: Springer Nature remains neutral with regard to jurisdictional claims in published maps and institutional affiliations.

nature research

Corresponding author(s): Ildiko Szabo

Last updated by author(s): March 26th, 2019

Reporting Summary

Nature Research wishes to improve the reproducibility of the work that we publish. This form provides structure for consistency and transparency in reporting. For further information on Nature Research policies, see Authors & Referees and the Editorial Policy Checklist.

Statistics

For all statistical analyses, confirm that the following items are present in the figure legend, table legend, main text, or Methods section.

n/a	Confirmed	
☐	☒	The exact sample size (*n*) for each experimental group/condition, given as a discrete number and unit of measurement
☐	☒	A statement on whether measurements were taken from distinct samples or whether the same sample was measured repeatedly
☐	☒	The statistical test(s) used AND whether they are one- or two-sided *Only common tests should be described solely by name; describe more complex techniques in the Methods section.*
☒	☐	A description of all covariates tested
☒	☐	A description of any assumptions or corrections, such as tests of normality and adjustment for multiple comparisons
☐	☒	A full description of the statistical parameters including central tendency (e.g. means) or other basic estimates (e.g. regression coefficient) AND variation (e.g. standard deviation) or associated estimates of uncertainty (e.g. confidence intervals)
☒	☐	For null hypothesis testing, the test statistic (e.g. *F*, *t*, *r*) with confidence intervals, effect sizes, degrees of freedom and *P* value noted *Give P values as exact values whenever suitable.*
☒	☐	For Bayesian analysis, information on the choice of priors and Markov chain Monte Carlo settings
☒	☐	For hierarchical and complex designs, identification of the appropriate level for tests and full reporting of outcomes
☒	☐	Estimates of effect sizes (e.g. Cohen's *d*, Pearson's *r*), indicating how they were calculated

Our web collection on statistics for biologists contains articles on many of the points above.

Software and code

Policy information about availability of computer code

Data collection	PCLAMP8.0 and to collect data.
Data analysis	PCLAMP8.0, Origin 6.0, FijiImageJ, Microsoft Excel

For manuscripts utilizing custom algorithms or software that are central to the research but not yet described in published literature, software must be made available to editors/reviewers. We strongly encourage code deposition in a community repository (e.g. GitHub). See the Nature Research guidelines for submitting code & software for further information.

Data

Policy information about availability of data

All manuscripts must include a data availability statement. This statement should provide the following information, where applicable:

- Accession codes, unique identifiers, or web links for publicly available datasets
- A list of figures that have associated raw data
- A description of any restrictions on data availability

All data are available through contacting the corresponding authors.

Field-specific reporting

Please select the one below that is the best fit for your research. If you are not sure, read the appropriate sections before making your selection.

☒ Life sciences ☐ Behavioural & social sciences ☐ Ecological, evolutionary & environmental sciences

For a reference copy of the document with all sections, see nature.com/documents/nr-reporting-summary-flat.pdf

Life sciences study design

All studies must disclose on these points even when the disclosure is negative.

Sample size	Sample size was chosen in a way to obtain statistically significant differences working with at least 3 biological replicates.
Data exclusions	No data were excluded.
Replication	At least 3 biological replicates have been performed in addition to technical replicates.
Randomization	Allocation was dependent on the genotype. Within the same genotype selection of samples was random.
Blinding	Stomata area measurements were blinded and performed by two independent researchers.

Reporting for specific materials, systems and methods

We require information from authors about some types of materials, experimental systems and methods used in many studies. Here, indicate whether each material, system or method listed is relevant to your study. If you are not sure if a list item applies to your research, read the appropriate section before selecting a response.

Materials & experimental systems

n/a	Involved in the study
☐	☒ Antibodies
☐	☐ Eukaryotic cell lines
☐	☐ Palaeontology
☐	☐ Animals and other organisms
☐	☐ Human research participants
☐	☐ Clinical data

Methods

n/a	Involved in the study
☐	☐ ChIP-seq
☐	☐ Flow cytometry
☐	☐ MRI-based neuroimaging

Antibodies

Antibodies used	Antibodies anti-AEQ (Abcam), anti-GFP (Sigma), anti-AOX and anti-D1 (Agrisera).
Validation	The antibodies used in this study were commercially available and validated by the supplier.

Eukaryotic cell lines

Policy information about cell lines

Cell line source(s)	*State the source of each cell line used.*
Authentication	*Describe the authentication procedures for each cell line used OR declare that none of the cell lines used were authenticated.*
Mycoplasma contamination	*Confirm that all cell lines tested negative for mycoplasma contamination OR describe the results of the testing for mycoplasma contamination OR declare that the cell lines were not tested for mycoplasma contamination.*
Commonly misidentified lines (See ICLAC register)	*Name any commonly misidentified cell lines used in the study and provide a rationale for their use.*

Palaeontology

Specimen provenance	*Provide provenance information for specimens and describe permits that were obtained for the work (including the name of the issuing authority, the date of issue, and any identifying information).*
Specimen deposition	*Indicate where the specimens have been deposited to permit free access by other researchers.*
Dating methods	*If new dates are provided, describe how they were obtained (e.g. collection, storage, sample pretreatment and measurement), where they were obtained (i.e. lab name), the calibration program and the protocol for quality assurance OR state that no new dates are provided.*

☐ Tick this box to confirm that the raw and calibrated dates are available in the paper or in Supplementary Information.

Animals and other organisms

Policy information about studies involving animals; ARRIVE guidelines recommended for reporting animal research

Laboratory animals	*For laboratory animals, report species, strain, sex and age OR state that the study did not involve laboratory animals.*
Wild animals	*Provide details on animals observed in or captured in the field; report species, sex and age where possible. Describe how animals were caught and transported and what happened to captive animals after the study (if killed, explain why and describe method; if released, say where and when) OR state that the study did not involve wild animals.*
Field-collected samples	*For laboratory work with field-collected samples, describe all relevant parameters such as housing, maintenance, temperature, photoperiod and end-of-experiment protocol OR state that the study did not involve samples collected from the field.*
Ethics oversight	*Identify the organization(s) that approved or provided guidance on the study protocol, OR state that no ethical approval or guidance was required and explain why not.*

Note that full information on the approval of the study protocol must also be provided in the manuscript.

Human research participants

Policy information about studies involving human research participants

Population characteristics	*Describe the covariate-relevant population characteristics of the human research participants (e.g. age, gender, genotypic information, past and current diagnosis and treatment categories). If you filled out the behavioural & social sciences study design questions and have nothing to add here, write "See above."*
Recruitment	*Describe how participants were recruited. Outline any potential self-selection bias or other biases that may be present and how these are likely to impact results.*
Ethics oversight	*Identify the organization(s) that approved the study protocol.*

Note that full information on the approval of the study protocol must also be provided in the manuscript.

Clinical data

Policy information about clinical studies

All manuscripts should comply with the ICMJE guidelines for publication of clinical research and a completed CONSORT checklist must be included with all submissions.

Clinical trial registration	*Provide the trial registration number from ClinicalTrials.gov or an equivalent agency.*
Study protocol	*Note where the full trial protocol can be accessed OR if not available, explain why.*
Data collection	*Describe the settings and locales of data collection, noting the time periods of recruitment and data collection.*
Outcomes	*Describe how you pre-defined primary and secondary outcome measures and how you assessed these measures.*

ChIP-seq

Data deposition

☐ Confirm that both raw and final processed data have been deposited in a public database such as GEO.

☐ Confirm that you have deposited or provided access to graph files (e.g. BED files) for the called peaks.

Data access links *May remain private before publication.*	*For "Initial submission" or "Revised version" documents, provide reviewer access links. For your "Final submission" document, provide a link to the deposited data.*
Files in database submission	*Provide a list of all files available in the database submission.*
Genome browser session (e.g. UCSC)	*Provide a link to an anonymized genome browser session for "Initial submission" and "Revised version" documents only, to enable peer review. Write "no longer applicable" for "Final submission" documents.*

Methodology

Replicates	*Describe the experimental replicates, specifying number, type and replicate agreement.*
Sequencing depth	*Describe the sequencing depth for each experiment, providing the total number of reads, uniquely mapped reads, length of reads and whether they were paired- or single-end.*
Antibodies	*Describe the antibodies used for the ChIP-seq experiments; as applicable, provide supplier name, catalog number, clone*

Antibodies	*name, and lot number.*
Peak calling parameters	*Specify the command line program and parameters used for read mapping and peak calling, including the ChIP, control and index files used.*
Data quality	*Describe the methods used to ensure data quality in full detail, including how many peaks are at FDR 5% and above 5-fold enrichment.*
Software	*Describe the software used to collect and analyze the ChIP-seq data. For custom code that has been deposited into a community repository, provide accession details.*

Flow Cytometry

Plots

Confirm that:

☐ The axis labels state the marker and fluorochrome used (e.g. CD4-FITC).

☐ The axis scales are clearly visible. Include numbers along axes only for bottom left plot of group (a 'group' is an analysis of identical markers).

☐ All plots are contour plots with outliers or pseudocolor plots.

☐ A numerical value for number of cells or percentage (with statistics) is provided.

Methodology

Sample preparation	*Describe the sample preparation, detailing the biological source of the cells and any tissue processing steps used.*
Instrument	*Identify the instrument used for data collection, specifying make and model number.*
Software	*Describe the software used to collect and analyze the flow cytometry data. For custom code that has been deposited into a community repository, provide accession details.*
Cell population abundance	*Describe the abundance of the relevant cell populations within post-sort fractions, providing details on the purity of the samples and how it was determined.*
Gating strategy	*Describe the gating strategy used for all relevant experiments, specifying the preliminary FSC/SSC gates of the starting cell population, indicating where boundaries between "positive" and "negative" staining cell populations are defined.*

☐ Tick this box to confirm that a figure exemplifying the gating strategy is provided in the Supplementary Information.

Magnetic resonance imaging

Experimental design

Design type	*Indicate task or resting state; event-related or block design.*
Design specifications	*Specify the number of blocks, trials or experimental units per session and/or subject, and specify the length of each trial or block (if trials are blocked) and interval between trials.*
Behavioral performance measures	*State number and/or type of variables recorded (e.g. correct button press, response time) and what statistics were used to establish that the subjects were performing the task as expected (e.g. mean, range, and/or standard deviation across subjects).*

Acquisition

Imaging type(s)	*Specify: functional, structural, diffusion, perfusion.*
Field strength	*Specify in Tesla*
Sequence & imaging parameters	*Specify the pulse sequence type (gradient echo, spin echo, etc.), imaging type (EPI, spiral, etc.), field of view, matrix size, slice thickness, orientation and TE/TR/flip angle.*
Area of acquisition	*State whether a whole brain scan was used OR define the area of acquisition, describing how the region was determined.*

Diffusion MRI ☐ Used ☐ Not used

Preprocessing

Preprocessing software	*Provide detail on software version and revision number and on specific parameters (model/functions, brain extraction, segmentation, smoothing kernel size, etc.).*

Normalization

If data were normalized/standardized, describe the approach(es): specify linear or non-linear and define image types used for transformation OR indicate that data were not normalized and explain rationale for lack of normalization.

Normalization template

Describe the template used for normalization/transformation, specifying subject space or group standardized space (e.g. original Talairach, MNI305, ICBM152) OR indicate that the data were not normalized.

Noise and artifact removal

Describe your procedure(s) for artifact and structured noise removal, specifying motion parameters, tissue signals and physiological signals (heart rate, respiration).

Volume censoring

Define your software and/or method and criteria for volume censoring, and state the extent of such censoring.

Statistical modeling & inference

Model type and settings

Specify type (mass univariate, multivariate, RSA, predictive, etc.) and describe essential details of the model at the first and second levels (e.g. fixed, random or mixed effects; drift or auto-correlation).

Effect(s) tested

Define precise effect in terms of the task or stimulus conditions instead of psychological concepts and indicate whether ANOVA or factorial designs were used.

Specify type of analysis: ☐ Whole brain ☐ ROI-based ☐ Both

Statistic type for inference
(See Eklund et al. 2016)

Specify voxel-wise or cluster-wise and report all relevant parameters for cluster-wise methods.

Correction

Describe the type of correction and how it is obtained for multiple comparisons (e.g. FWE, FDR, permutation or Monte Carlo).

Models & analysis

n/a	Involved in the study
☐	☐ Functional and/or effective connectivity
☐	☐ Graph analysis
☐	☐ Multivariate modeling or predictive analysis

Functional and/or effective connectivity

Report the measures of dependence used and the model details (e.g. Pearson correlation, partial correlation, mutual information).

Graph analysis

Report the dependent variable and connectivity measure, specifying weighted graph or binarized graph, subject- or group-level, and the global and/or node summaries used (e.g. clustering coefficient, efficiency, etc.).

Multivariate modeling and predictive analysis

Specify independent variables, features extraction and dimension reduction, model, training and evaluation metrics.

nature plants

SUPPLEMENTARY INFORMATION

https://doi.org/10.1038/s41477-019-0434-8

In the format provided by the authors and unedited.

A chloroplast-localized mitochondrial calcium uniporter transduces osmotic stress in *Arabidopsis*

Enrico Teardo[1,5], Luca Carraretto[1,5], Roberto Moscatiello[1], Enrico Cortese[1], Mattia Vicario[1], Margherita Festa[1], Lorenzo Maso[1], Sara De Bortoli[1], Tito Calì[2], Ute C. Vothknecht[3], Elide Formentin[1,4]*, Laura Cendron[1], Lorella Navazio[1,4]* and Ildiko Szabo[1,4]*

[1]Department of Biology, University of Padova, Padova, Italy. [2]Department of Biomedical Sciences, University of Padova, Padova, Italy. [3]IZMB - Plant Cell Biology, University of Bonn, Bonn, Germany. [4]Botanical Garden, University of Padova, Padova, Italy. [5]These authors contributed equally: Enrico Teardo, Luca Carraretto. *e-mail: elide.formentin@unipd.it; lorella.navazio@unipd.it; ildiko.szabo@unipd.it

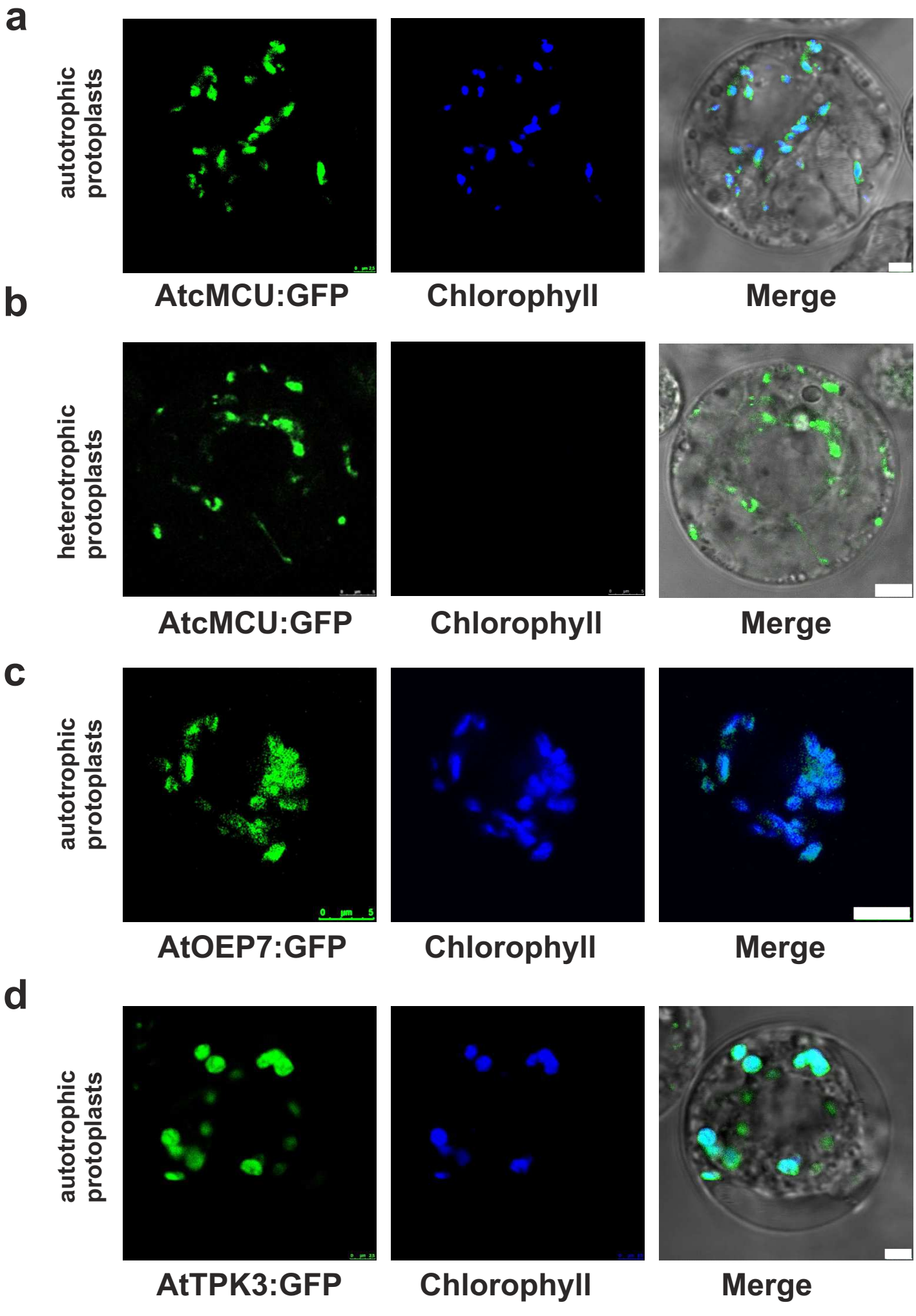

Supplementary Figure 1.

Supplementary Figure 1. An isoform of the mitochondrial calcium uniporter (cMCU) displays localization to chloroplasts when expressed in cultured Arabidopsis cells. a-d Confocal microscopy analyses of protoplasts derived from autotrophic or heterotrophic cell suspension cultures transiently transformed with cMCU:GFP **(a,b)**, with the outer envelope membrane OEP7:GFP **(c)** and with the thylakoid-located TPK3 channel **(d)**. Bars in a) and d): 2,5 µm and in b) and c): 5 µm.

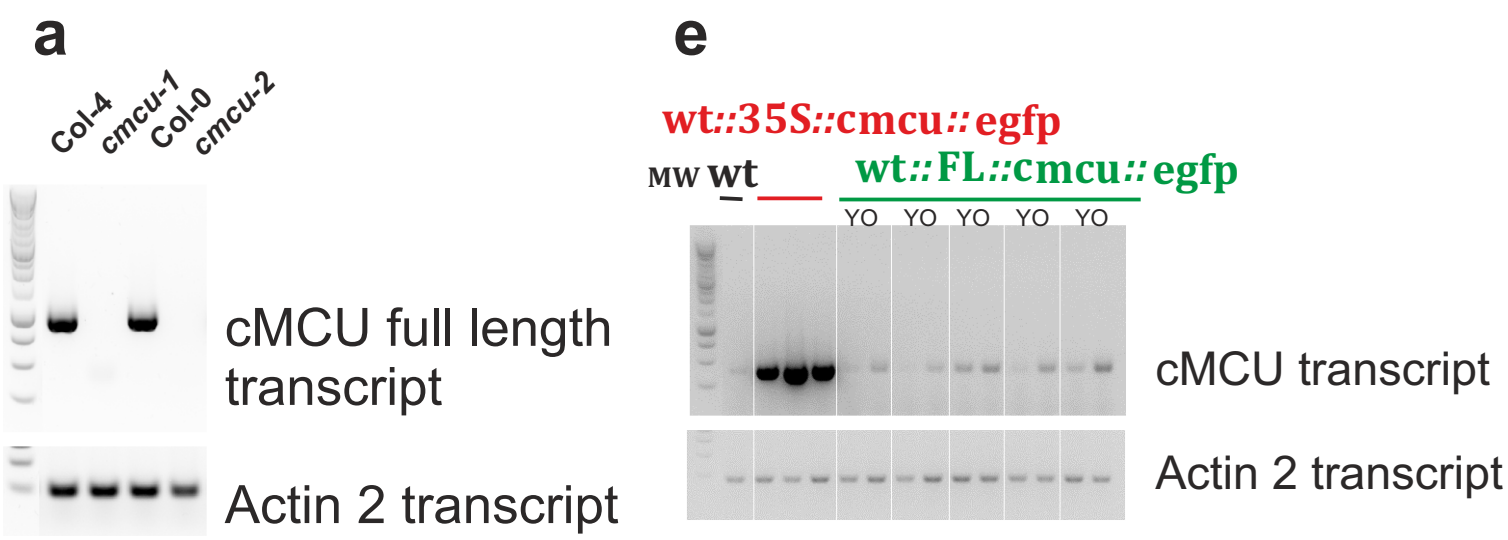

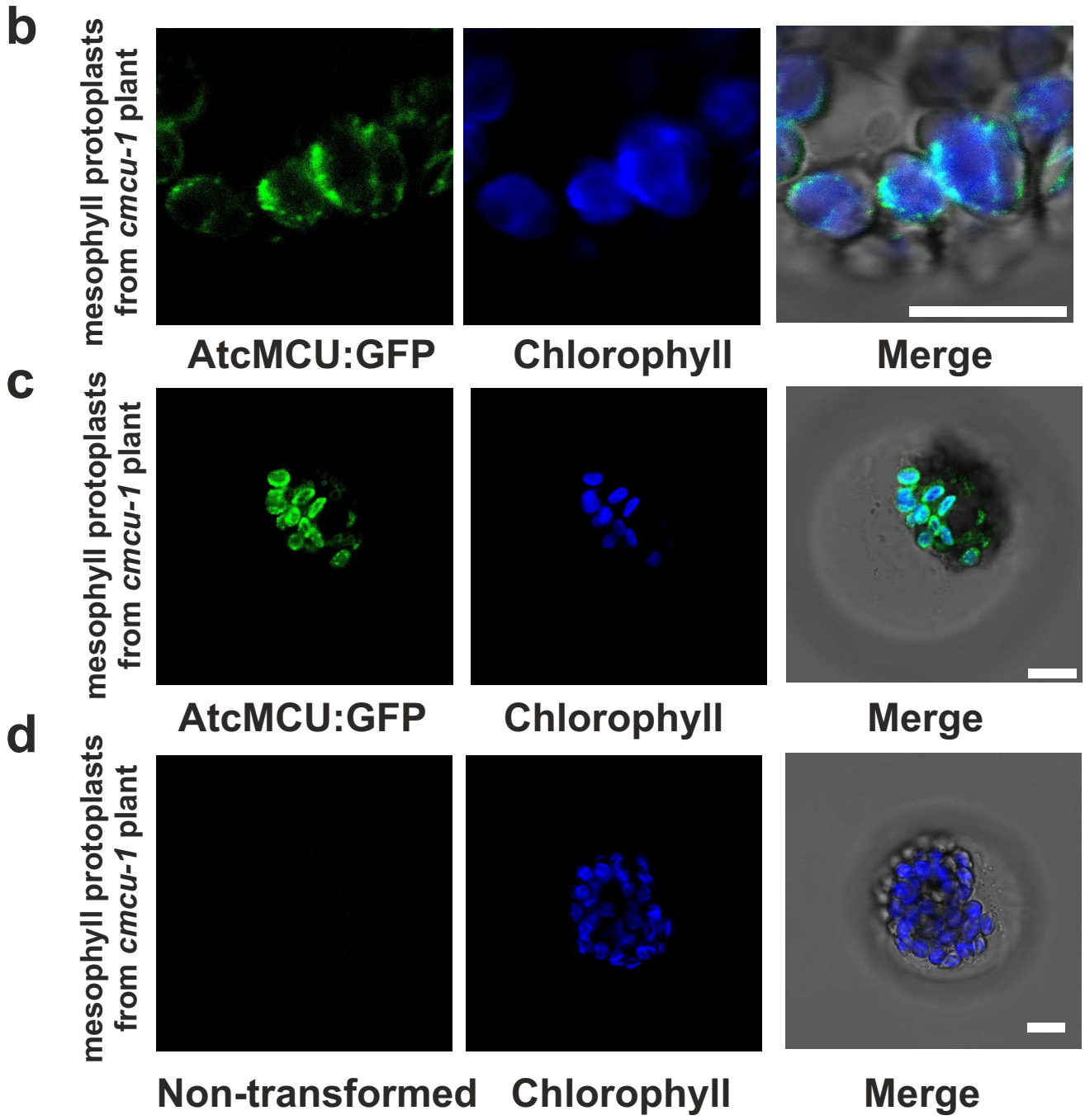

Supplementary Figure 2.

Supplementary Figure 2. Localization of AtcMCU to chloroplasts in cMCU KO plants transiently transformed with cMCU-GFP. **(a)** Transcript level of cMCU in the indicated lines. After genotyping, transcript analysis was made to confirm the absence of cMCU transcript. (**b, c**) Examples of confocal images of protoplasts from cMCU KO plants that were transiently transformed with cMCU-GFP. (**d)** Representative control image obtained from non-transformed cMCU KO plant protoplasts under the same settings of the confocal microscope of (b) and (c). Bars: 10 μm. **(e)** Analysis of cMCU transcript level in the stable lines shows the over-expression in the 2x35S promoter lines and a comparable transcript level (increasing in old leaves (O) with respect to young leaves (Y) in the full locus lines) as revealed by qPCR.

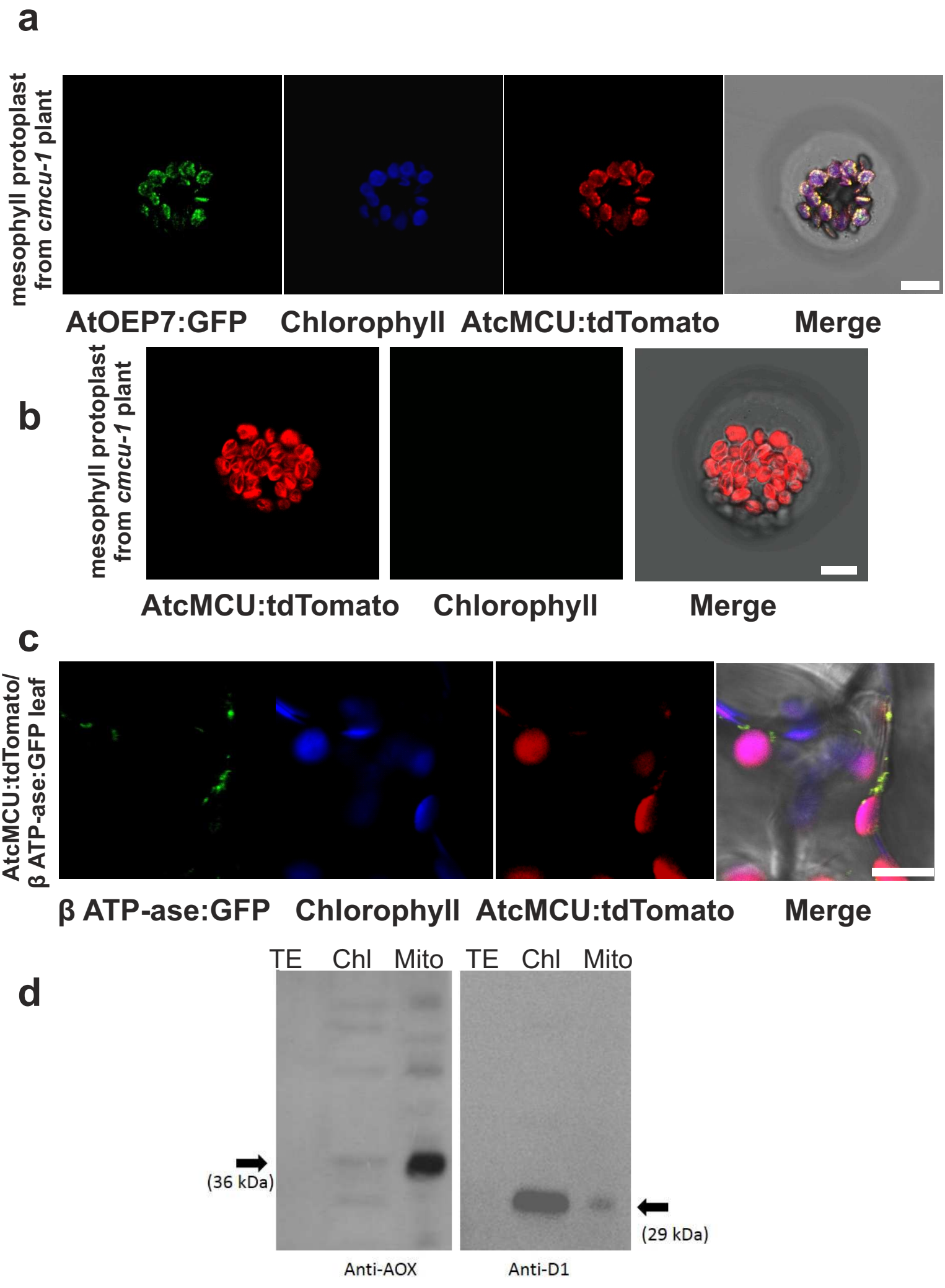

Supplementary Figure 3.

Supplementary Figure 3. Co-localization of AtcMCU and AtOEP7, a marker of the chloroplast envelope membrane. **(a)** Localization of cMCU to chloroplasts in mesophyll cell-derived protoplasts from cMCU KO Arabidopsis plants following transient expression of both OEP7:GFP and cMCU:tdTomato. Autofluorescence of chlorophyll and fluorescence of GFP were recorded following excitation at 488 nm, while that of tdTomato at 543 nm on the same sample in sequential order. (**b**) control images of cMCU:tdTomato -expressing protoplasts excited at only 543 nm, where chlorophyll excitation is negligible. (**c**) Images from intact plants stably expressing mitochondrial β-F1-ATPase-EGFP that have been transformed with cMCU:tdTomato (see also Supplementary Video 1). Bars: 10 μm. (**d**) Purity of chloroplasts isolated from Arabidopsis plants used in Fig. 1d was assessed using an antibody against mitochondrial alternative oxidase and against chloroplast D1 protein. TE: total extract; Chl: chloroplasts; Mito: mitochondria.

Supplementary Figure 4.

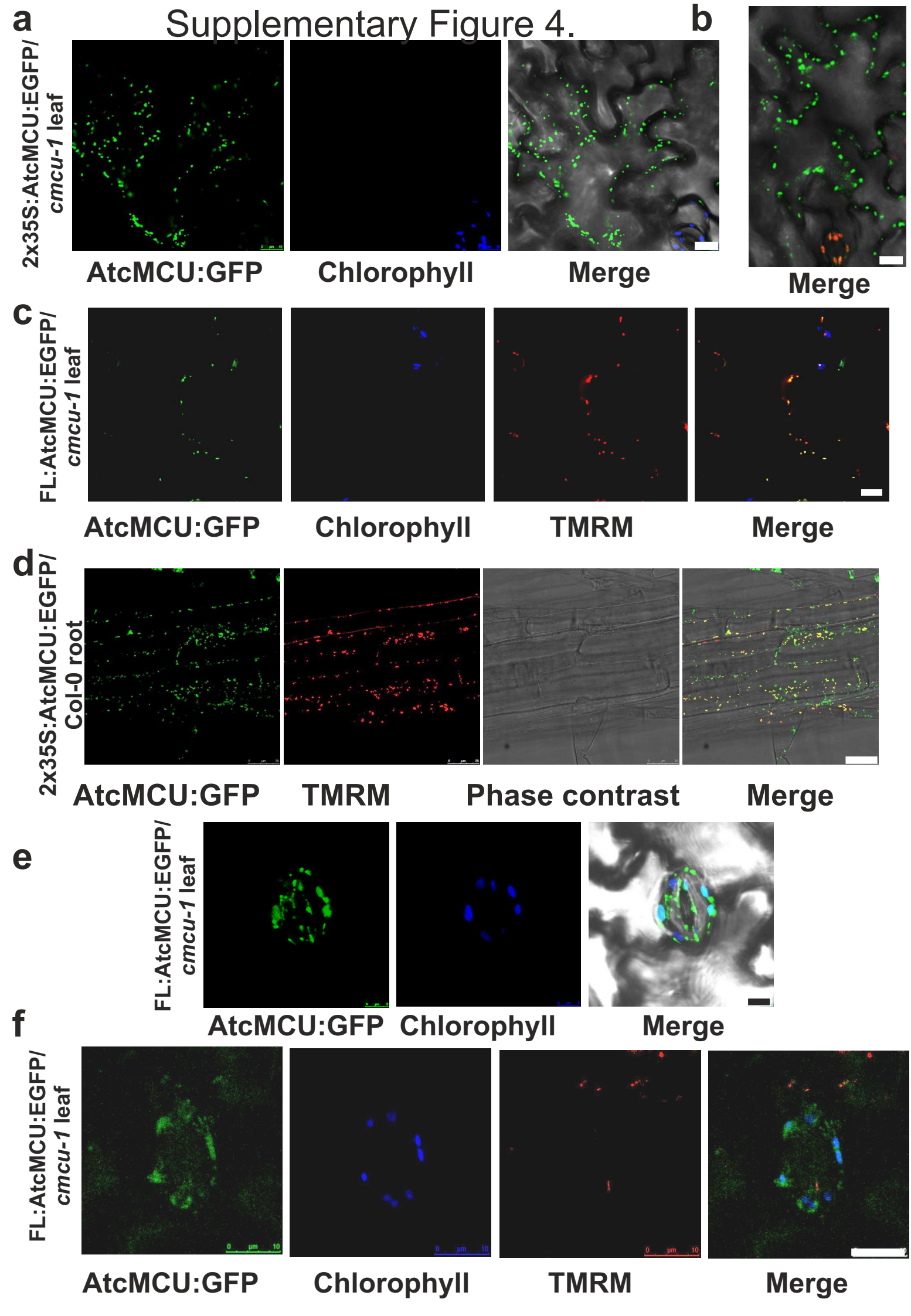

Supplementary Figure 4. Mitochondrial localization of cMCU in epidermal cells and in root of intact plants. (**a** and **b**) AtcMCU expressed in Arabidopsis plants of the indicated genetic background. For **a)** see Supplementary Video 3. (**c**) the same as in a and b, but mitochondrial localization is illustrated by co-localization of the cMCU-EGFP signal with TMRM, a membrane potential sensitive dye. In addition, these organelles were moving similarly to mitochondria (see Supplementary Video 2)[22]. From a-c, bars: 10 μm. **(d**) As in c, performed on root tissue. Bars: 25 μm. (**e,f)** cMCU:GFP co-localizes at least in part with auto-fluorescence of chlorophyll (blue) in guard cells of stomata, while does not fully co-localize with TMRM-stained mitochondria (red) (see also Supplementary Video 4). Bars in e: 5μm, in f: 10 μm.

a

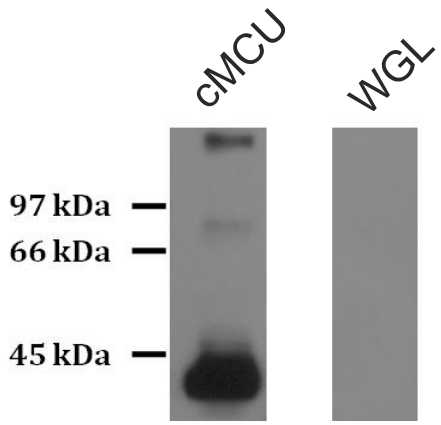

anti-His tag (1: 1000)

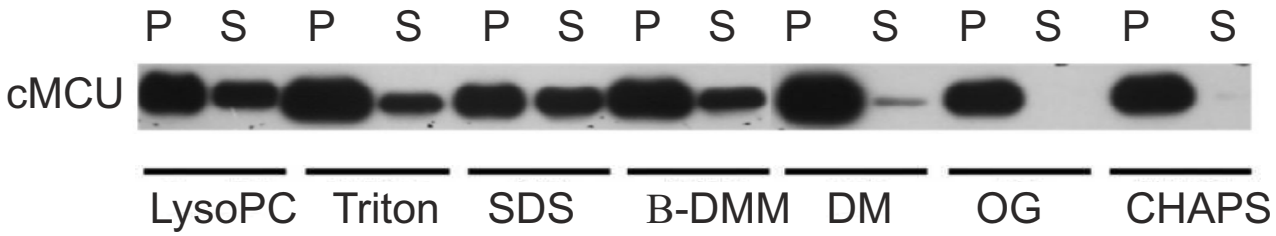

anti-His tag (1: 1000)

b

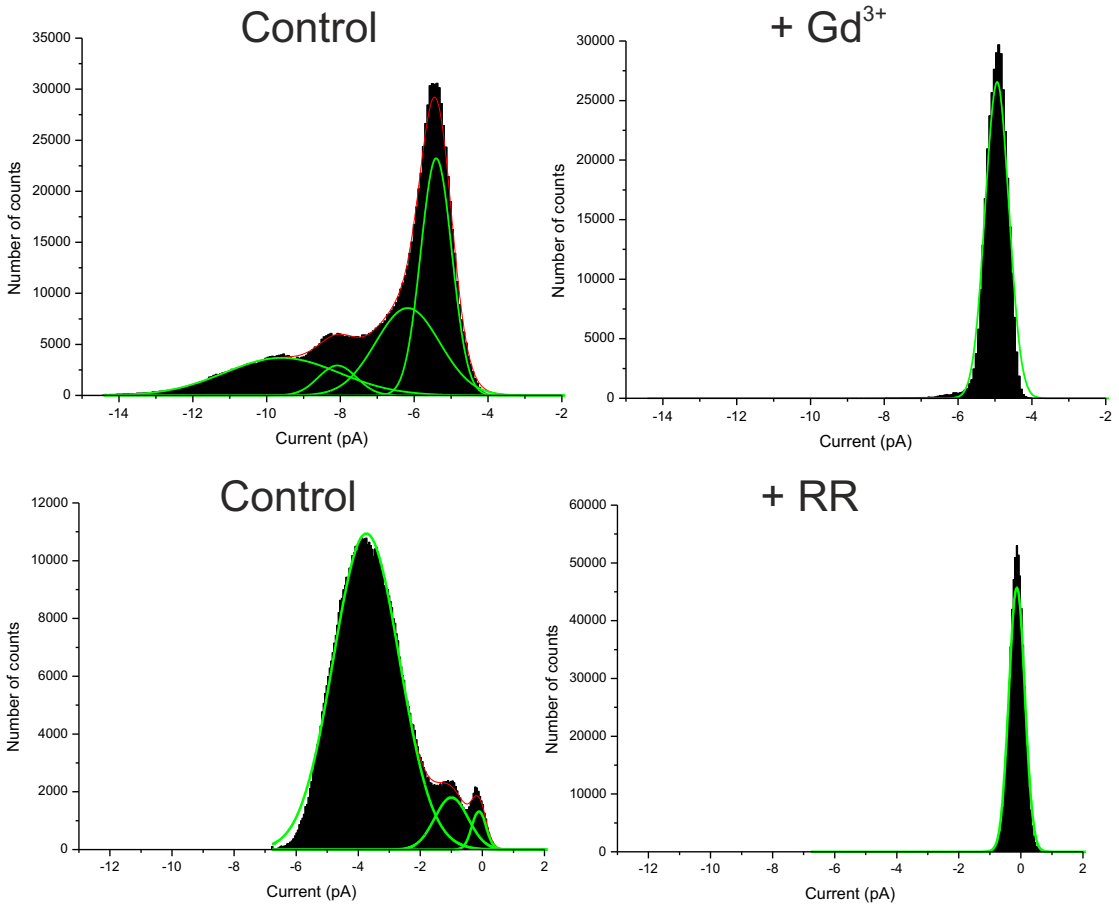

Supplementary Figure 5.

Supplementary Figure 5. In vitro characterization of cMCU (a) cMCU was expressed using a Wheat Germ Lysate Kit. Empty reaction mix (WGL) and mix following expression of the protein were separated by SDS-PAGE and assayed with anti-His tag antibody (upper part). Solubilization of *in vitro*-expressed cMCU with 2% (w/v) of each indicated detergent (lower part). SDS was used as a positive control. Following centrifugation, pellets (P) and supernatants (S) were separated by SDS-PAGE; anti-His tag antibody was used to detect cMCU. Non-denaturant β-DDM (β-dodecyl-maltoside) was selected for protein treatment before electrophysiological experiments. **(b)** Amplitude histograms obtained from the same experiment shown in Fig. 2 a and b. 100 mM Na-gluconate solution (n=12) (upper panels) and in 100 mM Ca-gluconate (n=7)(lower panels) before (left histograms) and after (right histograms) addition of 100 µM Gadolinium (n=6) or of 10 µM Ruthenium Red (RR)(n=5). Vcis: -60 mV (a) and -120 mV (b).

a

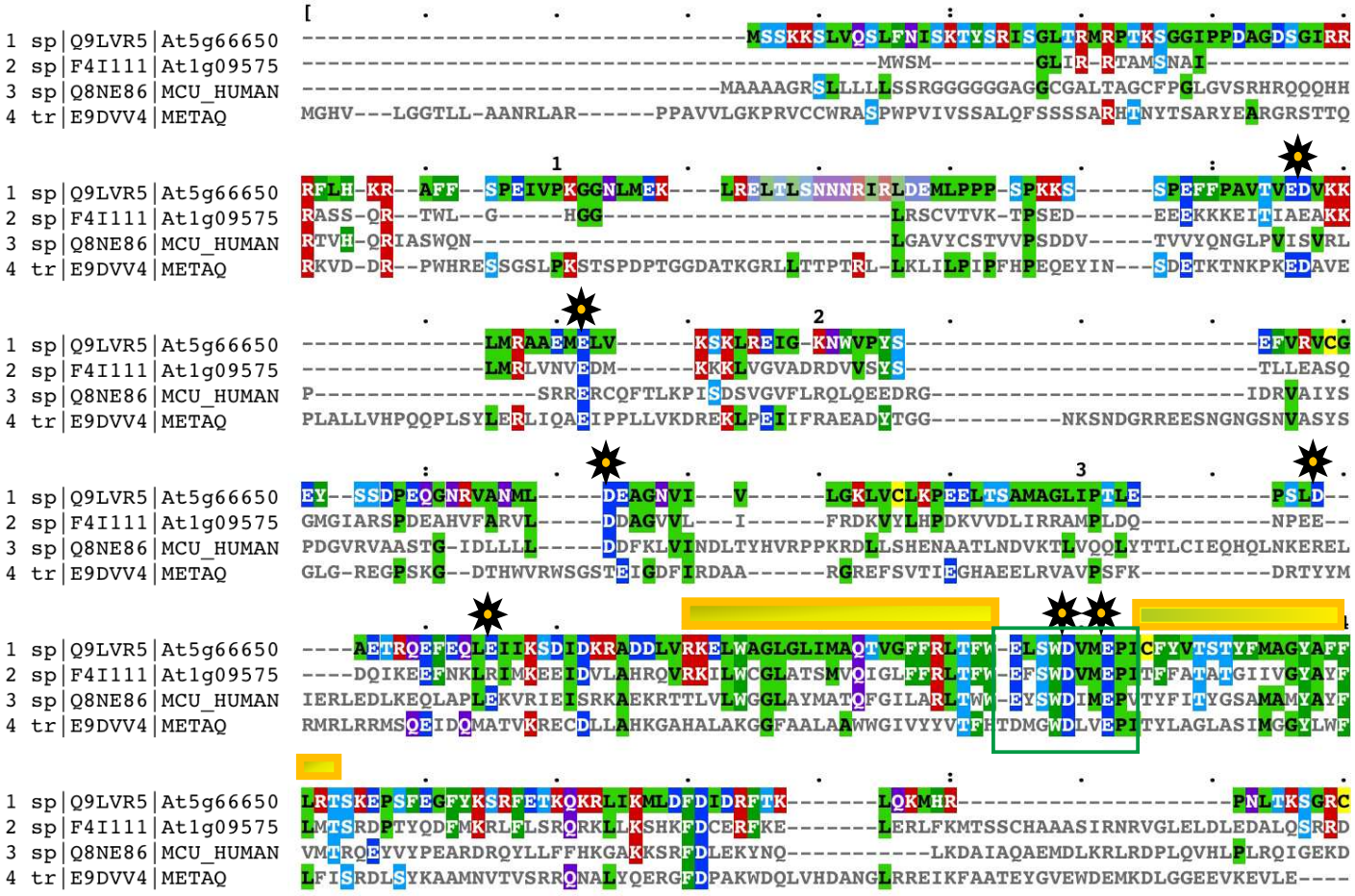

b

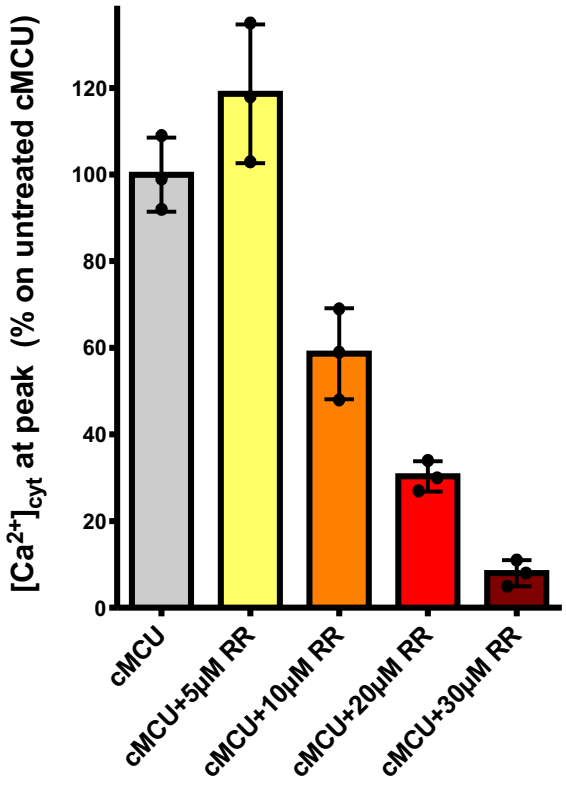

Supplementary Figure 6

Supplementary Figure 6. The N-terminal domain of cMCU. (a) Sequence alignment (ClustalW, Mview) of chloroplast localized MCU (at5g66650) with mitochondrial MCU isoforms: *Arabidopsis thaliana* at5g09575, human MCU (Q8NE86) and metazoan MCU (E9DVV4). Membrane spanning regions are shown by yellow bars. Acidic residues in partially conserved EF-hand like stretches (grey bars), mutated in *E. coli* Ca^{2+} uptake studies, are indicated by black and yellow asterisks. Numbering system is indicated as follow: black dots every ten aminoacids while 1,2,3 correspond to 100, 200 and 300 aa respectively. Colored boxes are used to group aminoacids according to their properties (acidic, basic, hydrophilic, amidic, hydrophobic, aromatic and sulphur containing side chains). **(b)** Monitoring of Ca^{2+} uptake at different doses of RR in *E. coli* (n=3 biological replicates ±SEM). Quantification of data shown in Fig. 2e.

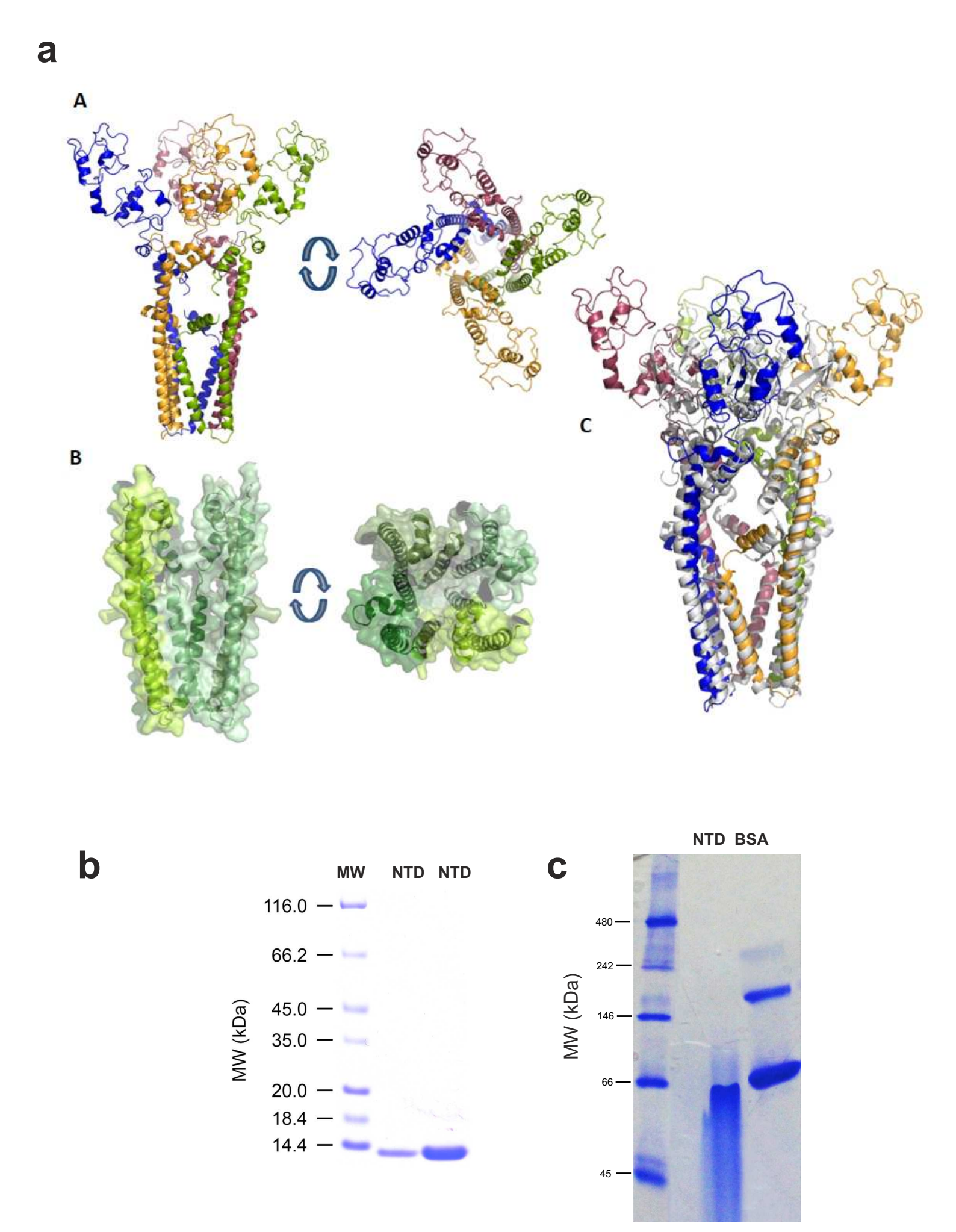

Supplementary Figure 7

Supplementary Figure 7. Homology modelling of cMCU and its tetramerization. (a) A. Homology modelling of the cMCU uniporter (A, B, C): the model (side view, left and top view, right) has been obtained by a combined approach, through the server Phyre2, followed by manual adjustments, crude molecular dynamics and geometry optimization (Phenix Interface). Membrane spanning subdomain (192-312), including the pore and the channel vestibule (shown in panel B) has been modelled and assembled into a tetramer based on templates 6C5W, 6D80, 6DT0, while the the N-terminus domain has been tentatively built based on the homology with Roco proteins dimerization domain (3DPU. 4WNR) and calmodulin-like structures (e.g.4I2Y, 1SW8). Each of the protomer forming the tetramer is shown by cartoon view in a different color (A,C). C. Superposition of cMCU model (blue, yellow, pink and gold) and mitocondrial uniporter structure from *Neurospora crassa* (tetrameric assembly in grey). **(b)** Commassie blu staining of SDS-PAGE where 2 and 4 µg (lanes 1 and 2, respectively) of purified cMCU-NTD (NTD) were loaded. **(c)** Native PAGE analysis of purified NTD (5 µg) and BSA (as control), stained with Coomassie Blue.

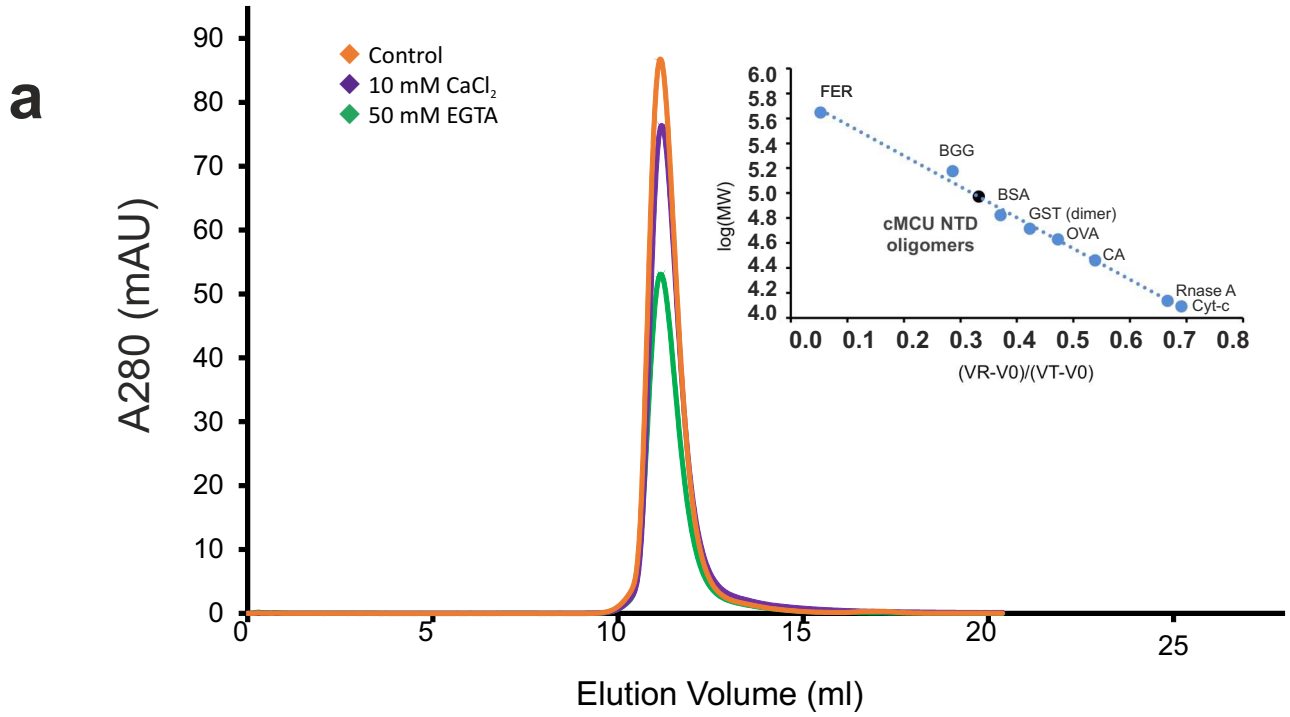

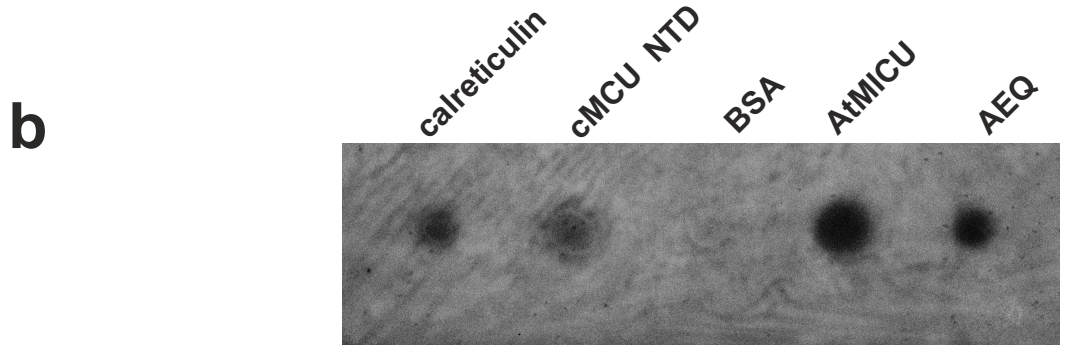

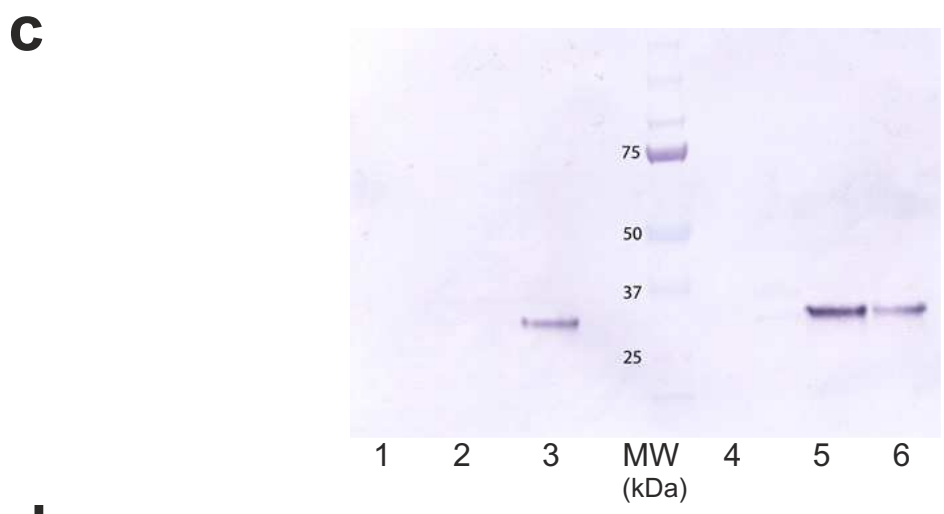

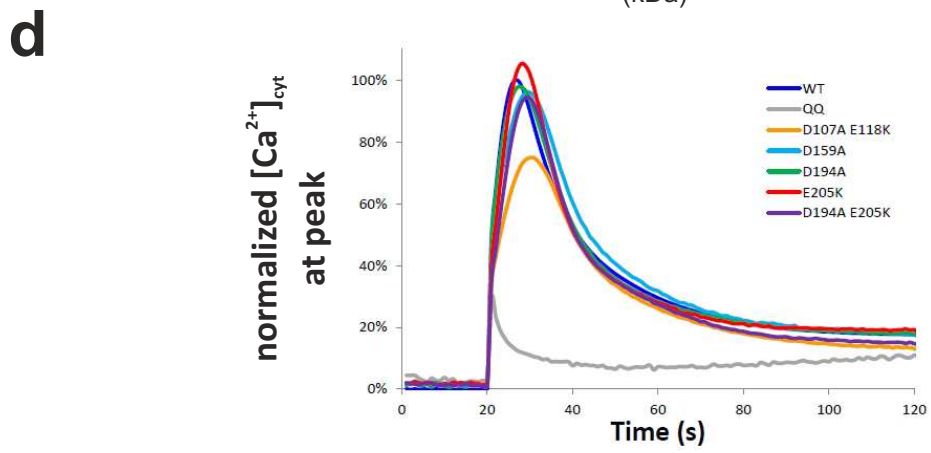

Supplementary Figure 8

Supplementary Figure 8. Calcium binding by the N-terminal domain of cMCU. (a) Size exclusion chromatography of cMCU-NTD as purified and after treatments with EGTA or $CaCl_2$. Inset: FER: ferritin (443,000 Da with 24 subunits); BGG: Bovine Gamma Globulin (150,000 Da); BSA: bovine serum albumin (66,400 Da); OVA: ovalbumin (42,700 Da), GST: Glutathione S-transferase (59,200 Da in dimeric form); CA: carbonic anhydrase (29,000 Da); RNase A: ribonuclease A (13,700 Da) and Cyt-C: cytochrome C (12,400 Da). **(b)** $^{45}Ca^{2+}$-ligand overlay analysis of Arabidopsis cMCU NTD. Proteins were dot-blotted onto nitrocellulose and then incubated with $^{45}CaCl_2$ in a calcium overlay assay. ^{45}Ca-labeled proteins were visualized by autoradiography (7-d exposure) (5 µg each). Spinach calreticulin (lane 1), AtMICU (lane 4) and aequorin (lane 5) were used as positive controls, BSA (lane 3) was used as negative control and lane 2 contained cMCU NTD. **(c)** Immunoblot analysis of recombinant cMCUΔSP (cMCU sequence from P61 to C321) QQ double mutant in *E. coli* (DE3) cell culture, with and without EGTA added to the medium (LB broth). The samples (total lysate) has been separated by SDS-PAGE and detected by mouse anti-His antibody. 1: -I pET28a::AtcMCUΔSP; 2: +I pET28a::AtcMCUΔSP; 3: +I pET28a::AtcMCUΔSP plus 0.3 mM EGTA; MW standard; 4: -I pET28a::AtcMCUΔSPΔQQ; 5: +I pET28a::AtcMCUΔSPΔQQ ; 6: +I pET28a::AtcMCUΔSPΔQQ plus 0.3 mM EGTA**. (d)** Cytosolic $[Ca^{2+}]$ response monitored in vivo in *E. coli* cells transformed with AEQ and wt cMCU (pET28a::cMCUΔSP) or one of the following mutated variants: D107A/E118K, D159A, D194A, E205K, D194A/E205K, E248Q/D251Q (QQ mutant). Ca^{2+} dynamics were monitored for 100 seconds after 500 µM free $[Ca^{2+}]$ stimulus. Traces represent average $[Ca^{2+}]$ responses of $n \geq 6$ independent experiments. Quantification of data is shown in Fig. 2f.

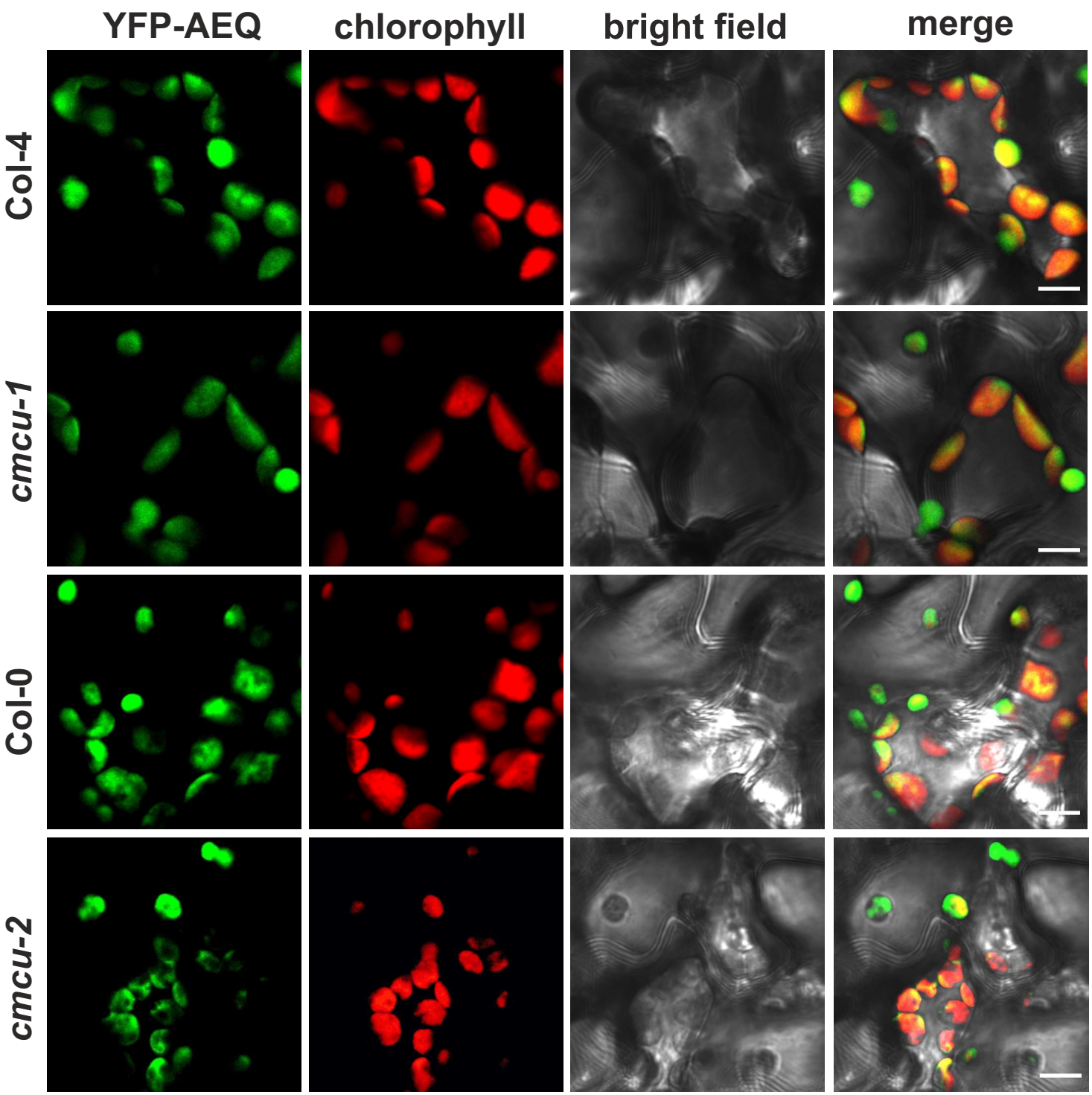

Supplementary Figure 9.

Supplementary Figure 9. Expression of YFP-aequorin in chloroplast stroma. Confocal microscopy analysis of mesophyll cells from wild-type (Col-4 and Col-0) and cMCU knockout (*cmcu-1* and *cmcu-2*) lines stably expressing YFP-aequorin in the chloroplast stroma. Bar:10 µm.

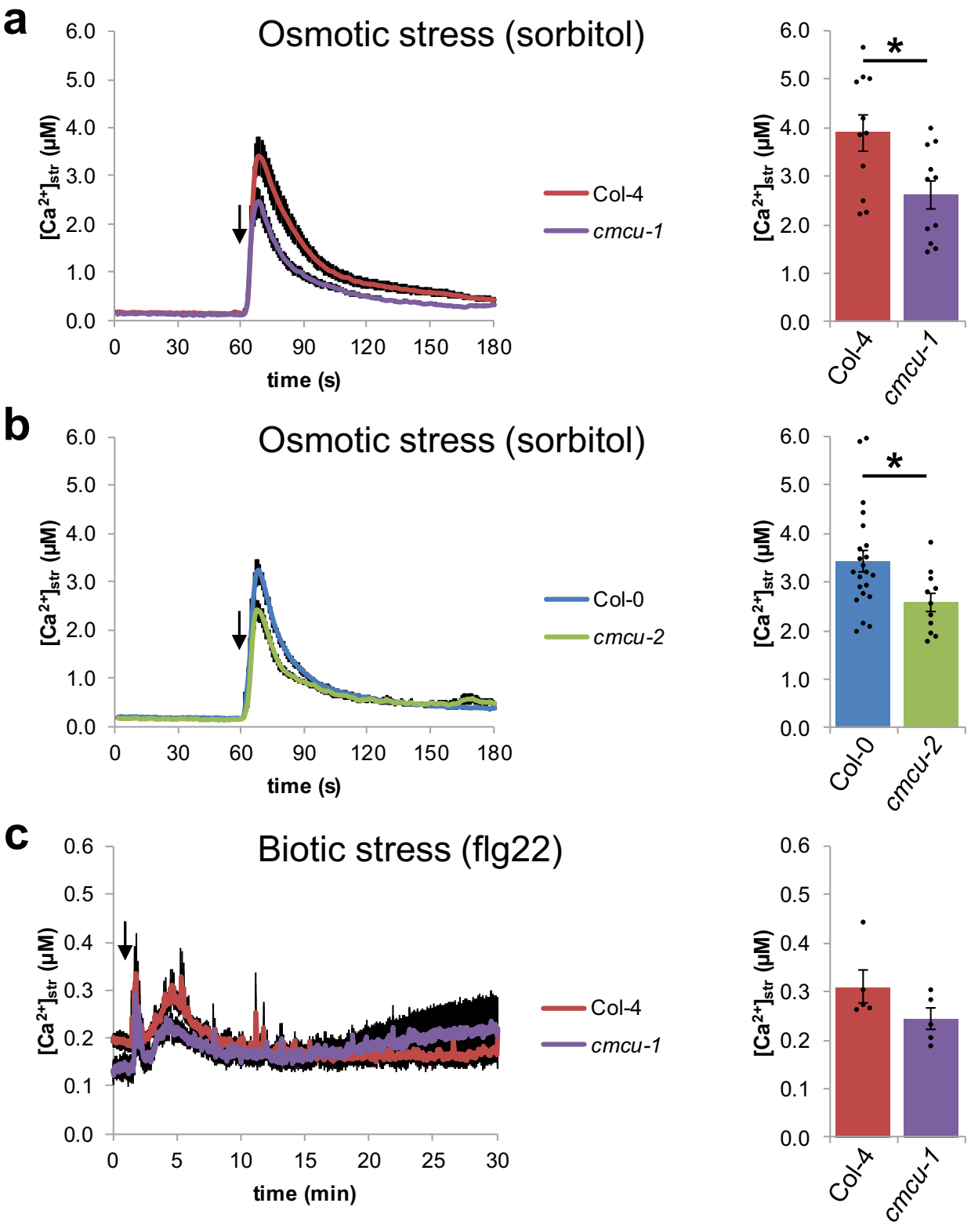

Supplementary Figure 10.

Supplementary Figure 10. cMCU-dependent changes in chloroplast stroma calcium level. (**a-b**) $[Ca^{2+}]_{str}$ was measured in two Arabidopsis WT ecotypes (Col-4, red trace; Col-0, blue trace) and in two independent cMCU knockout lines (*cmcu-1*, violet trace; *cmcu-2*, green traces) in response to 600 mM sorbitol. Traces represent average Ca^{2+} responses ± SEM (black shading) of n≥10 independent plants from ≥3 biological replicates. The stimulus was applied after 60 s (arrow). Right panels: Statistical analysis of $[Ca^{2+}]$ at the peak * P<0.05 (Student's t test). **(c)** Stromal Ca^{2+} response upon treatment with flg22 (1 μM) of WT and MCU KO plants.

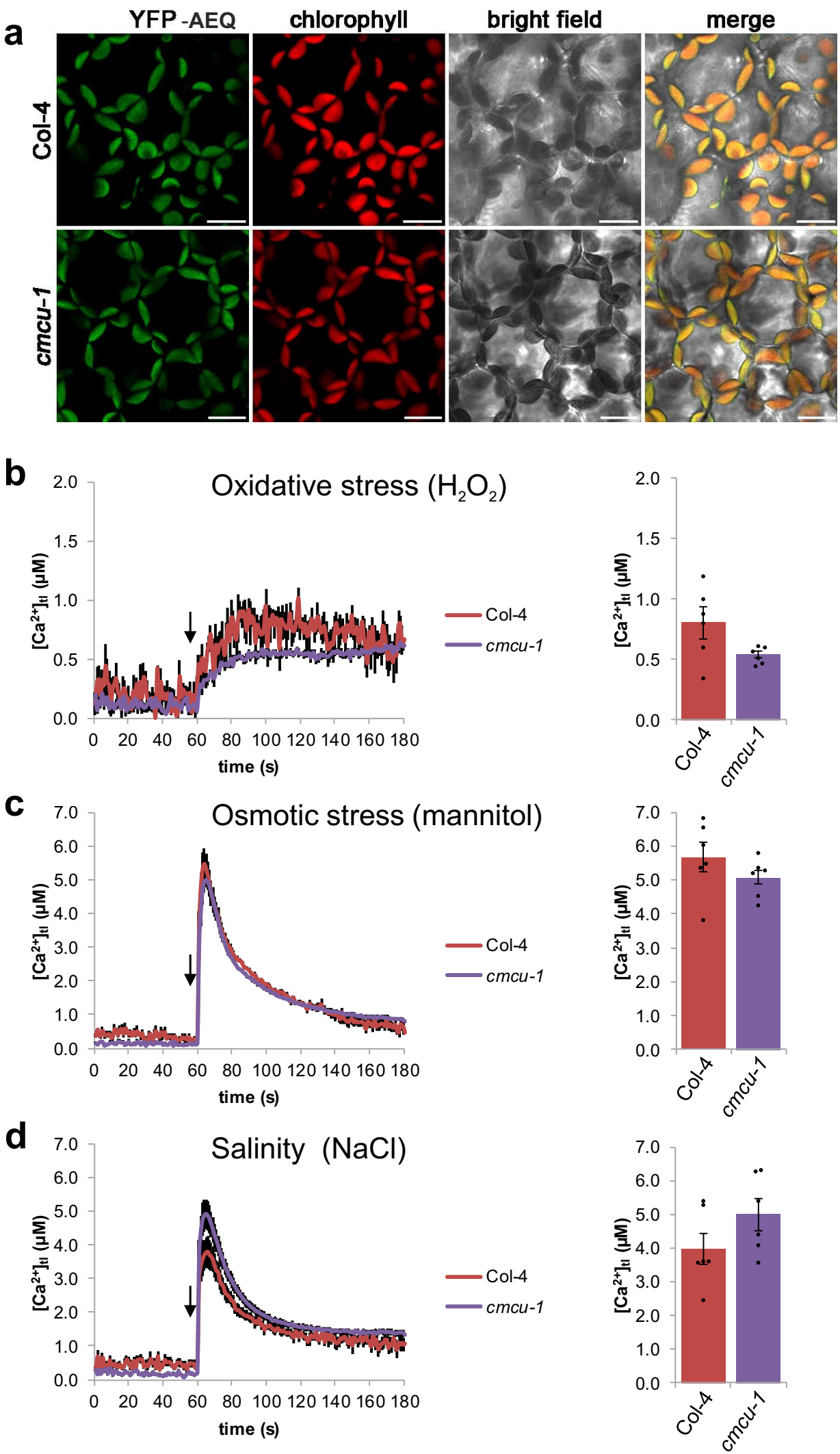

Supplementary Figure 11.

Supplementary Figure 11. Lack of cMCU-dependent changes in calcium level in the thylakoid lumen. (**a)** Confocal microscopy images of mesophyll cells from WT (Col-4) and cMCU knockout (*cmcu-1*) lines stably expressing YFP-aequorin in the thylakoid lumen. Bar, 10 µm. **(b-d)** $[Ca^{2+}]_{tl}$ was measured in Arabidopsis WT (red traces) and cMCU knockout (violet traces) lines in response to 10 mM H_2O_2, 600 mM mannitol, 300 mM NaCl. Traces represent average Ca^{2+} responses ± SEM (black shading, n=6). Stimuli were applied after 60 s (arrow). No statistically significant differences among $[Ca^{2+}]$ at the peak were observed (Student's t test).

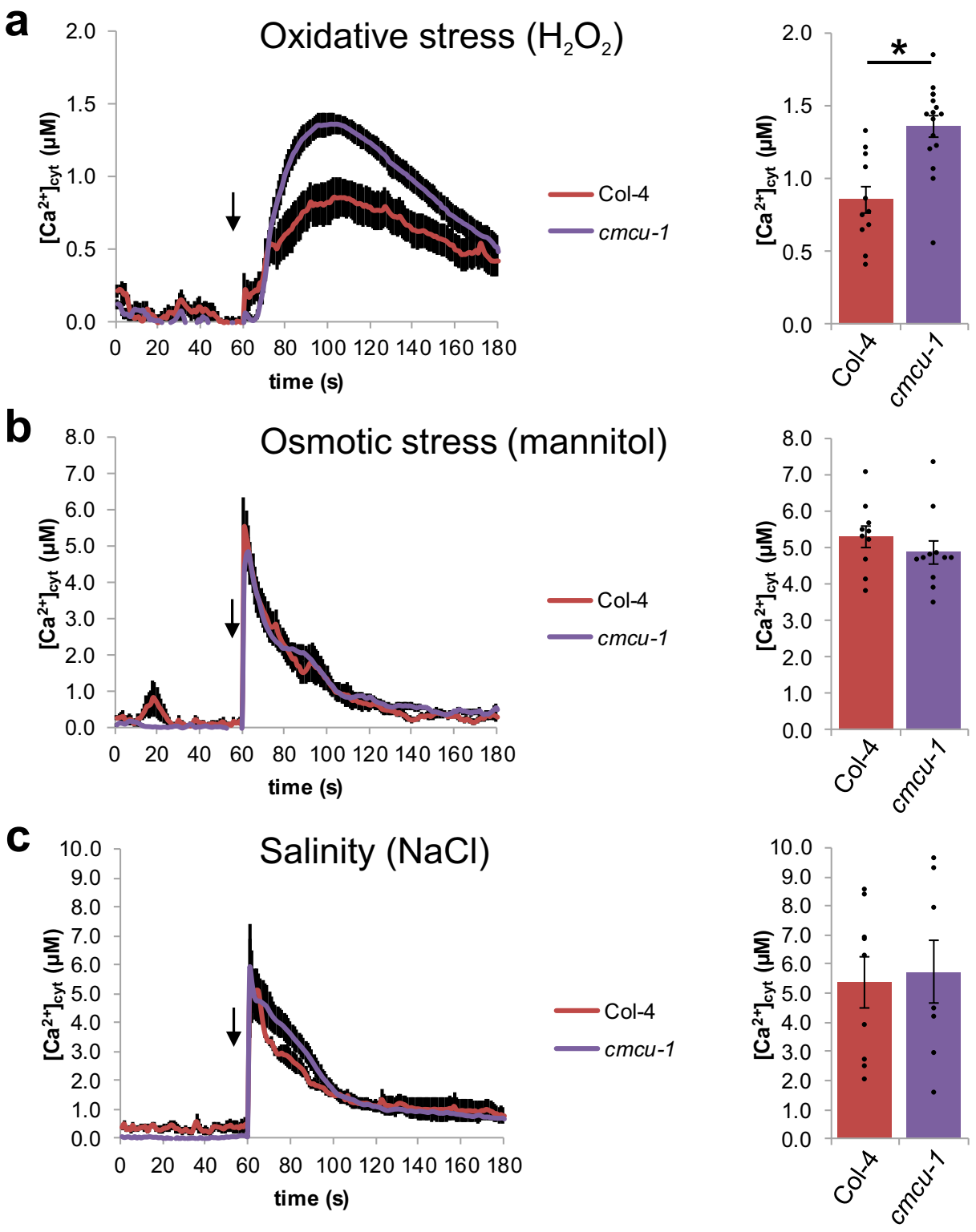

Supplementary Figure 12.

Supplementary Figure 12. cMCU-dependent changes cytosolic calcium level upon stimulation. (a-c) Monitoring of $[Ca^{2+}]_{cyt}$ in Arabidopsis wild-type (red trace) and chl-MCU knockout (violet trace) lines. Ca^{2+} dynamics were monitored in Arabidopsis seedlings stably expressing YFP-aequorin targeted to the cytosol. Traces represent average $[Ca^{2+}]$ responses ± SEM (black shading) of n≥6 independent experiments. The different stimuli were applied after 60 s. Statistical analysis of $[Ca^{2+}]$ at the peak. * $P<0.05$ (Student's *t* test).

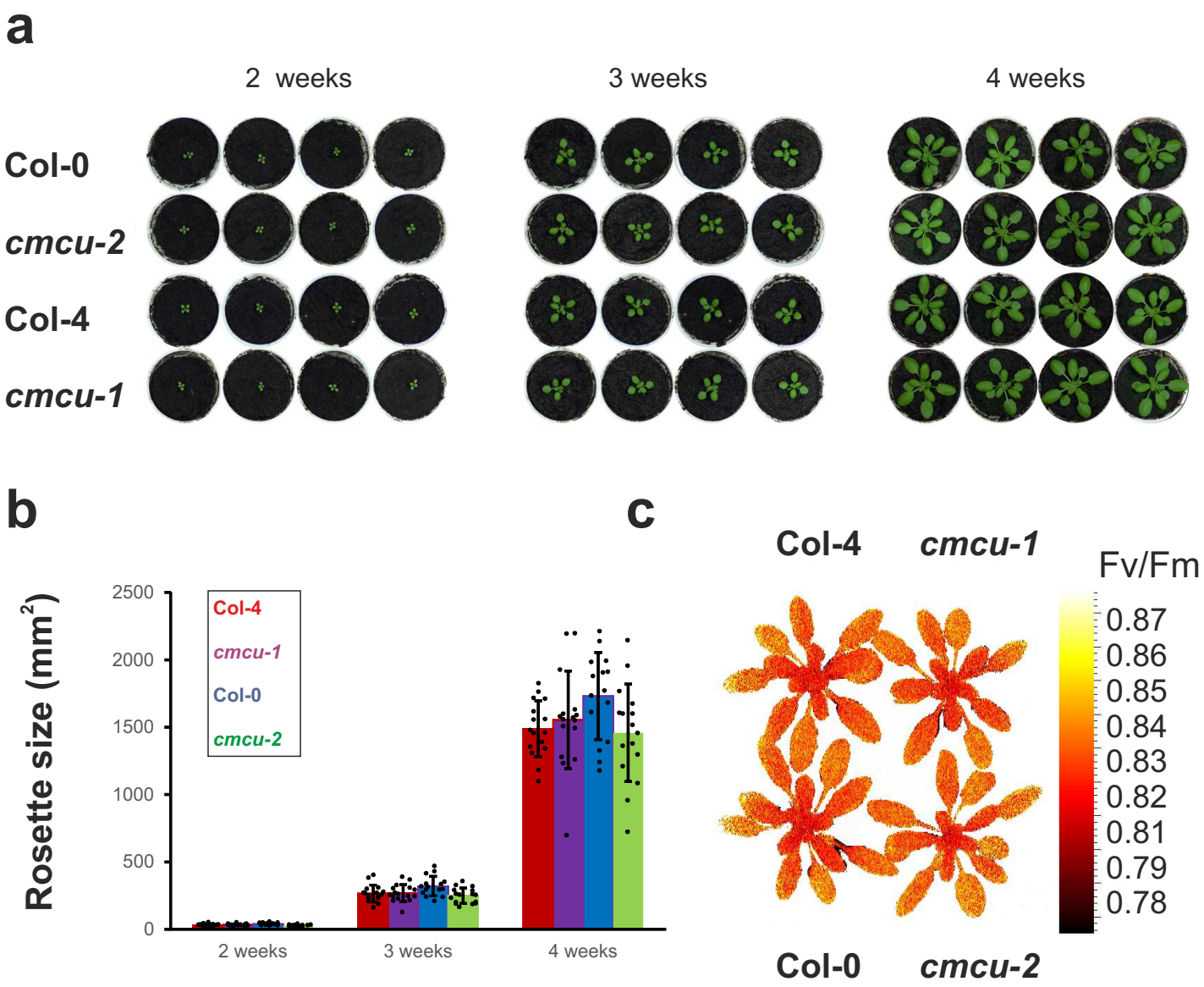

Supplementary Figure 13.

Supplementary Figure 13. Growth and phenotypic analysis of cMCU knock-out mutants. (a-d) Mutant plants not subjected to stress display the characteristics of WT plants. **(a,b)** WT and mutant plants have similar growth under normal conditions, as illustrated by mean rosette size at 4 weeks in **b** (n=16, ±SEM**). (c)** Photosynthetic efficiency of cMCU mutants is not altered. PAM image analysis (**c**) of 4-week old plants (n=5, ±SD). **(d)** Chloroplast ultrastructure is not altered in the mutant plants. Representative images (of 20 images for each line) are shown. Bars: 500 nm. **(e)** MAPK3/6 phosphorylation in plants pre-treated with N-acetyl cystein (1 mM), a potent anti-oxidant (representative of 3 Western blots giving similar results). Loading control: staining with Ponceau Red.

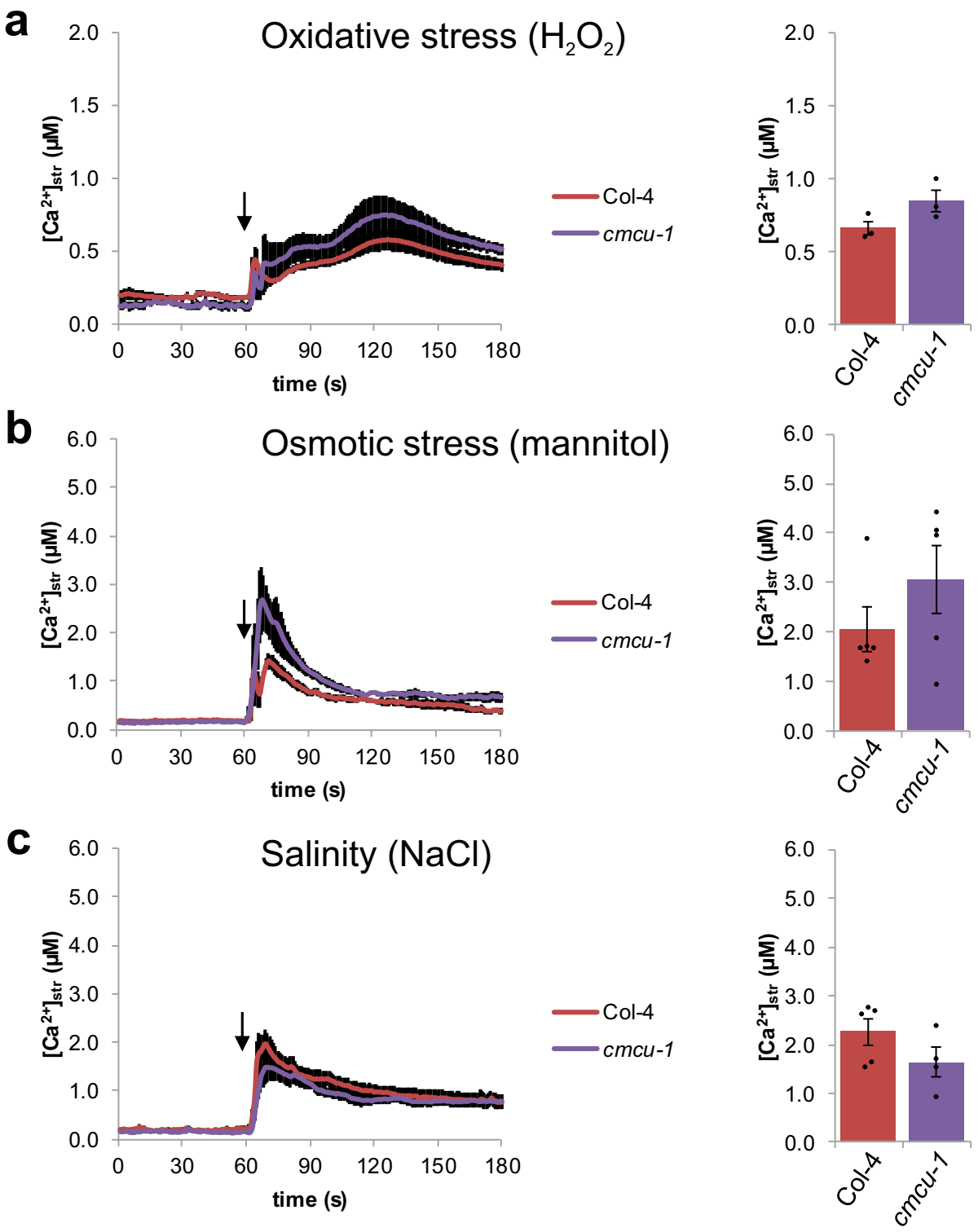

Supplementary Figure 14.

Supplementary Figure 14. Lack of cMCU-dependent changes in chloroplast stroma calcium level in the dark. (a-c) Measurement of stromal [Ca^{2+}] changes in wild-type versus cMCU knock-out seedlings after 8 h darkness. $[Ca^{2+}]_{str}$ was measured in Arabidopsis WT (Col-4, red traces) and cMCU knockout (*cmcu-1*, violet traces) lines in response to 10 mM H_2O_2 (a), 600 mM mannitol (b), 300 mM NaCl (c). Traces represent average Ca^{2+} responses ± SEM (black shading, n≥3). Stimuli were applied after 60 s (arrow). Right panels: Statistical analysis of [Ca^{2+}] at the peak. No statistically significant differences were observed (Student's t test).

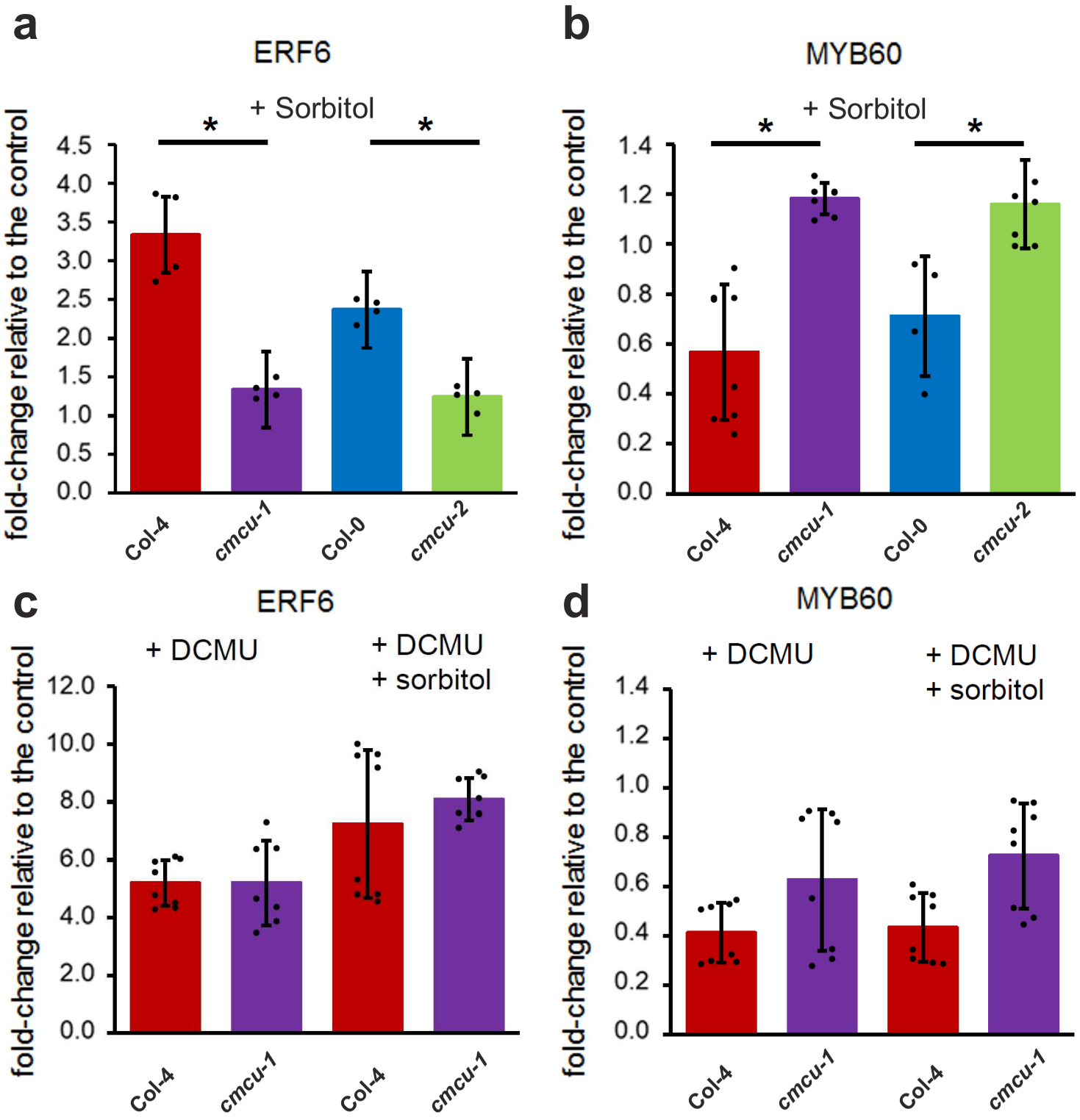

Supplementary Figure 15.

Supplementary Figure 15. Analysis of ERF6 and MYB60 transcription factor levels upon application of sorbitol. (a,b) Transcript level analysis of ERF6 and MYB60 transcription factors challenged with sorbitol, respectively. Illuminated leaves were treated as in Fig. 3g,h for 10 minutes and qPCR was performed to compare transcript levels of ERF6 and MYB60 with respect to mock-treated plants. **(c,d)** as in a and b, following addition of 10 μM DCMU to intact leave slices. DCMU and sorbitol were added together. Experiments in (a-d) were repeated 3 times for 3 leaves/plant in two different sets of Arabidopsis plants. Values are mean ± SEM. Statistically significant differences are indicated by asterisks ($p<0.05$, t-test).

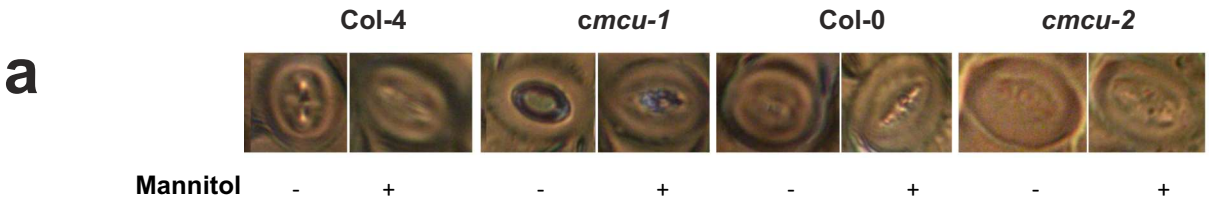

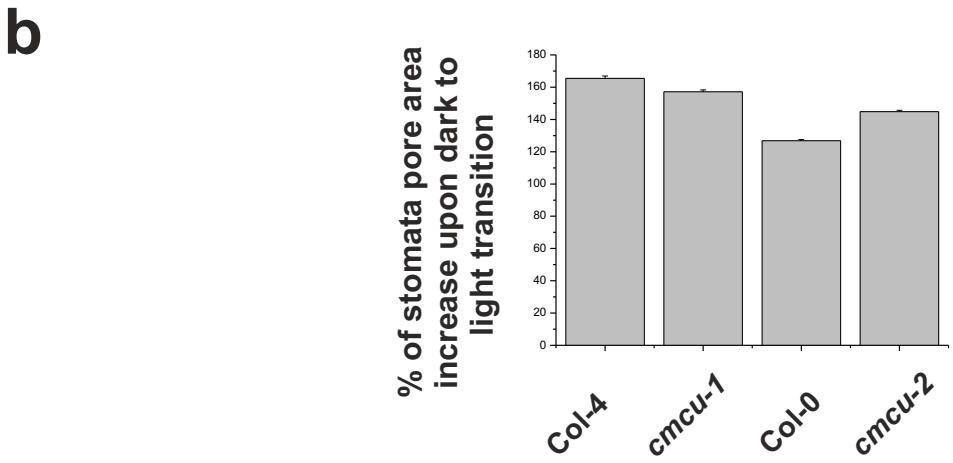

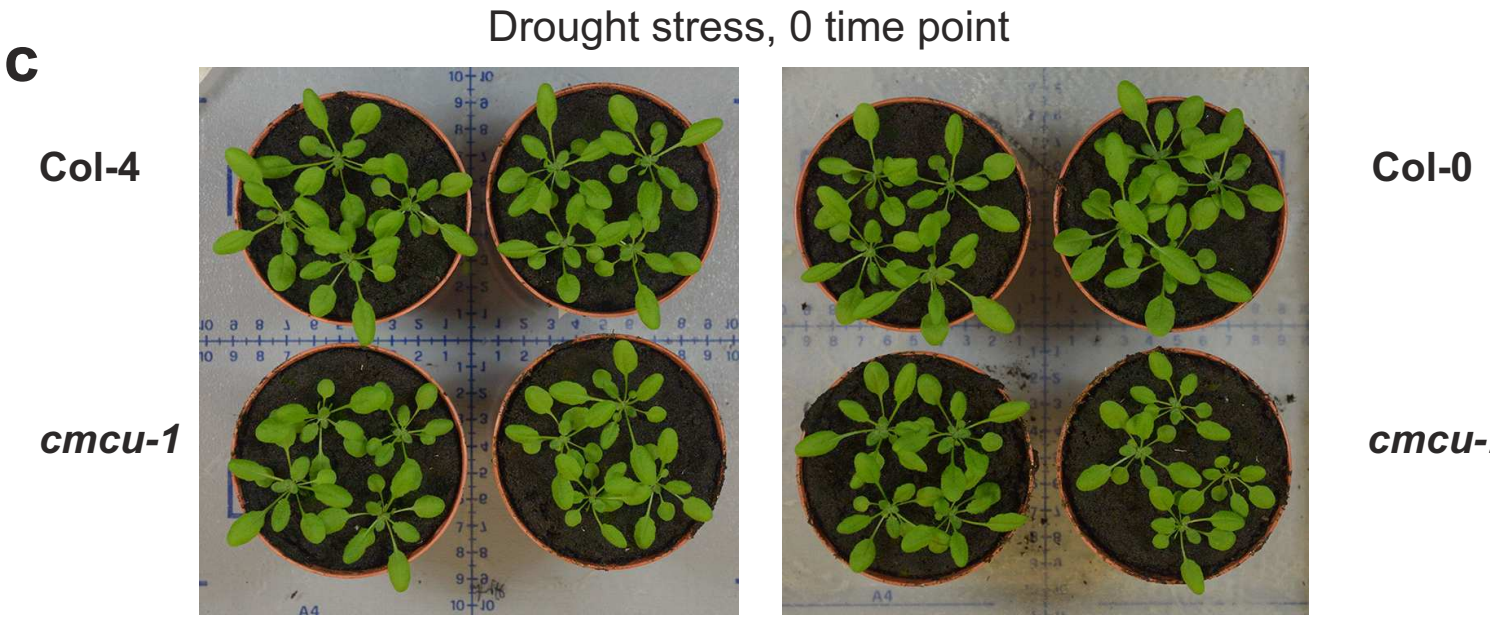

Supplementary Figure 16.

Supplementary Figure 16. Drought stress response in cMCU mutants. **(a)** Representative images of stomata under the indicated conditions. **(b)** Mean stomata size was determined in epidermal strips following dark to light transitions. n≥95 for each sample. SEM is shown. **(c)** Arabidopsis plants grown for 4 weeks under the same conditions and at the same time were subjected to drought stress.

a

Drought stress, 15 days

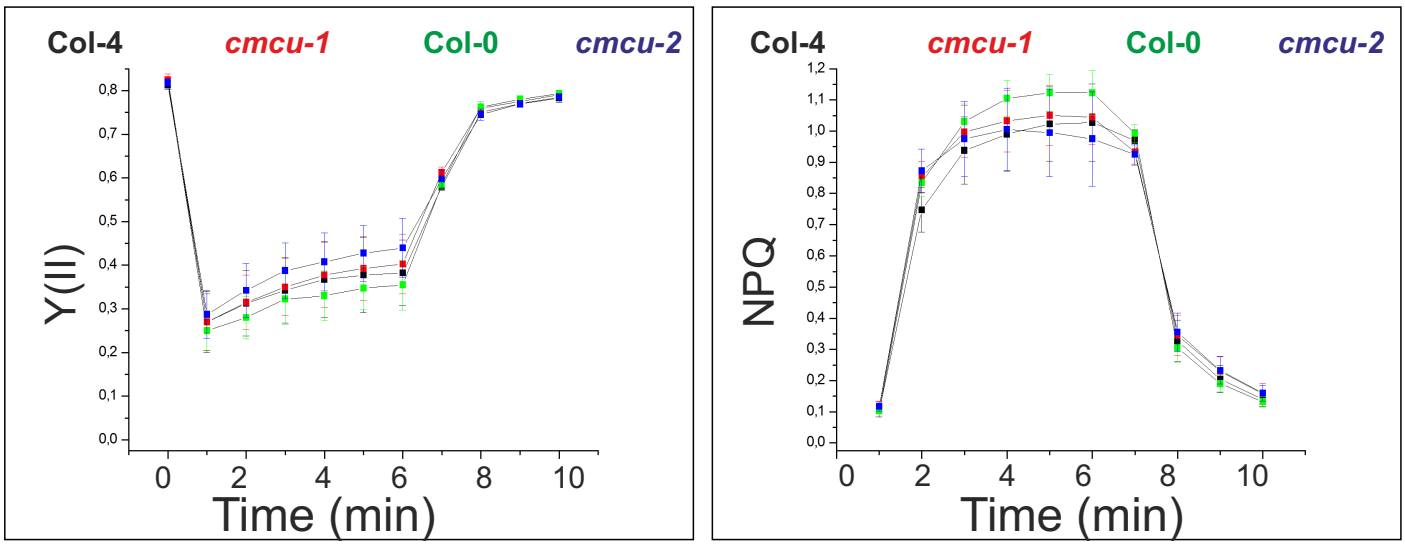

b

Drought stress, 18 days

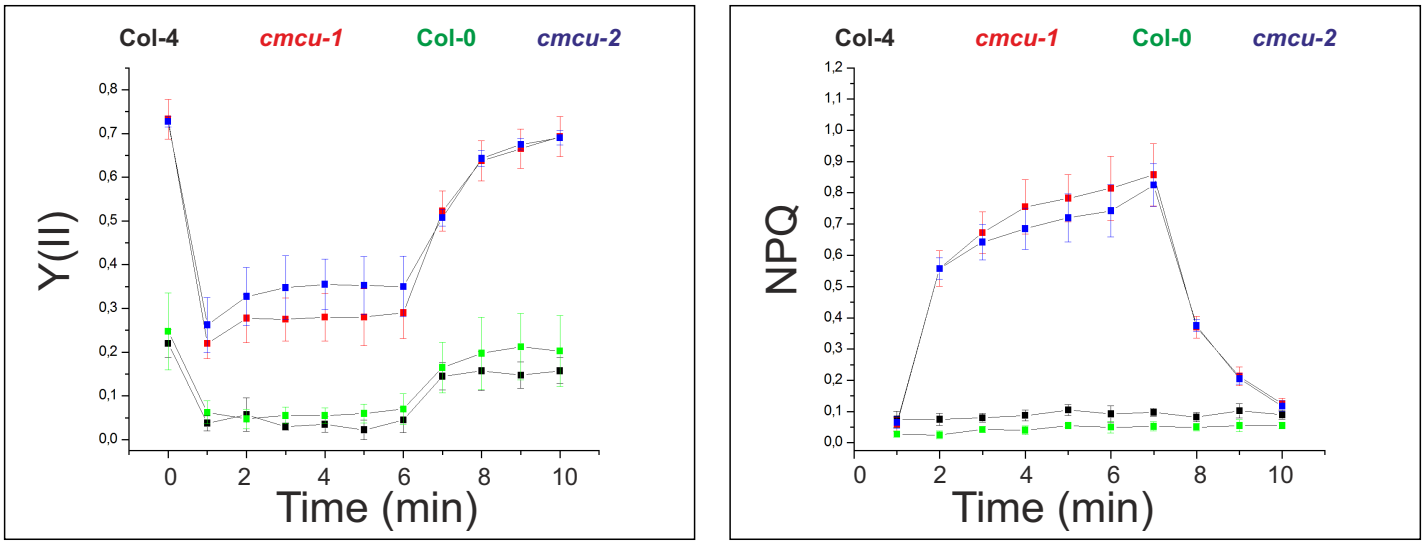

c

Drought stress, 18 days+ 1 day water

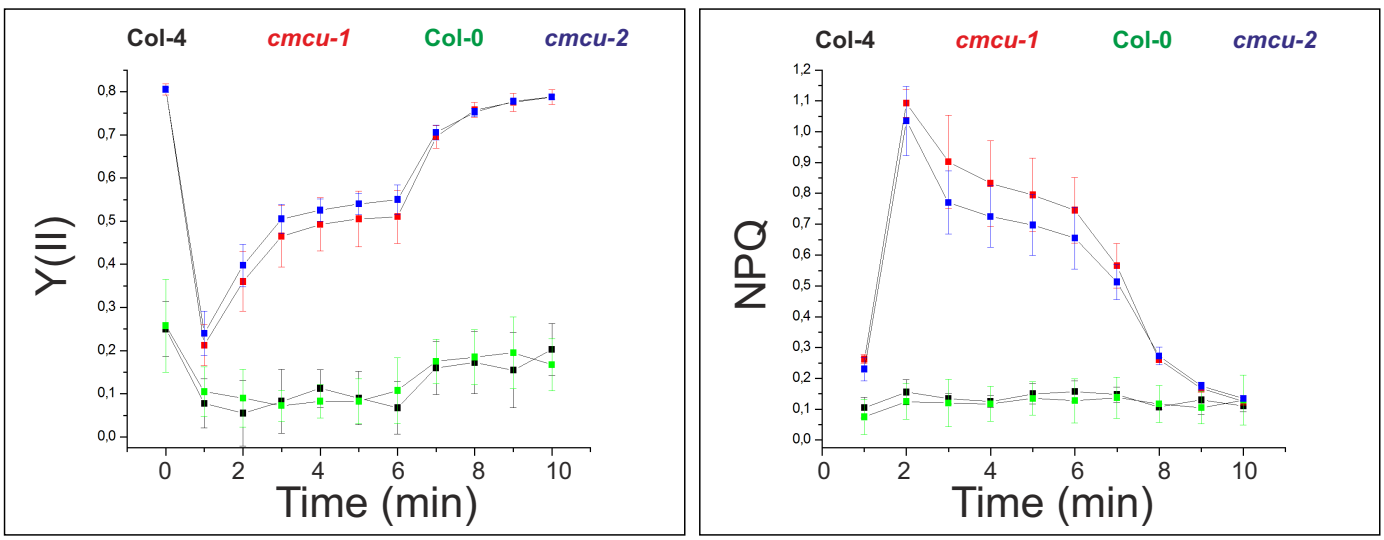

Supplementary Figure 17.

Supplementary Figure 17. Analysis of photosynthetic parameters of cMCU knock-out plants (**a)** Plants at the beginning of the drought period are shown as a control for plants shown in Figure 4c. **(b-c)** NPQ and Y(II) graphs for WT and mutant plants at the indicated times following drought stress and re-watering (n≥5, ±SD). Y(II) is indicative of the Photosystem II charge separation while NPQ indicates the non-photochemical quenching, i.e. a photoprotective mechanism.

Supplementary Videos:

Supplementary Video 1. Plants stably expressing mitochondrial β-F1-ATPase-EGFP (green) that have been transformed with cMCU:tdTomato (red). Chlorophyll autofluorescence is in blue.

Supplementary Video 2. cMCU:EGFP in epidermal cells stained with TMRM, a dye that accumulates in the mitochondria in a membrane potential-dependent manner

Supplementary Video 3. cMCU:EGFP in epidermal cells. Please note co-localization of cMCU with chloroplasts in the guard cell (chlorophyll autofluorescence is in red).

Supplementary Video 4. cMCU:EGFP in guard cells stained with TMRM (accumulates in mitochondria). cMCU:GFP co-localizes at least in part with auto-fluorescence of chlorophyll (blue) in guard cells of stomata, while does not co-localize with TMRM-stained mitochondria (red).

Supplementary Table 1. Primers used in this study.

Primer	Sequence 5'- 3'	Restriction site	Final vector
cMCU_NdeI_for	ctaCATATGTCGTCGAAGAAATCCCT	NdeI	pET28a and pIVEX1.4WG
cMCU_SacI_rev	tagGAGCTCTCAACAACGACCAGATTTAG	SacI	pET28a and pIVEX1.4WG
cMCUΔSP_NdeI_for	tttCATATGAAAGGTGGTAACTTGATGGAG	NdeI	pET28a and pIVEX1.4WG
cMCU_QQ_for	GTGGCAAGTGATGCAACCTATATGCTTCTACGTAAC		pET28a
cMCU_QQ_rev	GGTTGCATCACTTGCCACGACAGTTCCCAAAAC		pET28a
cMCU NTD for	GAAGGAGATATACATATGGCGGTCACGGTGGAAGACGTG		pETite::AtMCU NTD
cMCU NTD rev	AGAGCCGATGATCTGGTTCGACATCATCACCACCATCAC		pETite::AtMCU NTD
HA1-Aeq for	GAAGATCTTTATGATGTTCCTGATTATGC		pACYCDuet-1(HA1-Aeq)
HA1-Aeq rev	GCGCTCGAGTTAGGGGACAGCTCCACCG		pACYCDuet-1(HA1-Aeq)
cMCU_PstI_for	ctaCTGCAGAATGTCGTCGAAGAAATCCCT	PstI	pGREAT:GFP::35S
cMCU_D107A_for	CGGTCACGGTGGAAGCCGTGAAGAAGCTCATG		pET28a
cMCU_D107A_rev	CATGAGCTTCTTCACGGCTTCCACCGTGACCG		pET28a
cMCU_E118K_for	GAGCAGCGGAAATGAAGCTGGTGAAATCGAAGC		pET28a
cMCU_E118K_rev	GCTTCGATTTCACCAGCTTCATTTCCGCTGCTC		pET28a
cMCU D159A fw	GTCGCGAATATGCTTGCCGAAGCTGGAAACGTC		pET28a

cMCU D159A rv	GACGTTTCCAGCTTCGGCAAGCATATTCGCGAC		pET28a
cMCU_D194A_for	CTCGAACCCAGTCTCGCCGCCGAGACAAGAC		pET28a
cMCU_D194A_rev	GTCTTGTCTCGGCGGCGAGACTGGGTTCGAG		pET28a
cMCU_E205K_for	CAAGACAAGAGTTCGAACAACTTAAGATCATAAAATCAGATATCGAC		pET28a
cMCU_E205K_rev	GTCGATATCTGATTTTATGATCTTAAGTTGTTCGAACTCTTGTCTTG		pET28a
cMCU_SmaI_rev	tagCCCGGGTAAACAACGACCAGATTTAG	SmaI	pGREAT:GFP::35S
cMCU_FL_AgeI_for	ctaACCGGTcatcccgtccttaaggaaaat	AgeI	pGREAT:GFP::FL
cMCU_FL_XhoI	tagCTCGAGAAACAACGACCAGATTTAG	XhoI	pGREAT:GFP::FL
cMCU_for	TACAGTTCGGATCCTGAACAAGG		Transcript analysis
cMCU_rev	CTTCGTCTCGAACCGGCTTTTG		Transcript analysis
Act_for	ATTCAGATGCCCAGAAGTCTTGTTCC		Transcript analysis
Act_rev	ACCACCGATCCAGACACTGTACTTCC		Transcript analysis
ERF6_for	ACGAATTGTCTCCGTTGCCT		qPCR
ERF6_rev	CGGTTTGGGAGTGACGAGAT		qPCR
MYB60_for	GTTCCCACCAACACTGGGTTA		qPCR
MYB60_rev	GCTATGGACGCCCATTTGTT		qPCR
ACT2_for	CATTCCAGCAGATGTGGATCTC		qPCR
ACT2_rev	ACCCCAGCTTTTTAAGCCTTTG		qPCR

Teardo et al, SUPPLEMENTARY METHODS

Supplementary materials and methods

Cloning and qPCR

RNeasy Plant Mini kit (Qiagen) was used to extract total RNA from Arabidopsis leaves: 5 µg of RNA were reversely transcribed with the SuperScriptII Reverse Transcriptase (Invitrogen). The coding sequence (CDS) of cMCU was amplified by PCR and cloned into the following vectors: pGREAT::EGFP[1] for confocal microscopy; pIVEX1.4 WG (Roche) for *in vitro* expression; pET28a (Novagen) for *E. coli* expression. Several construct were generated in pET28a vector: pET28a::cMCUΔSP (cMCU sequence from P61 to C321); pET28a::cMCUΔSP(QQ) (the same as before with two single point mutations in the pore loop, D248Q e E251Q, loss-of-function mutation; pET28a::cMCUNTD1 (128 aminoacids, from L83 to D210 located in the soluble n-terminal region) for purification. Further constructs were designed and obtained for structural and functional studies as follows: pET28a::cMCUΔSP(D107A E118K), pET28a::cMCUΔSP(D159A)/pET28a::cMCUΔSP(D194A), pET28a::cMCUΔSP(E205K), pET28a::cMCUΔSP(D194A E205K) pETite::cMCUNTD2, coding for N terminal domain cMCU from A102 to R220, Cterm-His6-tagged, and pACYCDuet-1(HA1-Aeq) coding for hemagglutinin epitope (HA)-tagged wild type Aequorin.

The entire cMCU gene locus (At5g66650) was also cloned for localization study from Arabidopsis genomic DNA (pGREAT:FL:cMCU:EGFP vector): Plant Promoter DB (http://ppdb.agr.gifu-u.ac.jp/ppdb/cgi-bin/index.cgi) was used to determine the promoter length. A 3 kb region upstream the ATG codon was amplified together with the entire At5g66650 gene by PCR and cloned into pGREAT::EGFP vector after removing the internal 2x35S over-expressing promoter. Thus, expression of cMCU::EGFP protein is driven by its endogenous promoter. Another version of the pGREAT::cMCU::EGFP, where the green fluorescence protein was replaced by a dimeric tdTomato (pGREAT::35S::cMCU::tdTomato), was also obtained and used for mesophyll protoplast transformation and *Agrobacterium tumefaciens*-mediated leaf transfection.

100 mg of plant material was used for RNA extraction and retrotranscription (Plant RNeasy mini kit, Qiagen; Superscript II Reverse Transcriptase, Thermo Fisher Scientific). Quantitative RT-PCR was performed using GoTaq® qPCR Master Mix (Promega) in an AB Applied Biosystems 7500 Real-Time PCR System, by using standard cycling parameters. *Actin2* (*At3g18780*) was amplified as the reference gene . Enzymes are from NEB Biolabs (USA).

In vitro expression of cMCU

cMCU protein was expressed in an *in vitro* wheat germ lysate system based on the continuous exchange cell-free (CECF) technique, using the RTS 100 Wheat Germ CECF Kit (Roche) according to manufacturer instruction. After expression, the reaction mixture was directly solubilized with different detergents added at a final concentration of 2 % (w/v). After centrifugation, the supernatant containing the solubilized proteins selected for electrophysiological characterization was diluted 1:10 in 10 mM HEPES, pH 7.4 and used in planar lipid bilayer experiments either directly (5 µl of mixture was added to 3 recording solution of the chamber) or following incorporation into liposomes as in [2]. Detergents alone, added at the same final concentration, never induced activity (n=30).

Bilayer experiments

An asolectin solution in decane/chloroform with a 100:1 ratio per mg of lipids was used for artificial membrane construction. A membrane of 100 mV/pF was constructed between 2 compartments (*cis*/*trans*) and 3 ml of Na-gluconate (low divalent cation medium, 100 mM Na-gluconate, 5 mM EDTA, 10 mM HEPES, pH 7.4) or $CaCl_2$ (100 mM $CaCl_2$, 10 mM HEPES pH 7.4) or Ca-gluconate (100 mM Ca-gluconate, 10 mM HEPES pH 7.4)[3] were added to the *cis* and *trans* compartments. 10 µL of the solubilized and diluted cMCU was added to the *cis* side. Control experiments (n = 50) showed no activity without addition of the protein. $GdCl_3$ or RR were added to both compartments to the required concentration for inhibition assays. Analysis of data was performed using the PCLAMP8.0 and Origin 6.1 programs (for Gaussian and linear fitting). Conductance value was determined from the slope of the fitting of current-voltage relationship.

Protoplast transformation

Arabidopsis suspension cell cultures containing either chloroplasts or amyloplasts were established and maintained as recently described[4]. The same enzymatic digestion was used for rosette leaves of 4-week-old plants. Protoplasts were isolated from mid-exponential phase (4-day-old) cultured cells or from leaves and transformed by PEG with 8 µg of either pGREAT:cMCU:EGFP plasmid DNA or of pGREAT:cMCU:tdTomato plasmid DNA, then kept at 23°C in W5 solution supplemented with 5 mM glucose and ampicillin 100 µg/ml for up to 3 days[5].

Plant growth, transformation and phenotyping

Arabidopsis plants were grown under controlled conditions: 20°C, long day photoperiod (16h light (white led light, 3000 K, Philips), 8h dark), 120 µmol photons m^{-2} s^{-1}, 60% relative humidity. Seeds were surface-sterilized, incubated for 2 days at 4°C in the dark, and allowed to germinate in half-strength Murashige and Skoog (MS; Duchefa, Netherlands) medium solidified with 0.8% (w/v) plant agar supplemented with 1% sucrose. Seedlings were picked and transferred to soil.

Two independent T-DNA insertion lines for the At5g66650 locus were obtained from NASC (European Arabidopsis Stock Centre): SK16605 from Saskatoon Arabidopsis T-DNA mutant

collection (*cmcu-1*) and SALK_031408 from the SALK collection (*cmcu-2)*. Total genomic DNA was extracted from each line following standard procedures for plant genotyping. Transcript analysis was also performed to confirm the lack of the transcript in the two knockout lines. Primers used are listed in table S1.

The subcellular localization of the cMCU was examined through the agroinfiltration of 4-week-old Arabidopsis thaliana wt Col-0 plant leaves. For stable transformation, Arabidopsis plants (*cmcu-1*) were transformed by floral dip with *Agrobacterium tumefaciens* GV3101, carrying the pGREAT:35S:cMCU:EGFP or pGREAT:FL:cMCU:EGFP constructs in the presence of pSoup.

For plant phenotyping, the following parameters were considered at weeks 3, 4, 5 and 6. Rosetta area was measured by using ImageJ software (Rasband, W.S., ImageJ, U.S. National Institutes of Health, Bethesda, Maryland, USA, http://imagej.nih.gov/ij/, 1997-2014). PAM imaging was used to detect chlorophyll fluorescence using FluorCam7 (Photon Systems Instruments) applying a saturation pulse of 5322 μE m^{-2} s^{-1} for 800 ms; PSII quantum yield (YII) and NPQ (non-photochemical quenching) were analyzed.

Isolation of purified chloroplasts and mitochondria

The expression of the cMCU:EGFP fusion protein was tested on Percoll-purified chloroplasts obtained as described in [6]. Purified mitochondria from the same Arabidopsis line were obtained as in [7].

Stress assays and measurement of stomata area and absolute water content

Stress assays: For MAPK assay, Arabidopsis leaves were cut, weighted and incubated for 24 h in water to dephosphorylate MAPKs. Following, stress stimuli (or water for mock treatment) were applied as a 2x solution and leaves were collected. For MAPK assay and qPCR, leaves were grinded in liquid nitrogen and dissolved in loading buffer in a 1:1 ratio (v:w). After boiling, samples were loaded on SDS-PAGE and immunoblotted with Phospho-p44/42 MAPK (Erk1/2) (Thr202/Tyr204) antibody (Cell Signaling Technology)[8]. For qPCR, leaf slices were powdered in liquid nitrogen and cDNA was synthetized as described above. Drought assay: 4 week-old plants were subjected to drought stress through long-term water starvation. Then, recovery was achieved by irrigation. Plants were photographed and PAM Imaging was used to test photosynthetic efficiency during drought stress.

Determination of stomatal pore area: after stress treatment, leaves were collected and the abaxial sides were coated with nail polish to fix stomata. Tape was used to remove the epidermal layer and stomata size was measured by using an optic microscope. The length and width of the stomatal pore were determined by ImageJ and the stomata area was calculated as the area of the ellipse fitting the stomata.

Determination of absolute water content: 4 week-old plants were cut below the rosette and the weight was measured every 20 minutes; dry weight was obtained after over-night incubation at 70°C. Absolute water content was calculated as the difference between fresh and dry weight. Transpiration rate was calculated as normalized percentage variation of plant weight.

Transmission electron microscopy and confocal microscopy

Transmission electron microscopy and confocal microscopy was performed as previously described [1]. Plants were examined to detect transformation after 4 days using the confocal microscope Leica TCS SP5 II (Leica Microsystems). Images were collected with Leica Application Suite software (LAS AF, Leica Microsystems). Chlorophyll and EGFP were excited at 488 nm, tdTomato was excited at 543 nm. For fluorescence emission, we used wavelengths of 515-525 nm, 560-620 nm and 680-720 nm for EGFP, tdTomato and chlorophyll, respectively.

Aequorin-based Ca^{2+} measurements

For Ca^{2+} measurements, Arabidopsis WT and knock-out lines were transformed with constructs encoding YFP-aequorin chimeras targeted to the cytosol, chloroplast stroma[9] or thylakoid lumen[10]. Successful transformation and expression of the constructs was confirmed in the T2 generation by Western blot analyses using an anti-aequorin antibody (Abcam, Cambridge, UK) and confocal microscopy analysis of YFP fluorescence.

7-day-old seedlings were used in Ca^{2+} assays after reconstitution in H_2O with 5 µM native coelenterazine (Cat#303, Prolume Ltd., Pinetop, AZ, USA) for 4 h in the dark, followed by 16 h exposure to the light. Ca^{2+} measurements were performed by using an Envision Multilabel Plate Reader (Perkin-Elmer) equipped with a two-injector unit. Seedlings were floated onto 200 µl H_2O in 24-well CulturPlate microplates. After measuring luminescence from each well for 60 s, seedlings were challenged with an equal volume of different 2-fold concentrated solutions, mimicking salt stress (0.3 M NaCl), drought (0.6 M mannitol/sorbitol), oxidative stress (10 mM H_2O_2) or pathogen attack (1 µM flg22). At the end of the experiments, discharge of the remaining aequorin pool was carried out by automatic injection of 200 µl discharge solution (1 M $CaCl_2$, 30% ethanol). The curve representing the relationship between photon emission by aequorin and Ca^{2+} concentration has been mathematically modeled to develop an algorithm that is currently employed in the calibration of light emission to [Ca^{2+}] values, using a custom-made macro-enabled Excel workbook[11,12].

***Arabidopsis thaliana* cMCU uniporter expression in *E. coli* and Ca^{2+} uptake measurements**

E. coli C41(DE3) and ArcticExpress competent cells were transformed with pET28a::cMCUΔSP or or one of the plasmids encoding for cMCUΔSP mutants: pET28a::cMCUΔSP(QQ)/ (D107A E118K)/(D159A)/ (D194A)/ (E205K)/ (D194A E205K). The day after a single colony was used to inoculate a liquid culture (LB medium supplemented with kanamycin) at 30°C. When the OD_{600}

reached 0.6, protein expression was induced at 18°C with 0.5 mM IPTG in the presence or absence of 0.2 mM EGTA.

Cell extracts were prepared by solubilizing cells in Laemmli sample buffer (50 mM Tris-HCl pH6.8, 100 mM DTT, 2% (w/v) SDS, 0.05% (w/v) bromphenol blue). Samples were heated for 5 min at 100°C, loaded on a NuPAGE Novex 4-12% Bis-Tris Gels (Thermo Fisher) and blotted onto a PVDF membrane. The membrane was incubated overnight with anti-His mouse monoclonal primary antibody at 4°C diluted in TBS-T (Tris Buffered Saline-Tween: 20 mM Tris, 0,137 M NaCl, 0,1% Tween 20 pH7,6) after 1h blocking in 5% milk in TBS-T. Detection was carried out by incubation with alkaline phosphatase-conjugated anti-mouse secondary antibody for one hour at room temperature followed by incubation with the 1-step NBT/BCIP substrate solution (Thermo Fischer Scientific).

For Ca^{2+} uptake measurements, C41(DE3) *E. coli* competent cells were co-transformed with pACYCDuet-1(HA1-Aeq) and pET28a::cMCUΔSP or with pACYCDuet-1(HA1-Aeq) and pET28a::cMCUΔSP(QQ) mutant as well as the other mutants mentioned in Fig. 2. In parallel, C41(DE3) *E. coli* competent cells were transformed with the only aequorin expressing pACYCDuet-1(HA1-Aeq) as a control. Subsequently, a single colony was used to inoculate a liquid culture (LB medium) overnight at 37°C containing the appropriate antibiotics. The day after, overnight cultures were diluted 1:50 in 50 mL of fresh medium and grown at 37°C until OD_{600} reached 0.4, before the induction of protein expression using 1 mM IPTG for 2 h at room temperature in the presence of 0.25 mM EGTA.

Cells were harvested, resuspended in 1 mL of buffer solution containing 25 mM HEPES pH 7.5, 125 mM NaCl, 1 mM $MgCl_2$, 500 µM EGTA and reconstituted with 5 µM celenterazine for 90 minutes at room temperature in dark conditions. After reconstitution, cells were plated onto a 96 well plate and challenged with Ca^{2+} pulses of different concentrations. For inhibition studies, Ruthenium Red was added to the samples 10 min before Ca^{2+} stimuli. Experiments were stopped by lysing the cells with a hypotonic Ca^{2+} rich solution (1 mM $CaCl_2$, 30% ethanol). All the experiments were carried out in a Perkin-Elmer Envision plate reader equipped with a two-injection unit, and conversion of luminescence into [Ca^{2+}] values was performed as described above for Arabidopsis seedlings.

Expression and purification of cMCU N-terminal domains

For cMCUNTD expression, *E. coli* C41(DE3) cells harboring the corresponding expression plasmids have been cultured in LB medium. Protein expression was induced by adding 0.5 mM IPTG and prolonged for 18 hours at 28°C. Cell pellets were resuspended in Buffer A (200 mM NaCl, 20 mM Hepes, pH 7.5) in the presence of protease inhibitors (Complete Mini EDTA free, Roche) and lysed twice by cell homogenizer (Constant Ltd, One-shot Cell Disruptor) at 1.35 MPa. Clarified

supernatants were purified by affinity chromatography on Nichel-charged resin (HisTrap excel, GE-Healthcare). The 6xHis-tagged cMCUNTD protein were eluted by an Imidazole gradient ranging from 20 to 500 mM in Buffer A. Eluted peaks were checked by SDS-PAGE electrophoresis and fractions with highest purity collected and concentrated by ultrafiltration (10 kDa MWCO) to 30 mg/ml. Protein samples were further purified by size-exclusion chromatography on a Superose 12 column HR10/300 (GE-Healthcare) and the fractions obtained stored at -80° C. cMCUNTD was used for structural and functional studies. Protein concentration was estimated by UV-visible absorption at 280 nm, using theoretical absorption coefficient (0.59 $ml*cm^{-1}*mg^{-1}$) calculated by ProtParam software (ExPASy server).

Size exclusion chromatography studies

Size exclusion chromatography analyses were run on a Superose 12 10/300 column (GE Healthcare), equilibrated in GF buffer (20 mM HEPES, 200 mM NaCl, 5% v/v glycerol pH 7.5), 0.6 ml/min flow rate. Samples elution was monitored by UV absorbption at 280 nm. For calcium buffered experiments, cMCUNTD2 was treated with 10 mM EGTA or 10 mM $CaCl_2$ in buffer GF, loaded on the same column and run in the same conditions as the untreated sample.

Cross linking studies

The applied method was originally described for the crosslinking of protein crystals and subsequently adapted to study protein oligomers in native conditions[13]. By this approach, the glutaraldehyde vapours are exploited as crosslinking reagent, avoiding the direct mixing with the protein and assuring very mild conditions. The reservoir chambers of a MRC maxi 48-well crystallization plate (Molecular Dimensions Ltd) were filled with 100 ul of 25 % (v/v) glutaraldehyde solution. 15 µl of 0.2 mg/ml purified cMCUNTD were deposited on the top of each sitting drop well and the chamber rims closed by transparent Clear-seal film to guarantee saturation by cross-linking reagent vapour. All the steps were carried out at room temperature. The reaction in each well was sequentially blocked at 0, 15, 30, 60, 120, 180, 240, 300 minutes by SDS-page denaturing buffer before analysing the results by SDS-PAGE electrophoresis (4-12 % precast gels). The acrylamide gel was stained by Silver staining and the size of the different oligomers compared to a mix of protein standards (Precision Plus Protein Standards Dual color, Bio-Rad).

Molecular model of mitochondrial calcium uniporter

The model has been predicted using the fold recognition server Phyre 2.0 [14]. The software has identified best template structures based on heuristics in order to maximise confidence, percentage identity and alignment coverage, the first four with a homology confidence (Phyre 2.0 parameter) higher than 90%. According to the overall model built by multi-template modelling tool Poing (Phyre 2.0) and further refined by simulated annealing and geometries optimization by Phenix Interface[15].

N-terminus domain (38-187) has been studied and predicted as part of the overall protomer but also separately, through a dedicated search. Both the servers identified a significant identity (between 25 and 30%) of the transmembrane region, forming the pore and vestibule of the uniporter (192-312), with the structure of MCU uniporters from fungi, recently determined by single particle cryo-EM studies and X-Ray crystallography (6DT0, 6C5W, 6D80). N-terminus domain (38-187) has been reconstructed according to its similarity toward the following PDB structures: 4WNR, 3DPU, 4I2Y. The homology toward 4WNR and 3DPU RocCOR proteins structures pertains the residues range 119-186 (based on 25% sequence identity) and concerns structural elements involved in the oligomerization and conformational dynamics of Leucine-rich-repeat RocCOR domain, while 4I2Y, and many others, with similar and weaker homologies in the region 79-158, are strikingly involved in Ca^{2+} binding (calmodulin or calmodulin-like domains, sensors, polcalcin etc.). The tetrameric assembly has been tentatively reconstructed with the help of molecular graphics tools for model building and refinement[16,17], according to 6DT0 assembly. Reciprocal orientation of N-terminus domain and the core of the uniporter is merely hypothetical, as well as N-term contacts are not predictable, based on similarities and feasible data.

$^{45}Ca^{2+}$ overlay

$^{45}Ca^{2+}$ overlay assay was carried out as described by Maruyama et al.[18]. Spinach calreticulin[19] recombinant aequorin[20] and Arabidopsis MICU[21] were used as positive controls, BSA (Sigma-Aldrich) was used as negative control. Proteins were spotted directly onto nitrocellulose membranes. $^{45}CaCl_2$ was purchased from Perkin-Elmer (Boston, MA, USA). $^{45}Ca^{2+}$ labeled proteins were visualized by autoradiography on Amersham Hyperfilm MP (GE Healthcare, Little Chalfont, Buckinghamshire, UK) after 7 d exposure.

Supplementary References

1 Carraretto, L. *et al.* A thylakoid-located two-pore K^+ channel controls photosynthetic light utilization in plants. *Science (New York, N.Y.)* **342**, 114-118, doi:10.1126/science.1242113 (2013).

2 Raffaello, A. *et al.* The mitochondrial calcium uniporter is a multimer that can include a dominant-negative pore-forming subunit. *The EMBO journal* **32**, 2362-2376, doi:10.1038/emboj.2013.157 (2013).

3 Patron, M. *et al.* MICU1 and MICU2 finely tune the mitochondrial Ca^{2+} uniporter by exerting opposite effects on MCU activity. *Molecular cell* **53**, 726-737, doi:10.1016/j.molcel.2014.01.013 (2014).

4 Sello, S. *et al.* Dissecting stimulus-specific Ca^{2+} signals in amyloplasts and chloroplasts of Arabidopsis thaliana cell suspension cultures. *Journal of experimental botany* **67**, 3965-3974, doi:10.1093/jxb/erw038 (2016).

5 Yoo, S. D., Cho, Y. H. & Sheen, J. Arabidopsis mesophyll protoplasts: a versatile cell system for transient gene expression analysis. *Nature protocols* **2**, 1565-1572, doi:10.1038/nprot.2007.199 (2007).

6 Seigneurin-Berny, D., Salvi, D., Dorne, A. J., Joyard, J. & Rolland, N. Percoll-purified and photosynthetically active chloroplasts from Arabidopsis thaliana leaves. *Plant physiology and biochemistry : PPB / Societe francaise de physiologie vegetale* **46**, 951-955, doi:10.1016/j.plaphy.2008.06.009 (2008).

7 Sweetlove, L. J., Taylor, N. L. & Leaver, C. J. Isolation of intact, functional mitochondria from the model plant Arabidopsis thaliana. *Methods in molecular biology (Clifton, N.J.)* **372**, 125-136, doi:10.1007/978-1-59745-365-3_9 (2007).

8 Flury, P., Klauser, D., Schulze, B., Boller, T. & Bartels, S. The anticipation of danger: microbe-associated molecular pattern perception enhances AtPep-triggered oxidative burst. *Plant physiology* **161**, 2023-2035, doi:10.1104/pp.113.216077 (2013).

9 Mehlmer, N. *et al.* A toolset of aequorin expression vectors for in planta studies of subcellular calcium concentrations in Arabidopsis thaliana. *Journal of experimental botany* **63**, 1751-1761, doi:10.1093/jxb/err406 (2012).

10 Sello, S. *et al.* Chloroplast Ca^{2+} fluxes into and across thylakoids revealed by thylakoid-targeted aequorin probes. *Plant Physiol*, **177**, 38-51, doi:10.1104/pp.18.00027 (2018). Brini,

11 M. *et al.* Transfected aequorin in the measurement of cytosolic Ca^{2+} concentration ([Ca^{2+}]c). A critical evaluation. *The Journal of biological chemistry* **270**, 9896-9903 (1995).

12 Ottolini, D., Cali, T. & Brini, M. Methods to measure intracellular Ca($^{2+}$) fluxes with organelle-targeted aequorin-based probes. *Methods in enzymology* **543**, 21-45, doi:10.1016/b978-0-12-801329-8.00002-7 (2014).

13 Fadouloglou, V. E., Kokkinidis, M. & Glykos, N. M. Determination of protein oligomerization state: two approaches based on glutaraldehyde crosslinking. *Analytical biochemistry* **373**, 404-406, doi:10.1016/j.ab.2007.10.027 (2008).

14 Kelley, L. A., Mezulis, S., Yates, C. M., Wass, M. N. & Sternberg, M. J. The Phyre2 web portal for protein modeling, prediction and analysis. *Nature protocols* **10**, 845-858, doi:10.1038/nprot.2015.053 (2015).

15 Adams, P. D. *et al.* PHENIX: a comprehensive Python-based system for macromolecular structure solution. *Acta crystallographica. Section D, Biological crystallography* **66**, 213-221, doi:10.1107/s0907444909052925 (2010).

16 Emsley, P. & Cowtan, K. Coot: model-building tools for molecular graphics. *Acta crystallographica. Section D, Biological crystallography* **60**, 2126-2132, doi:10.1107/s0907444904019158 (2004).

17 Hodis, E., Schreiber, G., Rother, K. & Sussman, J. L. eMovie: a storyboard-based tool for making molecular movies. *Trends in biochemical sciences* **32**, 199-204, doi:10.1016/j.tibs.2007.03.008 (2007).

18 Maruyama, K., Mikawa, T. & Ebashi, S. Detection of calcium binding proteins by ^{45}Ca autoradiography on nitrocellulose membrane after sodium dodecyl sulfate gel electrophoresis. *Journal of biochemistry* **95**, 511-519 (1984).

19 Navazio, L. *et al.* Evidence that spinach leaves express calreticulin but not calsequestrin. *Plant physiology* **109**, 983-990 (1995).

20 Moscatiello, R. *et al.* The intracellular delivery of TAT-aequorin reveals calcium-mediated sensing of environmental and symbiotic signals by the arbuscular mycorrhizal fungus Gigaspora margarita. *The New phytologist* **203**, 1012-1020, doi:10.1111/nph.12849 (2014).

21 Wagner, S. *et al.* The EF-Hand Ca^{2+} Binding Protein MICU Choreographs Mitochondrial Ca^{2+} Dynamics in Arabidopsis. *The Plant cell* **27**, 3190-3212, doi:10.1105/tpc.15.00509 (2015).

22 Teardo, E. et al. Alternative splicing-mediated targeting of the Arabidopsis GLUTAMATE RECEPTOR3.5 to mitochondria affects organelle morphology. Plant Physiology, 167, 216-227, doi:10.1104/pp.114.242602 (2015).

CHAPTER 4

Sensing environmental cues by chloroplast GLRs

Glutamate receptor-like channels (GLRs) are a group of ligand-gated non-selective cation channels with a widespread distribution inside the plant cell (Wudick *et al.*, 2018a,b). Due to the lack of a nervous system in plants, GLRs are obviously not linked to neurotransmission as instead is for the homologues belonging to the well-studied mammalian ionotropic glutamate receptors (iGluRs) family (Lacombe *et al.*, 2001; Julio-Pieper *et al.*, 2011). In particular, early evidence for the production of GLR agonists by plants led to the hypothesis of these molecules being defence-related compounds evolved as a survival strategy against herbivores. It was only with the sequencing of the *Arabidopsis thaliana* genome that GLRs channels were eventually identified and suggested to be involved in ion homeostasis for plant cells (Lam *et al.*, 1998; Weiland *et al.*, 2015). To date, more than twenty years later, our knowledge is now sufficiently broad to clearly link these ion channels to several physiological processes of the plant itself (De Vriese *et al.*, 2018). Most studies were indeed carried out in the model plant *Arabidopsis thaliana*, revealing that its genome encodes for 20 members of this channel family (Lam *et al.*, 1998; Davenport, 2002; Aouini *et al.*, 2012; Ni *et al.*, 2016); other higher plants, however, show a significantly different number of homologues – such as, for example, the poplar with its 61 GLRs (Ward *et al.*, 2009) – pointing to the general idea that GLRs families consist in large groups of functionally redundant genes (Roy *et al.*, 2008; De Vriese *et al.*, 2018). Actually, in the Arabidopsis genome (as well as in the *Solanum lycopersicum* one) genes encoding GLRs are often found in tandem along the same chromosome, meaning that many of them presumably originated as a result of single gene- or genome-wide duplication events (Taylor and Raes, 2004; Aouini *et al.*, 2012). Moreover, bioinformatic inquiries resulted in the separation of GLRs of Arabidopsis into three distinct clades (plus 10 additional subclades) which all demonstrate early evolutionary divergence with respect to animal iGluRs and according to which each gene derives its name (Chiu 1999, Davenport, 2002; Aouini *et al.*, 2012).

Owing to the high structural and sequence similarity between animal and plant glutamate receptors, plant GLRs are thought to function as Ca^{2+}-permeable channels involved in a great number of crucial plant cell processes (Kim *et al.*,

2001; Roy *et al.*, 2008; Tapken and Hollmann, 2008; Kwaaitaal *et al.*, 2011; Michard *et al.*, 2011; Forde *et al.*, 2014; Ortiz-Ramirez *et al.*, 2017; Vincent *et al.*, 2017; Toyota *et al.*, 2018). Indeed, comparative analyses with respect to the extensively-studied mammal iGluRs suggested that plant GLRs domain structures, channel orientation as well as the membrane topology are quite conserved (Lam *et al.*, 1998; Chiu *et al.*, 2002; Dubos *et al.*, 2003; Furukawa *et al.*, 2005; Price *et al.*, 2012; Weiland *et al.*, 2016). Moreover, also the tendency to form multimeric complexes is thought to be a retained character in plant GLRs, featuring a common hypothesis that suggests that GLRs actually assemble into tetrameric structures consisting in different subunits (Price *et al.*, 2013). Unfortunately, experiments performed in order to clarify whether these interactions occur in specific patterns ended in conflicting results and were thus unable to provide a definitive answer, possibly due to an intimate dependence of GLRs assembly on the peculiar metabolic state and/or cell type (Stephens *et al.*, 2008; Price *et al.*, 2013; Vincill *et al.*, 2013).

Conversely, plant GLRs show some distinctive differences at the level of key domains in terms of the channel functioning, thus providing a challenging scenario that need to be further investigated: it is well assessed, indeed, that GLRs ion selectivity cannot be directly compared to that of iGluRs, since crucial residues in the selectivity filter are not conserved in all GLRs homologues (De Bortoli *et al.*, 2016). In a similar way, the lack of two highly conserved residues in one of the transmembrane regions as well as the presence of second (instead of just one) ligand-binding motif in the N-terminal domain are both remarkable differences that could significantly alter the channel activity with respect to our current knowledge in the mammalian counterpart (Davenport, 2002, Acher and Bertrand, 2005). Moreover, increasing evidence also suggest that GLRs are not activated exclusively by glutamate and indeed the amino acidic range of plant GLRs agonists is broader compared to the animal one (each GLR member shows in fact its own specificity). Considering the high redundancy of plant GLRs genes and the numerous combinations that can be obtained by heterotetramerization as well as their differential expression profiles in distinct cell types or tissues, but also -the possibility for splicing variant, the above-mentioned GLRs distinctive

features may thus represent the molecular basis from which a great potential specificity (with a high spatial and temporal resolution) evolved in plant cells in order to precisely perceive and respond to environmental stimuli (Weiland *et al.*, 2015).

Electrophysiological studies performed on GLRs chimeras as well as patch clamp experiments carried out on full length GLRs expressed in heterologous systems have demonstrated the actual functioning of at least some GLRs (AtGLR1.1, 1.4, 3.4 and 3.7): other than being inhibited by classical iGluRs antagonists (6,7-dinitroquinoxaline-2,3-dione (DNQX), 5,7-dinitro-1,4-dihydro-2,3-quinoxalinedione (MNQX) and 2-amino-5-phosphonopentanoic acid (AP5) (Dubos *et al.*, 2003; Meyerhoff *et al.*, 2005; Vatsa *et al.*, 2011; De Vriese *et al.*, 2018)), these ion channels operate as non-selective cation channels (NSCCs) able to conduct both Na^+ and Ca^{2+}, with some of them being involved even in the transport of K^+, Mg^{2+} or Ba^{2+} (Roy *et al.*, 2008; Tapken and Hollmann, 2008; Vincill *et al.*, 2012; Tapken *et al.*, 2013). Their significance in terms of cellular and organellar ion homeostasis requires however an explanation, in particular considering that NSCCs are quite abundant both in plant and animal cells, although highly selective ion channels allow for a more precise recruitment of the required ion. In this context, several potential NSCCs advantages have been proposed, such as the use of a single channel to transport more than one ion species (and possibly different ions towards the two opposite directions) in order to quickly restore a membrane potential, or to allow the target cation uptake even if its specific highly-selective channel is blocked due to other bulky cations, as well as considering an indiscriminate flux of cations as a form of regulation for turgor-controlled ion channels (Davenport, 2002; Demidchik *et al.*, 2002).

Taken together, the data currently available indicate that glutamate, as well as other amino acids, may exert the role of short- and long-distance signalling molecules in the Ca^{2+}-mediated transduction of various physiological and developmental responses *via* the activity of GLRs. The consequent activation of GLRs channels located at the plasma membrane would thereby lead to an influx of Ca^{2+} from the extracellular space into the cytosol, thus generating

$[Ca^{2+}]_{cyt}$ transients that determine a cascade of downstream responses (Dennison and Spalding, 2000; Vatsa *et al.*, 2011; De Vriese *et al.*, 2018).

However, although most GLRs are predicted to have a plasma membrane targeting, GLR3.4 and 3.5 members were recently found to possess a dual intracellular localization: the former is in fact targeted both to the plasma membrane and to the inner envelope of chloroplasts, while the latter shows an alternative splicing-related targeting to either mitochondria or chloroplasts (Teardo *et al.*, 2010, 2011 and 2015). Due to reports suggesting GLR.3.4 transcript being upregulated in response to cold (Meyerhoff *et al.*, 2005), the research work of a previous Ph.D. student (Sara De Bortoli) in the group of Prof. I. Szabò (Department of Biology, University of Padova) focused on the search of a conditional phenotype to cold or chilling in the Arabidopsis knockout line lacking the above-mentioned channel. A similar effort was carried out also with other abiotic stimuli, and experiments were repeated in the *glr3.5* knockout line as well (the rationale being GLR3.5 as the homologue displaying the highest similarity and an identical pore region compared to GLR3.4) (De Bortoli, 2017, Ph.D. thesis).

The research work subsequently went on by transforming Arabidopsis *glr3.4* and *glr3.5* knockout lines with the construct encoding aequorin targeted to the chloroplast stroma. After analysis of aequorin expression via Western Blot analyses (see **Fig. 1**), as well as confirmation of the correct targeting of the YFP-tagged aequorin chimera to the chloroplast stroma by confocal microscopy observations (carried out by members of the Szabo's laboratory), transgenic lines stably expressing stromal aequorin were used in our laboratory for $[Ca^{2+}]$ measurement experiments in response to several abiotic and biotic stress conditions.

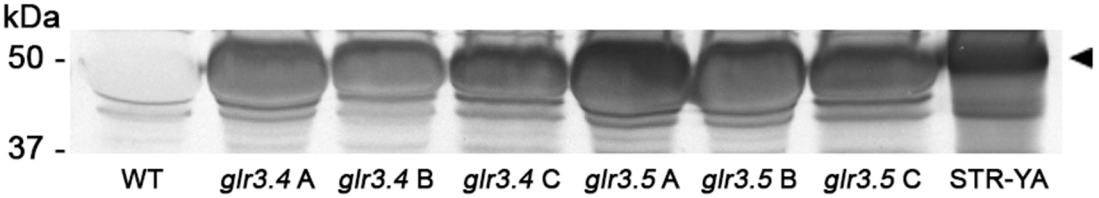

Fig. 1. Analysis of aequorin expression by immunoblotting in Arabidopsis *glr3.4* and *glr3.5* knockout transgenic lines stably transformed with a construct encoding YFP-aequorin targeted to the chloroplast stroma (STR-YA). Total protein extracts (50 µg) were separated by 12.5 % SDS-PAGE, transferred to PVDF and incubated with an anti-aequorin antibody (1:5000 diluted). Arrowhead indicates STR-YA transformed in a wild-type background and used as positive control. The wild-type (Col-0) line was used as negative control.

According to the aequorin-based Ca^{2+} assays that I performed (which are presented in **Fig. 2** and **3**), by comparing knockout mutants with wild-type controls, the GLR3.5 channel seems to be involved in response to cold, whereas the GLR3.4 shows instead a differential response to salinity. These preliminary results suggest that different Ca^{2+}-permeable channels may be involved in the transduction of specific environmental stimuli.

The present work, however, is clearly incomplete and further investigations will be carried out, after the end of my Ph.D. activity, in both the collaborating laboratories at the Department of Biology, University of Padova. In particular, a double *glr3.4glr3.5* knockout line transformed with stromal aequorin has just be obtained, so that in the future additional Ca^{2+} measurements, as well as the search for a conditional phenotype, will be performed in order to avoid potential compensatory effects between the two GLRs homologues. This issue must be taken into careful consideration, especially on the basis of a potential heterotetramerization between the two close GLR3.4 and 3.5 homologues. Moreover, the establishment of GLRs knockout transgenic lines stably expressing cytosolic aequorin is under way, allowing the monitoring of Ca^{2+} dynamics in another subcellular compartment strictly linked to chloroplasts in terms of Ca^{2+} handling and exchange of the ion during signalling events. Moreover, quantitative RT-PCR experiments aimed at the analysis of the relative expression levels of these channels will be performed under constitutive and stress-induced conditions. These studies may further advance our understanding of the precise physiological role and regulatory mechanisms of the two considered GLRs homologues.

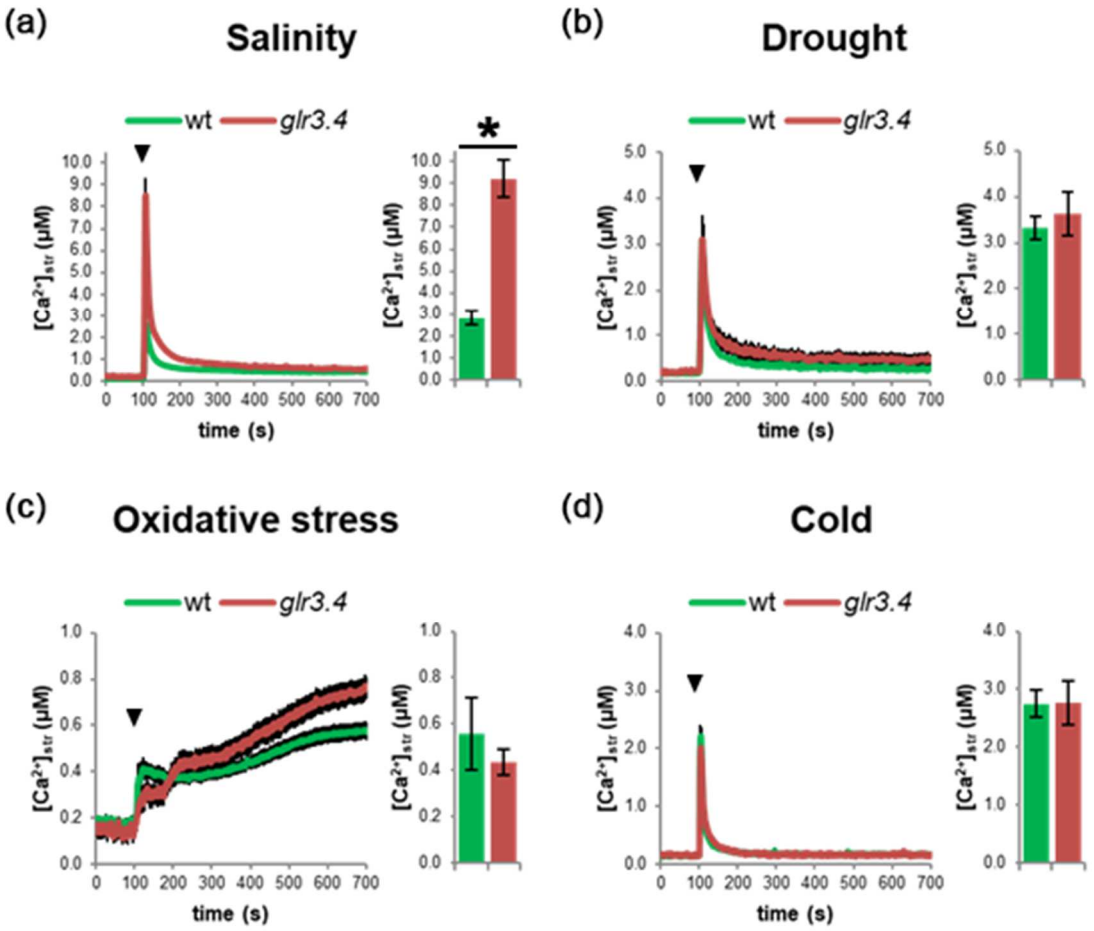

Fig. 2. Monitoring of $[Ca^{2+}]_{str}$ dynamics in response to environmental stimuli of abiotic nature. Ca^{2+} assays were conducted in Arabidopsis wild-type (green) and *glr3.4* knockout (red) lines stably-expressing STR-YA. Seedlings were challenged (100 s, black arrowhead) with: **(a)** 300 mM NaCl; **(b)** 600 mM mannitol; **(c)** 10 mM H_2O_2; **(d)** H_2O at 0°C. Data are the means (solid lines) ± SE (shadings) of ≥10 independent experiments. Asterisk indicates data that differ significantly ($P < 0.05$, Student's *t* test).

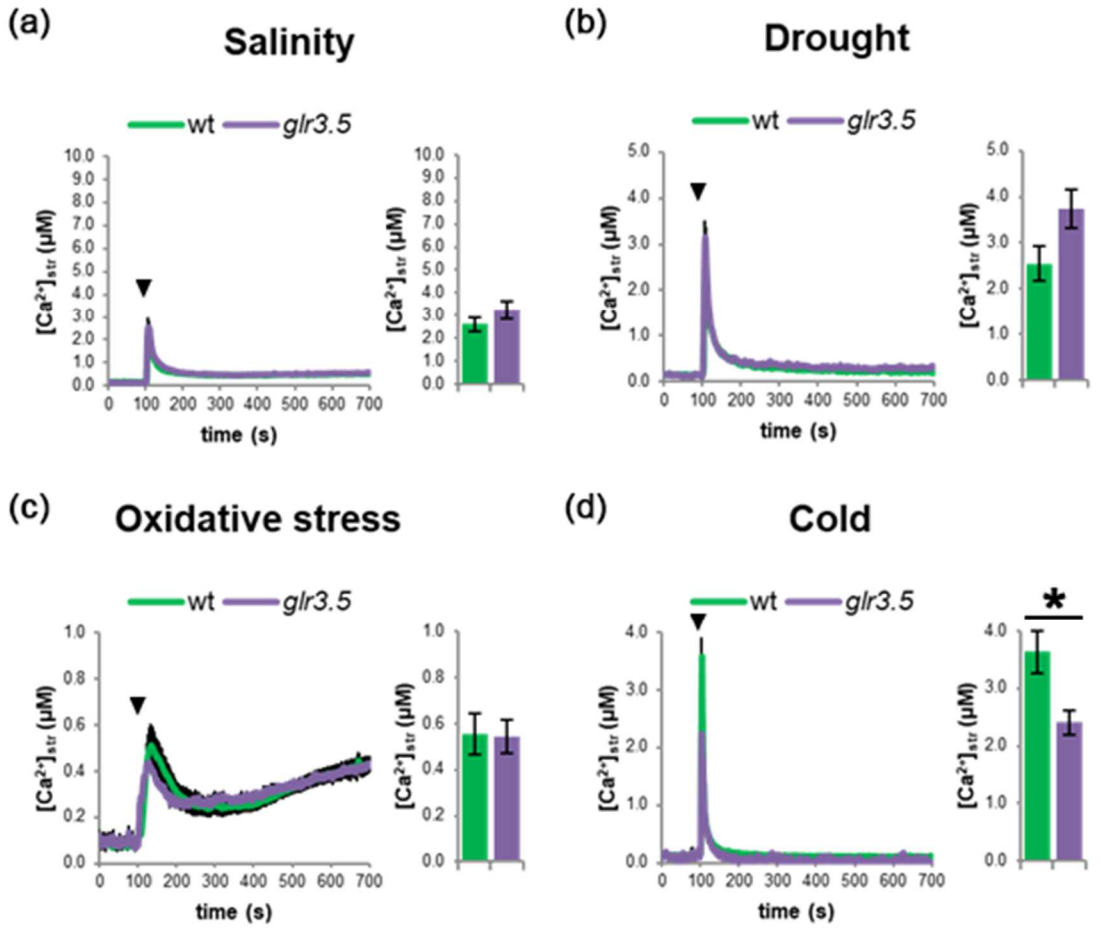

Fig. 3. Monitoring of $[Ca^{2+}]_{str}$ dynamics in response to environmental stimuli of abiotic nature. Ca^{2+} assays were conducted in Arabidopsis wild-type (green) and *glr3.4* knockout (violet) lines stably-expressing STR-YA. Seedlings were challenged (100 s, black arrowhead) with: **(a)** 300 mM NaCl; **(b)** 600 mM mannitol; **(c)** 10 mM H_2O_2; **(d)** H_2O at 0°C. Data are the means (solid lines) ± SE (shadings) of ≥10 independent experiments. Asterisk indicates data that differ significantly ($P < 0.05$, Student's *t* test).

REFERENCES

Acher FC, Bertrand HO (2005) Amino acid recognition by Venus flytrap domains is encoded in an 8-residue motif. Biopolymers **80:** 357-366

Aouini A, Matsukura C, Ezura H, Asamizu E (2012) Characterisation of 13 glutamate receptor-like genes encoded in the tomato genome by structure, phylogeny and expression profiles. Gene **493:** 36-43

Chiu J, DeSalle R, Lam HM, Meisel L, Coruzzi G (1999) Molecular evolution of glutamate receptors: a primitive signaling mechanism that existed before plants and animals diverged. Mol Biol Evol **16:** 826-838

Chiu JC, Brenner ED, DeSalle R, Nitabach MN, Holmes TC, Coruzzi GM (2002) Phylogenetic and expression analysis of the glutamate-receptor-like gene family in *Arabidopsis thaliana*. Mol Biol Evol **19:** 1066-1082

Davenport R (2002) Glutamate receptors in plants. Ann Bot **90:** 549-557

De Bortoli S, Teardo E, Szabo I, Morosinotto T, Alboresi A (2016) Evolutionary insight into the ionotropic glutamate receptor superfamily of photosynthetic organisms. Biophys Chem **218:** 14-26

De Bortoli S (2017) Characterization of ion channels in chloroplasts and mitochondria of land plants. Ph.D. thesis (Ph.D. Course in Biosciences and Biotechnologies, curriculum: Biochemistry and Biophysics), University of Padova

De Vriese K, Costa A, Beeckman T, Vanneste S (2018) Pharmacological strategies for manipulating plant Ca^{2+} signalling. Int J Mol Sci **19:** 1506

Demidchik V, Davenport RJ, Tester M (2002) Nonselective cation channels in plants. Annu Rev Plant Biol **53:** 67-107

Dennison KL, Spalding EP (2000) Glutamate-gated calcium fluxes in Arabidopsis. Plant Physiol **124:** 1511-1514

Dubos C, Huggins D, Grant GH, Knight MR, Campbell MM (2003) A role for glycine in the gating of plant NMDA-like receptors. Plant J **35:** 800-810

Forde BG, Roberts MR (2014) Glutamate receptor-like channels in plants: a role as amino acid sensors in plant defence? F1000Prime Rep **6:** 37

Furukawa H, Singh SK, Mancusso R, Gouaux E (2005) Subunit arrangement and function in NMDA receptors. Nature **438:** 185-192

Julio-Pieper M, Flor PJ, Dinan TG, Cryan JF (2011) Exciting times beyond the brain: metabotropic glutamate receptors in peripheral and non-neural tissues. Pharmacol Rev **63:** 35-58

Kim SA, Kwak JM, Jae SK, Wang MH, Nam HG (2001) Overexpression of the *AtGluR2* gene encoding an Arabidopsis homolog of mammalian glutamate receptors impairs calcium utilization and sensitivity to ionic stress in transgenic plants. Plant Cell Physiol **42:** 74-84

Kwaaitaal M, Huisman R, Maintz J, Reinstadler A, Panstruga R (2011) Ionotropic glutamate receptor (iGluR)-like channels mediate MAMP-induced calcium influx in *Arabidopsis thaliana*. Biochem J **440:** 355-365

Lacombe B, Becker D, Hedrich R, DeSalle R, Hollmann M, Kwak JM, Schroeder JI, Le Novere N, Nam HG, Spalding EP, Tester M, Turano FJ, Chiu J, Coruzzi G (2001) The

identity of plant glutamate receptors. Science **292:** 1486-1487

Lam HM, Chiu J, Hsieh MH, Meisel L, Oliveira IC, Shin M, Coruzzi G (1998) Glutamate-receptor genes in plants. Nature **396:** 125-126

Meyerhoff O, Muller K, Roelfsema MR, Latz A, Lacombe B, Hedrich R, Dietrich P, Becker D (2005) *AtGLR3.4*, a glutamate receptor channel-like gene is sensitive to touch and cold. Planta **222:** 418-427

Michard E, Lima PT, Borges F, Silva AC, Portes MT, Carvalho JE, Gilliham M, Liu LH, Obermeyer G, Feijo JA (2011) Glutamate receptor-like genes form Ca^{2+} channels in pollen tubes and are regulated by pistil D-serine. Science **332:** 434-437

Ni J, Yu Z, Du G, Zhang Y, Taylor JL, Shen C, Xu J, Liu X, Wang Y, Wu Y (2016) Heterologous expression and functional analysis of rice GLUTAMATE RECEPTOR-LIKE family indicates its role in glutamate triggered calcium flux in rice roots. Rice (N Y) **9:** 9

Ortiz-Ramirez C, Michard E, Simon AA, Damineli DSC, Hernandez-Coronado M, Becker JD, Feijo JA (2017) GLUTAMATE RECEPTOR-LIKE channels are essential for chemotaxis and reproduction in mosses. Nature **549:** 91-95

Price MB, Jelesko J, Okumoto S (2012) Glutamate receptor homologs in plants: functions and evolutionary origins. Front Plant Sci **3:** 235

Price MB, Kong D, Okumoto S (2013) Inter-subunit interactions between glutamate-like receptors in *Arabidopsis*. Plant Signal Behav **8:** e27034

Roy SJ, Gilliham M, Berger B, Essah PA, Cheffings C, Miller AJ, Davenport RJ, Liu LH, Skynner MJ, Davies JM, Richardson P, Leigh RA, Tester M (2008) Investigating glutamate receptor-like gene co-expression in *Arabidopsis thaliana*. Plant Cell Environ **31:** 861-871

Stephens NR, Qi Z, Spalding EP (2008) Glutamate receptor subtypes evidenced by differences in desensitization and dependence on the *GLR3.3* and *GLR3.4* genes. Plant Physiol **146:** 529-538

Tapken D, Hollmann M (2008) *Arabidopsis thaliana* glutamate receptor ion channel function demonstrated by ion pore transplantation. J Mol Biol **383:** 36-48

Tapken D, Anschutz U, Liu LH, Huelsken T, Seebohm G, Becker D, Hollmann M (2013) A plant homolog of animal glutamate receptors is an ion channel gated by multiple hydrophobic amino acids. Sci Signal **6:** ra47

Taylor JS, Raes J (2004) Duplication and divergence: the evolution of new genes and old ideas. Annu Rev Genet **38:** 615-643

Teardo E, Segalla A, Formentin E, Zanetti M, Marin O, Giacometti GM, Lo Schiavo F, Zoratti M, Szabo I (2010) Characterization of a plant glutamate receptor activity. Cell Physiol Biochem **26:** 253-262

Teardo E, Formentin E, Segalla A, Giacometti GM, Marin O, Zanetti M, Lo Schiavo F, Zoratti M, Szabo I (2011) Dual localization of plant glutamate receptor AtGLR3.4 to plastids and plasmamembrane. Biochim Biophys Acta **1807:** 359-367

Teardo E, Carraretto L, De Bortoli S, Costa A, Behera S, Wagner R, Lo Schiavo F, Formentin E, Szabo I (2015) Alternative splicing-mediated targeting of the Arabidopsis GLUTAMATE RECEPTOR3.5 to mitochondria affects organelle morphology. Plant Physiol **167:** 216-227

Toyota M, Spencer D, Sawai-Toyota S, Jiaqi W, Zhang T, Koo AJ, Howe GA, Gilroy S (2018) Glutamate triggers long-distance, calcium-based plant defense signaling. Science **361:** 1112-1115

Vatsa P, Chiltz A, Bourque S, Wendehenne D, Garcia-Brugger A, Pugin A (2011) Involvement of putative glutamate receptors in plant defence signaling and NO production. Biochimie **93:** 2095-2101

Vincent TR, Avramova M, Canham J, Higgins P, Bilkey N, Mugford ST, Pitino M, Toyota M, Gilroy S, Miller AJ, Hogenhout SA, Sanders D (2017) Interplay of plasma membrane and vacuolar ion channels, together with BAK1, elicits rapid cytosolic calcium elevations in Arabidopsis during aphid feeding. Plant Cell **29:** 1460-1479

Vincill ED, Bieck AM, Spalding EP (2012) Ca^{2+} conduction by an amino acid-gated ion channel related to glutamate receptors. Plant Physiol **159:** 40-46

Vincill ED, Clarin AE, Molenda JN, Spalding EP (2013) Interacting glutamate receptor-like proteins in Phloem regulate lateral root initiation in *Arabidopsis*. Plant Cell **25:** 1304-1313

Ward JM, Maser P, Schroeder JI (2009) Plant ion channels: gene families, physiology, and functional genomics analyses. Annu Rev Physiol **71:** 59-82

Weiland M, Mancuso S, Baluska F (2015) Signalling via glutamate and GLRs in *Arabidopsis thaliana*. Funct Plant Biol **43:** 10.1071/FP15109

Wudick MM, Michard E, Oliveira Nunes C, Feijo JA (2018a) Comparing plant and animal glutamate receptors: common traits but different fates? J Exp Bot **69:** 4151-4163

Wudick MM, Portes MT, Michard E, Rosas-Santiago P, Lizzio MA, Nunes CO, Campos C, Santa Cruz Damineli D, Carvalho JC, Lima PT, Pantoja O, Feijo JA (2018b) CORNICHON sorting and regulation of GLR channels underlie pollen tube Ca^{2+} homeostasis. Science **360:** 533-536

CHAPTER 5

Arabidopsis photosynthetic and heterotrophic cell suspension cultures

PROLOGUE

While physiological investigations in the plant biology fields often deal with entire plants subjected to a wide range of natural and/or artificial environmental conditions, the use of simplified systems such as cell suspension cultures still represents a valuable methodology for structural, metabolic and signalling studies (Hampp *et al.*, 2012). The demand in fact stems from the necessity to reduce the complexity of a whole plant system, in order to dissect intricate phenomena into their basic components. Plant cell suspension cultures indeed provide a convenient way to more easily analyze complex plant physiological processes. By resolving the complexity of an *in toto* plant into its elementary units, suspension-cultured cells often represent a useful tool to investigate a wide range of phenomena (Moscatiello *et al.*, 2013).

Indeed, in the last few decades the plant science field has made an extensive use of suspension-cultured cells as a key experimental technique in many fields of investigation: ion transport, secondary metabolite production, gene expression and defence responses are some examples of research topics that commonly employ explant-derived cell cultures to explore plant physiology at the cellular and molecular levels (Moscatiello *et al.*, 2013). Notably, Ca^{2+}-mediated signalling studies have greatly benefited from the use of these experimental systems, due to the fact that organisms *in toto* are not always suitable to dissect specific responses. For example, the Ca^{2+}-sensitive photoprotein aequorin allows for the monitoring of changes in the Ca^{2+}-dependent bioluminescence deriving from the whole plant, making it difficult to dissect the contribution of different tissue/cell types to the observed Ca^{2+} response. Moreover, the homogeneity of a cell suspension culture can help the amplification and hence the detection of even faint Ca^{2+} signals, as demonstrated by several works on Ca^{2+}-based signalling pathways during plant-microbe interactions (Lecourieux *et al.*, 2005; Moscatiello *et al.*, 2006; Navazio *et al.*, 2007a,b). On the other hand, studies based only on cell suspension cultures fail to unravel the potential systemic integration between different plant organs, suggesting the necessity to carry out *in vivo* studies in

order to confirm and expand *in vitro* observations (Choi *et al.*, 2017, Hilleary and Gilroy, 2018).

Suspension-cultured cell systems have proved to be fundamental keystones in the past by helping to uncover the role of several plant hormones (Caplin and Steward, 1948; Miller *et al.*, 1955; Skoog and Miller, 1957). More recently, they have become suitable intermediate step in plant genetic engineering, by allowing transient expression of new characters via transfection of exogenous DNA into protoplasts, that can be easily obtained in bulk quantities by the incubation of suspension-cultured cells with mixtures of cell wall-degrading enzymes. Also the pharmaceutical research field is greatly interested in this experimental system, since the employment of plant cell suspension cultures has allowed the large-scale production of secondary metabolites and other molecules of interest, such as recombinant proteins (Wilson and Roberts, 2012; Vasilev *et al.*, 2016; Schillberg *et al.*, 2019). Extensive efforts have been spent searching for specific stress conditions and/or stimulations which may increase the production and the accumulation of the desired compounds in *in vitro* culture conditions (see *e.g.* Guarnerio *et al.*, 2012; Toffali *et al.*, 2013; Commisso *et al.*, 2016). Accordingly, a more detailed knowledge of the different plant requirements could allow for the development of new strategies that use plant cell cultures as production platforms for the obtainment of valuable compounds for industrial applications (Schmitz *et al.*, 2016). In the Ca^{2+} signalling field, the generation of photosynthetic and heterotrophic cell suspension cultures of *Arabidopsis thaliana*, containing either chloroplasts or amyloplasts, respectively, has allowed the detection of stimulus-specific Ca^{2+} signals in the stroma of the two distinct plastid types (Sello *et al.*, 2016), as well as the elucidation of the role of thylakoids in shaping chloroplastic Ca^{2+} dynamics (see **Chapter 2**, Sello *et al.*, 2018).

Thanks to the functional plasticity that typically characterizes plastids, Arabidopsis cell cultures can be slowly interconverted between a heterotrophic and a photosynthetic state by a stepwise decrease in the sucrose concentration in the culture medium. However, until recent times, this interconversion has required a time-consuming procedure (about 2 years)

(Hampp *et al.*, 2012). More recently, a novel procedure developed in our laboratory has provided a faster and efficient method to obtain Arabidopsis photosynthetic cell suspension cultures (Sello *et al.*, 2017). The direct germination of Arabidopsis seeds on a hormone-containing medium (MS, 3% sucrose, 0.25 µg/µl 6-benzylaminopurine, 0.5 µg/µl 2,4-dichlorophenoxyacetic, 0.8% agar, pH 5.5) made it possible to generate green calli at the level of seedling hypocotyls in 3 weeks. The subsequent transfer of these calli into liquid culture medium containing the same concentrations of phytohormones and gradually decreasing sucrose levels allowed for the establishment of cell suspension cultures containing functional chloroplasts in a faster (about 2-3 months) and easier way than previously described procedures. The combined use of both heterotrophic and photosynthetic cell cultures may allow to obtain insights into the unique features of chloroplasts *versus* non-green plastids, as well as their integration in the structural and metabolic compartmentalization of the plant cell.

In this chapter I have described in detail the procedures commonly used in our laboratory to establish and maintain Arabidopsis photosynthetic and heterotrophic cell suspension cultures. This manuscript represents an invited contribution to the fourth edition of the Arabidopsis Protocols book for the Methods in Molecular Biology series of Springer, providing a handy manual for those who wish to approach to the field. After briefly dealing with theoretical aspects of plant suspension-cultured cells, the chapter mainly focuses on the detailed description of the procedures required to establish photosynthetic and heterotrophic cell suspension cultures of Arabidopsis. The intention was to provide researchers, who are starting to work with Arabidopsis cell cultures, with a beginner guide. Besides the detailed description of the protocols underlying the generation and maintenance of Arabidopsis cell suspension cultures, a section consisting in a list of experience-based tips was also included to facilitate a potential user in generating *in vitro* cell cultures. Figures illustrating macroscopic observations of the different cell cultures, together with confocal microscopy and transmission electron microscopy observations, were prepared. Moreover, data concerning the determination of the cell culture growth curve and evaluation of the photosynthetic efficiency of the cell

suspension cultures, measured by PAM analyses, were also provided. Photosynthetic and heterotrophic cell suspension cultures can be used for many different structural and functional studies, including signalling ones, as shown in **Chapter 2**. Moreover, they are also suitable experimental systems to perform intracellular localization studies of recombinant proteins, as demonstrated in **Chapter 3**.

The described protocols provide useful experimental tools to investigate the participation of chloroplasts, as well as non-green plastids, in intracellular Ca^{2+} handling and to highlight differences between the different functional types of plastids in terms of Ca^{2+} responses to environmental stimuli.

REFERENCES

Caplin SM, Steward FC (1948) Effect of coconut milk on the growth of explants from carrot root. Science **108:** 655-657

Choi WG, Miller G, Wallace I, Harper J, Mittler R, Gilroy S (2017) Orchestrating rapid long-distance signaling in plants with Ca^{2+}, ROS and electrical signals. Plant J **90:** 698-707

Commisso M, Toffali K, Strazzer P, Stocchero M, Ceoldo S, Baldan B, Levi M, Guzzo F (2016) Impact of phenylpropanoid compounds on heat stress tolerance in carrot cell cultures. Front Plant Sci **7:** 1439

Guarnerio CF, Fraccaroli M, Gonzo I, Pressi G, Dal Toso R, Guzzo F, Levi M (2012) Metabolomic analysis reveals that the accumulation of specific secondary metabolites in *Echinacea angustifolia* cells cultured in vitro can be controlled by light. Plant Cell Rep **31:** 361-367

Hampp C, Richter A, Osorio S, Zellnig G, Sinha AK, Jammer A, Fernie AR, Grimm B, Roitsch T (2012) Establishment of a photoautotrophic cell suspension culture of *Arabidopsis thaliana* for photosynthetic, metabolic, and signaling studies. Mol Plant **5:** 524-527

Hilleary R, Gilroy S (2018) Systemic signaling in response to wounding and pathogens. Curr Opin Plant Biol **43:** 57-62

Lecourieux D, Lamotte O, Bourque S, Wendehenne D, Mazars C, Ranjeva R, Pugin A (2005) Proteinaceous and oligosaccharidic elicitors induce different calcium signatures in the nucleus of tobacco cells. Cell Calcium **38:** 527-538

Miller CO, Skoog F, Von Saltza MH, Strong F (1955) Kinetin, a cell division factor from deoxyribonucleic acid. J Am Chem Soc **77:** 1392

Moscatiello R, Mariani P, Sanders D, Maathuis FJ (2006) Transcriptional analysis of calcium-dependent and calcium-independent signalling pathways induced by oligogalacturonides. J Exp Bot **57:** 2847-2865

Moscatiello R, Baldan B, Navazio L (2013) Plant cell suspension cultures. Methods Mol Biol **953:** 77-93

Navazio L, Baldan B, Moscatiello R, Zuppini A, Woo SL, Mariani P, Lorito M (2007a) Calcium-mediated perception and defense responses activated in plant cells by metabolite mixtures secreted by the biocontrol fungus *Trichoderma atroviride*. BMC Plant Biol **7:** 41

Navazio L, Moscatiello R, Genre A, Novero M, Baldan B, Bonfante P, Mariani P (2007b) A diffusible signal from arbuscular mycorrhizal fungi elicits a transient cytosolic calcium elevation in host plant cells. Plant Physiol **144:** 673-681

Schillberg S, Raven N, Spiegel H, Rasche S, Buntru M (2019) Critical analysis of the commercial potential of plants for the production of recombinant proteins. Front Plant Sci **10:** 720

Schmitz C, Fritsch L, Fischer R, Schillberg S, Rasche S (2016) Statistical experimental designs for the production of secondary metabolites in plant cell suspension cultures. Biotechnol Lett **38:** 2007-2014

Skoog F, Miller CO (1957) Chemical regulation of growth and organ formation in plant tissue cultures *in vitro*. Symp Soc Exp Biol **11:** 118-131

Sello S, Perotto J, Carraretto L, Szabo I, Vothknecht UC, Navazio L (2016) Dissecting stimulus-specific Ca^{2+} signals in amyloplasts and chloroplasts of *Arabidopsis thaliana* cell

suspension cultures. J Exp Bot **67:** 3965-3974

Sello S, Moscatiello R, La Rocca N, Baldan B, Navazio L (2017) A rapid and efficient method to obtain photosynthetic cell suspension cultures of *Arabidopsis thaliana*. Front Plant Sci **8:** 1444

Sello S, Moscatiello R, Mehlmer N, Leonardelli M, Carraretto L, Cortese E, Zanella FG, Baldan B, Szabo I, Vothknecht UC, Navazio L (2018) Chloroplast Ca^{2+} fluxes into and across thylakoids revealed by thylakoid-targeted aequorin probes. Plant Physiol **177:** 38-51

Toffali K, Ceoldo S, Stocchero M, Levi M, Guzzo F (2013) Carrot-specific features of the phenylpropanoid pathway identified by feeding cultured cells with defined intermediates. Plant Sci **209:** 81-92

Vasilev N, Boccard J, Lang G, Gromping U, Fischer R, Goepfert S, Rudaz S, Schillberg S (2016) Structured plant metabolomics for the simultaneous exploration of multiple factors. Sci Rep **6:** 37390

Wilson SA, Roberts SC (2012) Recent advances towards development and commercialization of plant cell culture processes for the synthesis of biomolecules. Plant Biotechnol J **10:** 249-268

This work is currently under revision as:

Photosynthetic and heterotrophic cell suspension cultures

Enrico Cortese[1], Luca Carraretto[1], Barbara Baldan[1,2] and Lorella Navazio[1,2]

[1]Department of Biology, University of Padova, 35131 Padova, Italy

[2]Botanical Garden, University of Padova, 35123 Padova, Italy

In Arabidopsis Protocols, Fourth Edition, Sanchez-Serrano JJ and Salinas J eds. Springer, Berlin (DE), Methods in Molecular Biology series.

Photosynthetic and heterotrophic cell suspension cultures

Enrico Cortese[1], Luca Carraretto[1], Barbara Baldan[1,2], and Lorella Navazio[1,2]

[1]Department of Biology, University of Padova, 35131 Padova, Italy

[2]Botanical Garden, University of Padova, 35123 Padova, Italy

Abstract

Cell suspension cultures represent a widely used experimental tool suitable to perform a variety of structural and physiological studies in a more simplified system compared to the organism *in toto*. In this chapter we describe the methods routinely used in our laboratory to establish and maintain Arabidopsis photosynthetic and heterotrophic cell suspension cultures, containing either chloroplasts or amyloplasts, respectively. The use of these *in vitro* systems may allow to obtain insights into the unique features of green plastids *versus* nongreen plastids, as well as their integration in the structural and metabolic compartmentalization of the plant cell.

Key words Arabidopsis, Seeds, Culture medium, Phytohormones, *In vitro* growth, Calli, Cell suspension cultures, Chloroplasts, Amyloplasts, Protoplasts.

Running Head Cell Suspension Cultures

1. Introduction

Arabidopsis in vitro cultures have been established a long time ago, with the first reports dating back to the sixties and seventies of the last century [1-2]. Methodologies for the production of calli - clusters of dedifferentiated cells growing on solid culture media - as well as the set up of Arabidopsis cell suspension cultures - cells growing in liquid culture media under constant shaking - have been described in details [*e.g.* 3-4]. In vitro technologies, allowing for the dissection of the entire Arabidopsis plant into its elementary units, represent an invaluable tool in basic research, and have greatly contributed to advancing our knowledge of the cellular and molecular biology, biochemistry, physiology of this model plant.

For a long time most techniques have allowed only for the obtainment of Arabidopsis heterotrophic cell suspension cultures - *i.e.* containing amyloplasts -, whereas the production of photosynthetic cell suspension cultures - *i.e.* containing chloroplasts - has proven more difficult to obtain. More recently, methods have been described to successfully establish them [5-6], and the advantages of working with Arabidopsis cell cultures containing functional chloroplasts have become increasingly evident [5, 7].

Cell suspension cultures can be used for a number of structural and functional studies, including signalling ones. The use of Arabidopsis photosynthetic and heterotrophic cell suspension cultures has recently highlighted differences between non-green plastids and chloroplasts in terms of organellar calcium signals in response to environmental stimuli [8]. Moreover, they have been useful to demonstrate the restriction of light-to-dark induced Ca^{2+} fluxes to chloroplasts only [8], and to investigate the integration of thylakoids in the Ca^{2+} signalling network [9].

Nevertheless, an intrinsic limitation of cell culture systems is given by their incompatibility with systemic signalling studies, focused on the communication and exchange of signals among different tissues and organs in the elaboration of long-distance responses [10-11].

Cell suspension cultures are also suitable experimental systems to perform intracellular localization studies of recombinant proteins. Indeed, they can be obtained from transgenic plants expressing fluorescently tagged versions of the proteins of interest [8]. Moreover, cell suspension cultures represent a convenient system for the isolation of protoplasts (*i.e.* cells enzymatically deprived of the cell wall), that can be isolated with high yields starting from mid-exponential phase suspension-cultured cells. Protoplasts can be useful for a number of studies, *e.g.* after transient expression of proteins of interest [12]. For example, we have recently demonstrated that an Arabidopsis homologue of the mitocondrial calcium uniporter (cMCU) localizes to the chloroplast envelope [13]. The intracellular localization of this organellar calcium-permeable channel was ascertained by using protoplasts obtained by both photosynthetic and heterotrophic cell cultures, transiently co-transformed with constructs encoding a GFP-fused version of cMCU and membrane markers of the different chloroplast subcompartments [13].

It has to be noted that photosynthetic and heterotropic cell suspension cultures are somehow interconvertible, by modulating sucrose concentration and light regime [5-6, 8]. This is possible thanks to the innate plasticity of plastids, highly dynamic organelles that can interconvert in response to developmental and environmental cues [14-15].

In this chapter, we describe in detail the protocols routinely used in our laboratory to establish and maintain Arabidopsis photosynthetic and heterotrophic cell suspension

cultures. This simple and precise guide will take the operator, including an absolute beginner, through the basic steps of Arabidopsis cell cultures. Modifications to the described protocols can be made and procedures can be tailored according to the host laboratory needs and habits.

2. Materials

2.1 Growth Facilities

The establishment and maintenance of plant cell cultures requires the availability of several *in vitro* growth facilities, such as a growth chamber equipped with light/temperature control and a laminar flow hood where all the procedures that require sterile conditions are conducted. The growth chamber for cell cultures is set at a temperature of 24°C and a photoperiod of 16 h light / 8 h dark.

Herewith is a list of laboratory equipment and material needed for the different procedures described in this Chapter to set up and maintain Arabidopsis photosynthetic and heterotrophic cell cultures.

2.2 Preparation of Phytohormones and Culture Media

1. 6-Benzylaminopurine (BAP).
2. 2,4-Dichlorophenoxyacetic acid (2,4-D).
3. Kinetin.
4. Murashige and Skoog basal medium (micro- and macroelements including vitamins).
5. Gamborg B5 basal medium (micro- and macroelements including vitamins).

6. Sucrose.
7. Plant agar.
8. 2-(N-Morpholino)ethanesulfonic acid (MES).
9. 1 N KOH.
10. 0.1 N HCl.
11. Ethanol.
12. Distilled H_2O.
13. 50 ml syringes.
14. Sterile disposable 0.22 μm filter units.
15. Sterile 1.5 ml Eppendorf-like tubes.
16. Pipet-aid and sterile disposable 2 ml pipettes.
17. Beakers, cylinders, Duran bottles.
18. Analytical balance.
19. Magnetic stirrer and stir bar.
20. pH meter.
21. Autoclave.
22. Oven.
23. Autoclave tape.
24. Refrigerator and freezer.

2.3 Preparation of plates containing agarized medium

1. Round sterile Petri dishes for cell cultures (100 mm diameter × 20 mm height).

2. Cell culture media (see Subheadings 3.2.2 and 3.3.2).

3. Proper antibiotic/herbicide, P20 micropipette and sterile tips (for transgenic lines).

4. Pipet-aid and sterile disposable 25 ml and 10 ml pipettes.
5. Parafilm.
6. Microwave oven.

2.4 Surface sterilization of seeds and sowing on Petri dishes

1. Seeds of *Arabidopsis thaliana*, Columbia 0 (Col-0) ecotype (*see* **Note 1**).
2. 1.5 ml or 2 ml Eppendorf-like tubes.
3. Filter paper.
4. P200 and P1000 micropipettes and sterile tips.
5. Ethanol.
6. Triton X-100.
7. Distilled H_2O.
8. Petri dishes containing Solid Medium for Green Callus Induction (see Subheading 3.2.2) or Solid Medium for Seed Germination (see Subheading 3.3.2).

2.5 Manipulation of callus cultures

1. Sterile forceps and scalpel.
2. Petri dishes containing the Solid Medium for Callus Maintenance (see Subheadings 3.3.2).
3. Parafilm.
4. Ethanol.
5. Bunsen burner.

2.6 Initiation of cell suspension cultures

1. Sterile 50 ml Erlenmeyer flasks.

2. Liquid Medium for Cell Suspension Cultures (see Subheadings 3.2.2 and 3.3.2).

3. Pipet-aid and sterile disposable 25 ml and 10 ml pipettes.

4. Proper antibiotic/herbicide, P20 micropipette and sterile tips (for transgenic lines).

5. Sterile forceps and scalpel.

6. Orbital shaker.

7. Bunsen burner.

8. Scissors.

2.7 Subculturing of cell suspension cultures

1. Sterile 100 ml (or larger volume) Erlenmeyer flasks.
2. Liquid Medium for Cell Suspension Cultures (see Subheadings 3.2.2 and 3.3.2).
3. Pipet-aid and sterile disposable 25 ml and 10 ml pipettes.
4. Proper antibiotic/herbicide, P20 micropipette and sterile tips (for transgenic lines).
5. Orbital shaker.
6. Scissors
7. Bunsen burner.

2.8 Measurement of fresh weight

1. 1.5 ml Eppendorf-like tubes.
2. Pipet-aid and sterile disposable 10 ml pipettes.
3. P1000 micropipette and sterile tips.
4. Sterile scalpel.
5. 1 ml syringe with a thin needle.
6. Benchtop centrifuge.

7. Analytical balance.

2.9 Protoplast Isolation

1. Cellulase "Onozuka" R-10.
2. Macerozyme R-10.
3. Liquid Medium for Cell Suspension Cultures (see Subheading 3.2.2 and 3.3.2).
4. Mannitol.
5. Analytic balance.
6. Beakers, cylinders.
7. Magnetic stirrer and stir bar.
8. Sterile 50 ml and 15 ml tubes.
9. Pipet-aid and sterile disposable 10 ml pipettes.
10. Sterile disposable vacuum filtration units.
11. Aluminum foil.
12. 50 μm nylon mesh.
13. 100 ml glass beaker.
14. Rubber bands.
15. Sterile scalpel.
16. Sterile disposable plastic Pasteur pipettes.
17. Orbital shaker.
18. Benchtop centrifuge.

2.10 Pulse-Amplitude Modulation Fluorometry

1. PAM imaging fluorometer.
2. Sterile disposable 6-well plates.

3. Methods

3.1 Sterility Conditions

The maintenance of sterility at all times is a *conditio sine qua non* for the establishment of *in vitro* cultures.

1. All appropriate manipulations must be carried out in a laminar flow hood, using sterile disposable plasticware (pipettes, tips, tubes, Petri dishes), sterilized glassware (Erlenmeyer flasks, beakers, bottles) and sterilized metalware (forceps, scalpels) (*see* **Note 2**).
2. Wash your hands and clean them with ethanol before working in the laminar flow hood, or wear gloves.
3. Wipe the bench under the laminar flow hood with denatured alcohol before and after use.
4. Never pass over open sterile labware with your hands or arms, when you are working in the laminar flow hood. Avoid to speak, caugh, sneeze.
5. Once a week, sterilize the environment under the laminar flow cabinet by using the UV lamp according to manufacturer's instructions.

3.2 Establishment and maintenance of photosynthetic cell suspension cultures

Herewith we describe a method based on the direct germination of Arabidopsis seeds on a sucrose-containing agarized culture medium supplemented with exogenous phytohormones, that leads to the formation of green calli at the hypocotyl level [6]. The subsequent transfer of these green calli in liquid media containing stepwise decreased sucrose concentrations allows for the set up of photosynthetic cell cultures

in a time interval greatly reduced in comparison to other described procedures (about 2-3 months).

For the establishment and maintenance of *in vitro* cultures, it is necessary to prepare in advance the required phytohormones and culture media, so that they are already available when needed.

3.2.1 Preparation of phytohormones

1. 0.25 mg/ml BAP.

Slowly dissolve 25 mg of BAP in 5 ml of 0.1 N HCl, then make up to 100 ml volume with distilled H_2O. In the laminar flow hood sterilize the solution by filtration through sterile disposable 0.22 µm filter units and store at 4°C.

2. 0.5 mg/ml 2,4-D.

Slowly dissolve 50 mg of 2,4-D in 5 ml of 95% (v/v) ethanol, then make up to 100 ml volume with distilled H_2O. Sterilize and store as described above.

3.2.2 Preparation of culture media

Culture media are based on Murashige and Skoog (MS) basal medium (micro- and macroelements including vitamins). Sterilize them by autoclaving on the same day of the preparation, because most of them contain sucrose. They can be stored at room temperature for several months (*see* **Note 3**).

1. Solid Medium for Green Callus Induction: full-strength MS, 3.0% (w/v) sucrose, 0.25 µg/ml BAP, 0.5 µg/ml 2,4-D, 0.8% (w/v) agar, pH 5.5.

To obtain this medium, first prepare a liquid medium containing a two-fold concentration of phytohormones (Component A), and a solid medium, containing a two-fold concentration of agar (Component B).

For Component A, dissolve 4.4 g of Murashige and Skoog basal medium in a beaker containing about 800 ml of deionized H_2O. Use a magnetic stirrer in order to ensure optimal and rapid dissolution of the reagents. Add 30 g sucrose and stir until completely dissolved. Adjust the pH to 5.5 using 1 N KOH. Add deionized H_2O and bring the volume up to 1 l in a cylinder. Transfer the solution into a 1 l Duran bottle. Autoclave for 20 min at 121°C. After autoclaving and cooling down the culture medium, in the laminar flow hood add 2 ml/l stock solutions of phytohormones (see Subheading 3.2.1) in order to obtain a 2X concentration. Gently shake the bottle (lid closed) to ensure accurate mixing.

For Component B, proceed as described above for Component A. After bringing the solution to pH 5.5, divide it into two 500 ml Duran bottles and add 8 g agar directly into each bottle (2X concentration of agar, 16 g/l) before autoclaving (*see* **Note 4**).

The medium for callus induction is obtained by mixing Component A and Component B in equal volume directly in the Petri dishes, as explained in Subheading 3.2.3.

2. Liquid Media for Photosynthetic Cell Suspension Cultures: full-strength MS, variable amount (w/v) of sucrose, 0.25 µg/ml BAP, 0.5 µg/ml 2,4-D, pH 5.5.

To set up photosynthetic cell suspension cultures, culture media containing progressively reduced sucrose concentrations (2%, 1%, 0.5%, w/v) are used. To prepare them, proceed as described above, adding the proper amount of sucrose (20 g/l, 10 g/l, 5 g/l) depending on the desired final concentration. Stir until dissolution, bring to pH and final volume, autoclave, and cool them down before adding 1 ml/l of the stock solution of phytohormones (see Subheading 3.2.1).

3.2.3 Preparation of plates containing agarized medium

1. By using the microwave at low power, melt Component B of the Solid Medium for Green Callus Induction (see Subheading 3.2.2) until it is fully melted (*see* **Note 5**).

2. Close the bottle and gently shake it in order to mix its content to homogeneity.

3. Let the medium cool down until you can easily handle the bottle in your hands without scorching (*see* **Note 6**).

4. By using the pipet-aid and a sterile disposable 10 ml pipette inside the laminar flow hood, transfer in round sterile Petri dishes (100 × 20 mm) 10 ml Component A and 10 ml Component B (*see* **Note 7**).

5. Gently mix the content of the Petri dish by sliding the plate on the surface of the bench under the laminar flow hood with a cross-like motion for 3 times.

6. Partially close the dish with its lid, placing it on top slightly inclined and let the medium solidify (it takes about 15 minutes).

3.2.4 Surface sterilization of seeds

1. Transfer the seeds into a clean 1.5 or 2 ml Eppendorf-like tube. This step can be performed on a bench, in the laboratory (*see* **Note 8**).

2. In the laminar flow hood, slowly add 1 ml of Seed Sterilization Solution 1 (70% ethanol, 0.05% Triton X-100) to the Eppendorf-like tube containing the seeds. Close the tube and shake it vigorously for 1 min by inverting it several times (*see* **Note 9**).

3. Remove the solution by using a P200 micropipette and a sterile tip. Make sure you do not suck the seeds into the tip.

4. Add 1 ml of Seed Sterilization Solution 2 (100% ethanol). Close the tube and shake it vigorously for 1 min as above (*see* **Note 9**). Immediately proceed with sowing on Petri dishes.

3.2.5 Sowing on Petri dishes and induction of green calli

1. In the laminar flow hood open a Petri dish containing Solid Medium for Green Callus Induction (see Subheading 3.2.2) and put the lid upside down.

2. Using a P1000 micropipette suck the seeds into a sterile tip (see **Note 10**) and transfer them onto the inner side of the Petri dish lid.

3. By using the same sterile tip, distribute the seeds so that they are homogenously scattered inside the Petri dish lid. Let the ethanol evaporate for a few min.

4. Reverse the Petri dish, containing the solid medium, upside down over the lid, containing the seeds. Overturn the closed Petri dish, in order to let the seeds fall onto the solid medium. If some of them remain on the lid, gently flick the lid with your fingers from outside to help their fall (*see* **Note 11**). If a large amount of seeds needs to be sown, use more than one Petri dish.

5. Seal the Petri dish with parafilm and place it horizontally, lid side up, in the growth chamber (*see* **Note 12**). After exactly 3 weeks, well-developed green calli will have formed at the hypocotyl level (Fig. 1A, 1D-E).

3.2.6 Initiation of photosynthetic cell suspension cultures

1. In the laminar flow hood carefully open a sterile 50 ml Erlenmeyer flask, and place the aluminum foil lid upside down.

2. Transfer in the flask, by using the pipet-aid and a sterile disposable pipette, 10 ml Liquid Medium for Cell Suspension Cultures containing 2% sucrose (see Subheading 3.2.2) (*see* **Note 7** and **Note 13**).

3. Using sterile forceps, transfer the green calli (Fig. 1A, D-E) one by one inside the Petri dish lid (placed upside down on the surface of the bench in the laminar flow hood).

4. With a sterile scalpel remove the residues of non-dedifferentiated cotyledons and cut the green calli in two or four pieces (*see* **Note 14**).

5. With sterile forceps carefully transfer the material deriving from about ten calli into the 50 ml Erlenmeyer flask containing the liquid culture medium (*see* **Note 15**).

6. Reduce the dimension of the aluminum foil lid by using scissors, taking care to preserve sterility during this operation (*see* **Note 16**).

7. Quickly pass the aluminum foil lid, as well as the flask neck, over the Bunsen burner flame (paying extreme attention not to burn your hands!) and close the flask by wrapping the aluminum foil around the top of the flask (Fig. 1B).

8. Place the flask on an orbital shaker set at 80 rpm with continuous motion in the growth chamber under a light intensity of 130 ± 20 µmol photons m^{-2} s^{-1} (to stimulate photosynthetic activity).

9. After a couple of days, gently resuspend the culture about ten times, using the pipet-aid and a sterile disposable 10 ml pipette deprived of the tip (*see* **Note 17**) to favour the fragmentation of calli.

10. After one week, by using the pipet-aid and a sterile disposable 10 ml pipette without the tip, transfer all the calli in a 100 ml sterile Erlenmeyer flask, containing 20 ml fresh medium with the same concentration (2%, w/v) of sucrose and phytohormones.

3.2.7 Set up and subculturing of photosynthetic cell suspension cultures

Cell suspension cultures are renewed weekly by transferring 1 ml packed cell volume (PCV) of late-exponential phase (7-day-old) (see Subheading 3.2.8) cells into 20 ml fresh culture medium. Sucrose concentration in the culture medium is gradually reduced from 2% to 1% and then to 0.5% (w/v) every 2-3 weeks, in order to stimulate the photosynthetic activity of the cells.

1. Transfer 20 ml fresh Liquid Medium for Photosynthetic Cell Cultures (containing stepwise 50% less sucrose content every 2-3 weeks) (see Subheading 3.2.2) into a sterile 100 ml Erlenmeyer flask.

2. Resuspend the content of the 7-day-old cell suspension culture at least ten times, by using the pipet-aid and a sterile disposable 10 ml pipette, taking care not to form air bubbles in the flask.

3. Suck in the pipette about 5 ml of the culture, then position the pipette tip against the inner bottom of the flask, slowly forcing out only the liquid medium (the cells will remain inside the tip). Repeat this step until you have amassed 1 ml PCV inside the tip (*see* **Note 18**).

4. Start the new subculture by transferring 1 ml PCV in the 100 ml Erlenmeyer flask containing 20 ml fresh culture medium prepared above (*see* **Note 19**).

5. Pipette up and down at least ten times in order to accurately resuspend the new subculture and fully release all the cells sticking inside the pipette.

6. Close the flask with the aluminum foil lid and place it on the orbital shaker in the growth chamber.

7. After about 2-3 months, fine photosynthetic cell suspension cultures, consisting in very small cell aggregates, are obtained (Fig. 1C). They contain chloroplasts as functional types of plastids, as confirmed by confocal microscopy

observations of chlorophyll autofluorescence (Fig. 1F-G) and transmission electron microscopy (TEM) analyses (Fig. 1H-K) For TEM procedures, see [16].

3.2.8 Determination of the cell suspension culture growth curve

The evaluation of the cell growth is important to determine the lag phase, exponential phase and stationary phase of the cell suspension culture. This is essential in order to identify the best time interval in which to perform experiments (usually with mid-exponential phase cells) and the subculturing time, when the cell culture has to be renewed in fresh culture medium (*i.e.* with late-exponential phase cells).

To determine the growth curve, the fresh weight (mg/ml) of the suspension-cultured cells can be measured at fixed days after the onset of the subculture, using the following procedure:

1. Weigh a 1.5 ml Eppendorf-like tube (*see* **Note 20**).
2. Open the Erlenmeyer flask containing the cell suspension culture and resuspend the flask content at least ten times, by using the pipet-aid and a sterile disposable 10 ml pipette.
3. Transfer exactly 1 ml of the resuspended cell culture into the tube by using a P1000 micropipette and a sterile tip with a wide bore (*see* **Note 21**).
4. Centrifuge the tube containing the cell culture aliquot at maximum speed for 1 min at room temperature.
5. Remove most of the culture medium by using a 1 ml syringe with a thin needle.
6. Centrifuge the tube again and remove all the remaining culture medium as above.

7. Weight the tube again and take note of the gross weight.

8. Subtract the tare to calculate the net weight and plot it against time in order to visualize the growth curve of the cell suspension culture (Fig. 1L).

3.3. Establishment and maintenance of heterotrophic cell suspension cultures

3.3.1 Preparation of phytohormones

1. 2 mg/ml kinetin.

Weigh 30 mg kinetin in a 15 ml tube, dissolve in 3 ml 0.1 N KOH, then make up to 15 ml volume with distilled H_2O. In the laminar flow hood sterilize the solution by filtration through sterile disposable 0.22 µm filter units and store at -20°C in 1 ml aliquots in sterile 1.5 ml Eppendorf-like tubes.

2. BAP and 2,4-D are prepared as described in Subheading 3.2.1.

3.3.2 Preparation of culture media

Culture media are based on MS and Gamborg B5 basal medium (micro- and macroelements including vitamins).

1. Solid Medium for Seed Germination: half-strength (½) MS, 1.5% (w/v) sucrose, 0.8% (w/v) agar, pH 5.5.

Dissolve 2.2 g/l MS basal medium and 15 g/l sucrose in distilled H_2O, bring to pH, make up to volume, add 8 g/l agar directly into the bottle and autoclave. Store at room temperature.

2. Solid Callus Induction Medium (CIM) for heterotrophic cultures: 3.2 g/l Gamborg B5 basal medium, 0.5 g/l MES, 2% (w/v) sucrose, 0.05 µg/ml kinetin, 0.5 µg/ml 2,4-D, 0.8% (w/v) agar, pH 5.7.

To obtain this medium, first prepare a liquid medium containing a two-fold concentration of phytohormones (Component A'), and a solid medium, containing a two-fold concentration of agar (Component B'), analogously to what described in Subheading 3.2.2. The medium for callus induction is obtained by mixing Component A' and Component B' in equal volume (10 ml + 10 ml) directly in the Petri dishes, as described in Subheading 3.3.3.

3. Solid Medium for Heterotrophic Callus Maintenance: full-strength MS, 3% (w/v) sucrose, 0.25 µg/ml BAP, 0.5 µg/ml 2,4-D, 0.8% (w/v) agar, pH 5.5.
First prepare a liquid culture medium containing a twofold concentration of phytohormones (Component A'') and a solid medium containing a twofold concentration of agar (Component B''), analogously to what described in Subheading 3.2.2. Combine them in equal volumes (10 ml + 10 ml) when you prepare the plates containing agarized medium, as described in Subheading 3.3.3.

3. Liquid Medium for Heterotrophic Cell Suspension Cultures: full-strength MS, 3% (w/v) sucrose, 0.25 µg/ml BAP, 0.5 µg/ml 2,4-D, pH 5.5.
Proceed as explained for photosynthetic cell cultures in Subheading 3.2.2, but adding 30 g/l sucrose.

3.3.3. Preparation of plates containing agarized medium

1. For seed germination: melt the Solid Medium for Seed Germination (see Subheading 3.3.2) in a microwave oven and then transfer 20 ml in a Petri dish.

2. For callus induction: transfer 10 ml of Component A' + 10 ml Component B' of CIM (see Subheading 3.3.2) in a Petri dish and gently mix (see Subheading 3.2.3).

3. For callus maintenance: transfer 10 ml of Component A'' + 10 ml Component B'' of Solid Medium for Heterotrophic Callus Maintenance (see Subheading 3.3.2) in a Petri dish and gently mix (see Subheading 3.2.3).

3.3.4 Surface sterilization of seeds, Sowing on Petri dishes and Growing of seedlings

Surface sterilize the seeds as described in Subheading 3.2.4. Proceed with sowing as described in Subheadings 3.2.5, by transferring the seeds on Petri dishes containing Solid Medium for Seed Germination (see Subheading 3.3.2). After 1 week the seeds will have germinated and developed into small seedlings (Fig. 2A).

3.3.5 Induction and maintenance of heterotrophic calli

1. In the laminar flow hood gently transfer the seedlings onto the inner side of the Petri dish lid by using sterile forceps.
2. Remove the roots by using the sterile scalpel.
3. Excise the cotyledons and the hypocotyl, then transfer them separately in two different Petri dishes containing CIM for heterotrophic cell cultures (see Subheading 3.3.2) (Fig. 2B-C).
4. Seal the Petri dishes with Parafilm and store them horizontally, lid side up, in the growth chamber. Greenish or pale yellow calli develop in about three weeks (Fig. 2D-E).
5. Every 3 weeks, transfer the calli into new Petri dishes, containing fresh CIM medium.

6. After the third renewal in CIM, calli will consist in big, yellow, friable clusters of completely dedifferentiated cells, almost indistinguishable regardless their origin from either cotyledons or hypocotyls (Fig. 2F).

7. Fractions of these calli can be subcultured monthly onto Solid Medium for Heterotrophic Callus Maintenance (see Subheading 3.3.2) (*see* **Note 22**) or used to set up heterotrophic cell suspension cultures.

3.3.6 Initiation and subculturing of heterotrophic cell suspension cultures

1. Proceed as described in Subheading 3.2.6, using as starting material heterotrophic calli (instead of the green ones), and the Liquid Medium for Heterotrophic Cell Suspension Cultures, containing 3% (w/v) sucrose (instead of progressively reduced sucrose concentrations) (see Subheading 3.3.2) (Fig. 2G).

2. Place the flask on an orbital shaker set at 80 rpm with continuous motion in the growth chamber under a light intensity of 50 ± 10 µmol photons m^{-2} s^{-1}.

3. Do the subculturing once a week, by transferring 1 ml PCV into 20 ml fresh medium, containing the same percentage of sucrose.

4. After about 2-3 months, fine heterotrophic cell suspension cultures are obtained (Fig. 2H). They are maintained in the darkness by wrapping the flasks in aluminum foil. They contain amyloplasts as functional types of plastids, as confirmed by the absence of chlorophyll autofluorescence (Fig. 2I-J), Lugol staining of starch granules (Fig. 2K-L) and TEM analyses (Fig. 2M-P).

3.4 Interconversion of photosynthetic and heterotrophic cell suspension cultures

Photosynthetic cell suspension cultures (see Subheading 3.2) and heterotrophic cell suspension cultures (see Subheading 3.3) are, at a certain degree, interconvertible.

Indeed, the gradual transfer of photosynthetic cultures to liquid culture media containing stepwise higher sucrose concentration allows, together with the gradual transition from a 16 h light/8 h dark photoperiod to a condition of constant darkness, for the obtainment of heterotrophic cell suspension cultures [6] (Fig. 3) (*see* **Note 23**). Even the transition in the other direction, *i.e.* from heterotrophic to autotrophic cell suspension cultures, has been obtained and described [5, 8].

3.4.1 Pulse Amplitude Modulation (PAM) fluorometry

The photosynthetic efficiency of the cell suspension cultures growing in the presence of different sucrose concentrations can be measured by Pulse Amplitude Modulation (PAM) analyses.

1. In the laminar flow hood transfer 3 ml of 6-day-old suspension cell culture into a sterile disposable 6-well plate.
2. Keep the plate in the dark for at least 20 min.
3. Measure at the PAM fuorometer the quantum yield of photosystem II (F_v/F_m, where F_v is the difference between the maximal (F_m) and the basal (F_0) fluorescence of chlorophyll).

Fig. 3 shows that the photosynthetic cell culture maintained in a culture medium containing 0.5% sucrose, although growing bit less than that maintained in 1% sucrose (Fig. 1L), exhibits the highest photosynthetic efficiency (*see* **Note 24**).

3.5 Isolation of protoplasts from cell suspension cultures

Protoplasts can be conveniently isolated from Arabidopsis cell suspension cultures, every week and with high yields, high percentage of vitality, and very good reproducibility [6]. They can be obtained from wild-type cultures, and then subjected

to transient transformation [12] or from transgenic lines, stably expressing proteins of interest (Fig. 4).

3.5.1 Preparation of Enzymatic Solution and Protoplast Resuspension Buffer

1. Enzymatic Solution: 1.5% (w/v) cellulase "Onozuka" R-10, 0.5% (w/v) Macerozyme R-10, 0.55 M mannitol in Liquid Culture Medium (see Subheadings 3.2.2 and 3.3.2) without phytohormones. Dissolve mannitol and the enzymes in the liquid medium and make up to volume. In the laminar flow hood sterilize the solution through sterile disposable vacuum filtration units. Store at -20°C in 10 ml aliquots in sterile 15 ml tubes, wrapped in aluminum foil (*see* **Note 25**).
2. Protoplast Resuspension Buffer: 0.55 M mannitol in Liquid Culture Medium (see Subheadings 3.2.2 and 3.3.2) without phytohormones. Sterilize the solution in autoclave and store at -20°C in sterile 15 ml tubes.

3.5.2 Preparation of protoplasts

1. Transfer 2.5 ml PCV of a mid-exponential phase (4 to 5-day-old) (see Subheading 3.2.8) cell suspension culture into a sterile 50 ml tube (*see* **Note 26**).
2. Add 10 ml Enzymatic Solution to the tube by using the pipet-aid and a sterile disposable 10 ml pipette.
3. Wrap the tube in aluminum foil and incubate for 2 h horizontally on the orbital shaker set at 80 rpm in the growth chamber.
4. At the end of the incubation time, in the laminar flow hood transfer the cell suspension on top of a sterile 50 μm concave nylon mesh, mounted on a 100 ml glass beaker thanks to a rubber band (*see* **Note 27**).

5. Let the solution completely leach through the nylon mesh, gently helping the process with the tip of a sterile disposable plastic Pasteur pipette.

6. Cut the rubber band with a sterile scalpel and discard the nylon mesh with the undigested cell debris on top.

7. Use a new sterile disposable plastic Pasteur pipette to transfer the filtered protoplast solution in a sterile 15 ml tube.

8. Centrifuge the tube at 60 *g* for 5 min at room temperature, brake off.

9. Discard the supernatant by using a sterile disposable plastic Pasteur pipette.

10. Add 5 ml of Protoplast Resuspension Buffer to the tube and gently resuspend the pellet by slowly swinging the tube.

11. Repeat centrifugation and washes twice.

12. Centrifuge the tube again, then resuspend the pellet in 1 ml of Protoplast Resuspension Buffer (*see* **Note 28**) (Fig. 4).

4. Notes

1. Arabidopsis seeds are kept in 1.5 ml or 2 ml Eppendorf-like tubes, that have to be properly labelled (especially if there are many different transgenic lines in the lab). For collection and preservation of seeds, see [17].

2. Erlenmeyer flasks and beakers, covered with thick aluminum foil, are sterilized in the oven at 180°C for 4 h. Bottles, tip boxes, cell culture media and all other solutions (except ethanol) are sterilized in autoclave at 121°C for 20 min. Before sterilization, apply autoclave tape on all glassware and tip boxes: it will become black after autoclaving. Forceps and scalpels can be wrapped in aluminum foil and sterilized in the oven.

3. Large volumes of liquid medium, such as 3 l or 5 l, can be prepared. Remember to clearly label bottles containing different culture media, possibly with different coloured tapes, to avoid confusion when you use them. Before use, gently shake the bottle containing the liquid medium in order to mix the content and resuspend salts potentially sedimented on the bottom. In case of bacterial/fungal contamination immediately discard it. Add the phytohormones when you start using a new liquid medium bottle. When you open the last bottle, remember to prepare new culture medium as soon as possible, in order not to run out of medium when you urgently need it.

4. Add the agar only after the pH has been adjusted and the medium (brought to the final volume) has been transferred into the bottle, because agar does not dissolve at room temperature. Use two 500 ml bottles instead of 1 l bottle, because microwave ovens (used later to melt the medium) are usually not high enough to host 1 l bottle.

5. Loosen the lid of the bottle before inserting it in the microwave oven, so that the hot air inside the bottle is not under excessive pressure. Do not completely remove the lid, otherwise sterility will be lost.

6. This is important to preserve phytohormone activity, once Component A and B have been mixed. On the other hand, avoid excessive cooling down, otherwise the medium will solidify again in the bottle or cause wrinkled plates.

7. If in vitro cultures have to be set up from a transgenic line, add the proper concentration of antibiotic/herbicide in the medium.

8. Seeds can be poured from the storage tube onto a clean filter paper. This step is particularly useful if you have to precisely count the seeds. To facilitate the transfer into the Eppendorf-like tube, fold the piece of filter paper like a chute or bend it in a funnel-shape manner. Alternatively, if only very few seeds are needed,

you can simply make them stick to your index finger and then carefully release them into the Eppendorf-like tube. Do not fill the tube with too many seeds (<0.5 cm^3 final volume), otherwise the sterilization process may be less efficient. If a large amount of seeds needs to be surface-sterilzed, subdivide them in multiple Eppendorf-like tubes. The number of seeds required for a single round Petri dish is usually small (20-50 maximum).

9. Do not incubate seeds in either Seed Sterilizations Solutions for more than 5 minutes. Exceeding this time interval may severely impair seed germination.

10. Try to suck the seeds in about 0.5 ml of ethanol. In this way the seeds will not remain in ethanol for too long because ethanol will dry out quickly.

11. The described procedure is, in our hands, the fastest and most straightforward way to sow the seeds on Petri dishes. Less experienced researchers may prefer to transfer the seeds individually by using a sterile toothpick, or a sterilized glass Pasteur pipette (previously bent and sealed at the tip on a Bunsen burner). In this case, pick up the seeds and transfer them in the Petri dishes by gently positioning the seeds on the surface of the agarized medium. To facilitate the transfer, touch the surface of the agarized medium with either the toothpick or the glass Pasteur pipette before picking up the seeds.

12. To better synchronize seed germination, after sowing the plates can be placed in the dark at 4°C for 2 days, before moving them to the growth chamber (stratification).

13. The volume of the liquid cell culture medium is always one fifth of the flask total volume, in order to ensure sufficient aeration of the cell suspension culture.

14. Forceps and scalpel need to be often re-sterilized during these operations. To do this, soak the tip of the metal labware in a tube containing 100% (v/v) ethanol,

then pass it on the flame of the Bunsen burner until it is red-hot. Cool it down before use. Pay extreme attention when you work with ethanol close to the Bunsen burner flame. Alternatively, a glassbeads sterilizer can be used, following manufacturer's instructions.

15. While transferring the callus portions, adopt the maximal care to maintain sterile conditions. To minimize the risk of contamination, avoid inserting the forceps in the flask, but rather drop each callus portion from the top of the flask mouth. Sterilize repeatedly the forceps and the scalpel, as described in **Note 14**.

16. Cut the aluminum foil lid so that about 1-2 cm of it are left around the mouth of the flask. This allows a better exposition of the cell cultures to the light regime of the growth chamber.

17. You can either buy sterile wide-bore pipettes or obtain them from standard pipettes, by manually removing the tip. To do so, simply break with your hands the tip while the pipette is still inside its sterile package, paying attention to maintain sterility.

18. In our hands this procedure is the fastest way to measure and transfer 1 ml PCV at every subculturing step. For less experienced researchers it may be easier to determine the PCV by transferring 5 ml of the cell suspension culture into a sterile 15 ml tube and centrifuging at 500 g for 2 min. The new subculture will be started by inoculating the appropriate volume of the 1-week old suspension culture, corresponding to 1 ml PCV, into 20 ml fresh culture medium.

19. When large volumes of suspension cell cultures are needed, subculturing can be performed in larger flasks, containing a larger volume of cell culture medium (*e.g.* 250 ml flasks, containing 50 ml culture medium; 500 ml flasks, containing 100 ml

culture medium; 1 l flasks, containing 200 ml culture medium). Remember to respect the rule of the inoculum size (1 ml PCV in 20 ml fresh medium).

20. If multiple measurements have to be carried out, weigh separately each tube, because there can be small differences in the weight between tubes.

21. Boxes of sterile tips with a wide bore can be prepared in advance, by cutting the tip ends with a sterile scalpel and then autoclaving them. Before the transfer, clean the micropipette with a paper towel and denatured alcohol. Use extreme caution while you enter the flask with the micropipette: avoid touching the inner glass sides, in order to minimize contamination risks.

22. Heterotrophic calli can be maintained in vitro almost indefinitely, by subculturing them once a month onto new plates. This is particularly useful, because they represent a reservoir of cells ready to use when cell suspension cultures have to be set up again, for example in the unfortunate event of a fungal/bacterial contamination.

23. Changes in sucrose concentration must be stepwise and the subcultures have to be kept in the same concentration of sucrose for 2-3 weeks.

24. In our hands, total deprivation of sugar in the culture medium is not advisable because, although not compromising the photosynthetic activity of the cell culture, it causes a drastic reduction of the cell growth rate, making the performance of weekly experiments unfeasible.

25. The Enzymatic Solution cannot be autoclaved, because enzymes are thermolabile. Moreover, it must be protected from light, because the enzymes are photolabile.

26. Determine the PCV as detailed in **Note 18**. Then transfer the cell culture volume corresponding to 2.5 ml PCV in the 50 ml tube, centrifuge at 500 g for 2 min and discard the supernatant.

27. Prepare this filter system by using non sterile labware, wrap it in aluminum foil and sterilize by autoclaving.

28. If required, a counting assay can be carried out to determine protoplasts concentration, viability and yield by using a light microscope, Trypan blue staining and a Bürker chamber, as previously described [3].

Acknowledgements

We are grateful to R. Moscatiello and S. Sello (Padova, Italy) for fruitful discussion. We thank T. Morosinotto and I. Szabò (Padova, Italy) for the kind availability of the PAM imaging apparatus. This work was supported by Progetti di Ricerca di Interesse Dipartimentale (PRID 2018) (prot. BIRD180317) and Dotazione Ordinaria della Ricerca 2018-2019 to LN.

References

1. Loewenberg JR (1965) Callus cultures of Arabidopsis. Arabidopsis Inf Serv 2:34
2. Negrutiu I, Jacobs M (1975) *Arabidopsis thaliana* as a model system in somatic cell genetics II. Cell suspension culture. Plant Sci Lett 8:7-15
3. Moscatiello R, Baldan B, Navazio L (2013) Plant cell suspension cultures. Methods Mol Biol 953:77-93
4. Barkla BJ, Vera-Estrella R, Pantoja O (2014) Growing Arabidopsis in vitro: cell suspensions, in vitro culture, and regeneration. Methods Mol Biol 1062:53-62

5. Hampp C, Richter A, Osorio S et al (2012) Establishment of a photoautotrophic cell suspension culture of *Arabidopsis thaliana* for photosynthetic, metabolic, and signaling studies. Mol Plant 5:524-7
6. Sello S, Moscatiello R, La Rocca N et al (2017) A rapid and efficient method to obtain photosynthetic cell suspension cultures of *Arabidopsis thaliana*. Front Plant Sci 8:1444
7. Gutiérrez J, González-Pérez S, García-García F et al (2014) Programmed cell death activated by Rose Bengal in *Arabidopsis thaliana* cell suspension cultures requires functional chloroplasts. J Exp Bot 65:3081-95
8. Sello S, Perotto J, Carraretto L et al (2016) Dissecting stimulus-specific Ca^{2+} signals in amyloplasts and chloroplasts of *Arabidopsis thaliana* cell suspension cultures. J Exp Bot 67:3965-74
9. Sello S, Moscatiello R, Mehlmer N et al (2018) Chloroplast Ca^{2+} fluxes into and across thylakoids revealed by thylakoid-targeted aequorin probes. Plant Physiol 177:38-51
10. Choi WG, Miller G, Wallace I et al (2017) Orchestrating rapid long-distance signaling in plants with Ca^{2+}, ROS and electrical signals. Plant J 90:698-707
11. Hilleary R, Gilroy S (2018) Systemic signaling in response to wounding and pathogens. Curr Opin Plant Biol 43:57-62
12. Jian LW *** (2019) Transient expression in protoplasts. Chapter *** In: Sánchez-Serrano JJ, Salinas J (eds) Arabidopsis Protocols 4th edition. Springer ***
13. Teardo E, Carraretto L, Moscatiello R et al (2019) A chloroplast-localized mitochondrial calcium uniporter transduces osmotic stress in *Arabidopsis*. Nat Plants 5:581-588

14. Jarvis P, López-Juez E (2013) Biogenesis and homeostasis of chloroplasts and other plastids. Nat Rev Mol Cell Biol 14:787-802

15. Sadali NM, Sowden RG, Ling Q, Jarvis RP (2019) Differentiation of chromoplasts and other plastids in plants. Plant Cell Rep doi: 10.1007/s00299-019-02420-2

16. Otegui M *** (2019) Electron microscopy for ultrastructure determination. Chapter *** In: Sánchez-Serrano JJ, Salinas J (eds) Arabidopsis Protocols 4th edition. Springer ***

17. Somers D *** (2019) Handling Arabidopsis plants: growth, preservation of seeds, transformation and genetic crosses. Chapter *** In: Sánchez-Serrano JJ, Salinas J (eds) Arabidopsis Protocols 4th edition. Springer ***

[*** *to be updated with the correct information, when available*]

Figure captions

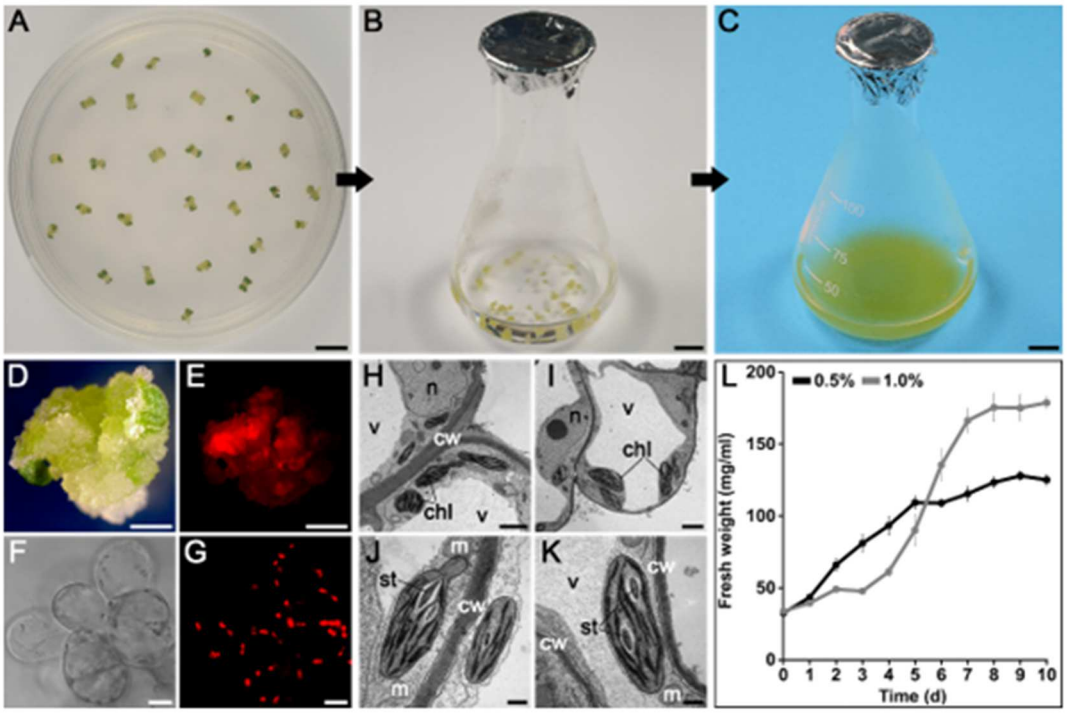

Fig. 1 Establishment and maintenance of Arabidopsis photosynthetic cell suspension cultures. (**A**) Exogenous hormone-induced production of green calli after 3 weeks from sowing Arabidopsis seeds on MS, 3% (w/v) sucrose, 0.25 µg/ml BAP, 0.5 µg/ml 2,4-D, 0.8% (w/v) agar. Bar, 1 cm. Insert: magnification of a green callus. (**B**) Initiation of photosynthetic cell suspension cultures, by transferring 10 green calli into a 50 ml Erlenmeyer flask, containing 10 ml of MS, 2% (w/v) sucrose, 0.25 µg/ml BAP, 0.5 µg/ml 2,4-D, Bar, 1 cm; (**C**) Photosynthetic cell suspension culture, maintained in 100 ml Erlenmeyer flask containing 20 ml of MS with the same concentration of phytohormones and a stepwise reduced sucrose content, down to 0.5% (w/v). Bar, 1 cm. (**D-E**) Stereomicroscopy observations of a green callus (**D**), showing chlorophyll autofluorescence (**E**). Bar, 1 mm. (**F-K**) Confocal microscopy (**F-G**) and TEM (**H-K**) analyses of cell suspension cultures, containing chloroplasts as functional types of plastids. F, bright field; G, chlorophyll autofluorescence. Bar, 25 µm. (**H-K**) Ultrastructure of photosynthetic suspension-cultured cells. chl, chloroplasts; cw, cell wall; m, mitochondria; st, starch; v, vacuole. Bars: H-I, 2 µm;

J-K, 500 nm. (**L**) Growth curve of photosynthetic cell suspension culture, growing in 1% (grey trace) and 0.5% (black trace) sucrose-containing medium. Data are the means ± SE of n ≥ 6 independent replicates for each time point.

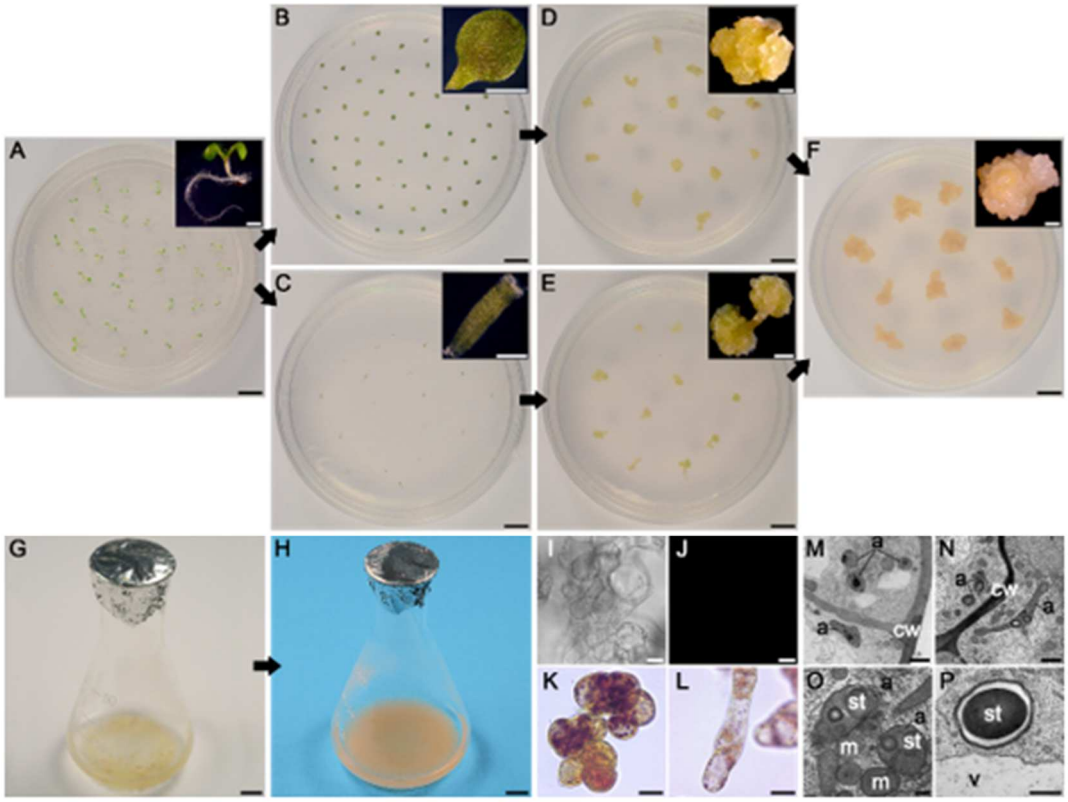

Fig. 2 Establishment and maintenance of Arabidopsis heterotrophic cell suspension cultures. (**A**) 7-day-old seedlings growing on MS½, 1.5% (w/v) sucrose, 0.8% (w/v) agar. Bar, 1 cm. (**B-C**): After 1 week from sowing of seeds, cotyledons (**B**) and hypocotyls (**C**) are axenically cut from seedlings and transferred on CIM (3.2 g/l Gamborg B5 basal medium, 0.5 g/l MES, 2% (w/v) sucrose, 0.05 µg/ml kinetin, 0.5 µg/ml 2,4-D, 0.8% (w/v) agar, pH 5.7). (**D-E**) After 3 additional weeks, heterotrophic calli start developing from cotyledons (**D**) and hypocotyls (**E**), respectively. (**F**) After 3 subsequent transfers on fresh CIM (carried out every 3 weeks) heterotrophic calli consist in huge clusters of dedifferentiated cells, regardless

their organ origin. In the inserts (**A-F**), stereomicroscopy images of the material contained in the different plates are shown. (**G**) Initiation of heterotrophic cell suspension cultures, by transferring calli into a 50 ml Erlenmeyer flask, containing 10 ml of MS, 3% (w/v) sucrose, 0.25 µg/ml BAP, 0.5 µg/ml 2,4-D. Bar, 1 cm; (**H**) 100 ml Erlenmeyer flask containing 20 ml of MS supplemented with the same concentration of sucrose and phytohormones. Bars: A-H, 1 cm. (**I-L**) Confocal and light microscopy observations of heterotrophic cell suspension cultures, showing the lack of chlorophyll autofluorescence (**J**) and the presence of Lugol-stained starch granules (**K-L**). (**M-P**) TEM analyses of heterotrophic cell suspension cultures, confirming the occurrence of amyloplasts. a, amyloplasts; cw, cell wall; m, mitochondria; st, starch; v, vacuole. Bars: I-L, 25 µm; M-N, 2 µm; O-P, 500 nm.

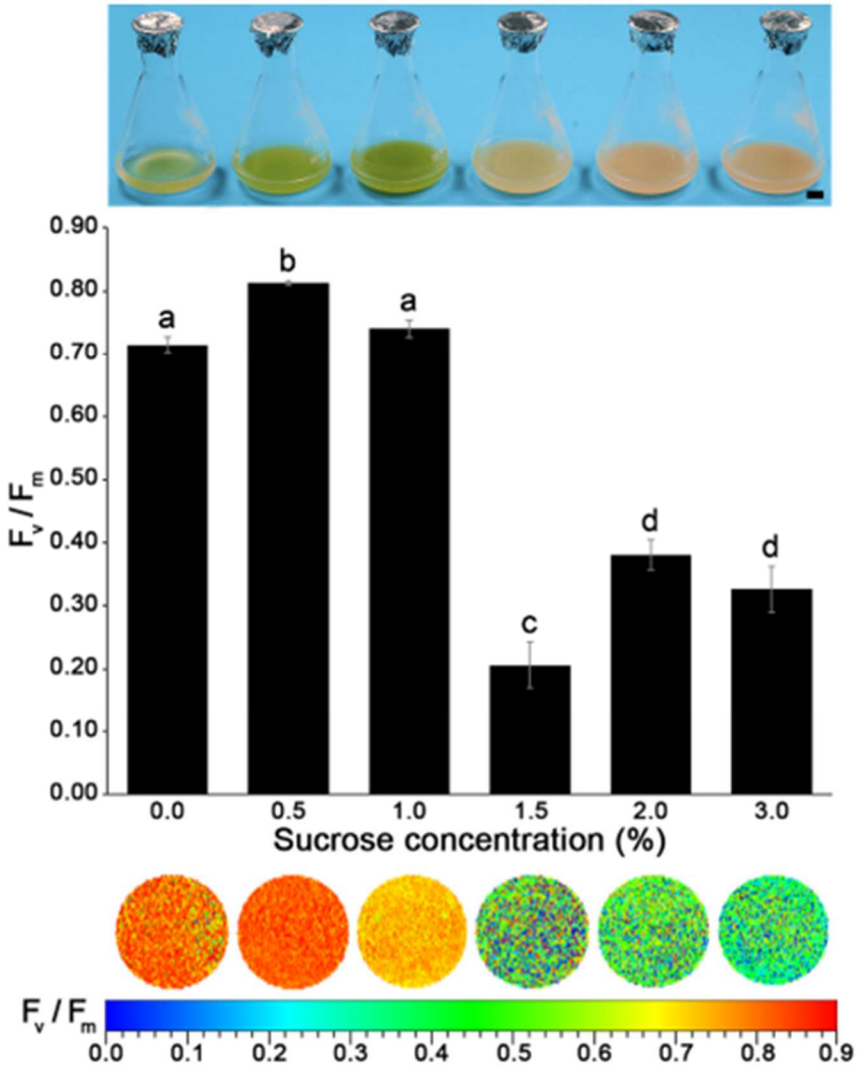

Fig. 3 Phenotype and photosynthetic activity of Arabidopsis cell suspension cultures maintained in different sucrose concentrations. Representative photographs of the flasks and PAM imaging analyses were carried out on 6-day-old cell suspension cultures. PAM data are the means ± SE of 3 independent experiments, each one conducted in triplicate. Bars labeled with a different letter differ significantly ($P < 0.05$) by Student's *t* test. The sample spots shown under the bars are representative of the F_v/F_m mean value of the different cell suspension cultures.

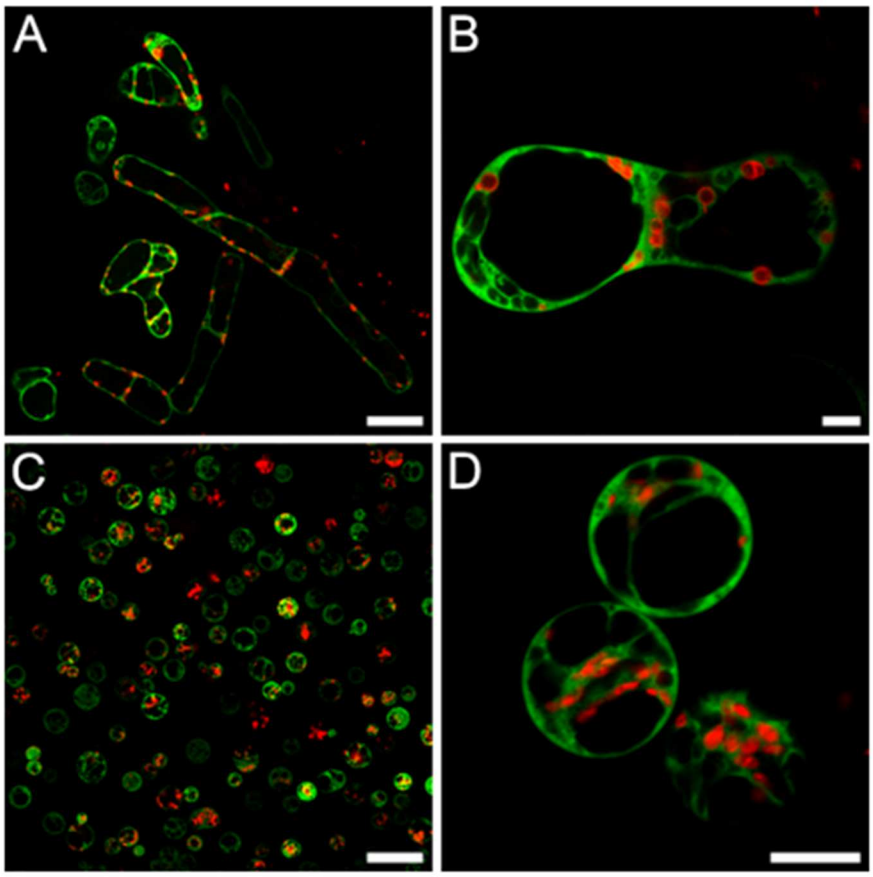

Fig. 4 Arabidopsis photosynthetic cell suspension cultures stably expressing a YFP-tagged cytosolic protein (aequorin) [8] (**A-B**) and freshly isolated protoplasts from them derived (**C-D**). Confocal microscopy analyses were carried out with excitation at 488 nm, emission at 505-530 nm for YFP and at 680-720 nm for chlorophyll. An overlay of the two channels is shown. Bars: A-C, 50 μm; B-D, 10 μm.

CHAPTER 6

Monitoring Ca^{2+} dynamics in the plant ER

This manuscript is in preparation:

Quantitative analysis of Ca^{2+} signatures in the plant endoplasmic reticulum by an aequorin-based approach

Enrico Cortese, Roberto Moscatiello, Francesca Pettiti, Luca Carraretto, Barbara Baldan, Ildiko Szabo, Marisa Brini, Lorella Navazio

Department of Biology, University of Padova, Via U. Bassi 58/B, 35131 Padova, Italy

ABSTRACT

In contrast to animal cells, the involvement of the plant endoplasmic reticulum (ER) in Ca^{2+} handling has long been overlooked, possibly clouded by the prominent role commonly ascribed to the vacuole and because of the lack of direct measurements of ER luminal Ca^{2+}. In this work a construct encoding a new ER-targeted aequorin-based probe was designed, by fusing the cDNA for a mutated version of aequorin, characterized by a reduced Ca^{2+} affinity, to the nucleotide sequence encoding a defective, uncleavable N-terminal ER signal peptide. The expression of the recombinant probe was evaluated by RT-PCR and immunoblot analyses, and the correct targeting was confirmed by confocal microscopy observations and immunogold labelling. Monitoring ER Ca^{2+} dynamics *in vivo* required separate steps of ER Ca^{2+} emptying (during reconstitution of the holoprotein with the prosthetic group coelenterazine) and subsequent Ca^{2+} refilling (before challenge with the different stimuli). The use of this novel ER-targeted aequorin chimera provided the first actual measurements of $[Ca^{2+}]$ in the plant ER, highlighting significant differences with the animal counterpart. Moreover, the observed stimulus-specific ER $[Ca^{2+}]$ increases suggest that the plant ER acts more as a Ca^{2+} sink than as a Ca^{2+} source, in contrast to the well-recognized role of this compartment as a major stimulus-releasable Ca^{2+} store in animal cells.

INTRODUCTION

The ever-expanding field of organellar calcium signalling has led to a well-established knowledge on how cells and their intracellular compartments orchestrate complex and specific responses to a wide range of physiological stimuli (Dodd *et al.*, 2010; Carafoli and Krebs, 2016; Kudla *et al.*, 2018). In animals, in particular, the advances obtained through the implementation of new technologies applied to Ca^{2+}-sensors (Pérez Koldenkova and Nagai, 2013) resulted in a clear photography of the complexity of the Ca^{2+} signalling network, opening up the possibility to study the fine-tuned integration of the internal compartments in achieving an efficient Ca^{2+} homeostasis and signal transduction (Brini *et al.*, 2013a and 2013b). In plants, despite the crucial role played by Ca^{2+} in the transduction of a plethora of environmental stimuli (Feijó and Wudick, 2018), precise knowledge of the exact role of intracellular Ca^{2+} stores is still incomplete and under frantic exploration, with compartments such as the vacuole, peroxisomes and the endoplasmic reticulum about which only partial or putative estimates are available of basal [Ca^{2+}] and its changes (Costa *et al.*, 2018).

Concerning the plant endoplasmic reticulum (ER) – and in contrast to the well explored animal counterpart (Sammels *et al.*, 2010; Raffaello *et al.*, 2016), where reports of free [Ca^{2+}] in the lumen range between 50 and 500 μM on a total [Ca^{2+}] of 2 mM (Rizzuto *et al.*, 2009), thus highlighting this compartment as a major intracellular store for Ca^{2+} – the little information available in terms of its Ca^{2+} storage properties comes either from the presence of Ca^{2+} buffering proteins in the ER lumen (mainly calreticulin, whose high-capacity and low-affinity Ca^{2+}-binding properties points to submillimolar $[Ca^{2+}]_{ER}$, (Joshi *et al.*, 2019)) and from circumstantial estimates carried out with cameleon-based Ca^{2+} sensors (Iwano *et al.*, 2009; Bonza *et al.*, 2013; Corso *et al.*, 2018). These fluorescent Ca^{2+} reporters, although representing a useful tool to image Ca^{2+} dynamics, are not the ideal method to accurately and precisely measure [Ca^{2+}] and its changes (Ottolini *et al.*, 2014).

Concerning Ca^{2+} transporters localized at ER membranes, two distinct types of Ca^{2+} ATPases were identified, ECAs and ACAs (Bonza *et al.*, 2013). In

particular, ECA1 proved to be fundamental for proper ER Ca^{2+} homeostasis, as its specific blocker cyclopiazonic acid (CPA) led to a reduced ER luminal [Ca^{2+}] and a parallel increase in the cytosolic one (Zuppini *et al.*, 2004; Bonza *et al.*, 2013). More recently, the ER-located Ca^{2+}/cation exchanger CCX2 was reported to be involved in the Ca^{2+}-mediated signal transduction taking place upon perception of an osmotic stress (Corso *et al.*, 2018). Conversely, no molecular identification of Ca^{2+}-permeable channels present at the ER membranes is yet available, despite biochemical evidence for the occurrence of voltage-gated (Klüsener *et al.*, 1995) and ligand-gated (Navazio *et al.*, 2000 and 2001) ER Ca^{2+} mobilization pathways involved in Ca^{2+} fluxes between this compartment and the cytosol.

The plant ER is also known to be able of multiple contacts with other intracellular compartments through which Ca^{2+} fluxes may happen. For example, due to its continuity to the nuclear outer membrane, the ER may play a key role in the modulation of nucleus-associated Ca^{2+} oscillations during plant-microbe symbioses (Capoen *et al.*, 2011; Charpentier *et al.*, 2016). Moreover, spatially-confined microdomains between the ER and the plasma membrane (the so-called ER-PM contact sites, EPCSs) have been detected both in plants (Bayer *et al.*, 2017; Wang *et al.*, 2017) and animal systems (Son *et al.*, 2016; Demaurex and Guido, 2017) where they are crucial for lipid transfer as well as in generating cytosolic Ca^{2+} signals through ER Ca^{2+} release (Saheki and De Camilli, 2017) and subsequent replenishment (Chung *et al.*, 2017). So far, knowledge about contacts sites joining the ER to mitochondria and their role in shaping the cytosolic Ca^{2+} signalling is limited to the animal field (Rizzuto *et al.*, 2012; Brini *et al.*, 2017), with no accurate reports in plant cells (Costa *et al.*, 2018). Distinctive of plant cells are, however, interactions occurring between the ER and stromules, stroma-filled protrusions stemming from both green and non-green plastids: these organelle projections were observed to extend and retract from the plastid body in an ER-aided manner (Schattat *et al.*, 2011) and were demonstrated to be the site of lipid exchange (Block and Jouhet, 2015; Liu and Li, 2019). The possible occurrence of ion fluxes at these contact sites, and in particular a potential ER-plastid

crosstalk in terms of Ca^{2+} handling, adds a further level of complexity to the already intricate plant calcium signalling scenario (Mehrshahi *et al.*, 2013).

In order to shed light on the precise role of the ER in terms of Ca^{2+}-mediated environmental signal transduction, one of the major research line that I have pursued during my Ph.D. project aimed at the precise measurement of the Ca^{2+} concentration in this intracellular compartment, as well as at the monitoring of the ER Ca^{2+} dynamics taking place during stress-related events. The results presented in this chapter were achieved by the design of a novel ER-targeted aequorin-based Ca^{2+} sensor, engineered by fusing a defective, uncleavable signal peptide (*floury2*, fl2) (Coleman *et al.*, 1995; Gillikin *et al.*, 1997) to a mutated version of aequorin endowed with a reduced Ca^{2+} affinity (Montero *et al.*, 1995). Confocal and electron microscopy analyses confirmed the correct targeting of fl2-fused probes to the ER membranes. The proper functionality of the probe was confirmed by *in vitro* reconstitution assays. However, preliminary *in vivo* reconstitution assays demonstrated that the protocol typically applied to seedlings expressing aequorin targeted to the cytosol or chloroplasts (Sello *et al.*, 2018) could not be applied in the case of the ER-targeted aequorin probe, due to the expecting much higher [Ca^{2+}] in the ER lumen, causing the irreversible discharge of the probe prior to Ca^{2+} measurements. A long setup phase was therefore necessary, that led to the formulation of a procedure involving a "Ca^{2+} emptying step" before aequorin reconstitution, followed by a "Ca^{2+} refilling step", analogously to what described for the animal counterpart (Ottolini *et al.*, 2014). Experiments carried out with the new probe reconstitution protocol provided the first accurate measurements of $[Ca^{2+}]_{ER}$ (about 7-8 µM) for the plant ER under resting conditions. Monitoring of ER Ca^{2+} dynamics in response to different abiotic and biotic stresses provided evidence for stimulus-specific Ca^{2+} increases in response to salinity, drought and oxidative stress, whereas no changes in $[Ca^{2+}]_{ER}$ were observed in response to elicitors of plant defence responses. Pharmacological approaches demonstrated the involvement of the ER-type Ca^{2+} ATPase ECA1 (Bonza *et al.*, 2011) in the observed Ca^{2+} fluxes. The comparison of cytosolic and ER Ca^{2+} traces highlighted a temporal delay in the generation of ER Ca^{2+} transients with respect to cytosolic ones, suggesting a

functional link further supported by data obtained when seedlings were pre-treated with the extracellular chelator EGTA. Experiments carried out on Arabidopsis seedlings stably expressing aequorin in the chloroplast stroma suggested an even more complex scenario, with the participation of these organelles either in between the cytosol and the ER, or at a later stage.

In summary, this work adds to the currently available toolkit of Ca^{2+} indicators a new aequorin-based probe, that has at last allowed for quantitative measurements of $[Ca^{2+}]_{ER}$. Aequorin-based Ca^{2+} measurements have increased our knowledge about plant ER as a major intracellular Ca^{2+} store in the plant cell, highlighting its role as a Ca^{2+} sink for the ion rather than a Ca^{2+} source, thereby shaping intracellular Ca^{2+} signals. The obtained results also pave the way for a better understanding of how the ER, chloroplasts and the cytosol functionally interact to maintain Ca^{2+} homeostasis and handle the complex signalling events taking place in the plant cell upon environmental stimulation.

RESULTS AND DISCUSSION

Targeting an aequorin probe to the plant endoplasmic reticulum

In order to quantify free [Ca^{2+}] that is present in resting condition in the plant ER, as well as the Ca^{2+} dynamics triggered upon perception of common environmental stimuli, in this work Arabidopsis seedlings were transformed with the aim of a stable expression of an aequorin-based Ca^{2+} probe targeted to the ER. The nucleotide sequence encoding *floury2* (fl2), a defective, uncleavable N-terminal ER signal peptide originally described in the nineties and responsible for an abnormal retention of storage α-zeins in the ER of a maize mutant (Gillikin *et al.*, 1997) was fused to the cDNA for a mutated version of aequorin, characterized by a point substitution (Asp119→Ala) leading to a reduced Ca^{2+} affinity (Montero *et al.*, 1995) and previously successfully used for Ca^{2+} investigations in the animal field (Ottolini *et al.*, 2014).

The sequence for this aequorin chimera was cloned in an expression cassette under the control of the 35S CaMV promoter in the pGreen 0029 plasmid. Arabidopsis seedlings were transformed via the floral dip technique using *Agrobacterium tumefaciens* (Clough and Bent, 1998).

After selection of the primary F_1 transformants on kanamycin (50 µg/ml), expression of the fl2_AEQmut probe in the transgenic seedlings was checked by RT-PCR and immunoblot analyses carried out on total RNA and protein extracts, respectively. 11 out the 12 independent F_2 sublines were positive at the level of aequorin gene expression (**Fig. 1a**), with sublines #6 and #10 revealing the highest protein level (**Fig. 1b**).

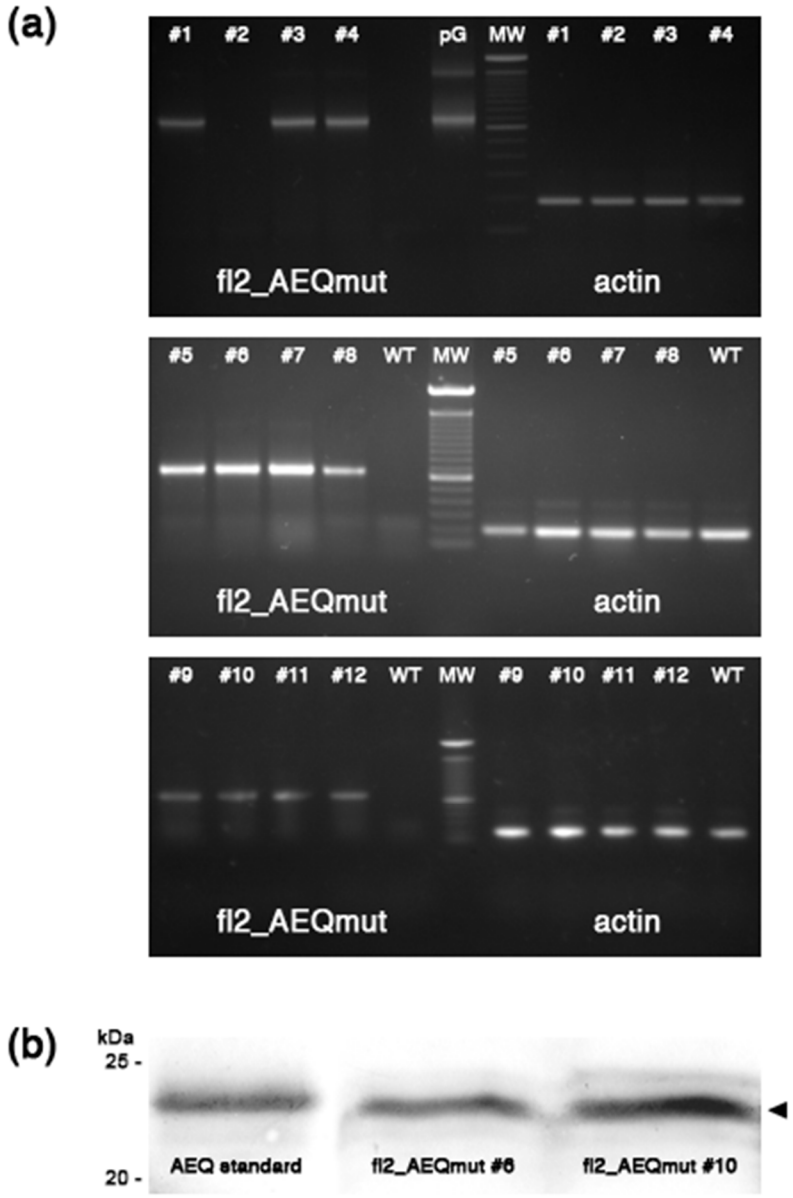

Fig. 1. Analysis of aequorin expression by RT-PCR **(a)** and immunoblotting **(b)** in Arabidopsis transgenic lines stably transformed with the fl2_AEQmut construct. RT-PCR analyses were performed on 12 different F_2 kanamycin-resistant sublines; a wild-type line (WT) was used as negative control. Actin was used as a housekeeping gene. Among the 12 screened sublines, only one (fl2_AEQmut #2) turned out to be a false positive. For immunoblot analyses, total protein extracts (50 µg) were separated by 12.5 % SDS-PAGE, transferred to PVDF and incubated with an anti-aequorin antibody (1:5000 diluted). An His-tagged aequorin (Moscatiello *et al.*, 2014) was used as a control. Only the two lines fl2_AEQmut #6 and #10 showing the highest expression levels are shown. Arrow indicates fl2-aequorin.

Analysis of the subcellular localization of the fl2-fused probes

To investigate the subcellular localization of fl2-fused recombinant proteins, a construct encoding fl2_YFP was engineered and used in transient and stable transformation of Arabidopsis. The former method was conducted by agroinfiltrating fully-expanded leaves of 1-month-old seedlings or by PEG-related transformation of protoplasts derived from 4-days-old heterotrophic suspension-cultured wild-type cells (**Fig. 2a**). Confocal microscopy observations were also performed on leaves and roots of stably transformed seedlings, as well as on cell suspension cultures from them derived (**Fig. 2b**, **c**). In all cases the YFP fluorescent signal was consistent with the distribution of ER membranes. The red signal due to chlorophyll autofluorescence never overlapped with the YFP one, but rather highlighted the close vicinity between ER and chloroplasts, which seem to be caged by a YFP-labelled reticular structure (**Fig. 2a**, **b**). Co-localization studies carried out on both seedlings and *in vitro* cell cultures by using the ER marker ER-Tracker Red further confirmed the ER targeting of fl2-fused proteins.

The actual localization at the ER level not only of the fl2_YFP probe but also of the fl2_AEQmut probe was ascertained by immunofluorescence (**Fig. S1**) and immunogold experiments (**Fig. 3**) carried out by using the anti-aequorin antibody on transgenic seedlings and cell cultures derived from them. TEM analyses after immunogold labelling showed the presence of electron-dense gold particles in close proximity with the rough ER membranes, whose profiles are clearly distinguishable due to ribosomes decorating their external surfaces.

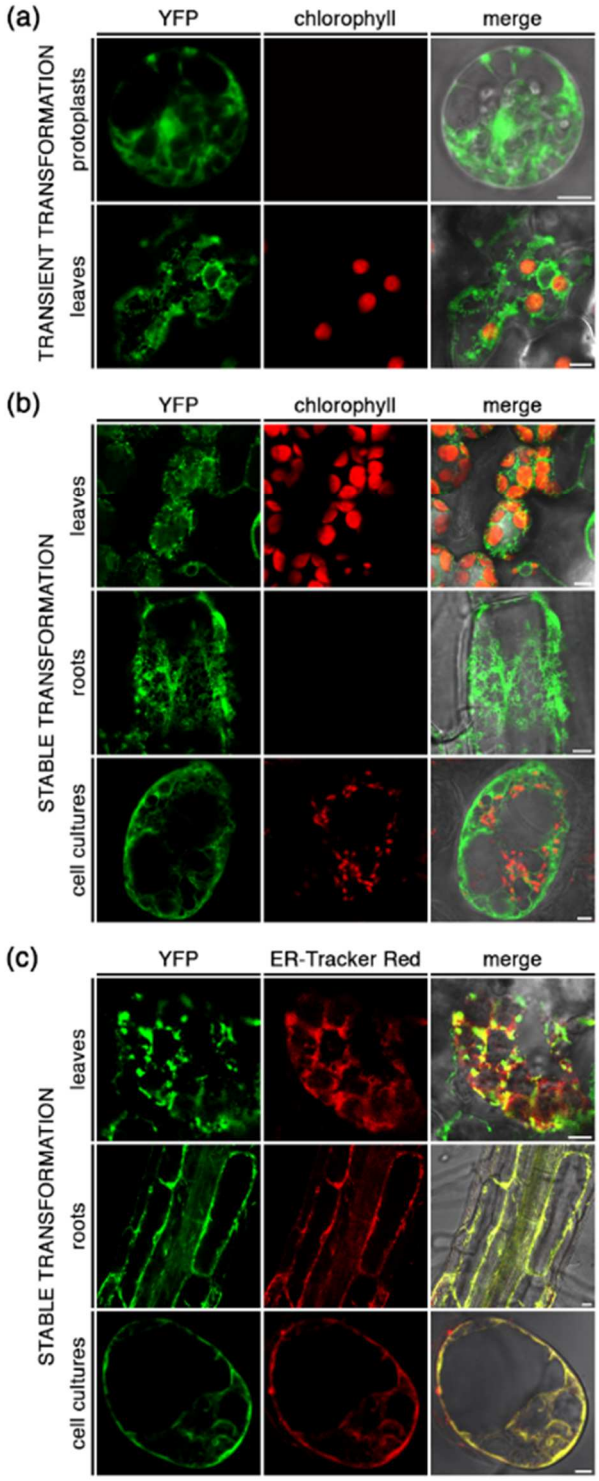

Fig. 2. Confocal microscopy analyses demonstrated the ER localization of the fl2_YFP probe in Arabidopsis: **(a)** transient transformation was carried out by PEG-mediated delivery of the fl2_YFP construct in protoplasts derived from wild-type heterotrophic cell suspension cultures and in wild-type leaves infiltrated with *Agrobacterium tumefaciens* carrying the fl2_YFP construct. **(b, c)** Leaves and roots from stably transformed seedlings, as well as cell cultures from them derives, were used. Fluorescence microscopy images with a YFP, chlorophyll and N21 filter plus an overlay of the two channels are shown. In **(c)**, co-localization studies using the ER marker ER-Tracker Red were performed. In all images, the fl2_YFP signal shows a reticular distribution compatible with ER profiles **(a, b)**, perfectly overlapping with the red fluorescent signal of the ER marker **(c)**. Bars = 5 µm.

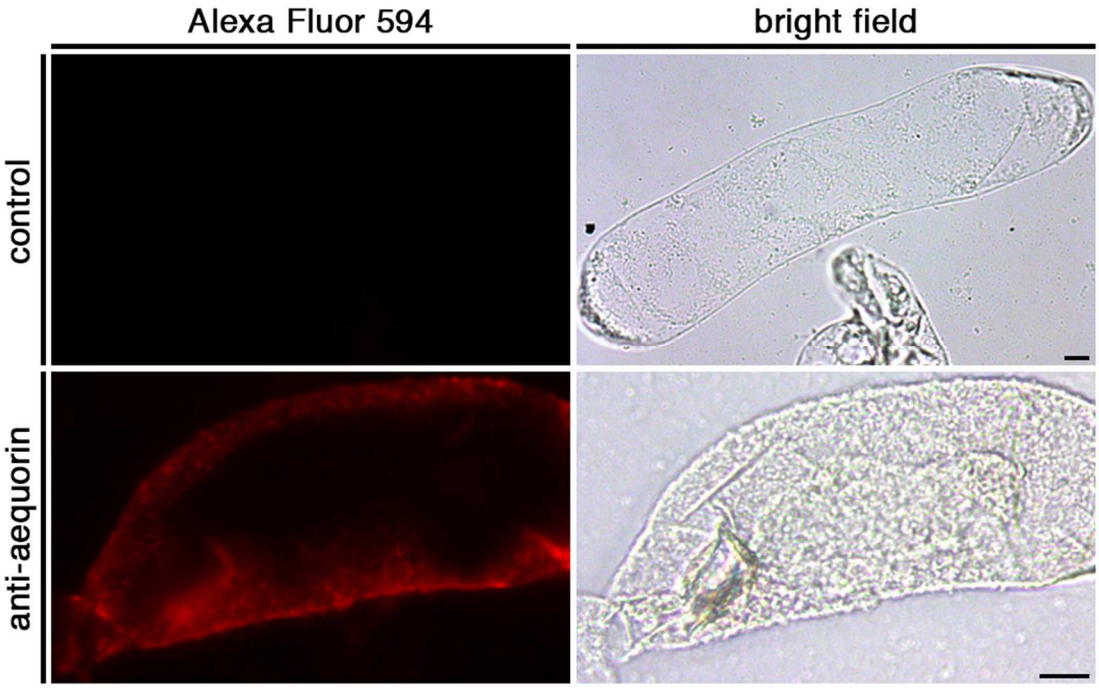

Fig. S1. Immunofluorescence analyses in Arabidopsis heterotrophic cell suspension cultures stably-expressing the fl2_AEQmut probe. After fixation, cells were incubated with anti-aequorin antibody followed by a red fluorescent Alexa Fluor 594 secondary antibody. Bright field and fluorescence microscopy images of the same field are shown. A clear red fluorescent signal was observed in the decorated sample, but not in the control (incubated only with secondary antibody). Bars = 10 µm.

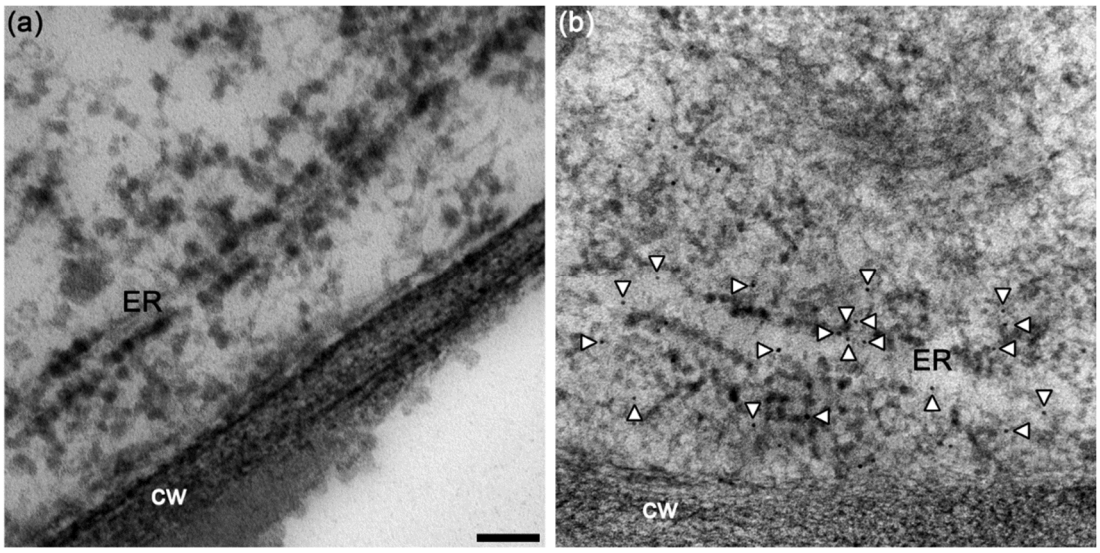

Fig. 3. Immunocytochemical analyses of fl2-aequorin subcellular localization in transgenic Arabidopsis seedlings. Immunogold labelling was carried out by incubation with anti-aequorin antibody followed by a secondary antibody conjugated with 10 nm diameter gold particles. White arrowheads indicate gold particles. Immunogold-labelled particles, present only in the decorated sample **(b)**, but not in the control (incubated only with secondary antibody) **(a)**, are visible at the level of ER profiles. Bars = 100 nm.

Setup of an efficient aequorin reconstitution protocol to enable *in vivo* ER Ca^{2+} measurements

Once the expression and correct targeting of the Ca^{2+} probe had been assessed, the next step was to perform *in vitro* and *in vivo* Ca^{2+} measurements. The functioning of the ER-targeted aequorin probe was verified by *in vitro* reconstitution assays. Light emitted by total proteins contained in the lysates from wild-type and transgenic lines was monitored after reconstitution of the apoprotein with coelenterazine. The luminescence signal detected in protein extracts from *A. thaliana* transformed with the fl2_AEQmut construct confirmed the functionality of the reporter (**Fig. S2**).

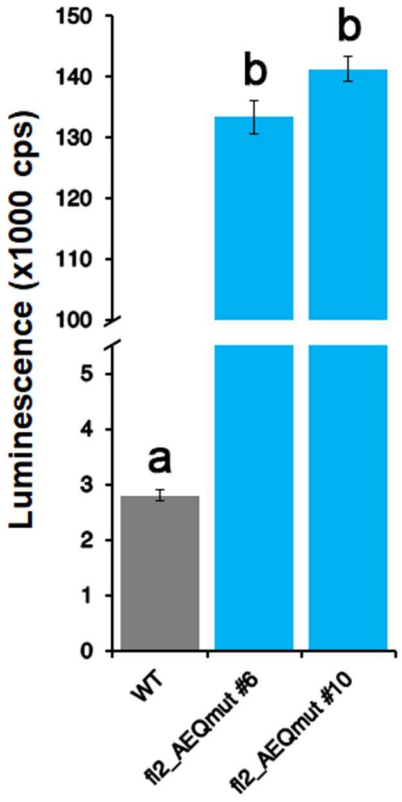

Fig. S2. *In vitro* reconstitution assays in fl2_AEQmut Arabidopsis transgenic lines. A wild-type line was used as negative control. Both fl2_AEQmut #6 and #10 Arabidopsis transgenic lines (light blue bars) showed significantly higher luminescence levels with respect to the wild-type one (grey bar) and are suitable for subsequent *in vivo* Ca^{2+} measurements at the luminometer. Luminescence data are presented as means ± SE of ≥3 independent experiments and bars labelled with different letters differ significantly ($P < 0.05$, Student's *t* test).

As a first trial for *in vivo* experiments, 2-weeks-old fl2_AEQmut Arabidopsis seedlings were simply challenged with a discharge solution (1 M $CaCl_2$, 30 % (v.v) ethanol) in order to evaluate the total luminescence available. However, standard reconstitution protocols commonly employed in aequorin-based Ca^{2+} assays (overnight reconstitution with 5 µM wild-type coelenterazine) proved unsuitable, since recorded luminescence levels were too low for adequate analyses (**Fig. S3**). This was likely due to the high [Ca^{2+}] expected in the ER, in agreement with the reports in the animal field (Brini, 2008), leading to an almost complete discharge of the Ca^{2+} probe during the holoprotein reconstitution procedure, despite the use of a mutated version of aequorin endowed with a reduced affinity for Ca^{2+}. A step of temporary emptying of this compartment was necessary to allow proper reconstitution of the fl2_AEQmut probe, and to this aim a large screening of different reconstitution procedures was carried out, both by reducing the incubation time interval and by applying specific ionophores or blockers of ER-located Ca^{2+} ATPases. These approaches were conducted not only with wild-type coelenterazine but also with coelenterazine n, a synthetic derivative that further reduces the aequorin affinity for Ca^{2+} with the aim of lowering its rate of consumption even in high [Ca^{2+}] compartments (Ottolini *et al.*, 2014). As shown in **Fig. S3**, the use of coelenterazine n proved to be inadequate to our aims, since it was found to reduce the luminescence emitted by aequorin. On the other hand, the use of wild-type coelenterazine and the combination of a reduced incubation time (2 h) plus a pre-treatment with the ER-type Ca^{2+} ATPase blocker cyclopiazonic acid (CPA) revealed suitable levels of emitted luminescence, and was therefore chosen as the appropriate reconstitution protocol for all the subsequent Ca^{2+} assays.

Following ER Ca^{2+} emptying, and in agreement with standard procedures commonly employed for studies in mammalian cells, prior to the addition of any tested stimulus it was necessary to remove CPA by extensive washing as well as to restore the resting $[Ca^{2+}]_{ER}$. ER refill by injection of 1 mM $CaCl_2$ induced a rapid and sustained increase in $[Ca^{2+}]_{ER}$, which mimicked what commonly observed for the animal counterpart, even if with a greatly reduced magnitude (**Fig. 4**).

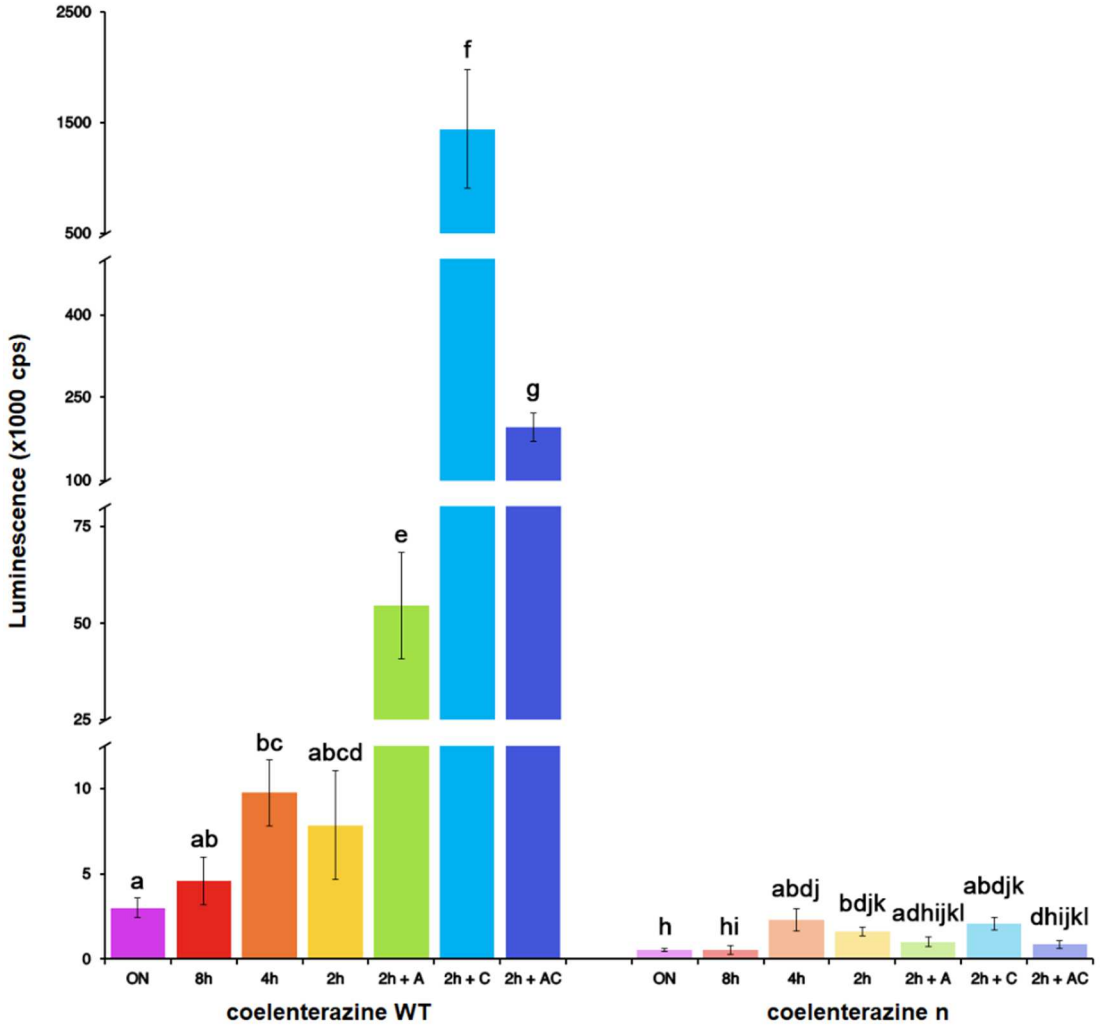

Fig. S3. *In vivo* reconstitution assays in fl2_AEQmut Arabidopsis transgenic lines in order to assess the best reconstitution protocol. Seedlings were reconstituted at 22 °C in the dark with 5 µM of either wild-type (dark bars) or n (light bars) coelenterazine for different incubation times: overnight (16 h, purple bars), 8 h (red bars), 4 h (orange bars), 2 h (green, light blue and blue bars). Prior to reconstitution, some seedlings were infiltrated with 10 µM A23187 (green bars), 50 µM CPA (light blue bars) or both (blue bars). The probe reconstitution protocol employing pre-treatment with CPA and 2 h incubation with wild-type coelenterazine provided the highest luminescence yield. Luminescence data collected are presented as means ± SE of ≥6 independent experiments and bars labelled with different letters differ significantly ($P < 0.05$, Student's *t* test).

The application of even higher $CaCl_2$ concentrations led to similar results, ruling out the possibility that the reached ER Ca^{2+} levels could be limited by the external Ca^{2+} concentration ($[Ca^{2+}]_{ext}$) provided: restored basal $[Ca^{2+}]_{ER}$ remained at about 7-8 µM even when the "refill" step was performed with a ten-fold concentration of $CaCl_2$ (**Fig. S4**). These Ca^{2+} levels were consistent in all the subsequent Ca^{2+} measurements presented throughout this work;

therefore, our *bona fide* suggestion is that they represent the actual free $[Ca^{2+}]$ present in the plant ER in resting conditions. A concentration value of $[Ca^{2+}]_{ER}$ just below 10 µM marks a striking difference with previously hypothesized values for $[Ca^{2+}]_{ER}$ of > 60 µM in Arabidopsis roots (Bonza *et al.*, 2013) or 100-500 µM in Arabidopsis pollen tubes (Iwano *et al.*, 2009). This discrepancy is likely to be due to the different Ca^{2+} indicator (cameleon) used in those previous studies, that, in contrast to aequorin, does not allow precise quantification of Ca^{2+} levels. Although $[Ca^{2+}]_{ER}$ in the plant ER was found to be up to 50 times lower than that measured in mammalian cells (Brini, 2008), it is still 100 times higher than $[Ca^{2+}]_{cyt}$, rendering this compartment the second main intracellular Ca^{2+} store of the plant cell, after the vacuole.

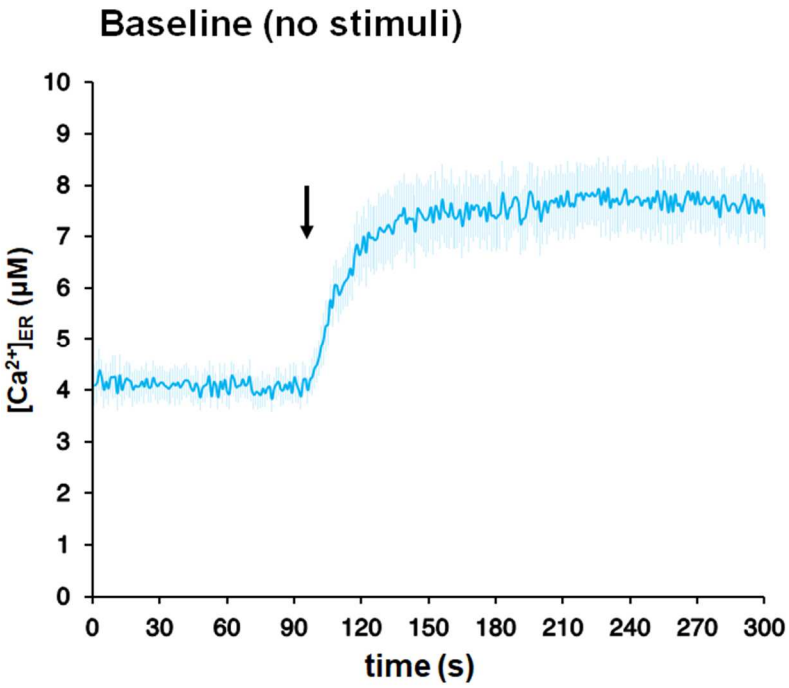

Fig. 4. Free basal $[Ca^{2+}]_{ER}$ in Arabidopsis seedlings in resting conditions. Ca^{2+} measurements were performed in Arabidopsis seedlings stably-expressing fl2_AEQmut. Data are the means (solid lines) ± SE (shadings) of >10 independent experiments. After 100 sec (black arrow) 1 mM $CaCl_2$ was added in order to restore the resting $[Ca^{2+}]_{ER}$.

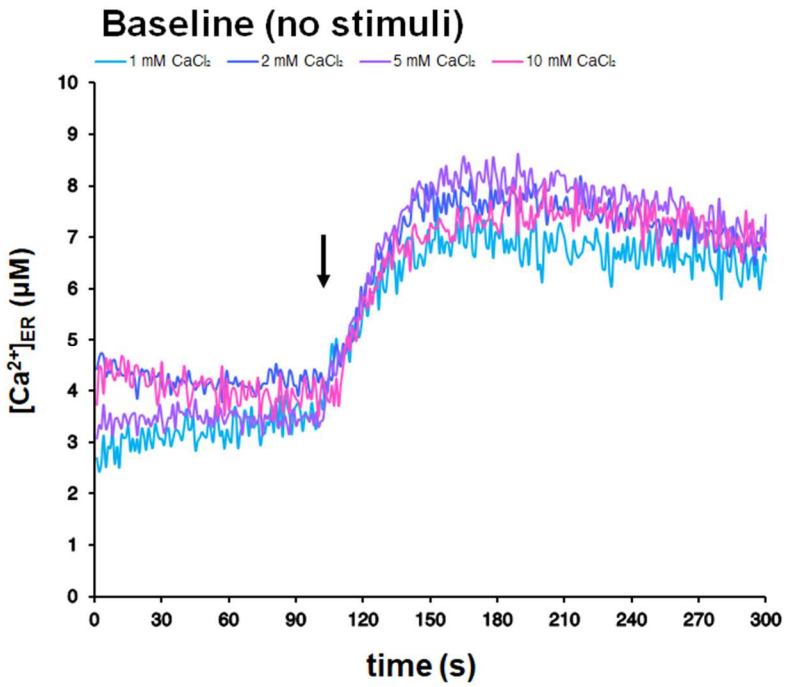

Fig. S4. Basal $[Ca^{2+}]_{ER}$ levels are independent of the injected $[CaCl_2]$ used in the refilling step. $[Ca^{2+}]_{ER}$ refill trials were performed in stably-expressing fl2_AEQmut Arabidopsis seedlings following the probe reconstitution protocol. Representative traces out of 3 independent experiments are shown. The application of various concentrations of $CaCl_2$ (100 s, black arrow: 1 mM (light blue trace), 2 mM (blue trace), 5 mM (violet trace) or 10 mM (pink trace)) led to similar basal $[Ca^{2+}]_{ER}$ levels.

Monitoring ER Ca^{2+} signals in response to abiotic and biotic environmental cues

Although the participation of organelles to plant intracellular Ca^{2+} signalling is increasingly emerging (Costa *et al.*, 2018), the relative contribution of the ER in shaping Ca^{2+} signatures still awaits further investigation. In particular, given the above-mentioned data – *i.e.* plant ER shows a higher $[Ca^{2+}]$ compared to other subcellular compartments – our expectations were to find this compartment able to release Ca^{2+} into the cytosol upon challenge with some physiological cues, similarly to animal ER which acts as a major Ca^{2+} mobilizable store of the cell. However, none of the tested abiotic stimuli (salinity, drought, oxidative stress) was able to trigger ER Ca^{2+} release but rather evoked transient $[Ca^{2+}]_{ER}$ increases characterized by stimulus-specific dynamics. Indeed, while application of a touch-control (H_2O) did not affect resting $[Ca^{2+}]_{ER}$ levels (**Fig. 5a**, insert), the application of 300 mM NaCl

(mimicking a salt stress) led to a rapid and transient increase in $[Ca^{2+}]_{ER}$ up to about 45 µM (**Fig. 5a**), which is 5-to-6 times higher than resting values. When Arabidopsis seedlings were challenged with 600 mM mannitol to simulate drought, a similar Ca^{2+} transient, peaking just above 30 µM, was recorded after about 30 sec (**Fig. 5b**), while an oxidative stress, represented by the injection of 10 mM H_2O_2, turned out to induce a much slower and less pronounced Ca^{2+} elevation, whose magnitude reached about 15 µM (**Fig. 5c**).

In subsequent experiments, biotic stimuli involve in the activation of plant defence responses were tested, in particular the flg22 peptide (1 µM), derived from bacterial flagellin (**Fig. S5a**), and OGs (20 µg/µl), pectic fragments of the plant cell wall originating after pathogen attack (**Fig. S5b**). In neither case a $[Ca^{2+}]_{ER}$ change was recorded, suggesting that other Ca^{2+} stores in the plant cell may be responsible for the Ca^{2+}-mediated signal transduction underlying these biotic interactions. Moreover, also a mixture of short chitin oligomers was tested (CO-MIX, 1 µM), but again no $[Ca^{2+}]_{ER}$ response was detected (**Fig. S5c**). However, this was expected, because short chitin chains have been demonstrated to represent a fungal symbiotic signal for arbuscular mycorrhizal (AM) symbiosis that is established between AM fungi and the 80 % of land plants, but not Arabidopsis.

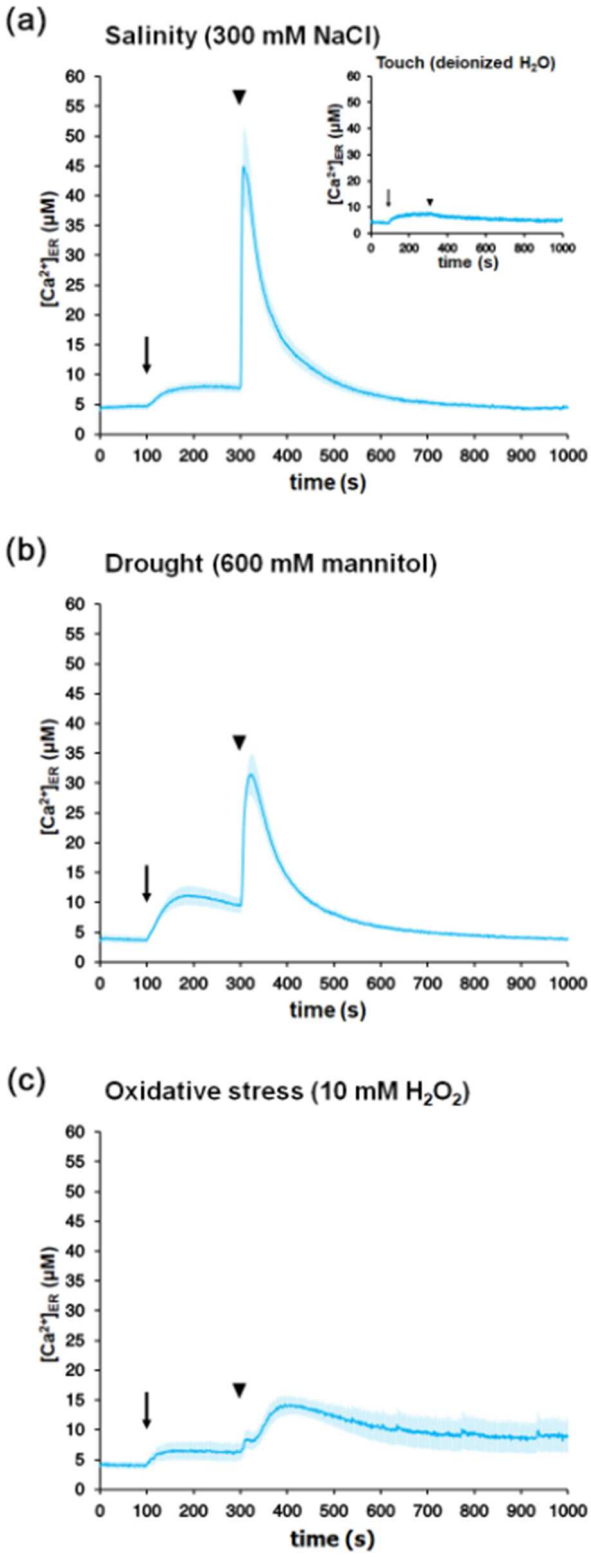

Fig. 5. Monitoring of $[Ca^{2+}]_{ER}$ dynamics in response to environmental stimuli of abiotic nature. Ca^{2+} assays were conducted in stably-expressing fl2_AEQmut Arabidopsis seedlings. Following the application of 1 mM $CaCl_2$ (100 s, black arrow) in order to restore the basal $[Ca^{2+}]_{ER}$, seedlings were challenged with (300 s, black arrowhead) **(a)** 300 mM NaCl; **(b)** 600 mM mannitol; **(c)** 10 mM H_2O_2. Data are the means (solid lines) ± SE (shadings) of ≥6 independent experiments. The insert in panel **(a)** shows a touch control (injection of an equal volume of H_2O)

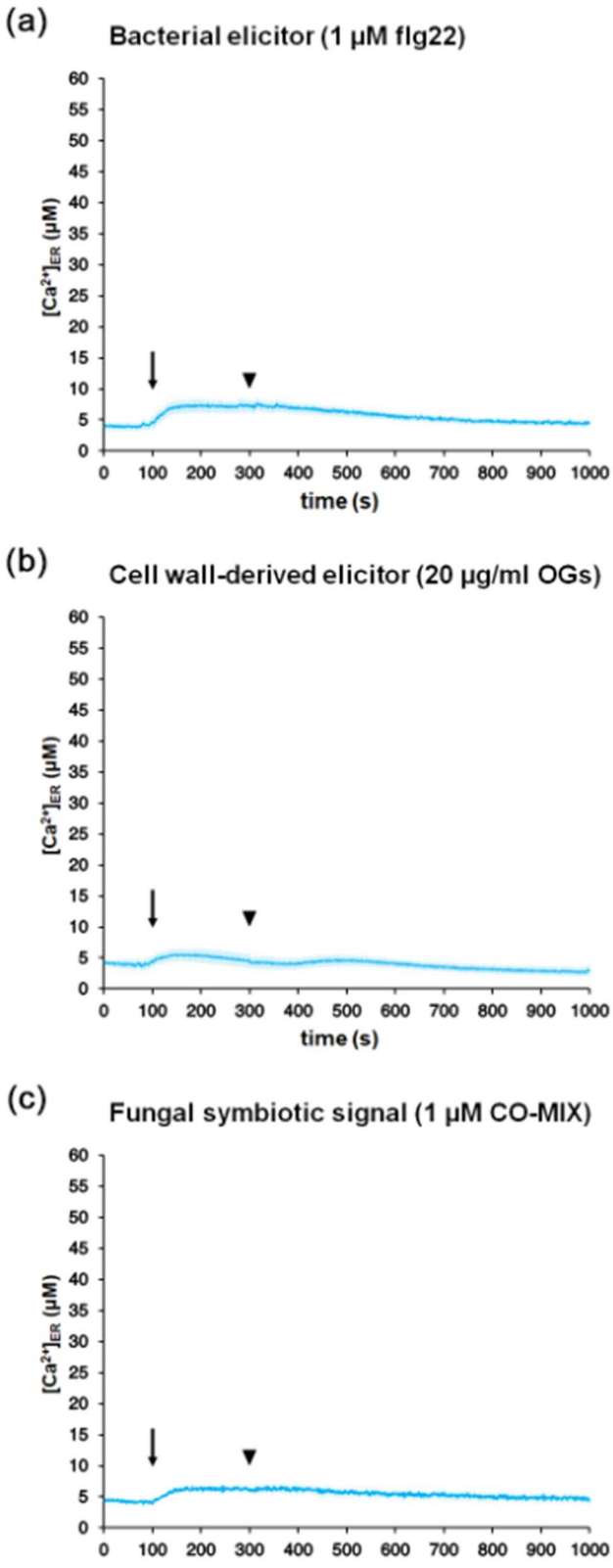

Fig. S5. Monitoring of $[Ca^{2+}]_{ER}$ dynamics in response to environmental stimuli of biotic nature. Ca^{2+} assays were conducted in stably-expressing fl2_AEQmut Arabidopsis seedlings. Following the application of 1 mM $CaCl_2$ (100 s, black arrow) in order to restore the basal $[Ca^{2+}]_{ER}$, seedlings were challenged with different biotic stresses (300 s, black arrowhead): **(a)** 1 µM flg22; **(b)** 20 µg/ml OGs; **(c)** 1 µM CO-MIX. Data are the means (solid lines) ± SE (shadings) of ≥3 independent experiments.

An ER Ca^{2+} ATPase is involved in the observed ER Ca^{2+} increases during signal transduction

A pharmacological approach based on the use of specific inhibitors of plant Ca^{2+} ATPases was applied to get insights into the putative Ca^{2+} transporters localized at the ER membrane and responsible for the observed ER Ca^{2+} increases. Due to the significant difference between $[Ca^{2+}]_{cyt}$ and $[Ca^{2+}]_{ER}$ (~100 nM in the cytosol *versus* ~10 µM in the ER, respectively) the participation of active Ca^{2+} transporters located at ER membranes seem to be likely. There are two types of ER Ca^{2+} ATPases: ECAs (ER-type Ca^{2+} ATPases) and ACAs (Autoinhibited Ca^{2+} ATPases). ECAs are a class of Ca^{2+} ATPases able to transport not only Ca^{2+} but also other divalent cations (such as Mn^{2+} and Zn^{2+}): they include two members targeted either to the ER (ECA1) or the Golgi and post-Golgi vesicles (ECA3), plus two members (ECA2 and 4) with still unidentified intracellular localization. They exhibit an affinity constant in the submicromolar range and they are specifically inhibited by cyclopiazonic acid (CPA), a pharmacological inhibitor already employed in this work in order to empty the ER during the aequorin *in vivo* reconstitution protocol. ACAs represent a wide family of Ca^{2+} ATPases that are found not only at the level of the ER membranes (ACA2 and possibly ACA1, about which discordant reports are present in literature pointing either to the ER or to the plastid inner envelope) but also at the tonoplast (ACA4 and 11) and plasma membrane (ACA 8, 9, 10 and perhaps even ACA12), with still unknown subcellular localization for ACA7 and 13: these Ca^{2+} pumps were reported to be highly specific for Ca^{2+} ions, to possess an affinity constant in the micromolar range (thus higher than that of ECAs) and to be blocked by fluorescein derivatives such as eosin yellow (EY) and erythrosin blue (EB) (De Michelis *et al.*, 1993; Bonza and De Michelis, 2011). To uncover the contribution of the different ER Ca^{2+} ATPases involved in Ca^{2+} increases during signal transduction, Ca^{2+} measurements were carried in fl2_AEQmut seedlings by pre-treating for 5 min Arabidopsis seedlings with either CPA (50 µM), eosin Y (1 µM) or erythrosine B (1 µM), before challenge with environmental stimuli. **Fig. 6** shows that, at least in the case of salt stress (300 mM NaCl) CPA caused a 50 % inhibition of the ER Ca^{2+} increase, whereas EY and EB did not induce any change in the

[Ca^{2+}] elevation with respect to the untreated control. These data indicated the main involvement of the ER-targeted ECA1 Ca^{2+} pump in the observed ER Ca^{2+} uptake. Since the contribution of ER-located ACAs seem to be negligible, it cannot be ruled out that also ER Ca^{2+} buffering proteins, such as calreticulin (Mariani *et al.*, 2003; Joshi *et al.*, 2019), may be involved in $[Ca^{2+}]_{ER}$ increases.

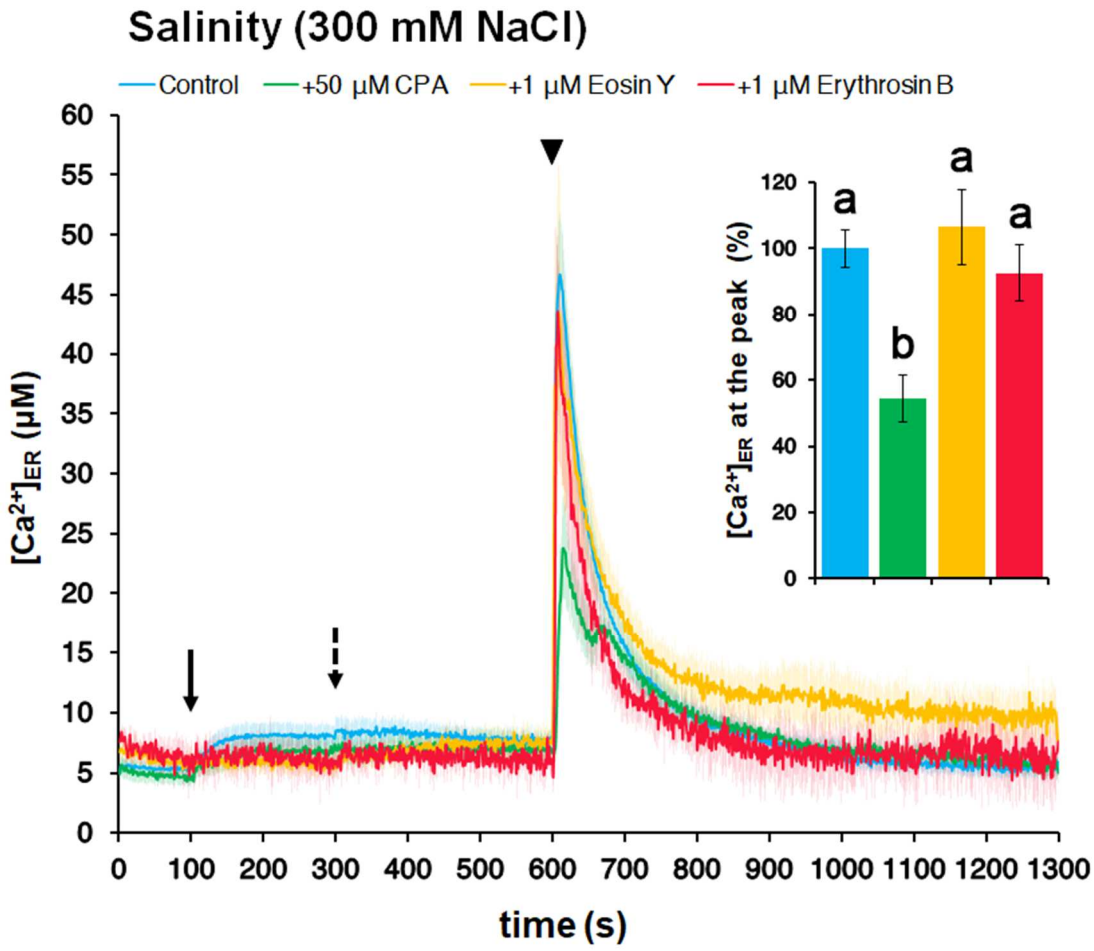

Fig. 6. Pharmacological approach for the analysis of salinity-induced ER Ca^{2+} fluxes. Ca^{2+} analyses were carried out in stably-expressing fl2_AEQmut Arabidopsis seedlings. Data are the means (solid lines) ± SE (shadings) of 6 independent experiments. Following the application of 1 mM $CaCl_2$ (100 s, black solid arrow) in order to restore the basal $[Ca^{2+}]_{ER}$, seedlings were incubated with H_2O (control, in light blue) or with different inhibitors of ER Ca^{2+} ATPases (50 µM CPA (green), 1 µM EY (yellow), 1 µM EB (red)) (300 s, black dashed arrow) and then challenged with 300 mM NaCl (600 s, black arrowhead). The inset shows statistical analyses of $[Ca^{2+}]_{ER}$ at the peak. Bars labelled with different letters differ significantly ($P < 0.05$, Student's *t* test).

Integration of ER Ca^{2+} dynamics in the plant cell Ca^{2+} signalling network: comparison of Ca^{2+} signatures evoked in the cytosol, ER, chloroplasts

Ca^{2+} assays in response to the same environmental stimuli were also carried out in Arabidopsis seedlings stably expressing aequorin in the cytosol and chloroplast stroma (Sello *et al.*, 2018), and the Ca^{2+} traces in the respective locations were compared to those in the ER. **Fig. 7** shows that in all the cases considered, ER Ca^{2+} transients temporally followed cytosolic Ca^{2+} changes. In particular, while the ER Ca^{2+} response evoked by salt stress (**Fig. 7a**) appeared only slightly delayed compared to the cytosolic one, $[Ca^{2+}]_{ER}$ elevations triggered by both drought (**Fig. 7b**) and oxidative stress (**Fig. 7c**) showed a Ca^{2+} peak occurring 20-60 sec after the cytosolic one. These data suggest that the ER is involved in the dissipation of the cytosolic Ca^{2+} signals, rather than in their generation.

Concerning the experiments carried out in Arabidopsis seedlings expressing the stroma-targeted aequorin probe, the comparison of the Ca^{2+} traces recorded in the different intracellular localizations (cytosol, ER, chloroplasts) suggest that chloroplasts are involved either in between the cytosol and the ER (**Fig. 7a**, **b**) or at a later stage (**Fig. 7c**), thus implying a complex interplay between these organelles in terms of Ca^{2+} handling.

To functionally link cytosolic and ER $[Ca^{2+}]$ elevations, an additional set of experiments was performed with the aim of elucidating a possible correlation between the two Ca^{2+} responses: Arabidopsis seedlings stably expressing aequorin either in the cytosol or in the ER were pre-treated with different concentrations of the extracellular Ca^{2+} chelator EGTA. **Fig. 8** shows that pre-treatment with either 1 or 5 mM EGTA reduced to about 50 % the magnitude of cytosolic Ca^{2+} elevations evoked in response of both high salinity (**Fig. 8a**) and drought (**Fig. 8c**), whereas $[Ca^{2+}]_{cyt}$ changes in response to oxidative stress remained unaltered (**Fig. 8e**).

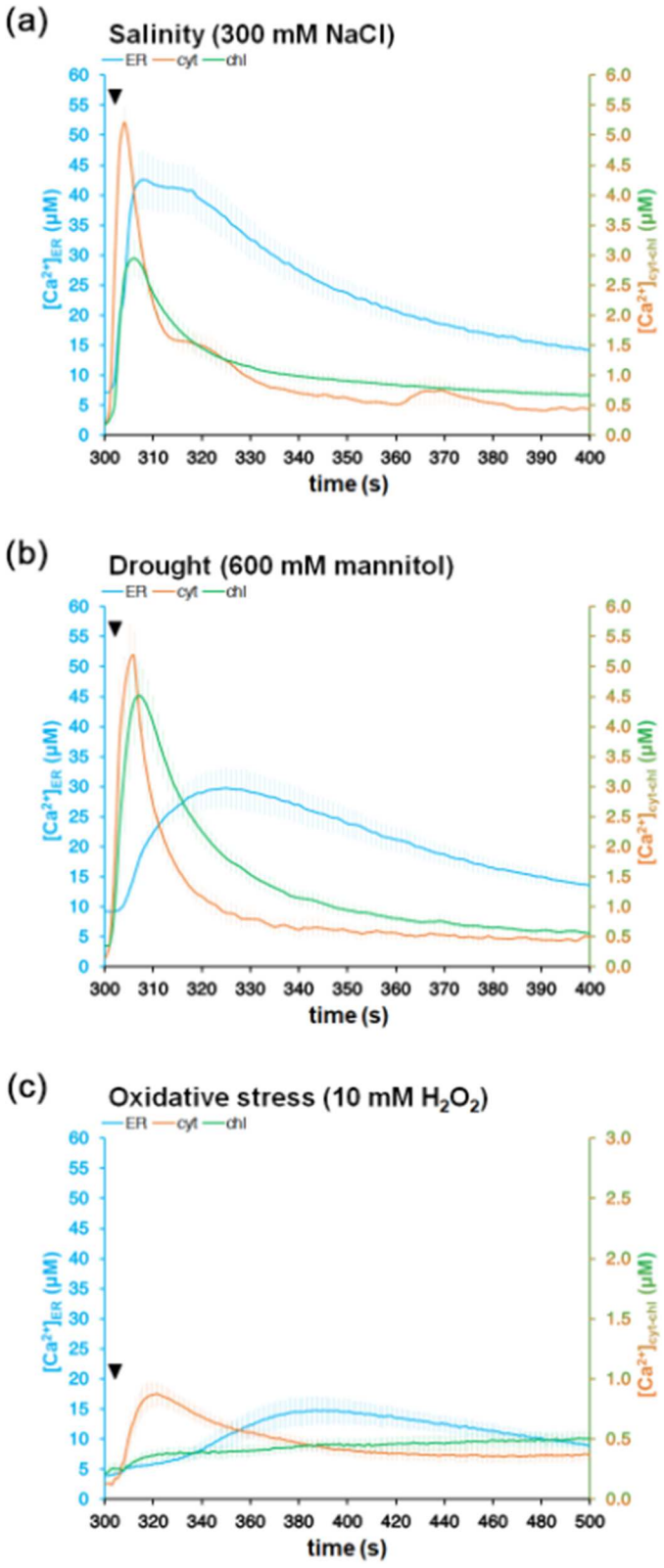

Fig. 7. Comparison between [Ca^{2+}] dynamics in the cytosol, chloroplast and ER in response to environmental stimuli. Ca^{2+} measurements were performed in Arabidopsis seedlings stably expressing aequorin in the cytosol (orange trace), in the chloroplast stroma (green trace) or in the ER (light blue trace). Seedlings were challenged with different abiotic stresses (300 s, black arrowhead): **(a)** 300 mM NaCl; **(b)** 600 mM mannitol; **(c)** 10 mM H_2O_2. Data are the means (solid lines) ± SE (shadings) of ≥6 independent experiments.

Similarly, salt- (**Fig. 8b**) and drought- (**Fig. 8d**) induced ER Ca^{2+} responses were highly reduced (at about 50 %) by 1 mM EGTA pre-treatment and completely abolished by 5 mM EGTA. On the other hand, pre-treatment of seedlings with 1 mM EGTA did not reduce the magnitude of the ER Ca^{2+} transient in response to an oxidative stress (**Fig. 8f**) and 5 mM EGTA caused a significant reduction in the ER Ca^{2+} uptake that however was not as harsh as that recorded for the other two abiotic stimuli. Taken together, these data indicate the existence of not only a temporal but also a causal link between the Ca^{2+} transients in the cytosol and the ER. Indeed, the abolishment of the $[Ca^{2+}]_{cyt}$ changes observed in response to a salt and osmotic stress in the presence of EGTA was mirrored by a corresponding inhibition of the $[Ca^{2+}]_{ER}$. The slightly different scenario observed in response to oxidative stress is probably due to a different management of the Ca^{2+} uptake from the apoplast and/or Ca^{2+} release from intracellular storage compartments (such as the vacuole) in response to distinct environmental stimulations. Indeed, it is known that Ca^{2+} signalling in response to salinity and drought partially relies on the entry into the cell of external Ca^{2+} (Knight *et al.*, 1997), whereas oxidative stress may be mainly transduced through the release of Ca^{2+} from intracellular pools (Rentel and Knight, 2004).

In summary, in this work a novel genetically-encoded calcium probe targeted to the ER was engineered, which provided accurate quantifications of $[Ca^{2+}]$ in the plant ER and for its variations in response to different environmental stimuli. Our findings add new insights into the role of this compartment in Ca^{2+} homeostasis and signalling in the plant cell.

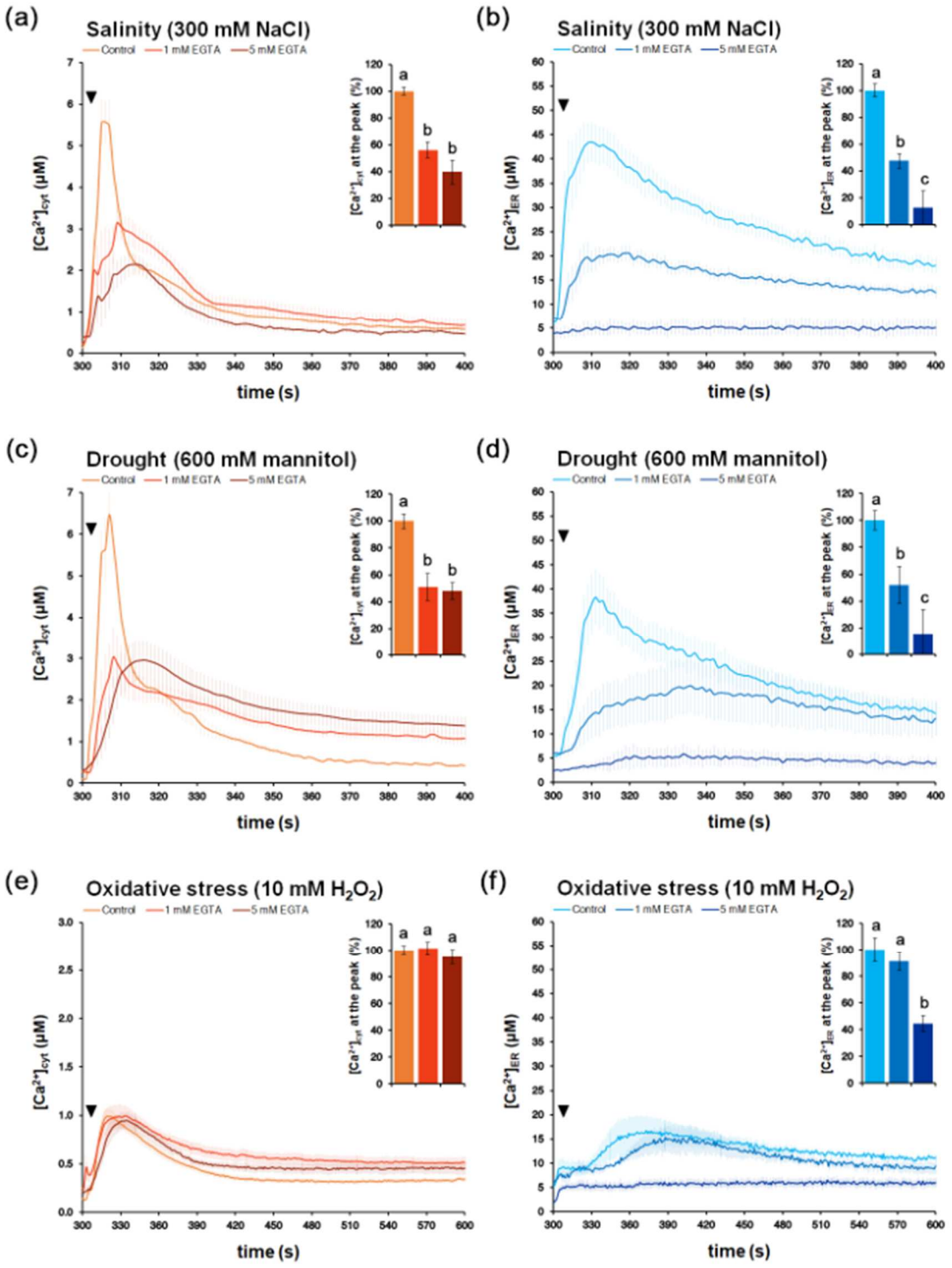

Fig. 8. Effect of pre-treatment with EGTA on abiotic stresses-triggered $[Ca^{2+}]_{cyt}$ and $[Ca^{2+}]_{ER}$. Ca^{2+} assays were conducted in Arabidopsis seedlings stably expressing either the Cyt-YA **(a, c, e)** or the fl2_AEQmut **(b, d, f)** probes. Seedlings were pre-treated with various concentrations of EGTA (100 µM control (light traces), 1 mM (intermediate traces), 5 mM (dark traces)) for 10 min, then challenged with different abiotic stresses (300 s, black arrowhead): **(a, b)** 300 mM NaCl; **(c, d)** 600 mM mannitol; **(e, f)** 10 mM H_2O_2. Insets show statistical analyses for $[Ca^{2+}]$ at the peak and bars labelled with different letters differ significantly ($P < 0.05$, Student's *t* test). Data are the means (solid lines) ± SE (shadings) of ≥6 independent experiments.

MATERIALS AND METHODS

Molecular cloning and construction of expression plasmids

In order to monitor the calcium concentration in the plant ER, the signal peptide of the maize mutant *floury2* (Coleman *et al*., 1995) was fused to a mutated version of aequorin, endowed with a reduced Ca^{2+} affinity (Montero *et al*., 1995). The sequence encoding aequorin was amplified by PCR using as forward primer XbaI_fl2_aeq, encoding the 21 amino acid (α-helix) of the uncleaved signal peptide of the 24-kDa α-zein protein, and Aeq_rev as reverse primer (**Table S1**). After digestion with XbaI and SacI, the amplicon (751 bp) was cloned into the 35S-CaMV cassette (677 bp) of the plasmid p35SCaMV. The entire cassette 35-CaMV-fl2_AEQmut was then amplified in order to create additional restriction sites (NotI and XhoI) and moved into the binary vector pGreen 0029. To obtain the fl2_YFP construct, the sequence encoding the YFP was amplified by PCR using XbaI_fl2_Yfp and Yfp_rev as primers (**Table S1**). The amplicon (808 bp) was digested with XbaI and SacI and cloned into the 3535S-CaMV cassette. After digestion with EcoRV the entire cassette was then moved into the binary vector pGreen 0029.

Table S1. Nucleotide sequences of the primers used in this work for the targeting of the fl2-fused probes to the ER.

Primer	Sequence
XbaI_fl2_aeq	5'-cttactctagaatggctaccaagatattagccctccttgcgcttcttgccctttagtgagcgcaacaaatgtgaagctttatgatgttcctga-3'
Aeq_rev	5'-tgatagagctcgaattcatcagtgttttat-3'
35S NotI_for	5'-atggcggccgcgatatcgtacccctactccaaaaat-3'
35S XhoI_rev	5'-catgctcgaggatatcgatctggattttagta-3'
XbaI_fl2_Yfp	5'-cttactctagaatggctaccaagatattagccctccttgcgcttcttgccctttagtgagcgcaacaaatgtgggcagcaagggcgaggagct-3'
Yfp_rev	5'-tgatagagctcctagatcaccttgtacagc-3'
XbaI_fl2	5'- cttactctagaatggctaccaagatattag-3'

Generation of transgenic Arabidopsis lines

Arabidopsis thaliana wild-type plants belonging to Columbia 0 ecotype were grown on soil and transformed by the floral dip technique (Clough and Bent, 1998) with the pGreen 0029-fl2_AEQmut construct in order to generate multiple independent transgenic lines. The same approach was repeated also for the pGreen 0029-fl2_YFP construct. The seeds of the F_1 generation were surface-sterilized and screened on agarized (0.8 % w/v) half-strength Murashige and Skoog (MS) medium, pH 5.5 supplemented with 1.5 % (w/v) sucrose and containing 50 µg/ml kanamycin (seedlings were grown at 22 °C under a 16 h-light/8 h-dark cycle). Plants which survived were transferred in single pots and grown on soil so that their F_2

generation seeds could be collected separately: the progeny of each F_1 seedling was subsequently screened for aequorin expression both at the DNA and protein levels.

Analysis of aequorin expression

Leaves from each of the Arabidopsis fl2_AEQmut independent transgenic lines were collected from the F_2 generation (kanamycin-resistant, 1-month-old plants) and flash-frozen in liquid nitrogen. Total RNA was extracted using the RNeasy Plant Mini Kit (Qiagen) and then reverse transcribed with SuperScript III (Thermo Fisher Scientific) according to the manufacturer's instructions. Primers designed on the cDNA sequence of fl2_AEQmut and on the coding sequence of actin (used as control) were used to analyze gene expression (**Table S1**).

Total protein crude extracts were obtained by grinding leaves in presence of a lysis buffer (0.1 M Tris-HCl pH 7.8, 0.2 M NaCl, 0.2 % Triton X-100, 1 mM EDTA, 1 µM leupeptin, 0.5 mM PMSF). After centrifugation at 13000g at 4 °C for 5 min the were collected and protein concentration was determined by Bradford assay (Bradford, 1976). Equal amounts (50 µg) of total protein crude extracts were loaded onto 12.5 % polyacrylamide gels and separated by SDS-PAGE, then transferred to polyvinylidene difluoride (PVDF) membranes (Immobilon-P, Millipore) and immunoblotted with a polyclonal anti-aequorin antibody (Abcam) diluted 1:5000 (1 h incubation).

Setup of cell suspension cultures from the transformed Arabidopsis lines

Arabidopsis fl2_AEQmut sublines #6 and #10 (F_2), which revealed the highest expression of the probe – as well as the fl2_YFP subline (F_2) showing the highest YFP fluorescence – were used to establish photosynthetic and heterotrophic cell suspension cultures as described by Cortese *et al.* (*in revision, Sept. 2019*; see **Chapter 5**).

For photosynthetic cultures, seeds were surface-sterilized and sown on agarized (0.8 w/v) full-strength MS medium pH 5.5 supplemented with 3 % (w/v) sucrose, 0.5 µg ml^{-1} 2,4-dichlorophenoxyacetic acid, 0.25 µg ml^{-1} BAP and 50 µg/ml kanamycin. After 3 weeks, de-differentiated hypocotyl-derived green calli were excised from cotyledons and roots by using a sterile scalpel, then transferred to a liquid version of the same medium as above with the sole exception of sucrose concentration which started at 2 % (w/v) and was progressively reduced by half (down to 0.5 % w/v) every 2 or 3 weeks of subculturing. To stimulate photosynthesis, cell suspension cultures were maintained on an orbital shaker (80 rpm) at 22 °C under a 16 h-light/8 h-dark cycle with an illumination rate of 110 µmol photons m^{-2} s^{-1}. Heterotrophic cultures were obtained by surface-sterilizing seeds and sowing them on agarized (0.8 w/v) half-strength MS medium pH 5.5 supplemented with 1.5 % (w/v) sucrose and 50 µg/ml kanamycin. After 1 week, well-developed cotyledons and hypocotyls were excised with a sterile scalpel and transferred separately to agarized (0.8 % w/v) Callus Induction Medium supplemented with 2 % (w/v) sucrose and 50 µg/ml kanamycin. Two renewals on similar, fresh medium were performed after 3 weeks each, while for the third time now developed yellow calli were transferred to exactly the same liquid medium employed for

photosynthetic cultures (as described above) with the sole difference of gradually increasing the sucrose concentration up to 3 % (w/v) instead of reducing it.

Protoplast isolation

Protoplast isolation was carried out from 4-days-old photosynthetic wild-type Arabidopsis cell cultures by incubating 2 ml of packed cell volume with 5 volumes of 0.75 % (w/v) cellulase 'Onozuka' R-10, 0.25 % (w/v) macerozyme R-10 (Yakult Honsha Co., Ltd.), 0.55 M mannitol in cell culture medium for 2 h in the dark. Protoplasts were separated from cellular debris and undigested cells by filtration through 55 µm nylon meshes, centrifuged at 60 × g for 5 min at room temperature, washed twice with isosmotic buffer (0.55 M mannitol in cell culture medium) and resuspended at a final density of 10^6 protoplasts ml^{-1}.

fl2_YFP transient expression in Arabidopsis wild-type lines

Transient expression of the fl2_YFP construct for localization studies was performed both on isolated protoplasts and on fully-expanded leaves in 4-weeks-old wild-type Arabidopsis seedlings. The former ones were transformed by PEG as described by Yoo and colleagues (Yoo *et al.*, 2007), whereas the latter ones were subjected to standard agroinfiltration procedure (Lee and Yang, 2006).

Fluorescence and confocal microscopy analyses

Developing calli from fl2_YFP sublines were observed with a LEICA MZ16F fluorescence stereomicroscope equipped with a GFP filter (excitation at 450/490 nm and emission at 500/550 nm) and a chlorophyll filter (excitation at 460/500 nm and emission above 605 nm).
Confocal microscopy observations of fl2_YFP transformed seedling (14-days-old) and cell suspension cultures (4-days-old) as well as on agroinfiltrated leaves (1-month-old) or transformed protoplasts (4-days-old) were performed with a Leica TCS SP5 II confocal laser scanning system mounted on a Leica DMI6000 inverted microscope. Samples were excited with two argon lasers set at 488 nm (for YFP and chlorophyll) and 543 nm (for the ER-Tracker Red), while fluorescence emissions were collected at 505 to 540 nm for YFP, 680 to 720 nm for chlorophyll or 600 to 633 nm for the ER-Tracker Red.

Immunofluorescence

fl2_AEQmut heterotrophic cell suspension cultures were fixed in 3.8 % (w/v) paraformaldehyde for 15 min. After extensive washing in phosphate-buffered saline (PBS), cells were sedimented onto poly-L-lysine coverslips and permeabilized with 0.1 % (w/v) Triton X-100 in PBS for 3 min. Unspecific binding sites were blocked with 1 % (w/v) BSA in PBS for 15 min and then labelling was performed with the anti-aequorin primary antibody diluted 1:1000 for 1 h at 37 °C in a moist chamber, followed by Alexa Fluor 594 donkey anti-rabbit Ig (Thermo Fisher Scientific) diluted 1:250 for 30 min at room temperature. All incubations were followed by three washes (2 min each) in PBS and 0.1 % (w/v) Tween-20, with an additional

wash with distilled H_2O before the addition of the mounting medium ProLong Gold antifade reagent (Thermo Fisher Scientific). Cells were observed under a Leica DM5000B fluorescence microscope, with excitation at 515/560 nm and emission above 580 nm and images acquired with a Leica DFC300FX digital camera, using the LAS software.

Immunogold labelling

Leaf and root fragments from 2-week-old Arabidopsis plants were fixed overnight at 4 °C in 4 % (v.v) paraformaldehyde and 0.25 % (v.v) glutaraldehyde in 0.1 M cacodylate buffer, pH 7.4. After three washes in cacodylate buffer, dehydration in a graded ethanol series was performed. Samples were then embedded progressively in medium-grade London Resin White (PolySciences). Ultrathin sections (500 Å) were obtained on a Reichert-Jung ultramicrotome and mounted on uncoated nickel grids. For immunogold labelling, grids were incubated for 45 min in 0.1 % (v.v) Tween 20, 1 % (w/v) BSA in TBS, and then for 1 h with rabbit anti-aequorin antibody at a 1:500 dilution. After three washes with 0.1 % (v.v) Tween 20 in TBS, samples were incubated for 1 h with an anti-rabbit secondary antibody conjugated with colloidal gold particles of 10 nm diameter (Sigma-Aldrich) diluted 1:100. After two washes as above and one wash in distilled H_2O, samples were exposed to osmium tetroxide vapours overnight. After extensive washing with distilled H_2O, samples were counterstained with uranyl acetate and lead citrate and observed using a Tecnai 12-BT transmission electron microscope (FEI) operating at 120 kV and equipped with a Tietz camera.

***In vitro* reconstitution of apoaequorin to aequorin**

Total protein crude extracts were obtained as described above, with the sole exception of a non-denaturing buffer composed of 150 mM Tris-HCl, 10 mM EGTA, 0.8 mM PMSF, pH 8.0 (reconstitution buffer). 50 µg of total protein crude extracts were resuspended at 1 µg/µl in reconstitution buffer and incubated with 1 mM β-mercaptoethanol and 5 µM coelenterazine for 4 h at 4 °C in the dark. Aequorin luminescence was detected from 50 µl of the *in vitro* aequorin reconstitution mixture and integrated for a 200 sec time interval after the addition of an equal volume of 100 mM $CaCl_2$.

***In vivo* reconstitution of apoaequorin to aequorin**

14-to-17-days-old Arabidopsis fl2_AEQmut seedlings (F_3) grown in sterility conditions on agarized medium were transferred in a microtitration plate well and incubated in 600 µM EGTA solution additioned with 5 µM coelenterazine (wild-type or n variant) for time intervals ranging from 2 h to about 16 h (overnight) at 22 °C. To set up an efficient *in vivo* reconstitution protocol, different procedures were experimented by pre-treating seedlings with 10 µM ionophore A23187, 50 µM cyclopiazonic acid (CPA) or both in the presence of 600 µM EGTA. Solutions were syringe-infiltrated to create vacuum, then after 10 min either wild-type or n coelenterazine was added and incubation prolonged for 2 h. At the end of the *in vivo* aequorin reconstitution, seedlings were washed individually via syringe-infiltration with a 100 µM EGTA solution and

allowed to recover for at least 10 min. Each seedling was then subjected to *in vivo* probe discharge by applying the same procedure described for *in vitro* assays. In some experiments, Arabidopsis seedlings stably expressing aequorin either targeted to the cytosol or to the chloroplast stroma (Sello *et al.*, 2018) were used. Luminescence data were converted off-line into [Ca^{2+}] values by using computer algorithms based on the Ca^{2+} response curves of wild-type aequorin or mutated aequorin (Ottolini *et al.*, 2014).

Aequorin-based Ca^{2+} measurement assays

The best reconstitution protocol (pre-treatment with 50 µM CPA + 2 h wild-type coelenterazine incubation) was applied to all the subsequent Ca^{2+} measurements carried out at the luminometer. Each of the independent experiments (with the exception of higher-EGTA (1 and 5 mM) pre-treated runs) started with a single fl2_AEQmut seedling incubated in a 100 µM EGTA solution, to which an equal volume of a two-fold (2 mM) $CaCl_2$ solution was added after 100 sec in order to restore resting $[Ca^{2+}]_{ER}$. ER refill trials with higher concentration of $CaCl_2$ followed the same procedure but with appropriate [$CaCl_2$] solutions. At 300 sec, an equal volume of a two-fold concentrated solution for each tested stimulus was injected in the luminometer chamber. Discharge solution (1 M $CaCl_2$, 30 % (v.v) ethanol) was applied at 1000 sec and Ca^{2+} dynamics were recorded up to complete discharge of the remaining aequorin pool.

REFERENCES

Bayer EM, Sparkes I, Vanneste S, Rosado A (2017) From shaping organelles to signalling platforms: the emerging functions of plant ER-PM contact sites. Curr Opin Plant Biol **40:** 89-96

Block MA, Jouhet J (2015) Lipid trafficking at endoplasmic reticulum-chloroplast membrane contact sites. Curr Opin Cell Biol **35:** 21-29

Bonza MC, De Michelis MI (2011) The plant Ca^{2+}-ATPase repertoire: biochemical features and physiological functions. Plant Biol (Stuttg) **13:** 421-430

Bonza MC, Loro G, Behera S, Wong A, Kudla J, Costa A (2013) Analyses of Ca^{2+} accumulation and dynamics in the endoplasmic reticulum of Arabidopsis root cells using a genetically encoded Cameleon sensor. Plant Physiol **163:** 1230-1241

Bradford MM (1976) A rapid and sensitive method for the quantitation of microgram quantities of protein utilizing the principle of protein-dye binding. Anal Biochem **72:** 248-254

Brini M (2008) Calcium-sensitive photoproteins. Methods **46:** 160-166

Brini M, Cali T, Ottolini D, Carafoli E (2013a) Intracellular calcium homeostasis and signaling. Met Ions Life Sci **12:** 119-168

Brini M, Ottolini D, Cali T, Carafoli E (2013b) Calcium in health and disease. Met Ions Life Sci **13:** 81-137

Brini M, Leanza L, Szabo I (2017) Lipid-mediated modulation of intracellular ion channels and redox state: physiopathological implications. Antioxid Redox Signal

Carafoli E, Krebs J (2016) Why calcium? How calcium became the best communicator. J Biol Chem **291:** 20849-20857

Chung WY, Jha A, Ahuja M, Muallem S (2017) Ca^{2+} influx at the ER/PM junctions. Cell Calcium **63:** 29-32

Clough SJ, Bent AF (1998) Floral dip: a simplified method for *Agrobacterium*-mediated transformation of *Arabidopsis thaliana*. Plant J **16:** 735-743

Coleman CE, Lopes MA, Gillikin JW, Boston RS, Larkins BA (1995) A defective signal peptide in the maize high-lysine mutant floury 2. Proc Natl Acad Sci U S A **92:** 6828-6831

Corso M, Doccula FG, de Melo JRF, Costa A, Verbruggen N (2018) Endoplasmic reticulum-localized CCX2 is required for osmotolerance by regulating ER and cytosolic Ca^{2+} dynamics in *Arabidopsis*. Proc Natl Acad Sci U S A **115:** 3966-3971

Costa A, Navazio L, Szabo I (2018) The contribution of organelles to plant intracellular calcium signalling. J Exp Bot **69:** 4175-4193

Demaurex N, Guido D (2017) The role of mitochondria in the activation/maintenance of SOCE: Membrane contact sites as signaling hubs sustaining store-operated Ca^{2+} entry. Adv Exp Med Biol **993:** 277-296

De Michelis MI, Camelli A, Rasi-Caldogno F (1993) The Ca^{2+} pump of the plasma membrane of *Arabidopsis thaliana*: characteristics and sensitivity to fluorescein derivatives. Botanica Acta **106:** 20-25

Dodd AN, Kudla J, Sanders D (2010) The language of calcium signaling. Annu Rev Plant Biol **61:** 593-620

Feijó JA, Wudick MM (2018) 'Calcium is life'. J Exp Bot **69:** 4147-4150

Gillikin JW, Zhang F, Coleman CE, Bass HW, Larkins BA, Boston RS (1997) A defective signal peptide tethers the floury-2 zein to the endoplasmic reticulum membrane. Plant Physiol **114:** 345-352

Iwano M, Entani T, Shiba H, Kakita M, Nagai T, Mizuno H, Miyawaki A, Shoji T, Kubo K, Isogai A, Takayama S (2009) Fine-tuning of the cytoplasmic Ca^{2+} concentration is essential for pollen tube growth. Plant Physiol **150:** 1322-1334

Joshi R, Paul M, Kumar A, Pandey D (2019) Role of calreticulin in biotic and abiotic stress signalling and tolerance mechanisms in plants. Gene **714:** 144004

Klusener B, Boheim G, Liss H, Engelberth J, Weiler EW (1995) Gadolinium-sensitive, voltage-dependent calcium release channels in the endoplasmic reticulum of a higher plant mechanoreceptor organ. EMBO J **14:** 2708-2714

Knight H, Trewavas AJ, Knight MR (1997) Calcium signalling in *Arabidopsis thaliana* responding to drought and salinity. Plant J **12:** 1067-1078

Kudla J, Becker D, Grill E, Hedrich R, Hippler M, Kummer U, Parniske M, Romeis T, Schumacher K (2018) Advances and current challenges in calcium signaling. New Phytol **218:** 414-431

Lee MW, Yang Y (2006) Transient expression assay by agroinfiltration of leaves. Methods Mol Biol **323:** 225-229

Liu L, Li J (2019) Communications between the endoplasmic reticulum and other organelles during abiotic stress response in plants. Front Plant Sci **10:** 749

Mariani P, Navazio L, Zuppini A (2003) Calreticulin and the endoplasmic reticulum in plant cell biology. *In* P Eggleton, M Michalak, eds, Calreticulin: Second Edition. Springer US, Boston, MA, pp 94-104

Mehrshahi P, Stefano G, Andaloro JM, Brandizzi F, Froehlich JE, DellaPenna D (2013) Transorganellar complementation redefines the biochemical continuity of endoplasmic reticulum and chloroplasts. Proc Natl Acad Sci U S A **110:** 12126-12131

Montero M, Brini M, Marsault R, Alvarez J, Sitia R, Pozzan T, Rizzuto R (1995) Monitoring dynamic changes in free Ca^{2+} concentration in the endoplasmic reticulum of intact cells. EMBO J **14:** 5467-5475

Moscatiello R, Sello S, Novero M, Negro A, Bonfante P, Navazio L (2014) The intracellular delivery of TAT-aequorin reveals calcium-mediated sensing of environmental and symbiotic signals by the arbuscular mycorrhizal fungus *Gigaspora margarita*. New Phytol **203:** 1012-1020

Navazio L, Bewell MA, Siddiqua A, Dickinson GD, Galione A, Sanders D (2000) Calcium release from the endoplasmic reticulum of higher plants elicited by the NADP metabolite nicotinic acid adenine dinucleotide phosphate. Proc Natl Acad Sci U S A **97:** 8693-8698

Navazio L, Mariani P, Sanders D (2001) Mobilization of Ca^{2+} by cyclic ADP-ribose from the endoplasmic reticulum of cauliflower florets. Plant Physiol **125:** 2129-2138

Ottolini D, Cali T, Brini M (2014) Methods to measure intracellular Ca^{2+} fluxes with organelle-targeted aequorin-based probes. Methods Enzymol **543:** 21-45

Perez Koldenkova V, Nagai T (2013) Genetically encoded Ca^{2+} indicators: properties and

evaluation. Biochim Biophys Acta **1833:** 1787-1797

Raffaello A, Mammucari C, Gherardi G, Rizzuto R (2016) Calcium at the center of cell signaling: interplay between endoplasmic reticulum, mitochondria, and lysosomes. Trends Biochem Sci **41:** 1035-1049

Rentel MC, Knight MR (2004) Oxidative stress-induced calcium signaling in *Arabidopsis*. Plant Physiol **135:** 1471-1479

Rizzuto R, Marchi S, Bonora M, Aguiari P, Bononi A, De Stefani D, Giorgi C, Leo S, Rimessi A, Siviero R, Zecchini E, Pinton P (2009) Ca^{2+} transfer from the ER to mitochondria: when, how and why. Biochim Biophys Acta **1787:** 1342-1351

Rizzuto R, De Stefani D, Raffaello A, Mammucari C (2012) Mitochondria as sensors and regulators of calcium signalling. Nat Rev Mol Cell Biol **13:** 566-578

Saheki Y, De Camilli P (2017) Endoplasmic reticulum-plasma membrane contact sites. Annu Rev Biochem **86:** 659-684

Sammels E, Parys JB, Missiaen L, De Smedt H, Bultynck G (2010) Intracellular Ca^{2+} storage in health and disease: a dynamic equilibrium. Cell Calcium **47:** 297-314

Schattat M, Barton K, Baudisch B, Klosgen RB, Mathur J (2011) Plastid stromule branching coincides with contiguous endoplasmic reticulum dynamics. Plant Physiol **155:** 1667-1677

Sello S, Moscatiello R, Mehlmer N, Leonardelli M, Carraretto L, Cortese E, Zanella FG, Baldan B, Szabo I, Vothknecht UC, Navazio L (2018) Chloroplast Ca^{2+} fluxes into and across thylakoids revealed by thylakoid-targeted aequorin probes. Plant Physiol **177:** 38-51

Son A, Park S, Shin DM, Muallem S (2016) Orai1 and STIM1 in ER/PM junctions: roles in pancreatic cell function and dysfunction. Am J Physiol Cell Physiol **310:** C414-422

Wang JZ, Li B, Xiao Y, Ni Y, Ke H, Yang P, de Souza A, Bjornson M, He X, Shen Z, Balcke GU, Briggs SP, Tissier A, Kliebenstein DJ, Dehesh K (2017) Initiation of ER body formation and indole glucosinolate metabolism by the plastidial retrograde signaling metabolite, MEcPP. Mol Plant **10:** 1400-1416

Yoo SD, Cho YH, Sheen J (2007) *Arabidopsis* mesophyll protoplasts: a versatile cell system for transient gene expression analysis. Nat Protoc **2:** 1565-1572

Zuppini A, Navazio L, Mariani P (2004) Endoplasmic reticulum stress-induced programmed cell death in soybean cells. J Cell Sci **117:** 2591-2598

CHAPTER 7

NAADP-gated Ca^{2+} release in response to a fungal hydrophobin

PROLOGUE

Among all the environmental threats that plants have to face due to their sessile nature, interactions of biotic nature are one of the most diversified and widespread classes. Plant interacting organisms can be represented by animal pests (such as insects or nematodes), pathogenic fungi and bacteria as well as parasitic protists or even algae and other plants (Rubiales and Heide-Jørgensen, 2011; Brooks *et al.*, 2015; Schwelm *et al.*, 2018). However, not all interactions – especially the microbial ones – are *de facto* harmful or unfavourable to the plant host. Indeed, plant associations with specific groups of bacteria and fungi are of primary importance for the mineral nutrition and the general fitness of the host plant and the integrated functioning of whole ecosystems (Lanfranco *et al.*, 2016; Zipfel and Oldroyd, 2017). This is the case, in particular, for the mutualistic interactions that plants establish with Gram-negative bacteria collectively called rhizobia, leading to nitrogen-fixing symbiosis or fungi of the Glomeromycotina subphylum, leading to arbuscular mycorrhiza. The occurrence of these beneficial synergies is in fact based on the mutualistic exchange of mineral nutrients and organic compounds between the two symbionts and it is mediated by a precise recognition of the partners thanks to a molecular dialogue taking place in the rhizosphere (Oldroyd, 2013; Bonfante *et al.*, 2015).

A similar situation also regards the advantageous interplay between plants and biocontrol agents, both of bacterial or fungal nature, that were extensively demonstrated to help the plant host in priming its defence responses, thus allowing the plant to be ready to withstand future infections (Prime-A-Plant *et al.*, 2006). Moreover, biocontrol agents have been shown to act as biostimulants and biofertilizers, hence promoting plant growth and development (Benítez *et al.*, 2004; Hermosa *et al.*, 2012; Woo *et al.*, 2014; López-Bucio *et al.*, 2015). Some biocontrol agents such as the filamentous fungi belonging to the *Thricoderma* genus, which were defined as opportunistic and avirulent plant symbionts (Harman *et al.*, 2004), have also been demonstrated to produce indirect beneficial effects for the plant partner by fighting fungal phytopathogens found in the soil (Punja and Utkhede, 2003;

Vinale *et al.*, 2008): thanks to their mycoparasitic activity, *Thricoderma* spp. digest and penetrate the cell wall of other plant-deleterious fungi in order to feed on them (Brotman *et al.*, 2010; Harman *et al.*, 2004); likewise, they compete with them for nutrients during their early saprophytic phase and inhibit their growth through the production of several antibiotic compounds (Harman *et al.*, 2004). However, the exact nature of the compounds contained in the fungal exudates has been determined only for a few of the many secreted metabolites (Vinale *et al.*, 2008); furthermore, the specific molecules perceived by the plant and responsible for the activation of the "priming" effect are largely unknown together with the precise signal transduction pathway triggered during the early stages of the plant host-microbe recognition. Cytosolic Ca^{2+} transients as well as the activation of plant defence responses leading to programmed cell death were found to be triggered in soybean cell suspension cultures when treated with *Thricoderma atroviride* culture filtrates (Navazio *et al.*, 2007), but the precise mechanisms underlying these events have not yet been elucidated.

On the other hand, information about the molecules involved in the plant-fungus physical interactions is rapidly emerging, with recent works elucidating the role of hydrophobins in plant root colonization by the biocontrol fungus (Whiteford and Spanu, 2002; Brotman *et al.*, 2010; Hermosa *et al.*, 2012; Ruocco *et al.*, 2015) as well as in inducing plant defences and raising antifungal activity against phytopathogens (Guzmán-Guzmán *et al.*, 2017; Przylucka *et al.*, 2017). Hydrophobins form a family of small amphypatic proteins ubiquitously and exclusively found in filamentous fungi, where they mediate the adhesion of fungal hyphae to the plant root surface (Whiteford and Spanu, 2002). Despite their low degree of amino acidic identity, hydrophobins are all characterized by 4 well-conserved disulphide bonds which are responsible for the autonomous assembly in amphypatic monolayers (REF Sunde *et al.*, 2008; Cox and Hooley, 2009). Thanks to their ability to convert hydrophobic surfaces into hydrophilic ones and *vice versa*, hydrophobins are a crucial element of the cell wall of fungal hyphae, as well as of the fungal exudates, with a role in mediating the fungus-environment interactions: by reducing the surface tension of the water-air interface they work as natural

surfactants, hence allowing the emergence of aerial hyphae, the production of fruit bodies, the sporulation process and the cell penetration (Whiteford and Spanu, 2002; Elliot and Talbot, 2004; Cox and Hooley, 2009). To this extent, hydrophobins were suggested to be required for the establishment of plant-fungus interactions of both symbiotic and pathogenic behaviour, in particular at the early stages of the root colonization (Whiteford and Spanu, 2002): *Thricoderma* hydrophobins were also thought to possibly protect the growing hyphae from defence compounds released by the plant, thus allowing this avirulent, opportunistic fungus to effectively penetrate the root and colonize the intercellular spaces (Hermosa *et al.*, 2012). A *Thricoderma* mutant lacking the hydrophobin-encoding gene *TasHyd1* was indeed found to be unable to colonize the plant root, while its mycoparasitic activities were totally unaffected (Viterbo and Chet, 2006).

The data presented in this chapter concern the analysis of Ca^{2+}-mediated responses triggered in the model legume *Lotus japonicus* in response to the major hydrophobin secreted by the biocontrol fungus *Thricoderma longibrachiatum*. I was involved in this research work as a side project of my Ph.D. activity.

Before the start of my Ph.D. activity, *Lotus japonicus* wild-type and *Ljsym4*-2 mutant plants were subjected to an *Agrobacterium tumefaciens*-mediated transformation-regeneration protocol (Lombari *et al.*, 2003; Barbulova *et al.*, 2005) in order to produce transgenic lines stably expressing the Ca^{2+} reporter aequorin in the cytosol. The *Ljsym4-2* mutant was chosen because it is unable to establish symbioses with either rhizobia and arbuscular mycorrhizal fungi (Bonfante *et al.*, 2000), due to the lack of the *CASTOR* gene encoding a cation channel essential for nuclear and perinuclear Ca^{2+} spiking required in legume root symbioses (Charpentier *et al.*, 2008 and 2016; Venkateshwaran *et al.*, 2012). The subsequent generation of cell suspension cultures from the transgenic lines allowed to carry out measurements assays of the cytosolic [Ca^{2+}] and its variations in response to HYTLO1, a hydrophobin abundantly secreted in the culture medium by the fungus *Thricoderma longibrachiatum* strain MK1 (Ruocco *et al.*, 2015). Transient Ca^{2+} elevations with similar kinetics

were observed upon challenge with HYTLO1 in both the transgenic lines, whereas the *Ljsym4-2* mutant displayed an altered Ca^{2+} response to the symbiotic signals Myc factors and Nod factors. A pharmacological approach employing Ca^{2+} chelators as well as inhibitors of Ca^{2+} channels or of enzymes involved in the generation of Ca^{2+} mobilizing agents allowed to investigate the origin of the observed Ca^{2+} fluxes: in particular EGTA (a chelating agent for extracellular Ca^{2+}) and Ned-19 (a competitive antagonist of nicotinic acid adenine dinucleotide phosphate (NAADP) (Naylor *et al.*, 2009)) both reduced to 50% the amplitude of the recorded $[Ca^{2+}]_{cyt}$ elevation, indicating the mobilization of Ca^{2+} from both the extracellular space and an internal store sensitive to NAADP, most likely the ER. Indeed, although the molecular identity of NAADP receptors in plants still remains elusive, early biochemical evidence of Ca^{2+} release from ER vesicle preparations had previously indicated a potential ER localization for NAADP-gated Ca^{2+}-permeable channels (Navazio *et al.*, 2000).

The effect of HYTLO1 perception on the expression of defence-related genes (such as *MPK3*, *WRKY33*, *CP450* and *PR1*) were also evaluated by quantitative RT-PCR: all these genes, except *PR1*, were shown to be upregulated after different time intervals (2 h, 4 h or 24 h) of incubation with HYTLO1 in both the wild-type and *Ljsym4-2* mutant lines. The viability of *L. japonicus* cell cultures treated up to 24 h with HYTLO1 was found to be unaffected with respect to the control, suggesting that the hydrophobin does not induce the hypersensitive response leading to programmed cell death (Pontier *et al.*, 1998a and 1998b; Heath 2000)). Taken together, the above data suggest that the fungal hydrophobin can be considered as a mild elicitor of plant defence responses. The upregulation of the plant defence-related genes was found to be Ca^{2+}-dependent, because the combined application of EGTA and Ned-19 was responsible for a drastic reduction (more than 85%) of their expression levels. Immunofluorescence and immunogold labelling experiments carried out with affinity-purified polyclonal antibodies raised against HYTLO1 showed that the hydrophobin forms a protein film covering the plant cell wall, with a certain degree of permeation into the apoplastic space. This suggest the possibility that HYTLO1 may interact with specific

binding sites at the plasma membrane. The *in vivo* secretion of a battery of cell wall-degrading enzymes by *Thricoderma* may facilitate the access of the hydrophobin to potential plasma membrane-located receptors (Markovich and Kononova, 2003). In agreement with cell viability data, transmission electron microscopy analyses demonstrated that the ultrastructural organization of *L. japonicus* cells was well preserved after 24 h treatment with HYTLO1.

In conclusion, the use of aequorin-expressing cell suspension cultures of *L. japonicus* allowed for the monitoring of the cytosolic Ca^{2+} transients evoked in the early phases of the recognition of a biocontrol fungus. On the basis of the observed upregulation of plant defence genes, but no activation of cell death, HYTLO1 may be considered as a mild elicitor pre-alerting the plant prior to a potential subsequent attack by real pathogens, a phenomenon called “priming” (Prime-A-Plant *et al.*, 2006). The dependence of the defence priming on $[Ca^{2+}]_{cyt}$ elevations was demonstrated by using the extracellular Ca^{2+} chelator EGTA and Ned-19, a potent inhibitor of the NAADP receptor in animal cells. This pharmacological approach showed the involvement of both the extracellular milieu and a NAADP-sensitive internal storage compartment in the observed Ca^{2+} fluxes. This study adds new valuable insights into the Ca^{2+}-mediated signal transduction evoked in the plant cell in response to a key metabolite secreted by a biocontrol fungus and provides the first evidence for the involvement of NAADP-gated Ca^{2+} release in a signalling pathway triggered by a biotic stimulus. On the basis of the previously suggested presence of a Ca^{2+} release pathway activated by NAADP at higher plants ER (Navazio *et al.*, 2000), this work suggests the occurrence of ER-mediated Ca^{2+} release into the cytosol during a beneficial plant-microbe interaction.

REFERENCES

Barbulova A, D'Apuzzo E, Rogato A, Chiurazzi M (2005) Improved procedures for in vitro regeneration and for phenotypic analysis in the model legume *Lotus japonicus*. Funct Plant Biol **32:** 529-536

Benítez T, Rincon AM, Limon MC, Codon AC (2004) Biocontrol mechanisms of *Trichoderma* strains. Int Microbiol **7:** 249-260

Bonfante P, Genre A, Faccio A, Martini I, Schauser L, Stougaard J, Webb J, Parniske M (2000) The *Lotus japonicus LjSym4* gene is required for the successful symbiotic infection of root epidermal cells. Mol Plant Microbe Interact **13:** 1109-1120

Bonfante P, Genre A (2015) Arbuscular mycorrhizal dialogues: do you speak 'plantish' or 'fungish'? Trends Plant Sci **20:** 150-154

Brooks F, Rindi F, Suto Y, Ohtani S, Green M (2015) The Trentepohliales (Ulvophyceae, Chlorophyta): An Unusual Algal Order and its Novel Plant Pathogen-*Cephaleuros*. Plant Dis **99:** 740-753

Brotman Y, Kapuganti JG, Viterbo A (2010) Trichoderma. Curr Biol **20:** R390-391

Charpentier M, Bredemeier R, Wanner G, Takeda N, Schleiff E, Parniske M (2008) *Lotus japonicus* CASTOR and POLLUX are ion channels essential for perinuclear calcium spiking in legume root endosymbiosis. Plant Cell **20:** 3467-3479

Charpentier M, Sun J, Vaz Martins T, Radhakrishnan GV, Findlay K, Soumpourou E, Thouin J, Very AA, Sanders D, Morris RJ, Oldroyd GE (2016) Nuclear-localized cyclic nucleotide-gated channels mediate symbiotic calcium oscillations. Science **352:** 1102-1105

Cox PW, Hooley P (2009) Hydrophobins: New prospects for biotechnology. Fungal Biol Rev **23:** 40-47

Elliot MA, Talbot NJ (2004) Building filaments in the air: aerial morphogenesis in bacteria and fungi. Curr Opin Microbiol **7:** 594-601

Guzmán-Guzmán P, Aleman-Duarte MI, Delaye L, Herrera-Estrella A, Olmedo-Monfil V (2017) Identification of effector-like proteins in *Trichoderma* spp. and role of a hydrophobin in the plant-fungus interaction and mycoparasitism. BMC Genet **18:** 16

Harman GE, Howell CR, Viterbo A, Chet I, Lorito M (2004) *Trichoderma* species–opportunistic, avirulent plant symbionts. Nat Rev Microbiol **2:** 43-56

Heath MC (2000) Hypersensitive response-related death. Plant Mol Biol **44:** 321-334

Hermosa R, Viterbo A, Chet I, Monte E (2012) Plant-beneficial effects of *Trichoderma* and of its genes. Microbiology **158:** 17-25

Lanfranco L, Bonfante P, Genre A (2016) The Mutualistic Interaction between Plants and Arbuscular Mycorrhizal Fungi. Microbiol Spectr **4**

Lombari P, Ercolano E, El Alaoui H, Chiurazzi M (2003) A new transformation-regeneration procedure in the model legume *Lotus japonicus*: root explants as a source of large numbers of cells susceptible to *Agrobacterium*-mediated transformation. Plant Cell Rep **21:** 771-777

López-Bucio J, Pelagio-Flores R, Herrera-Estrella A (2015) *Trichoderma* as biostimulant: Exploiting the multilevel properties of a plant beneficial fungus. Sci Hortic **196:** 109-123

Markovich NA, Kononova GL (2003) Lytic enzymes of *Trichoderma* and their role in

protecting plants from fungal diseases. Prikl Biokhim Mikrobiol **39:** 389-400

Navazio L, Bewell MA, Siddiqua A, Dickinson GD, Galione A, Sanders D (2000) Calcium release from the endoplasmic reticulum of higher plants elicited by the NADP metabolite nicotinic acid adenine dinucleotide phosphate. Proc Natl Acad Sci U S A **97:** 8693-8698

Navazio L, Baldan B, Moscatiello R, Zuppini A, Woo SL, Mariani P, Lorito M (2007) Calcium-mediated perception and defense responses activated in plant cells by metabolite mixtures secreted by the biocontrol fungus *Trichoderma atroviride*. BMC Plant Biol **7:** 41

Naylor E, Arredouani A, Vasudevan SR, Lewis AM, Parkesh R, Mizote A, Rosen D, Thomas JM, Izumi M, Ganesan A, Galione A, Churchill GC (2009) Identification of a chemical probe for NAADP by virtual screening. Nat Chem Biol **5:** 220-226

Oldroyd GE (2013) Speak, friend, and enter: signalling systems that promote beneficial symbiotic associations in plants. Nat Rev Microbiol **11:** 252-263

Pontier D, Balague C, Roby D (1998a) The hypersensitive response. A programmed cell death associated with plant resistance. C R Acad Sci III **321:** 721-734

Pontier D, Tronchet M, Rogowsky P, Lam E, Roby D (1998b) Activation of hsr203, a plant gene expressed during incompatible plant-pathogen interactions, is correlated with programmed cell death. Mol Plant Microbe Interact **11:** 544-554

Prime APG, Conrath U, Beckers GJ, Flors V, Garcia-Agustin P, Jakab G, Mauch F, Newman MA, Pieterse CM, Poinssot B, Pozo MJ, Pugin A, Schaffrath U, Ton J, Wendehenne D, Zimmerli L, Mauch-Mani B (2006) Priming: getting ready for battle. Mol Plant Microbe Interact **19:** 1062-1071

Przylucka A, Akcapinar GB, Chenthamara K, Cai F, Grujic M, Karpenko J, Livoi M, Shen Q, Kubicek CP, Druzhinina IS (2017) HFB7 - A novel orphan hydrophobin of the *Harzianum* and *Virens* clades of *Trichoderma*, is involved in response to biotic and abiotic stresses. Fungal Genet Biol **102:** 63-76

Punja ZK, Utkhede RS (2003) Using fungi and yeasts to manage vegetable crop diseases. Trends Biotechnol **21:** 400-407

Rubiales D, Heide-Jørgensen HS (2011) Parasitic Plants. In eLS (Ed.) doi:10.1002/9780470015902.a0021271

Ruocco M, Lanzuise S, Lombardi N, Woo SL, Vinale F, Marra R, Varlese R, Manganiello G, Pascale A, Scala V, Turra D, Scala F, Lorito M (2015) Multiple roles and effects of a novel *Trichoderma* hydrophobin. Mol Plant Microbe Interact **28:** 167-179

Schwelm A, Badstober J, Bulman S, Desoignies N, Etemadi M, Falloon RE, Gachon CMM, Legreve A, Lukes J, Merz U, Nenarokova A, Strittmatter M, Sullivan BK, Neuhauser S (2018) Not in your usual Top 10: protists that infect plants and algae. Mol Plant Pathol **19:** 1029-1044

Sunde M, Kwan AH, Templeton MD, Beever RE, Mackay JP (2008) Structural analysis of hydrophobins. Micron **39:** 773-784

Venkateshwaran M, Cosme A, Han L, Banba M, Satyshur KA, Schleiff E, Parniske M, Imaizumi-Anraku H, Ane JM (2012) The recent evolution of a symbiotic ion channel in the legume family altered ion conductance and improved functionality in calcium signaling. Plant Cell **24:** 2528-2545

Vinale F, Sivasithamparam K, Ghisalberti EL, Marra R, Woo SL, Lorito M (2008) *Trichoderma*–plant–pathogen interactions. Soil Biol Biochem **40:** 1-10

Viterbo A, Chet I (2006) *TasHyd1*, a new hydrophobin gene from the biocontrol agent *Trichoderma asperellum*, is involved in plant root colonization. Mol Plant Pathol **7:** 249-258

Whiteford JR, Spanu PD (2002) Hydrophobins and the interactions between fungi and plants. Mol Plant Pathol **3:** 391-400

Woo SL, Ruocco M, Vinale F, Nigro M, Marra R, Lombardi N, Pascale A, Lanzuise S, Manganiello G, Lorito M (2014) *Trichoderma*-based products and their widespread use in agriculture. Open Mycol J **8:** 71-126

Zipfel C, Oldroyd GE (2017) Plant signalling in symbiosis and immunity. Nature **543:** 328-336

This work was published as:

The Hydrophobin HYTLO1 Secreted by the Biocontrol Fungus *Trichoderma longibrachiatum* Triggers a NAADP-Mediated Calcium Signalling Pathway in *Lotus japonicus*

Roberto Moscatiello[1], Simone Sello[1], Michelina Ruocco[2], Ani Barbulova[3], Enrico Cortese[1], Sebastiano Nigris[4], Barbara Baldan[1,4], Maurizio Chiurazzi[3], Paola Mariani[1], Matteo Lorito[5] and Lorella Navazio[1,4]

[1]Department of Biology, University of Padova, Via U. Bassi 58/B, 35131 Padova, Italy

[2]Institute for Sustainable Plant Protection, CNR, Via Università 133, 80055 Portici (NA), Italy

[3]Institute of BioSciences and BioResourses, CNR, Via P. Castellino 111, 80131 Napoli, Italy

[4]Botanical Garden, University of Padova, Via Orto Botanico 15, 35123 Padova, Italy

[5] Department of Agricultural Sciences, University of Napoli "Federico II", Via Università 100, 80055 Portici (NA), Italy

in International Journal of Molecular Sciences, September 2018, vol. 19, issue 9, 2596.

International Journal of
Molecular Sciences

MDPI

Article

The Hydrophobin HYTLO1 Secreted by the Biocontrol Fungus *Trichoderma longibrachiatum* Triggers a NAADP-Mediated Calcium Signalling Pathway in *Lotus japonicus*

Roberto Moscatiello [1], Simone Sello [1], Michelina Ruocco [2], Ani Barbulova [3], Enrico Cortese [1], Sebastiano Nigris [4], Barbara Baldan [1,4], Maurizio Chiurazzi [3], Paola Mariani [1], Matteo Lorito [5] and Lorella Navazio [1,4,*]

1 Department of Biology, University of Padova, Via U. Bassi 58/B, 35131 Padova, Italy; roberto.moscatiello@unipd.it (R.M); sello.simone@gmail.com (S.S.); enrico.cortese.1@phd.unipd.it (E.C.); barbara.baldan@unipd.it (B.B.); mariani@bio.unipd.it (P.M.)
2 Institute for Sustainable Plant Protection, CNR, Via Università 133, 80055 Portici (NA), Italy; michelina.ruocco@ipsp.cnr.it
3 Institute of BioSciences and BioResourses, CNR, Via P. Castellino 111, 80131 Napoli, Italy; ani@arterrabio.it (A.B.); maurizio.chiurazzi@ibbr.cnr.it (M.C.)
4 Botanical Garden, University of Padova, Via Orto Botanico 15, 35123 Padova, Italy; sebastiano.nigris@unipd.it
5 Department of Agricultural Sciences, University of Napoli "Federico II", Via Università 100, 80055 Portici (NA), Italy; lorito@unina.it
* Correspondence: lorella.navazio@unipd.it; Tel.: +39-049-827-6295

Received: 30 July 2018; Accepted: 29 August 2018; Published: 1 September 2018

Abstract: *Trichoderma* filamentous fungi are increasingly used as biocontrol agents and plant biostimulants. Growing evidence indicates that part of the beneficial effects is mediated by the activity of fungal metabolites on the plant host. We have investigated the mechanism of plant perception of HYTLO1, a hydrophobin abundantly secreted by *Trichoderma longibrachiatum*, which may play an important role in the early stages of the plant-fungus interaction. Aequorin-expressing *Lotus japonicus* suspension cell cultures responded to HYTLO1 with a rapid cytosolic Ca^{2+} increase that dissipated within 30 min, followed by the activation of the defence-related genes *MPK3*, *WRK33*, and *CP450*. The Ca^{2+}-dependence of these gene expression was demonstrated by using the extracellular Ca^{2+} chelator EGTA and Ned-19, a potent inhibitor of the nicotinic acid adenine dinucleotide phosphate (NAADP) receptor in animal cells, which effectively blocked the HYTLO1-induced Ca^{2+} elevation. Immunocytochemical analyses showed the localization of the fungal hydrophobin at the plant cell surface, where it forms a protein film covering the plant cell wall. Our data demonstrate the Ca^{2+}-mediated perception by plant cells of a key metabolite secreted by a biocontrol fungus, and provide the first evidence of the involvement of NAADP-gated Ca^{2+} release in a signalling pathway triggered by a biotic stimulus.

Keywords: aequorin; biocontrol fungi; calcium signalling; *Lotus japonicus*; hydrophobins; HYTLO1; NAADP; *Trichoderma*

1. Introduction

Trichoderma is a widely spread genus of free-living filamentous fungi belonging to Ascomycota, increasingly used in agricultural applications as biocontrol agents and biofertilizers [1–5]. The effects exerted by *Trichoderma* at the plant level are both indirect, due to the mycoparasitic activity on

a plethora of phytopathogens, and direct, due to the induction of plant defence responses and promotion of growth and development [6]. For its peculiar lifestyle traits, plant root colonization and favourable impact on plant physiology, *Trichoderma* has been defined as an opportunistic, avirulent plant symbiont [7]. Although the beneficial effects produced by *Trichoderma* on the plant have been extensively demonstrated, little is known about the molecular mechanisms underlying signal transduction during the early stages of the interactions of plants with these biocontrol fungi. The induction of pathogen resistance is accomplished through the secretion of a complex arsenal of fungal molecules encompassing cell wall-degrading enzymes, secondary metabolites with antibiotic activity, and other substances [8]. Culture filtrates of *Trichoderma atroviride*, grown alone or in co-culture with the phytopathogen *Botrytis cinerea*, have been shown to induce in soybean cell cultures transient elevation in cytosolic free Ca^{2+} concentrations and defence responses, such as reactive oxygen accumulation and programmed cell death [9]. Nevertheless, the molecular mechanisms causing the observed effects on the plant host has been determined only for a few of the many secreted metabolites found in *Trichoderma* [10].

Calcium is a universal signalling element involved in a plethora of transduction pathways in all eukaryotes [11–13], as well as in prokaryotes [14]. In plants, Ca^{2+} has been demonstrated to mediate a wide array of signalling cascades in response to both abiotic and biotic stimuli [15–17]. Changes in intracellular free Ca^{2+} levels are a common early event during many plant-microbe interactions, of both symbiotic and pathogenic nature [18]. In particular, the role of Ca^{2+} signalling in the establishment of plant defence responses has been known for many years [19].

In this work we have investigated the mechanism of plant perception and transduction of HYTLO1, a hydrophobin abundantly secreted in the culture medium by *Trichoderma longibrachiatum* strain MK1 [20]. Hydrophobins are a family of small amphypathic proteins found exclusively in filamentous fungi, which are known to mediate the interactions between the fungus and its environment. In addition to having a general role during formation of aereal hyphae, sporulation, and production of fruit bodies, hydrophobins are thought to be involved in plant-fungus interactions, both pathogenic and symbiotic, by mediating the adhesion of fungal hyphae to the root surface [21]. Information about the role of hydrophobins in biocontrol fungi in plant root colonization, induction of plant defences, antifungal activity against phytopathogens, as well as responses to abiotic stresses is rapidly emerging [20,22,23]. A *Trichoderma* mutant, defective for the *TasHyd1* gene encoding a hydrophobin, although unaffected in its mycoparasitic activity, was found to be unable to colonize the plant root apparatus [24].

By using the model legume *Lotus japonicus* [25,26] stably expressing the genetically encoded Ca^{2+} indicator aequorin, we demonstrated that HYTLO1 triggers in plant cells a signal transduction pathway leading to the activation of defence genes in a Ca^{2+}-dependent manner. Experiments performed by using the chemical probe Ned-19 [27] showed that the Ca^{2+} signalling pathway activated by HYTLO1 is mediated by nicotinic acid adenine dinucleotide phosphate (NAADP), a metabolite of nicotinamide adenine dinucleotide phosphate (NADP) which has been demonstrated to act as a potent Ca^{2+} mobilizing messenger in a wide variety of eukaryotes (see [28] for a review), including plants [29], as well as green and brown macroalgae [30,31]. The obtained data provide the first evidence for the involvement of this pyridine nucleotide-based Ca^{2+} agonist in a physiological event in higher plants and offer new insights into the mechanism of action of fungal hydrophobins.

2. Results

2.1. Generation of Transgenic L. japonicus Plants Stably Expressing the Bioluminescent Ca^{2+} Reporter Aequorin

To investigate the potential participation of calcium in the plant perception of HYTLO1, we transformed *Lotus japonicus* with a cDNA construct encoding the bioluminescent Ca^{2+} reporter aequorin. *L. japonicus* is a well-characterized model legume, widely used as an experimental system to

analyse different types of plant-microbe interactions along the symbiosis-pathogenesis spectrum [32]. The aequorin coding sequence was cloned between the Cauliflower Mosaic Virus 35S promoter (CaMV 35S) and the *Agrobacterium tumefaciens* nopaline synthase terminator (tNOS) sequences in the pCAMBIA vector [33] to obtain the T-DNA construct pAB1 (Figure S1A). PAB1 was then used for *Agrobacterium tumefaciens*-mediated transformation-regeneration procedure of *L. japonicus* [34,35] wild-type and *Ljsym4-2* mutant, where the latter is impaired in the symbioses with both arbuscular mycorrhizal (AM) fungi and rhizobia [36]. Transgenic plants were selected on hygromycin-containing medium and allowed to self-pollinate. Several independent lines of the first generation of transformants (T1), showing a hygromycin resistance segregation of 3:1 were tested by semi-quantitative RT-PCR to confirm aequorin expression and analyse the amount of transcript in the different transgenic lines. Homozygous plants of the second generation (T2), exhibiting the highest aequorin expression (Figure S1B), were selected to set up in vitro cell cultures. Suspension-cultured cells are particularly useful to understand some complex plant physiological processes, such as Ca^{2+}-mediated signal transduction events [37,38].

2.2. The Hydrophobin HYTLO1 Triggers a Transient Cytosolic Ca^{2+} Elevation in Aequorin-Expressing Lotus japonicus Cells

HYTLO1, the major hydrophobin secreted by the strain MK1 of *Trichoderma longibrachiatum*, has been previously isolated from the culture medium of the biocontrol fungus, purified to homogeneity, and cloned [20]. To check if the perception and signal transduction of this protein involves calcium as intracellular messenger, aequorin-expressing *L. japonicus* cell suspension cultures derived from the transgenic plants were challenged with HYTLO1. The hydrophobin (0.6 μM) was found to trigger a transient cytosolic Ca^{2+} increase that peaked (0.48 ± 0.09 μM; n = 10) about 6 min after the injection and slowly dissipated within 30 min. The kinetics of the cytosolic Ca^{2+} change ($[Ca^{2+}]_{cyt}$) was very similar in *L. japonicus* wild-type cells and *Ljsym4-2* mutant cells, stably expressing cytosolic aequorin (Figure 1A). The *Ljsym4-2* mutant is defective in the *CASTOR* gene that encodes a cation channel essential for nuclear and perinuclear Ca^{2+} spiking in legume root endosymbiosis [39–41].

As a comparison, the cytosolic Ca^{2+} transients evoked by the symbiotic signalling molecules Myc factors and Nod factors, produced by the arbuscular mycorrhizal fungus *Gigaspora margarita* and the specific rhizobial symbiont *Mesorhizobium loti* are respectively shown in Figure 1B,C. In these latter two cases the Ca^{2+} traces exhibited by the *Ljsym4-2* mutant differ from the wild-type for the lack of the second, flattened dome-shaped $[Ca^{2+}]_{cyt}$ elevation (after about 15 min), which is consistent with the sum of the perinuclear Ca^{2+} oscillations that were visualized in Ca^{2+} imaging experiments in *L. japonicus* wild-type, but not *CASTOR* mutant [39].

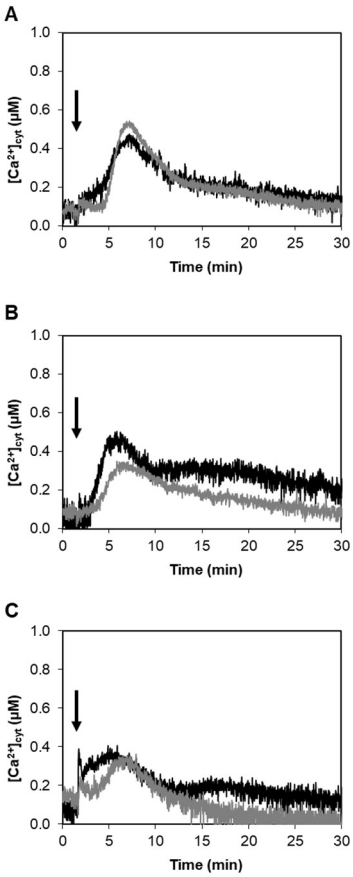

Figure 1. Monitoring of cytosolic Ca^{2+} concentration ($[Ca^{2+}]_{cyt}$) in aequorin-expressing *L. japonicus* in response to different biotic stimuli. Suspension-cultured cells of *L. japonicus* wild-type (black trace) and *Ljsym4-2* mutant (grey trace), stably transformed with a cDNA construct encoding cytosolic aequorin, were treated with: (**A**) the hydrophobin HYTLO1 (0.6 μM) purified from the biocontrol fungus *T. longibrachiatum*; (**B**) *Myc factors* from the AM fungus *G. margarita*; (**C**) *Nod factors* from the nitrogen-fixing symbiotic bacterium *M. loti*. Arrows indicate the time (100 s) of stimulation. These and the following traces are representative of at least 6 independent experiments that gave similar results.

2.3. HYTLO1 Activates the Expression of Defence Genes in L. japonicus *Cells, but Does Not Induce Cell Death*

We next evaluated the effect of the treatment of *L. japonicus* cells with HYTLO1 on the expression of some genes commonly involved in plant defence against phytopathogens, namely *MPK3*, encoding the mitogen-activated protein kinase 3, *WRKY33*, encoding the transcription factor WRK33, *CP450*, encoding the cytochrome P450, and *PR1*, encoding the pathogenesis-related protein 1. Exponentially growing *L. japonicus* cells of the wild-type line and *Ljsym4-2* mutant line were treated with 0.6 μM HYTLO1 for 2 h, 6 h, and 24 h. Semi-quantitative RT-PCR analyses conducted with the wild-type cells showed a variable range of responses to the HYTLO1 application. *MPK3* and *WRKY33* were significantly up-regulated (1.88 ± 0.09 and 1.61 ± 0.02, respectively) after 2 h of treatment, with a subsequent decay to basal expression levels in the following 24 h (Figure 2A,B). The *CP450* gene, although remaining at constitutive level after 2 h of treatment with HYTLO1, gradually increased its expression after 6 h (1.67 ± 0.43) up to more than a three-fold induction level compared to the control (3.61 ± 0.78) after 24 h (Figure 2C). On the other hand, the expression of *PR1* was not significantly modified by the treatment with 0.6 μM HYTLO1 for any of the considered time intervals (Figure 2D). Concerning the *Ljsym4-2* mutant line, the gene expression analysis showed a trend similar to that observed in the wild-type line, but with lower values (Figure 2A–D).

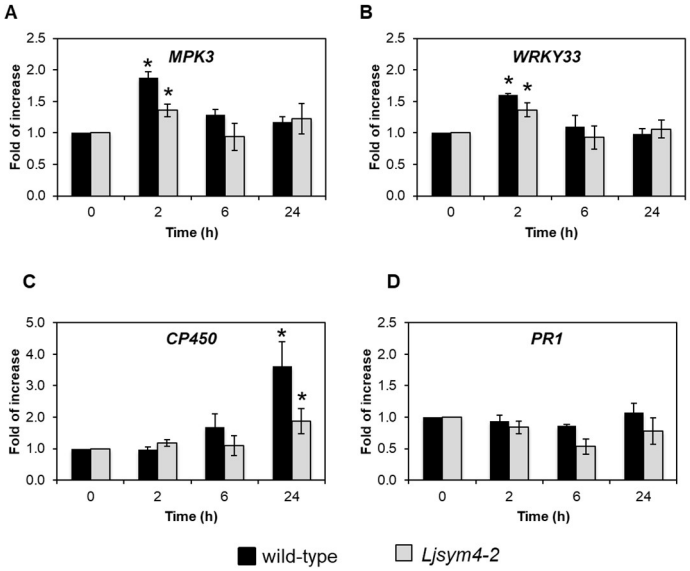

Figure 2. Analysis of HYTLO1-induced gene expression in *L. japonicus* cells. Semi-quantitative RT-PCR analysis of *L. japonicus MPK3* (**A**), *WRK33* (**B**), *CP450* (**C**), and *PR1* (**D**) in aequorin-expressing *L. japonicus* cell cultures of the wild-type line (black bars) and *Ljsym4-2* mutant line (grey bars) in control conditions and after treatment with HYTLO1 (0.6 μM) for different time intervals. Data are the means ± SE of three independent experiments. * indicates statistically significant difference at $P < 0.05$.

The results concerning the statistically significant differences between HYTLO1-treated samples and controls were validated by quantitative RT-PCR (Figure S2). Taken together, these data indicate that HYTLO1 can be considered as a mild elicitor of plant defence responses.

To evaluate the potential cytotoxicity of the fungal hydrophobin, we tested the viability of *L. japonicus* cells by using the Evans blue method [42]. This colorimetric assay revealed that the percentage of dead cells after treatment with HYTLO1 at 0.6 μM for up to 24 h did not significantly differ from that of control cells (Figure 3).

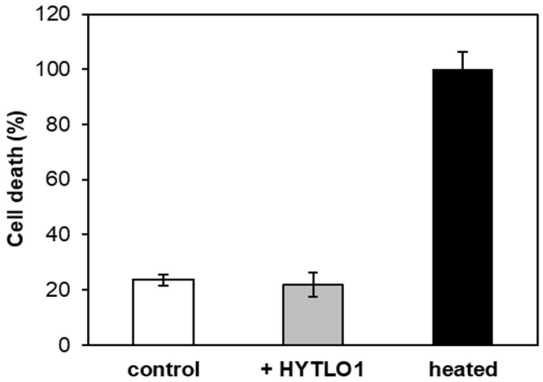

Figure 3. Effect of HYTLO1 on *L. japonicus* cell viability. Cell suspension cultures were treated with 0.6 μM HYTLO1 (grey bar) for 24 h. Cells incubated with the same percentage of ethanol (white bar) were used as control. 100% cell death corresponds to cells incubated for 20 min at 100 °C (black bar). Cell viability was determined by the Evans blue method. Data are the means ± SE of three independent experiments.

2.4. Origin of the HYTLO1-Elicited Cytosolic Ca^{2+} Fluxes in L. japonicus

To assess whether the transient elevation in $[Ca^{2+}]_{cyt}$ induced by HYTLO1 in *L. japonicus* plays a key role in the signalling pathway leading to the activation of defence genes, the effect of the

abolition of the Ca^{2+} change on downstream responses was analysed. Experiments based on the use of Ca^{2+} chelators, inhibitors of Ca^{2+} channels and of enzymes involved in the generation of Ca^{2+} mobilizing agents were carried out in the attempt to effectively block the HYTLO1-induced $[Ca^{2+}]_{cyt}$ transient. When cells, 10 minutes before HYTLO1 administration, were transferred to a culture medium depleted of $CaCl_2$ and containing 600 µM EGTA, about 56% reduction of the $[Ca^{2+}]_{cyt}$ peak was observed (Figure 4). Pre-treatment with 100 µM Ned-19, a competitive antagonist of the intracellular Ca^{2+}-mobilizing agent NAADP [27], caused inhibition of ~47% of the Ca^{2+} transient (Figure 4). These data indicate that in *L. japonicus* cells HYTLO1 mobilizes Ca^{2+} from both the extracellular space and from an intracellular compartment sensitive to NAADP. Moreover, the two stores (external and internal) seem to be involved almost at the same extent as sources of the ion for the transduction of this signal. As expected, the $[Ca^{2+}]_{cyt}$ elevation evoked by HYTLO1 was very efficiently blocked (83.2 ± 3.5%) by pre-treating *L. japonicus* cells with EGTA (600 µM) in combination with Ned-19 (100 µM) in Ca^{2+}-free medium (Figure 4). $LaCl_3$ (3 mM), a widely used inhibitor of Ca^{2+}-permeable channels located at the plasma membrane [43], caused a reduction of only ~33% of the HYTLO1-Ca^{2+} transient (Figure 4), suggesting that additional Ca^{2+} channels are involved in the Ca^{2+} influx activated by HYTLO1 from the extracellular medium. Nicotinamide (100 µM), an inhibitor of ADP-ribosyl cyclase, involved in the production of both cyclic ADP-ribose (cADPR) and NAADP [44,45], reduced by ~40% the $[Ca^{2+}]_{cyt}$ in response to HYTLO1 (Figure 4), confirming the participation of NAADP-gated Ca^{2+} channels in the generation of HYTLO1-induced Ca^{2+} fluxes.

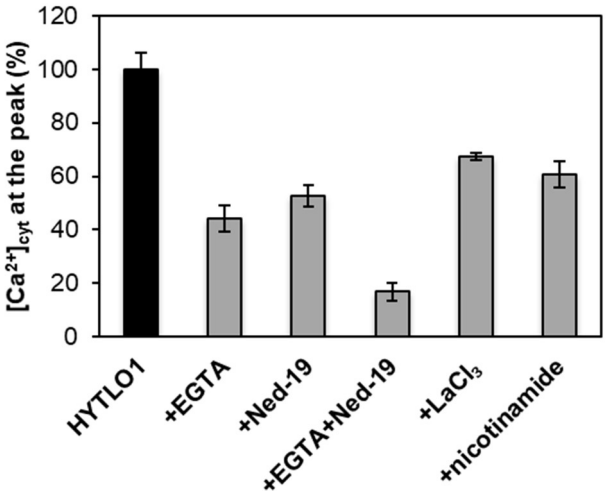

Figure 4. Pharmacological approach for the analysis of cytosolic Ca^{2+} fluxes induced by HYTLO1 in *L. japonicus* cells. Cell samples were incubated with: EGTA (600 µM), Ned-19 (100 µM) (singly or in combination with EGTA), $LaCl_3$ (3 mM), nicotinamide (100 µM). After 10 min (EGTA, $LaCl_3$, nicotinamide) or 30 min (Ned-19), cells were challenged with HYTLO1 (0.6 µM). For assays performed with EGTA, cells were previously washed extensively and resuspended in Ca^{2+}-free medium. Data are the means ± SE of five independent experiments.

2.5. HYTLO1-Induced Activation of Defence Gene Expression is Ca^{2+}-Dependent

In view of the efficient inhibition of the HYTLO1-induced Ca^{2+} transient obtained by the pre-treatment of *L. japonicus* cells with 600 µM EGTA and 100 µM Ned-19 in Ca^{2+}-free medium (Figure 5A), the same experimental condition was used to examine the effect of the abolition of the HYTLO1-induced Ca^{2+} signalling pathway at the level of gene expression. The change of expression of the defence genes *MPK3* and *WRKY33*, observed after 2 h treatment of wild-type cells with 0.6 µM HYTLO1 (Figure 2A,B), was reduced by more than 85% in the presence of EGTA + Ned-19 (Figure 5B). This result demonstrates that the activation of *MPK3* and *WRKY33* gene expression in response to HYTLO1 is Ca^{2+}-dependent.

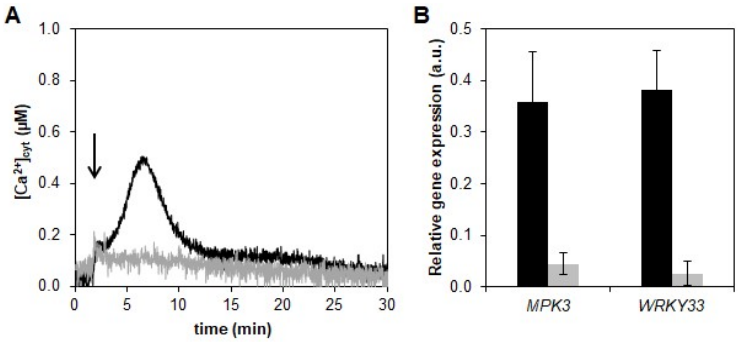

Figure 5. Effect of pretreatment with EGTA and Ned-19 on HYTLO1-induced $[Ca^{2+}]_{cyt}$ transient and gene expression in *L. japonicus* cells. (**A**) Monitoring of $[Ca^{2+}]_{cyt}$ in *L. japonicus* after treatment (arrow) with 0.6 μM HYTLO1 in regular cell culture medium (black trace) or after pretreatment with 600 μM EGTA and 100 μM Ned-19 in Ca^{2+}-free medium (grey trace). (**B**) RT-PCR analysis of the expression of *MPK3* and *WRKY33* after treatment with HYTLO1 (0.6 μM) for 2 h in regular medium (black bar) or in Ca^{2+} free medium supplemented with 600 μM EGTA and 100 μM Ned-19 (grey bar).

Even the expression of the *CP450* gene after 24 h HYTLO1 treatment was found to be significantly inhibited (~95%) by pre-treatment with EGTA + Ned-19 (Figure S3A). However, this result must be interpreted with caution; in fact, despite treatment with HYTLO1 not causing, by itself, any significant change in cell viability compared with the control (Figure 3), the pre-treatment with EGTA + Ned-19 caused, after 24 h, a significant rise of the cell death (Figure S3B). These data indicate the uselessness of a gene expression analysis after such a prolonged incubation time of the suspension-cultured cells with the above Ca^{2+} chelator and Ca^{2+} channel inhibitor.

2.6. HYTLO1 Perception Occurs at the Plant Cell Surface

Negative staining with 1% uranile acetate of a preparation of HYTLO1, dissolved in 50% ethanol, showed that this protein, similarly to other type II hydrophobins [20], forms in aqueous solution spherical air mycelles by autoassembling in amphypatic monolayer (Figure S4). Immunofluorescence analysis of HYTLO1-treated *L. japonicus* cells carried out with affinity-purified polyclonal antibodies raised against the purified protein indicated that HYTLO1 interacts with the plant cell surface, with no evidence for protein internalization inside the cell within 24 h (Figure S5).

Immunogold labelling observations showed that HYTLO1 covers the plant cell wall external surface by forming a protein film (Figure 6), with some evidence for the permeation of the fungal hydrophobin across the plant cell wall (Figure 6 and Figure S6).

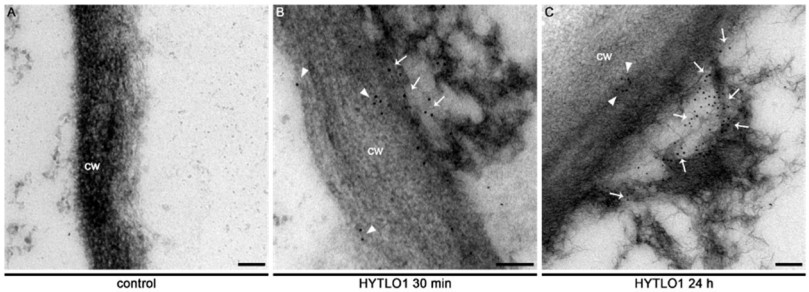

Figure 6. Immunocytochemical analysis of *L. japonicus* cells treated with HYTLO1. Cells were incubated: (**A**) in control conditions; (**B**) with HYTLO1 (0.6 μM) for 30 min; (**C**) with HYTLO1 (0.6 μM) for 24 h. Immunogold labelling was carried out by incubation with an affinity-purified anti-HYTLO1 antibody followed by a secondary antibody conjugated with 10 nm diameter-gold particles. Immunogold-labelled particles are visible at the external surface (arrows) and across the plant cell wall (arrowheads). cw, cell wall. Bars, 100 nm.

In agreement with cell viability data (Figure 3), transmission electron microscopy (TEM) analyses demonstrated that the ultrastructural organization of *L. japonicus* cells was well preserved after 24 h treatment with HYTLO1 (Figure 7).

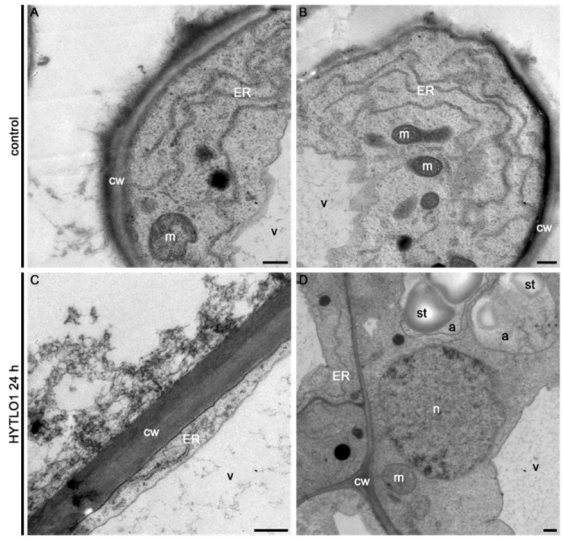

Figure 7. Electron microscopy observations of HYTLO1-treated *L. japonicus* cells. Cells were incubated: (**A**,**B**) in control conditions; (**C**,**D**) in the presence of HYTLO1 (0.6 μM) for 24 h. The ultrastructure of cells was found to be well-preserved even after 24 h treatment with the fungal hydrophobin. a, amyloplasts; cw, cell wall; ER, endoplasmic reticulum; m, mitochondria; n, nucleus; st, starch granules; v, vacuole. Bars, 500 nm.

3. Discussion

Hydrophobins are small molecular weight proteins that play multiple roles in the cell biology of filamentous fungi [46]. In particular, during the early phases of plant-fungus interactions they may play an important function by mediating adhesion to the root surface [21]. Nevertheless, their potential role as elicitors of plant defence responses has been relatively little investigated so far.

In this work we have demonstrated that HYTLO1, a hydrophobin abundantly secreted by the biocontrol fungus *Trichoderma longibrachiatum*, is perceived in a Ca^{2+}-dependent manner by *L. japonicus* suspension-cultured cells by inducing a fast, transient $[Ca^{2+}]_{cyt}$ (Figure 1A) and the subsequent activation of genes commonly considered as hallmarks of plant defence responses (Figure 2A–C). Unlike complex metabolite mixtures isolated from *Trichoderma* culture filtrates, which have been previously shown to cause programmed cell death in soybean cell cultures [9], no reduction in cell viability or ultrastructural alterations were observed after treatment of *L. japonicus* cells with HYTLO1 (Figures 3 and 7). On the other hand, our data suggest that the fungal hydrophobin acts as a mild proteinaceous elicitor, which may be able to pre-alert plant defence prior to a potential subsequent attack by a real pathogen—a mechanism commonly defined as "priming" [47].

Negative staining of preparations of pure HYTLO1 suggested the assembly of the protein in monolayers (Figure S4), that may help the fungus break the air-water interface during the early stages of plant-fungus interactions. Indeed, the peculiar physical features of these fungal proteins [48] have recently attracted a great deal of interest in view of their potential biotechnological applications as natural surfactants [49]. Unlike other hydrophobins, such as HYDPt-1 from the basidiomycete *Pisolithus tinctorius* that is exclusively located at the surface of fungal hyphae [50], HYTLO1 is secreted by *T. longibrachiatum* strain MK1 and interacts with the plant cell surface, as demonstrated by immunofluorescence (Figure S5) and immunogold labelling experiments (Figure 6 and Figure S6) with a specific antibody raised against the purified native protein.

The research work previously carried out by Lopez-Gomez et al. [51] in the same model legume *L. japonicus* highlighted the complex interplay of defence responses and symbiotic signalling pathways. Indeed, the notion that boundaries between pathogenesis and symbiosis are subtle and fluid is rapidly emerging [52]. Consistently, the *Ljsym4-2* mutant, which is characterized by an early block of the common symbiotic signalling pathway induced by both Myc factors and Nod factors, has shown altered gene expression profiles both in control conditions and after treatment with different biotic stimuli in several additional studies [53,54].

The new experimental system set up in this work, given by aequorin-expressing suspension-cultured cells of *L. japonicus*, derived from both wild-type and *Ljsym4-2* mutant, can be a useful tool to analyse Ca^{2+} signalling events not only during the beneficial interaction with an avirulent symbiont, such as the biocontrol fungus *Trichoderma* [7], but also in the establishment of symbioses with rhizobia and AM fungi. The *Ljsym4-2* mutant is defective in the *CASTOR* gene encoding for a K^+-permeable channel that has been clearly demonstrated to be an essential modulator of the Ca^{2+} spiking phenomenon originating in the nuclear and perinuclear region of legume cortical cells in response to endosymbiotic microbes [39,41,55,56]. The molecular identity of the nuclear-localized Ca^{2+} channels responsible for symbiotic Ca^{2+} oscillations has recently been unravelled [40]. Indeed, when the two *L. japonicus* cell lines were challenged with the microbial symbiotic molecules Myc factors and Nod factors, the $[Ca^{2+}]_{cyt}$ traces observed in the wild-type and mutant cell lines were clearly different, i.e., the *Ljsym4-2* lacked the second flattened Ca^{2+} increase occurring after about 15 min (Figure 1B,C). This differential Ca^{2+} response is likely due to the lack of the asynchronous cytosolic Ca^{2+} oscillations, stemming from the controlled Ca^{2+} release/uptake by the nuclear envelope in the mutant cell population, when compared to the wild-type [39,57,58]. On the other hand, the trace and kinetics of the cytosolic Ca^{2+} change triggered by the hydrophobin was found to be very similar in wild-type and *Ljsym4-2* mutant cell lines (Figure 1A). This was generally true also for the changes of expression of genes involved in plant defence (Figure 2 and Figure S2). These results indicate possible differences in the signalling transduction pathways triggered by factors secreted by different symbiotic partners, which can be consistent with the versatility of plant receptor-like kinases (RLKs) involved in the response to microbial signals [59]. On the basis of our TEM analyses of an HYTLO1-derived web-like network at the plant cell surface, we may hypothesize that the observed intracellular Ca^{2+} elevation and change in defence gene expression can originate, at least in part, by a mechanical stimulation exerted by the fungal biofilm. Mechanical stimuli generate Ca^{2+} signals in plants, and the specific plant mechanosensing mechanisms are biological processes that have recently attracted the attention of different research groups [60,61]. Moreover, it has been demonstrated that plant perception of soft mechanical stress can activate defence responses [62]. However, TEM observations of HYTLO1-treated *L. japonicus* cultured cells favoured the possibility that the 7.2 kDa hydrophobin [20] may also permeate the apoplastic compartment (Figure 6 and Figure S6), possibly interacting with the plasma membrane. Indeed, *Trichoderma* secretes in vivo a battery of cell wall degrading enzymes [63], which may further facilitate the access of secreted molecules, and then HYTLO1, to specific binding sites at the plasma membrane level. Further work will be required to identify potential receptors for hydrophobins.

The pharmacological approach used in this work suggests that HYTLO1 triggers both a Ca^{2+} influx from the extracellular milieu, as well as a Ca^{2+} release from a NAADP-sensitive intracellular Ca^{2+} store. NAADP is a pyridine nucleotide derivative that in the last two decades has been increasingly demonstrated to act as a potent Ca^{2+} mobilizing agent in animal cells, in addition to the well-established intracellular messenger inositol 1,4,5-trisphosphate ($InsP_3$) and cyclic ADP-ribose (cADPR) [28]. Although NAADP has been shown to trigger Ca^{2+} release also in higher plants [29], its involvement in plant physiological events had yet to emerge. By using Ned-19, a newly-developed chemical probe for NAADP [27], a NAADP-gated Ca^{2+} release was shown to occur in response to copper excess in the marine alga *Ulva compressa* [30], as well as in the brown alga *Ectocarpus siliculosus* [31]. These data suggest that the spectrum of photosynthetic organisms responsive to NAADP might be broader than previously envisaged. The results obtained in this work confirm that Ned-19 can be used as

a valuable tool to investigate NAADP-mediated Ca^{2+} signalling and highlight the participation of NAADP in a plant response to a biotic stimulus (a fungal proteinaceous elicitor). Interestingly, whereas members of the two-pore channel (*TPC*) gene family have been demonstrated to encode NAADP receptors in acidic organelles (endo-lysosomes) of animal cells (see [64,65] for review), the identity of NAADP receptors in plant cells still remain elusive. *TPC1*, the only member of the *TPC* gene family in *A. thaliana*, has been shown to encode the slow-vacuolar (SV) channel, a Ca^{2+}-permeable channel located at the vacuolar membrane [66] and regulated by voltage and Ca^{2+} (see [67–69] for review). Interestingly, NAADP was found to be completely ineffective in the activation of TPC1, as well as of other tonoplast cation channels [70]. Indeed, early biochemical studies, consisting in $^{45}Ca^{2+}$ release assays on sucrose-fractionated membrane vesicles, indicated an endoplasmic reticulum (ER)-localization for NAADP-gated Ca^{2+} release [29]. Interestingly, the recently reported crystal structure of *A. thaliana* TPC1 highlighted the presence of a Ned-19 binding site [71], suggesting the potential ability of this pharmacophore to allosterically block the channel activation. However, Ned-19 does not interact with the functionally-relevant voltage sensor [72]. Future in depth-studies will be necessary to further investigate the intracellular localization and additional physiological roles of plant NAADP receptors.

4. Materials and Methods

4.1. Chemicals

The hydrophobin HYTLO1 was isolated and purified to homogeneity from in vitro cultures of the biocontrol strain MK1 of *Trichoderma longibrachiatum*, as described by Ruocco et al. [20]. The pure protein was dissolved in 50% ethanol. Crude Myc factors were obtained by collecting the exudates of germinated spores of the arbuscular mycorrhizal fungus *Gigaspora margarita* (kindly provided by Paola Bonfante, Torino, Italy), lyophilizing and resuspending them in cell culture medium prior to cell treatment, as previously described [57]. Crude Nod factors extracted from *Mesorhizobium loti* were kindly provided by Makoto Hayashi (Yokohama, Japan). All chemicals used in the pharmacological analysis of Ca^{2+} fluxes (EGTA, $LaCl_3$, nicotinamide) were obtained from Sigma-Aldrich (St. Louis, MO, USA), except *trans*-Ned-19, that was purchased from ENZO Life Sciences (Farmingdale, New York, USA).

4.2. Plant Material

Lotus japonicus (ecotype Gifu) wild-type and *sym4-2* mutant seeds, defective in *CASTOR*, were kindly provided by J. Stougaard (Aarhus, Denmark) and M. Parniske (Munich, Germany), respectively.

4.3. Molecular Cloning and L. japonicus Transformation Procedures

To obtain the aequorin-expressing T-DNA construct, the aequorin cDNA was excised from the cytAEQ plasmid [73] by *Sma*I digestion. The 600 bp *Sma*I fragment was subcloned into the pSE380 plasmid (Thermo Fisher Scientific, Waltham, MA, USA) in order to gain additional restriction sites for the next step of subcloning. A *Bgl*II-*Sal*I fragment was then ligated between a CaMV-35S promoter sequence and a tNOS terminator into pCAMBIA1300 [33] *Bgl*II-*Sal*I double digested to obtain the pAB1 T-DNA construct (Figure S1A).

Agrobacterium tumefaciens-mediated *L. japonicus* transformation was performed as previously described [34,35]. Primary transformed plants of both wild-type and *Ljsym4-2* symbiotic mutant lines were selected on 5 µg/mL hygromicin B-containing medium and allowed to self-pollinate. Successful transformation and expression of the construct was confirmed by RT-PCR analysis of aequorin gene expression. Selected T2 homozygous plants (Figure S1B) were used to set up in vitro cell cultures.

4.4. Establishment of Aequorin-Expressing L. japonicus Cell Cultures

Aequorin-expressing cell cultures were set up by in vitro dedifferentiation of hypocotyls from transgenic *L. japonicus* seedlings. Briefly, hypocotyl explants from 8-day-old axenically grown seedlings were transferred on agarized (0.8%, *w*/*v*) Callus Induction Medium (CIM, 3.2 g/L Gamborg B5 basal medium, 0.5 g/L MES, 2% (*w*/*v*) sucrose, 0.5 µg/mL 2,4-dichlorophenoxyacetic acid (2,4-D), 0.05 µg/mL kinetin), supplemented with 5 µg/mL hygromycin B. After two subculturing steps, well-developed calli were transferred in Gamborg B5 liquid medium, pH 5.5, containing 2% (*w*/*v*) sucrose, 2 µg/mL 2,4-D, 5 µg/mL hygromycin B. Suspension-cultured cells were maintained at 24 °C on a rotary shaker at 80 rpm under 16 h light /8 h dark photoperiod. They were subcultured weekly by inoculating 1 mL packed cell volume into 20 mL fresh cell culture medium with, as described by Moscatiello et al. [37].

4.5. Cell Treatments

Exponentially-growing cells (five days) were treated with purified HYTLO1 (0.6 µM). The dose applied to cells was chosen on the basis of previous work concerning in vivo bioassays of physiological effects of HYTLO1 on plants [20]. In some experiments cells were treated with crude preparations of Myc factors or Nod factors. The final dose applied to cells corresponded to 10-fold concentrated AM fungal exudates and 1 µM Nod factors. In this latter case, suspension-cultured cells were grown in low nitrogen medium (containing 5 mM KNO_3) for two days prior to the onset of the Ca^{2+} measurement assays.

4.6. Aequorin-Based Ca^{2+} Measurements

Aequorin was reconstituted by overnight incubation of mid-exponential phase transgenic *L. japonicus* cell cultures with 5 µM coelenterazine (Prolume, Pinetop, AZ, USA) in darkness. Cells were then extensively washed with fresh culture medium and allowed to recover from the touch response for at least 15 min. Aequorin-based Ca^{2+} measurements were performed as recently described [38], by using 100 µL of reconstituted cell suspension culture (containing about 5 mg cells, fresh weight). For pharmacological studies, cells were pre-incubated with the appropriate inhibitor for 10 min ($LaCl_3$) or 30 min (Ned-19, nicotinamide). For experiments carried out in the absence of extracellular Ca^{2+}, cells were extensively washed with Ca^{2+}-free culture medium and then resuspended in the same medium containing 600 µM EGTA. In the case of molecules dissolved in ethanol (HYTLO1) or DMSO (Ned-19), control cells were treated with the same percentage (maximum 0.5%, *v*/*v*) of the organic solvent.

4.7. Immunofluorescence, Immunocytochemisty, and TEM Analyses

Immunofluorescence experiments were performed on *L. japonicus* suspension cultured cells as described by Zonin et al. [74]. Labelling was carried out by using affinity-purified polyclonal antibodies raised against purified native HYTLO1 (ProteoGenix, Schiltigheim, France), diluted 1:100, followed by Alexa Fluor 594 goat anti-rabbit IgG (Thermo Fisher Scientific). Working concentrations and specificity of the primary antibody were assessed in Western blot experiments against purified HYTLO1 and crude protein extracts from *L. japonicus* cells.

TEM analyses were performed as described by Tagu et al. [50]. Immunogold labelling (dilution 1:100) was performed as recently described [75]. Samples were observed with a Tecnai 12-BT transmission electron microscope (FEI, Eindhoven, The Netherlands) operating at 120 kV equipped with a Tietz camera.

For negative staining, purified HYTLO1 (0.6 µM) was adsorbed on carbon-coated EM grids, washed and stained on a drop of 1% uranyl acetate solution.

4.8. Gene Expression Analyses

For the screening of primary T1 transformants, total RNA was prepared from leaves of two week-old *L. japonicus* plants by the procedure reported by Kistner and Matamoros [76] and reversed-transcribed as described below. The oligonucleotides used for the PCR amplification are Aeq-for 5′-GCAAGCCAAACGACACAAAG-3′; Aeq-rev 5′-GAACCAACGCTCATCCGTAT-3′. The amplified 162 bp aequorin fragment was inserted in pCR2.1 cloning vector (Thermo Fisher Scientific) and confirmed by sequencing. The PCR program used was as follows: 94 °C for 5 min and 30 cycles of 94 °C for 30 s, 58 °C for 30 s, and 72 °C for 30 s. The ubiquitin gene (*UBI*, AW719589) was used as an internal standard to normalize expression levels (25 cycles of amplification; *UBI*-F-1 5′-TTCACCTTGTGCTCCGTCTTC-3′; *UBI*-R-1 5′-AACAACAGCACACACAGACAATCC-3′).Semi-quantitative RT-PCR analyses of defence gene expression in *L. japonicus* cell suspension cultures incubated in control conditions or after treatment with HYTLO1 were performed as recently described [75]. The defence-related genes encoding for the following proteins were chosen: MPK3, an enzyme frequently activated in signal transduction cascades in response to phytopathogens [77]; CP450, an enzyme involved in a wide range of biosynthetic reactions, including the synthesis of phytoalexins [78]; WRKY33, a transcriptional regulator involved in a large array of defence responses [79,80]; PR1, which expression is induced by many pathogens, and considered as a molecular marker of systemic acquired resistance (SAR) [81,82]. Transcript levels were normalized to *ATP synthase* [51]. The oligonucleotide primers were as described by [51] for *LjMPK3*, *LjWRKY33, LjCP450*, and *LjATPsyn*, and by [53] for *LjPR1*. The number of cycles exploited for a linear range of gene amplification in the RT-PCR reactions was experimentally determined. Densitometric analysis of agarose gels stained with 0.5 μg/mL ethidium bromide was carried out with the Quantity One software (Bio-Rad, Hercules, CA, USA). RT-PCR experiments were conducted in triplicate on at least three independent experiments.

Quantitative reverse transcription PCR, used to validate the data, was performed in 10 μL using HOT FIREPol EvaGreen qPcr Mix Plus (Solys BioDyne, Tartu, Estonia) and 2.5 ng of the different cDNA template. Three replicates were performed for each reaction. The qPCR reaction was conducted in a 7500 Real-Time PCR System (Thermo Fisher) according to the following cycle: 95 °C for 12 min; 95 °C for 15 s, 59 °C for 20 s, for 40 cycles. Differences in the target genes expression were evaluated by a relative quantification method normalizing the data to the endogenous reference gene *LjATPsyn*.

4.9. Cell Viability

Cell viability, after treatment for HYTLO1 for different time intervals, in the absence or presence of Ca^{2+} chelating agents/Ca^{2+} channel inhibitors, was determined by the Evans Blue method [42].

4.10. Statistical Analysis

Data are expressed as mean ± SE. The statistical significance of differences ($P < 0.05$) between means was evaluated using the Student's *t* test.

Supplementary Materials: Supplementary materials can be found at http://www.mdpi.com/1422-0067/19/9/2596/s1.

Author Contributions: R.M. set up *L. japonicus* cell cultures, performed Ca^{2+} measurements, gene expression analyses, analysed the data, and prepared the figures, with help from S.S., E.C., and S.N. M.R. purified HYTLO1 from *T. longibrachiatum* MK1 culture medium used for all the experiments and for antibody production. A.B. and M.C. designed the aequorin expression plasmid and generated *L. japonicus* transgenic lines. B.B. and L.N. performed TEM analyses. M.R., B.B., M.C., P.M., and M.L. contributed to discussion of the results and assisted in article editing. L.N. conceived the research, designed the experiments, and wrote the paper. All authors read and approved the final manuscript.

Funding: This research was funded by Dotazione Ordinaria della Ricerca Dipartimentale (DOR) 2016–2018 to L.N. and Programmi di Ricerca Scientifica di Rilevante Interesse Nazionale (PRIN) to M.L., L.N., and M.C.

Acknowledgments: We thank J. Stougaard (Aarhus, Denmark) and M. Parniske (Munich, Germany) for the kind gift of *L. japonicus* wild-type and *sym4-2* mutant seeds, respectively. We are grateful to M. Brini (Padova, Italy), P. Bonfante (Torino, Italy) and M. Hayashi (Yokohama, Japan) for kindly providing the cytAEQ plasmid, *G. margarita* spores and *M. loti* Nod factors, respectively. We also thank S. Marcato and the Electron Microscopy Service of the Department of Biology (Padova, Italy) for skilful technical assistance.

Conflicts of Interest: The authors declare no conflict of interest.

Abbreviations

Ca^{2+}	Calcium
cADPR	Cyclic ADP-ribose
2,4-D	Dichlorophenoxyacetic acid
EGTA	Ethylene glycol-bis(β-aminoethyl ether)-*N*,*N*,*N*′,*N*′-tetraacetic acid
NAADP	Nicotinic acid adenine dinucleotide phosphate
TEM	Transmission electron microscopy
TPC	Two-pore channel

References

1. Brotman, Y.; Kapuganti, J.G.; Viterbo, A. Trichoderma. *Curr. Biol.* **2010**, *20*, R390–R391. [CrossRef] [PubMed]
2. Harman, G.E.; Herrera-Estrella, A.H.; Horwitz, B.A.; Lorito, M. Special issue: *Trichoderma*—From basic Biology to Biotechnology. *Microbiology* **2012**, *158*, 1–2. [CrossRef] [PubMed]
3. Hermosa, R.; Viterbo, A.; Chet, I.; Monte, E. Plant-beneficial effects of *Trichoderma* and of its genes. *Microbiology* **2012**, *158*, 17–25. [CrossRef] [PubMed]
4. Woo, S.L.; Ruocco, M.; Vinale, F.; Nigro, M.; Marra, R.; Lombardi, N.; Pascale, A.; Lanzuise, S.; Manganiello, G.; Lorito, M. *Trichoderma*-based products and their widespread use in agriculture. *Open Mycol. J.* **2014**, *8*, 71–126. [CrossRef]
5. López-Bucio, J.; Pelagio-Flores, R.; Herrera-Estrella, A. *Trichoderma* as biostimulant: Exploiting the multilevel properties of a plant beneficial fungus. *Sci. Hortic.* **2015**, *196*, 109–123. [CrossRef]
6. Druzhinina, I.S.; Seidl-Seiboth, V.; Herrera-Estrella, A.; Horwitz, B.A.; Kenerley, C.M.; Monte, E.; Mukherjee, P.K.; Zeilinger, S.; Grigoriev, I.V.; Kubicek, C.P. *Trichoderma*: The genomics of opportunistic success. *Nat. Rev. Microbiol.* **2011**, *9*, 749–759. [CrossRef] [PubMed]
7. Harman, G.E.; Howell, C.R.; Viterbo, A.; Chet, I.; Lorito, M. *Trichoderma* species—Opportunistic, avirulent plant symbionts. *Nat. Rev. Microbiol.* **2004**, *2*, 43–56. [CrossRef] [PubMed]
8. Woo, S.L.; Scala, F.; Ruocco, M.; Lorito, M. The Molecular Biology of the interactions between *Trichoderma* spp., phytopathogenic fungi, and plants. *Phytopathology* **2006**, *96*, 181–185. [CrossRef] [PubMed]
9. Navazio, L.; Baldan, B.; Moscatiello, R.; Zuppini, A.; Woo, S.L.; Mariani, P.; Lorito, M. Calcium-mediated perception and defense responses activated in plant cells by metabolite mixtures secreted by the biocontrol fungus *Trichoderma atroviride*. *BMC Plant Biol.* **2007**, *7*, 41. [CrossRef] [PubMed]
10. Vinale, F.; Sivasithamparam, K.; Ghisalberti, E.L.; Marra, R.; Woo, S.L.; Lorito, M. *Trichoderma*–plant–pathogen interactions. *Soil Biol. Biochem.* **2008**, *40*, 1–10. [CrossRef]
11. Clapham, D.E. Calcium signaling. *Cell* **2007**, *131*, 1047–1058. [CrossRef] [PubMed]
12. Dodd, A.N.; Kudla, J.; Sanders, D. The language of calcium signaling. *Annu. Rev. Plant Biol.* **2010**, *61*, 593–620. [CrossRef] [PubMed]
13. Cai, X.; Clapham, D.E. Ancestral Ca^{2+} signaling machinery in early animal and fungal evolution. *Mol. Biol. Evol.* **2012**, *29*, 91–100. [CrossRef] [PubMed]
14. Domínguez, D.C.; Guragain, M.; Patrauchan, M. Calcium binding proteins and calcium signaling in prokaryotes. *Cell Calcium* **2015**, *57*, 151–165. [CrossRef] [PubMed]
15. Aldon, D.; Mbengue, M.; Mazars, C.; Galaud, J.P. Calcium signalling in plant biotic interactions. *Int. J. Mol. Sci.* **2018**, *19*, 665. [CrossRef] [PubMed]
16. Kudla, J.; Becker, D.; Grill, E.; Hedrich, R.; Hippler, M.; Kummer, U.; Parniske, M.; Romeis, T.; Schumacher, K. Advances and current challenges in calcium signaling. *New Phytol.* **2018**, *218*, 414–431. [CrossRef] [PubMed]
17. Costa, A.; Navazio, L.; Szabo, I. The contribution of organelles to plant intracellular calcium signalling. *J. Exp. Bot.* **2018**, *69*, 4175–4193. [CrossRef] [PubMed]

18. Zipfel, C.; Oldroyd, G.E. Plant signalling in symbiosis and immunity. *Nature* **2017**, *543*, 328–336. [CrossRef] [PubMed]
19. Lecourieux, D.; Ranjeva, R.; Pugin, A. Calcium in plant defence-signalling pathways. *New Phytol.* **2006**, *171*, 249–269. [CrossRef] [PubMed]
20. Ruocco, M.; Lanzuise, S.; Lombardi, N.; Woo, S.L.; Vinale, F.; Marra, R.; Varlese, R.; Manganiello, G.; Pascale, A.; Scala, V.; et al. Multiple roles and effects of a novel *Trichoderma* hydrophobin. *Mol. Plant Microbe Interact.* **2015**, *28*, 167–179. [CrossRef] [PubMed]
21. Whiteford, J.R.; Spanu, P.D. Hydrophobins and the interactions between fungi and plants. *Mol. Plant Pathol.* **2002**, *3*, 391–400. [CrossRef] [PubMed]
22. Guzmán-Guzmán, P.; Alemán-Duarte, M.I.; Delaye, L.; Herrera-Estrella, A.; Olmedo-Monfil, V. Identification of effector-like proteins in *Trichoderma* spp. and role of a hydrophobin in the plant-fungus interaction and mycoparasitism. *BMC Genet.* **2017**, *18*, 16. [CrossRef] [PubMed]
23. Przylucka, A.; Akcapinar, G.B.; Chenthamara, K.; Cai, F.; Grujic, M.; Karpenko, J.; Livoi, M.; Shen, Q.; Kubicek, C.P.; Druzhinina, I.S. HFB7—A novel orphan hydrophobin of the *Harzianum* and *Virens* clades of *Trichoderma*, is involved in response to biotic and abiotic stresses. *Fungal Genet. Biol.* **2017**, *102*, 63–76. [CrossRef] [PubMed]
24. Viterbo, A.; Chet, I. *TasHyd1*, a new hydrophobin gene from the biocontrol agent *Trichoderma asperellum*, is involved in plant root colonization. *Mol. Plant Pathol.* **2006**, *7*, 249–258. [CrossRef] [PubMed]
25. Kurt, H.; Jens, S. *Lotus japonicus*, an autogamous, diploid legume species for classical and molecular genetics. *Plant J.* **1992**, *2*, 487–496.
26. Jiang, Q.; Gresshoff, P.M. Classical and molecular genetics of the model legume *Lotus japonicus*. *Mol. Plant Microbe Interact.* **1997**, *10*, 59–68. [CrossRef] [PubMed]
27. Naylor, E.; Arredouani, A.; Vasudevan, S.R.; Lewis, A.M.; Parkesh, R.; Mizote, A.; Rosen, D.; Thomas, J.M.; Izumi, M.; Ganesan, A.; et al. Identification of a chemical probe for NAADP by virtual screening. *Nat. Chem. Biol.* **2009**, *5*, 220–226. [CrossRef] [PubMed]
28. Galione, A.; Morgan, A.J.; Arredouani, A.; Davis, L.C.; Rietdorf, K.; Ruas, M.; Parrington, J. NAADP as an intracellular messenger regulating lysosomal calcium-release channels. *Biochem. Soc. Trans.* **2010**, *38*, 1424–1431. [CrossRef] [PubMed]
29. Navazio, L.; Bewell, M.A.; Siddiqua, A.; Dickinson, G.D.; Galione, A.; Sanders, D. Calcium release from the endoplasmic reticulum of higher plants elicited by the NADP metabolite nicotinic acid adenine dinucleotide phosphate. *Proc. Natl. Acad. Sci. USA* **2000**, *97*, 8693–8698. [CrossRef] [PubMed]
30. González, A.; Cabrera Mde, L.; Henríquez, M.J.; Contreras, R.A.; Morales, B.; Moenne, A. Cross talk among calcium, hydrogen peroxide, and nitric oxide and activation of gene expression involving calmodulins and calcium-dependent protein kinases in *Ulva compressa* exposed to copper excess. *Plant Physiol.* **2012**, *158*, 1451–1462. [CrossRef] [PubMed]
31. González, A.; Sáez, C.A.; Moenne, A. Copper-induced activation of TRPs and VDCCs triggers a calcium signature response regulating gene expression in *Ectocarpus siliculosus*. *PeerJ.* **2018**, *6*, e4556. [CrossRef] [PubMed]
32. Mun, T.; Bachmann, A.; Gupta, V.; Stougaard, J.; Andersen, S.U. *Lotus* Base: An integrated information portal for the model legume *Lotus japonicus*. *Sci. Rep.* **2016**, *6*, 39447. [CrossRef] [PubMed]
33. Hajdukiewicz, P.; Svab, Z.; Maliga, P. The small, versatile *pPZP* family of *Agrobacterium* binary vectors for plant transformation. *Plant Mol. Biol.* **1994**, *25*, 989–994. [CrossRef] [PubMed]
34. Lombari, P.; Ercolano, E.; El Alaoui, H.; Chiurazzi, M. A new transformation-regeneration procedure in the model legume *Lotus japonicus*: Root explants as a source of large numbers of cells susceptible to *Agrobacterium*-mediated transformation. *Plant Cell Rep.* **2003**, *21*, 771–777. [PubMed]
35. Barbulova, A.; D'Apuzzo, E.; Rogato, A.; Chiurazzi, M. Improved procedures for in vitro regeneration and for phenotypic analysis in the model legume *Lotus japonicus*. *Funct. Plant Biol.* **2005**, *32*, 529–536. [CrossRef]
36. Bonfante, P.; Genre, A.; Faccio, A.; Martini, I.; Schauser, L.; Stougaard, J.; Webb, J.; Parniske, M. The *Lotus japonicus LjSym4* gene is required for the successful symbiotic infection of root epidermal cells. *Mol. Plant Microbe Interact.* **2000**, *13*, 1109–1120. [CrossRef] [PubMed]
37. Moscatiello, R.; Baldan, B.; Navazio, L. Plant cell suspension cultures. *Methods Mol. Biol.* **2013**, *953*, 77–93. [PubMed]

38. Sello, S.; Perotto, J.; Carraretto, L.; Szabò, I.; Vothknecht, U.C.; Navazio, L. Dissecting stimulus-specific Ca^{2+} signals in amyloplasts and chloroplasts of *Arabidopsis thaliana* cell suspension cultures. *J. Exp. Bot.* **2016**, *67*, 3965–3974. [CrossRef] [PubMed]
39. Charpentier, M.; Bredemeier, R.; Wanner, G.; Takeda, N.; Schleiff, E.; Parniske, M. *Lotus japonicus* CASTOR and POLLUX are ion channels essential for perinuclear calcium spiking in legume root endosymbiosis. *Plant Cell* **2008**, *20*, 3467–3479. [CrossRef] [PubMed]
40. Charpentier, M.; Sun, J.; Vaz Martins, T.; Radhakrishnan, G.V.; Findlay, K.; Soumpourou, E.; Thouin, J.; Véry, A.A.; Sanders, D.; Morris, R.J.; et al. Nuclear-localized cyclic nucleotide-gated channels mediate symbiotic calcium oscillations. *Science* **2016**, *352*, 1102–1105. [CrossRef] [PubMed]
41. Venkateshwaran, M.; Cosme, A.; Han, L.; Banba, M.; Satyshur, K.A.; Schleiff, E.; Parniske, M.; Imaizumi-Anraku, H.; Ané, J.M. The recent evolution of a symbiotic ion channel in the legume family altered ion conductance and improved functionality in calcium signaling. *Plant Cell* **2012**, *24*, 2528–2545. [CrossRef] [PubMed]
42. Baker, C.J.; Mock, N.M. An improved method for monitoring cell death in cell suspension and leaf disc assays using evans blue. *Plant Cell Tissue Organ Cult.* **1994**, *39*, 7–12. [CrossRef]
43. Knight, H.; Trewavas, A.J.; Knight, M.R. Calcium signalling in *Arabidopsis thaliana* responding to drought and salinity. *Plant J.* **1997**, *12*, 1067–1078. [CrossRef] [PubMed]
44. Abdul-Awal, S.M.; Hotta, C.T.; Davey, M.P.; Dodd, A.N.; Smith, A.G.; Webb, A.A. NO-Mediated $[Ca^{2+}]_{cyt}$ increases depend on ADP-ribosyl cyclase activity in Arabidopsis. *Plant Physiol.* **2016**, *171*, 623–631. [CrossRef] [PubMed]
45. Lin, W.K.; Bolton, E.L.; Cortopassi, W.A.; Wang, Y.; O'Brien, F.; Maciejewska, M.; Jacobson, M.P.; Garnham, C.; Ruas, M.; Parrington, J.; et al. Synthesis of the Ca^{2+}-mobilizing messengers NAADP and cADPR by intracellular CD38 enzyme in the mouse heart: Role in beta-adrenoceptor signaling. *J. Biol. Chem.* **2017**, *292*, 13243–13257. [CrossRef] [PubMed]
46. Wosten, H.A. Hydrophobins: Multipurpose proteins. *Annu. Rev. Microbiol.* **2001**, *55*, 625–646. [CrossRef] [PubMed]
47. Prime-A-Plant Group; Conrath, U.; Beckers, G.J.; Flors, V.; García-Agustín, P.; Jakab, G.; Mauch, F.; Newman, M.A.; Pieterse, C.M.; Poinssot, B.; et al. Priming: Getting ready for battle. *Mol. Plant Microbe Interact.* **2006**, *19*, 1062–1071. [CrossRef] [PubMed]
48. Sunde, M.; Kwan, A.H.; Templeton, M.D.; Beever, R.E.; Mackay, J.P. Structural analysis of hydrophobins. *Micron* **2008**, *39*, 773–784. [CrossRef] [PubMed]
49. Cox, P.W.; Hooley, P. Hydrophobins: New prospects for biotechnology. *Fungal Biol. Rev.* **2009**, *23*, 40–47. [CrossRef]
50. Tagu, D.; De Bellis, R.; Balestrini, R.; De Vries, O.M.H.; Piccoli, G.; Stocchi, V.; Bonfante, P.; Martin, F. Immunolocalization of hydrophobin HYDPt-1 from the ectomycorrhizal basidiomycete *Pisolithus tinctorius* during colonization of *Eucalyptus globulus* roots. *New Phytol.* **2001**, *149*, 127–135. [CrossRef]
51. Lopez-Gomez, M.; Sandal, N.; Stougaard, J.; Boller, T. Interplay of flg22-induced defence responses and nodulation in *Lotus japonicus*. *J. Exp. Bot.* **2012**, *63*, 393–401. [CrossRef] [PubMed]
52. Hacquard, S.; Spaepen, S.; Garrido-Oter, R.; Schulze-Lefert, P. Interplay between innate immunity and the plant microbiota. *Annu. Rev. Phytopathol.* **2017**, *55*, 565–589. [CrossRef] [PubMed]
53. Bastianelli, F.; Costa, A.; Vescovi, M.; D'Apuzzo, E.; Zottini, M.; Chiurazzi, M.; Lo Schiavo, F. Salicylic acid differentially affects suspension cell cultures of *Lotus japonicus* and one of its non-symbiotic mutants. *Plant Mol. Biol.* **2010**, *72*, 469–483. [CrossRef] [PubMed]
54. Francia, D.; Chiltz, A.; Lo Schiavo, F.; Pugin, A.; Bonfante, P.; Cardinale, F. AM fungal exudates activate MAP kinases in plant cells in dependence from cytosolic Ca ($^{2+}$) increase. *Plant Physiol. Biochem.* **2011**, *49*, 963–969. [CrossRef] [PubMed]
55. Chabaud, M.; Genre, A.; Sieberer, B.J.; Faccio, A.; Fournier, J.; Novero, M.; Barker, D.G.; Bonfante, P. Arbuscular mycorrhizal hyphopodia and germinated spore exudates trigger Ca^{2+} spiking in the legume and nonlegume root epidermis. *New Phytol.* **2011**, *189*, 347–355. [CrossRef] [PubMed]
56. Sieberer, B.J.; Chabaud, M.; Fournier, J.; Timmers, A.C.; Barker, D.G. A switch in Ca^{2+} spiking signature is concomitant with endosymbiotic microbe entry into cortical root cells of *Medicago truncatula*. *Plant J.* **2012**, *69*, 822–830. [CrossRef] [PubMed]

57. Navazio, L.; Moscatiello, R.; Genre, A.; Novero, M.; Baldan, B.; Bonfante, P.; Mariani, P. A diffusible signal from arbuscular mycorrhizal fungi elicits a transient cytosolic calcium elevation in host plant cells. *Plant Physiol.* **2007**, *144*, 673–681. [CrossRef] [PubMed]
58. Kosuta, S.; Hazledine, S.; Sun, J.; Miwa, H.; Morris, R.J.; Downie, J.A.; Oldroyd, G.E. Differential and chaotic calcium signatures in the symbiosis signaling pathway of legumes. *Proc. Natl. Acad. Sci. USA* **2008**, *105*, 9823–9828. [CrossRef] [PubMed]
59. Antolín-Llovera, M.; Ried, M.K.; Binder, A.; Parniske, M. Receptor kinase signaling pathways in plant-microbe interactions. *Annu. Rev. Phytopathol.* **2012**, *50*, 451–473. [CrossRef] [PubMed]
60. Monshausen, G.B.; Haswell, E.S. A force of nature: Molecular mechanisms of mechanoperception in plants. *J. Exp. Bot.* **2013**, *64*, 4663–4680. [CrossRef] [PubMed]
61. Kurusu, T.; Kuchitsu, K.; Nakano, M.; Nakayama, Y.; Iida, H. Plant mechanosensing and Ca^{2+} transport. *Trends Plant Sci.* **2013**, *18*, 227–233. [CrossRef] [PubMed]
62. Benikhlef, L.; L'Haridon, F.; Abou-Mansour, E.; Serrano, M.; Binda, M.; Costa, A.; Lehmann, S.; Métraux, J.P. Perception of soft mechanical stress in Arabidopsis leaves activates disease resistance. *BMC Plant Biol.* **2013**, *13*, 133. [CrossRef] [PubMed]
63. Markovich, N.A.; Kononova, G.L. Lytic enzymes of *Trichoderma* and their role in plant defense from fungal diseases: A review. *Appl. Biochem. Microbiol.* **2003**, *39*, 341–351. [CrossRef]
64. Galione, A. NAADP receptors. *Cold Spring Harb. Perspect. Biol.* **2011**, *3*, a004036. [CrossRef] [PubMed]
65. Morgan, A.J.; Davis, L.C.; Ruas, M.; Galione, A. TPC: The NAADP discovery channel? *Biochem. Soc. Trans.* **2015**, *43*, 384–389. [CrossRef] [PubMed]
66. Peiter, E.; Maathuis, F.J.; Mills, L.N.; Knight, H.; Pelloux, J.; Hetherington, A.M.; Sanders, D. The vacuolar Ca^{2+}-activated channel TPC1 regulates germination and stomatal movement. *Nature* **2005**, *434*, 404–408. [CrossRef] [PubMed]
67. Peiter, E. The plant vacuole: Emitter and receiver of calcium signals. *Cell Calcium* **2011**, *50*, 120–128. [CrossRef] [PubMed]
68. Hedrich, R.; Mueller, T.D.; Becker, D.; Marten, I. Structure and function of TPC1 vacuole SV channel gains shape. *Mol. Plant* **2018**, *11*, 764–775. [CrossRef] [PubMed]
69. Demidchik, V.; Shabala, S.; Isayenkov, S.; Cuin, T.A.; Pottosin, I. Calcium transport across plant membranes: Mechanisms and functions. *New Phytol.* **2018**. [CrossRef] [PubMed]
70. Boccaccio, A.; Scholz-Starke, J.; Hamamoto, S.; Larisch, N.; Festa, M.; Gutla, P.V.; Costa, A.; Dietrich, P.; Uozumi, N.; Carpaneto, A. The phosphoinositide PI (3,5) P_2 mediates activation of mammalian but not plant TPC proteins: Functional expression of endolysosomal channels in yeast and plant cells. *Cell. Mol. Life Sci.* **2014**, *71*, 4275–4283. [CrossRef] [PubMed]
71. Kintzer, A.F.; Stroud, R.M. Structure, inhibition and regulation of two-pore channel TPC1 from *Arabidopsis thaliana*. *Nature* **2016**, *531*, 258–262. [CrossRef] [PubMed]
72. Patel, S.; Penny, C.J.; Rahman, T. Two-pore channels enter the atomic era: Structure of plant TPC revealed. *Trends Biochem. Sci.* **2016**, *41*, 475–477. [CrossRef] [PubMed]
73. Brini, M.; Marsault, R.; Bastianutto, C.; Alvarez, J.; Pozzan, T.; Rizzuto, R. Transfected aequorin in the measurement of cytosolic Ca^{2+} concentration ($[Ca^{2+}]_c$). A critical evaluation. *J. Biol. Chem.* **1995**, *270*, 9896–9903. [CrossRef] [PubMed]
74. Zonin, E.; Moscatiello, R.; Miuzzo, M.; Cavallarin, N.; Di Paolo, M.L.; Sandonà, D.; Marin, O.; Brini, M.; Negro, A.; Navazio, L. TAT-mediated aequorin transduction: An alternative approach for effective calcium measurements in plant cells. *Plant Cell Physiol.* **2011**, *52*, 2225–2235. [CrossRef] [PubMed]
75. Sello, S.; Moscatiello, R.; Mehlmer, N.; Leonardelli, M.; Carraretto, L.; Cortese, E.; Zanella, F.G.; Baldan, B.; Szabò, I.; Vothknecht, U.C.; et al. Chloroplast Ca^{2+} fluxes into and across thylakoids revealed by thylakoid-targeted aequorin probes. *Plant Physiol.* **2018**, *177*, 38–51. [CrossRef] [PubMed]
76. Kistner, C.; Matamoros, M. RNA isolation using phase extraction and LiCl precipitation. In *Lotus Japonicus Handbook*; Márquez, A.J., Ed.; Springer: Dordrecht, The Netherlands, 2005; pp. 123–124.
77. Colcombet, J.; Hirt, H. *Arabidopsis* MAPKs: A complex signalling network involved in multiple biological processes. *Biochem. J.* **2008**, *413*, 217–226. [CrossRef] [PubMed]
78. Nafisi, M.; Goregaoker, S.; Botanga, C.J.; Glawischnig, E.; Olsen, C.E.; Halkier, B.A.; Glazebrook, J. *Arabidopsis* cytochrome P450 monooxygenase 71A13 catalyzes the conversion of indole-3-acetaldoxime in camalexin synthesis. *Plant Cell* **2007**, *19*, 2039–2052. [CrossRef] [PubMed]

79. Mao, G.; Meng, X.; Liu, Y.; Zheng, Z.; Chen, Z.; Zhang, S. Phosphorylation of a WRKY transcription factor by two pathogen-responsive MAPKs drives phytoalexin biosynthesis in *Arabidopsis*. *Plant Cell* **2011**, *23*, 1639–1653. [CrossRef] [PubMed]
80. Birkenbihl, R.P.; Diezel, C.; Somssich, I.E. Arabidopsis WRKY33 is a key transcriptional regulator of hormonal and metabolic responses toward *Botrytis cinerea* infection. *Plant Physiol.* **2012**, *159*, 266–285. [CrossRef] [PubMed]
81. Uknes, S.; Dincher, S.; Friedrich, L.; Negrotto, D.; Williams, S.; Thompson-Taylor, H.; Potter, S.; Ward, E.; Ryals, J. Regulation of pathogenesis-related protein-1a gene expression in tobacco. *Plant Cell* **1993**, *5*, 159–169. [CrossRef] [PubMed]
82. Maleck, K.; Levine, A.; Eulgem, T.; Morgan, A.; Schmid, J.; Lawton, K.A.; Dangl, J.L.; Dietrich, R.A. The transcriptome of *Arabidopsis thaliana* during systemic acquired resistance. *Nat. Genet.* **2000**, *26*, 403–410. [CrossRef] [PubMed]

A

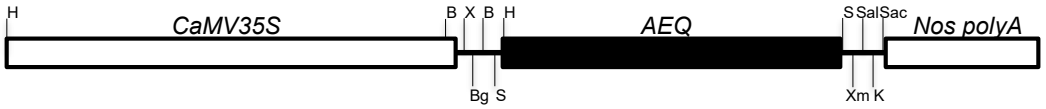

B

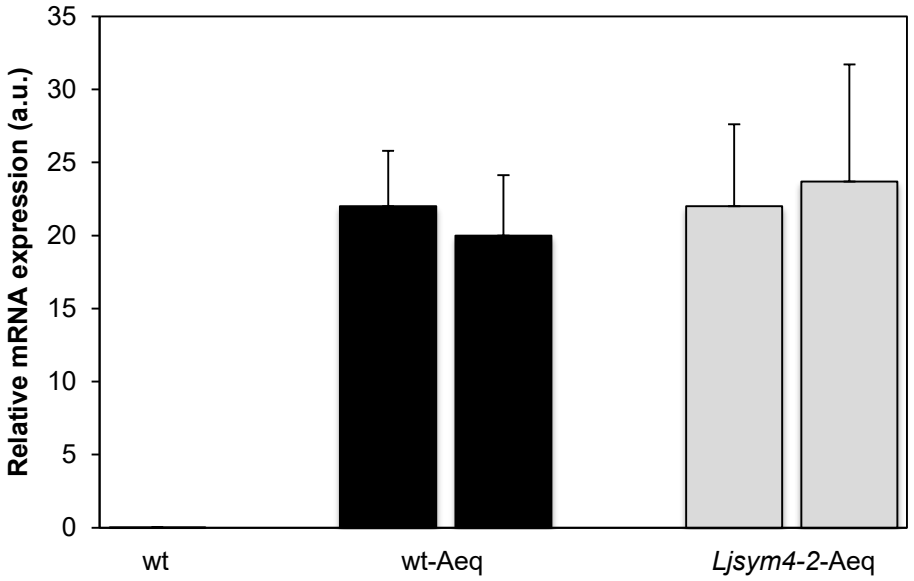

Figure S1. (**A**) Schematic map of the aequorin expressing cassette of pAB1 T-DNA construct. X, *Xba*I; Bg, *Bgl*II; B, *Bam*HI; S, *Sma*I; H, *Hind*III; Xm, *Xma*I; Sal, *Sal*I; K, *Kpn*I; Sac, *Sac*I. (**B**) Level of aequorin transcript in *L. japonicus* wild-type and *Ljsym4-2* mutant transformants of the T2 generation, selected to set up cell suspension cultures. Expression levels are normalized to that of the internal control ubiquitin. Data are the means ± SE of three independent experiments.

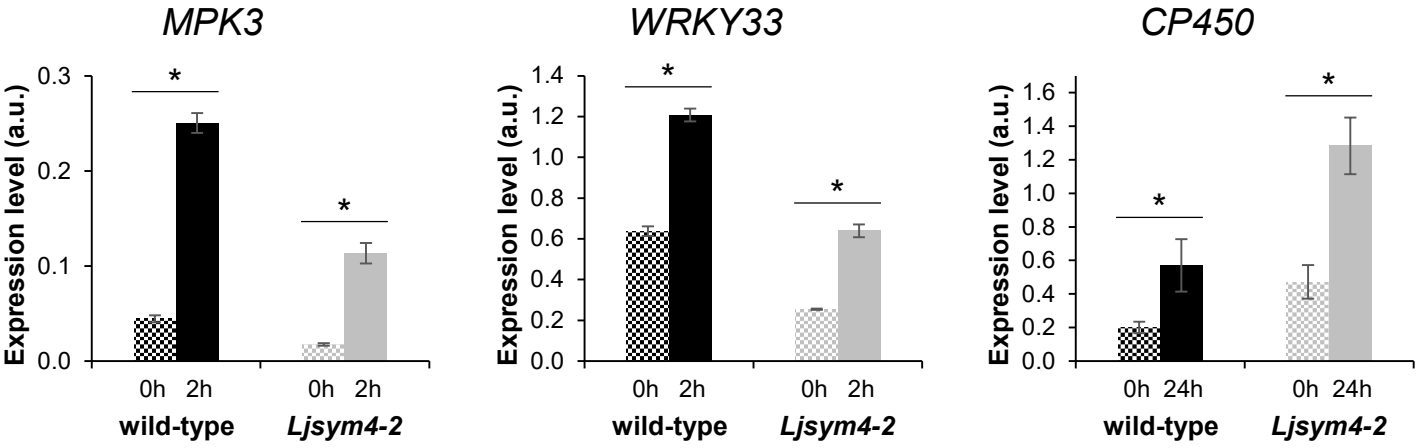

Figure S2. Quantitative RT-PCR analysis of *MPK3*, *WRKY33* and *CP450* transcripts in *L. japonicus* cell cultures of the wild-type line and *Ljsym4-2* mutant in control conditions (dotted bars) and after treatment with 0.6 μM HYTLO1 (solid bars) for different time intervals. Expression levels are normalized to the housekeeping gene *ATP synthase*. Data are the means ± SE of three replicates. * indicates statistically significant difference at $P<0.05$.

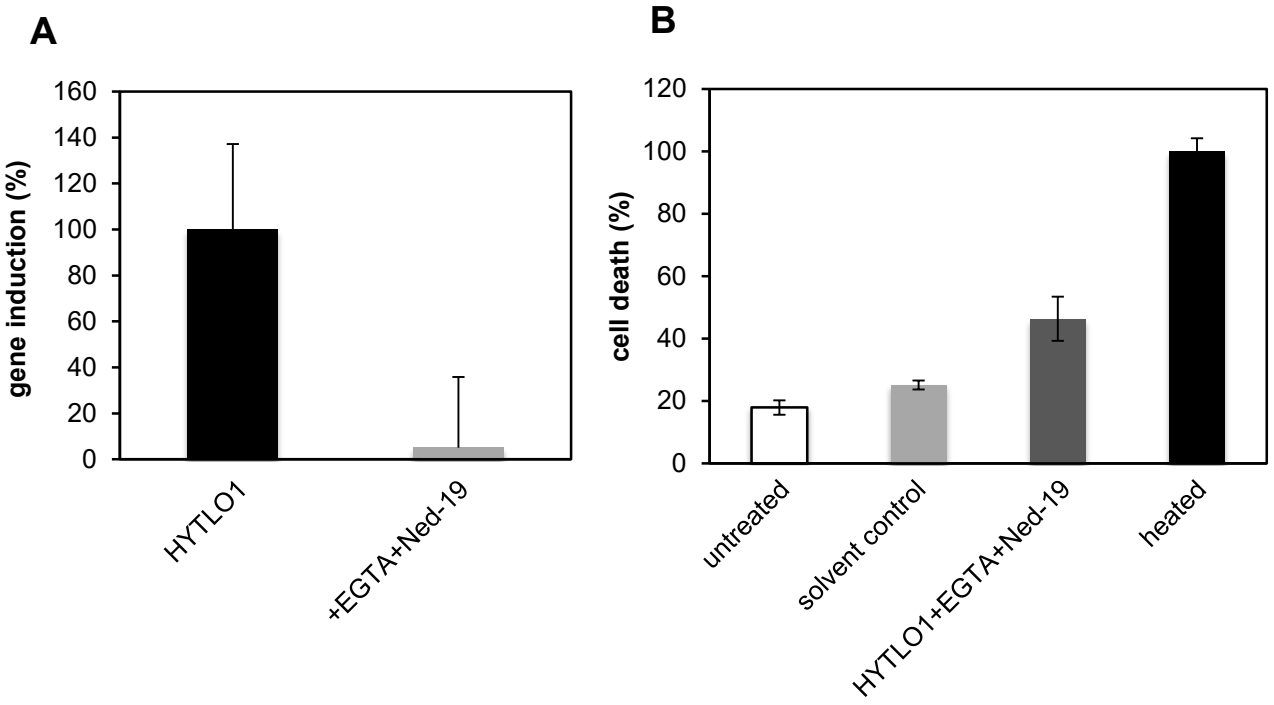

Figure S3. Effect of pretreatment with EGTA and Ned-19 on HYTLO1-induced *CP450* expression and cell viability in *L. japonicus* cells. (**A**) RT-PCR analysis of *CP450* expression after treatment with HYTLO1 (0.6 µM) for 24 h in regular cell culture medium (black bar) or after pre-treatment with 600 µM EGTA and 100 µM Ned-19 in Ca^{2+}-free medium (grey bar). (**B**) Cell viability assay after 24 h incubation in untreated samples (white bar), in Ca^{2+}-free medium supplemented with 600 µM EGTA and the solvents of Ned-19 (0.5% DMSO) and HYTLO1 (0.5% ethanol) (light grey bar), or in Ca^{2+}-free medium supplemented with 600 µM EGTA, 100 µM Ned-19 and 0.6 µM HYTLO1 (dark grey bar). 100% cell death corresponds to cells incubated for 20 min at 100°C (black bar). Data are the means ± SE of three independent experiments.

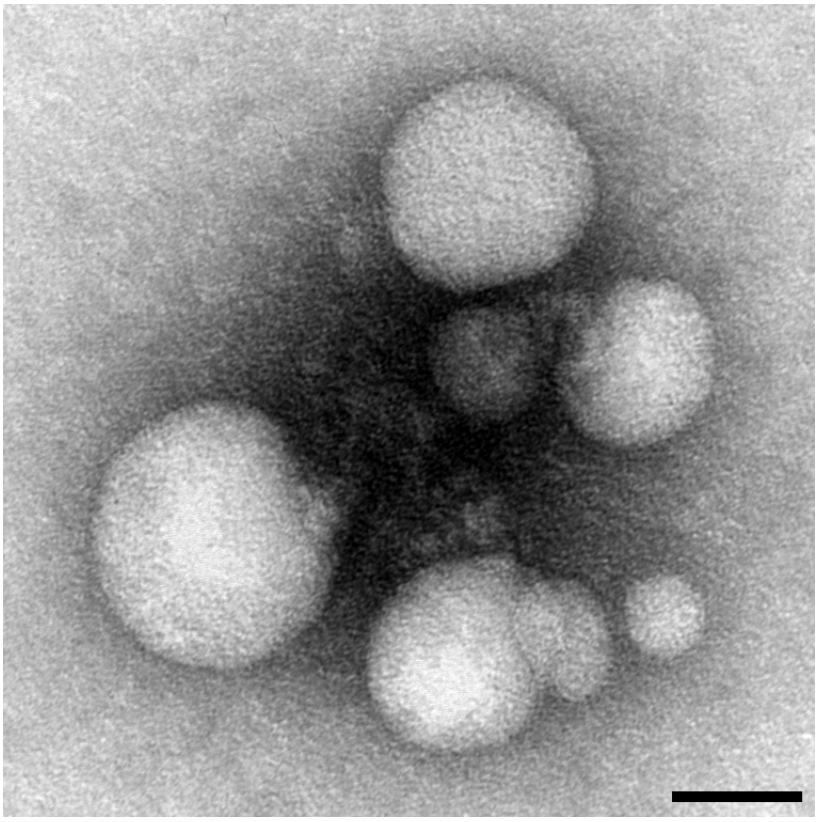

Figure S4. Negative staining with 1% uranyl acetate of purified HYTLO1. Bar, 50 nm.

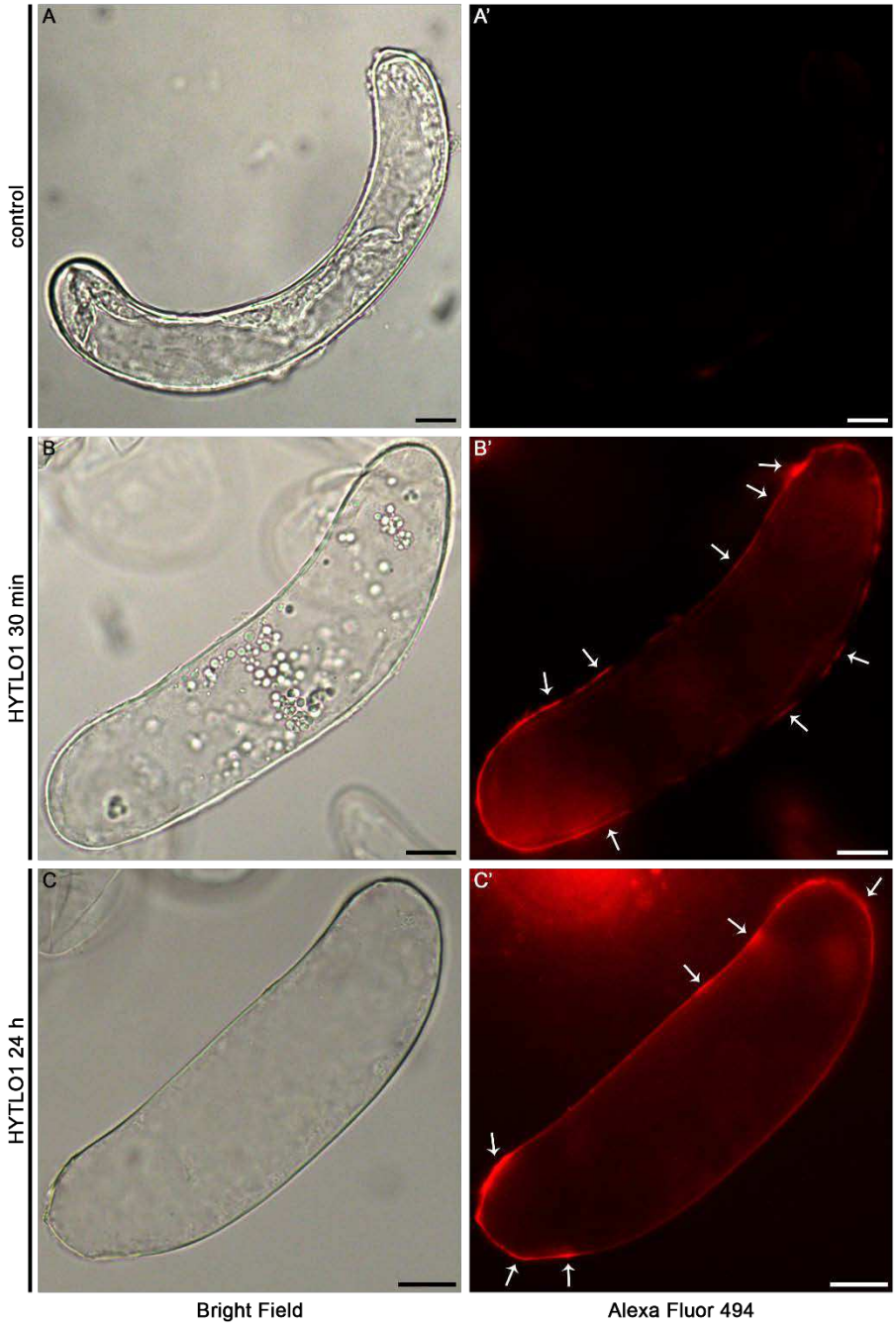

Figure S5. Immunofluorescence staining of *L. japonicus* cells treated with HYTLO1. Cells were incubated: (**A-A'**) in control conditions; (**B-B'**) with HYTLO1 (0.6 μM) for 30 min; (**C-C'**) with HYTLO1 (0.6 μM) for 24 h. After fixation, cells were incubated with an affinity-purified anti-HYTLO1 antibody followed by a red-fluorescent Alexa Fluor 494 secondary antibody. Bright field (**A-C**) and fluorescence microscopy (**A'-C'**) images of the same fields are shown. White arrows indicate an exclusive localization of the hydrophobin at the cell surface. Bars, 50 μm.

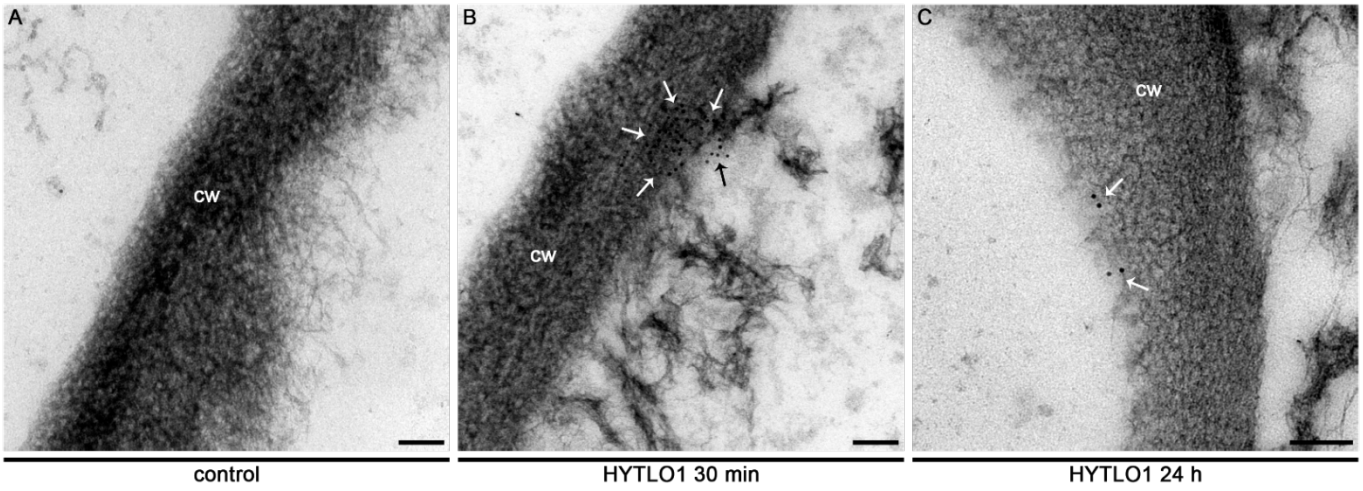

Figure S6. Immunocytochemical analysis of HYTLO1 in *Lotus japonicus* cells treated with the fungal hydrophobin. Untreated cells were used as negative control (**A**). Immunogold-labeled particles (arrows) are present across the plant cell wall width in 30 min-treated cells (**B**) and at the internal side of the cell wall in 24 h-treated cells (**C**). Bars, 100 nm.

CHAPTER 8

Conclusions

CONCLUSIONS

Plant organellar Ca^{2+} signalling is a rapidly expanding field of investigation that has recently benefited from the availability of novel specifically targeted reporters useful to monitor intracellular Ca^{2+} dynamics (Costa *et al.*, 2018). Whereas the scientific attention has mainly focused for a long time on the vacuole – as it is the major Ca^{2+} store of the plant cell – increasing evidence supports the idea that also other intracellular compartments may play a crucial role in the modulation of cytosolic Ca^{2+} signatures. In particular, recent investigations have shown that both chloroplasts and non-green plastids contribute to the fine-tuning of cytoplasmic Ca^{2+} signalling by generating their own stromal Ca^{2+} transients in response to different environmental stimuli (Sello *et al.*, 2016). Despite extensive research is currently ongoing to precisely address how chloroplasts are integrated in the whole cell Ca^{2+} signalling, when I started my Ph.D. no indications were available on the specific involvement of thylakoids in the generation of the chloroplast [Ca^{2+}] changes, as well as on the identity of the molecular players making these organellar Ca^{2+} fluxes possible. Likewise, also the endoplasmic reticulum (ER) is envisaged to exert a relevant role in transducing stress-related Ca^{2+} mediated events, in a similar fashion to the well-established function of this compartment in the animal counterpart. Nevertheless, only little was known about this putative Ca^{2+} store in plant cells, due to the lack of accurate measurements of the [Ca^{2+}] inside ER lumen.

This Ph.D. work thus aimed to elucidate the contribution of chloroplasts and (ER) to Ca^{2+} homeostasis and signalling in the plant cell and to investigate their potential interplay both under constitutive and stress-related conditions in the model plant *Arabidopsis thaliana*.

Concerning chloroplasts, the development of two new genetically encoded Ca^{2+} indicators (GECIs) targeted to either the thylakoid membrane or the thylakoid lumen allowed for the monitoring of Ca^{2+} dynamics inside this unique chloroplast internal membrane system. The accurate quantification of resting free [Ca^{2+}] levels as well as their variations during signal transduction events evoked by environmental stimuli was made possible by the use of aequorin

chimeras specifically targeted to these compartments, both in Arabidopsis entire seedlings and in cell suspension cultures from them derived. Among all the available GECIs, aequorin-based Ca^{2+}-biosensors are in fact the current method of choice for precise Ca^{2+} quantification (Ottolini *et al.*, 2014) thanks to their biochemical (insensitivity to pH and Mg^{2+} changes) and bioluminescent properties (high signal-to-noise ratio as well as lack of damaging excitation light) (Brini *et al.*, 2008). Moreover, aequorin is also an excellent tool to measure Ca^{2+} levels in chlorophyll-containing tissues even for long time intervals (Martì *et al.*, 2013; Costa *et al.*, 2018). Monitoring of subchloroplasts Ca^{2+} dynamics hence revealed the occurrence of stimulus-specific Ca^{2+} signals triggered by a wide range of different abiotic and biotic stimuli, each characterized by its own kinetics, with thylakoids that were found to actively contribute to the dissipation of stromal Ca^{2+} transients. Investigations on putative Ca^{2+}-permeable channels located at chloroplast membranes – cMCU and GLR3.4/3.5 – further highlighted the participation of chloroplasts in modulating the complex events involved in Ca^{2+} homeostasis and Ca^{2+}-mediated signal transduction. cMCU was identified and functionally characterized both *in vitro* and *in vivo*, revealing its involvement in osmotic stress-related signalling pathway that confer to the plant a certain degree of tolerance to water deprivation. GLR3.4 and GLR3.5, instead, seem to play a role in transducing different environmental stimuli (*i.e.* salinity and cold), but their full characterization is part of a still ongoing work in the laboratory and the precise characterization of their function will be better addressed in the future. Overall, the obtained data highlight the role of chloroplasts and of chloroplast-located Ca^{2+}-permeable channels in transducing Ca^{2+}-mediated stress signals in the plant cell.

Concerning the ER, the lack of a reliable quantification of its luminal $[Ca^{2+}]$ has been overcome thanks to the successful development of a low Ca^{2+}-affinity aequorin-based Ca^{2+} indicator targeted to the luminal side of the ER membrane. Accurate quantification of free basal $[Ca^{2+}]_{ER}$ as well as of its changes in response to external stresses revealed a significant difference for the plant ER with respect to the animal counterpart. Moreover, the observed increases in $[Ca^{2+}]_{ER}$ upon perception of some abiotic environmental stimuli

pointed to a role for the plant ER in the dissipation of cytosolic Ca^{2+} signatures, suggesting a role for this compartment more as a Ca^{2+} sink than as a Ca^{2+} source. The comparison between Ca^{2+} dynamics recorded in parallel in the ER, chloroplast stroma and cytosol provided useful information about the functional interaction of these intracellular Ca^{2+} stores in the modulation of cytosolic Ca^{2+} signals.

In conclusion, new organelle-targeted aequorin-based Ca^{2+} probes were developed, increasing the number of subcellular localizations for which Ca^{2+} indicators are currently available (**Fig. 1**). These new probes will surely serve as valuable tools in future studies of plant organellar Ca^{2+} signalling.
A chloroplast-located Ca^{2+}-permeable channel (cMCU) was identified and characterized, and research work on chloroplast-targeted members of the glutamate receptor-like family is ongoing.
Moreover, accurate quantifications of $[Ca^{2+}]$ in the plant ER and of its variations in response to different environmental stimuli were provided, adding insights into the role of this compartment in Ca^{2+} homeostasis and signalling.

As future perspectives, the newly developed organelle-targeted Ca^{2+} probes can be used to better explore the precise interplay between chloroplasts and ER in Ca^{2+} handling by using pharmacological approaches, based on Ca^{2+} chelators and specific inhibitors of organellar Ca^{2+} transporters, as well as knockout plants defective in the above-mentioned molecular players.

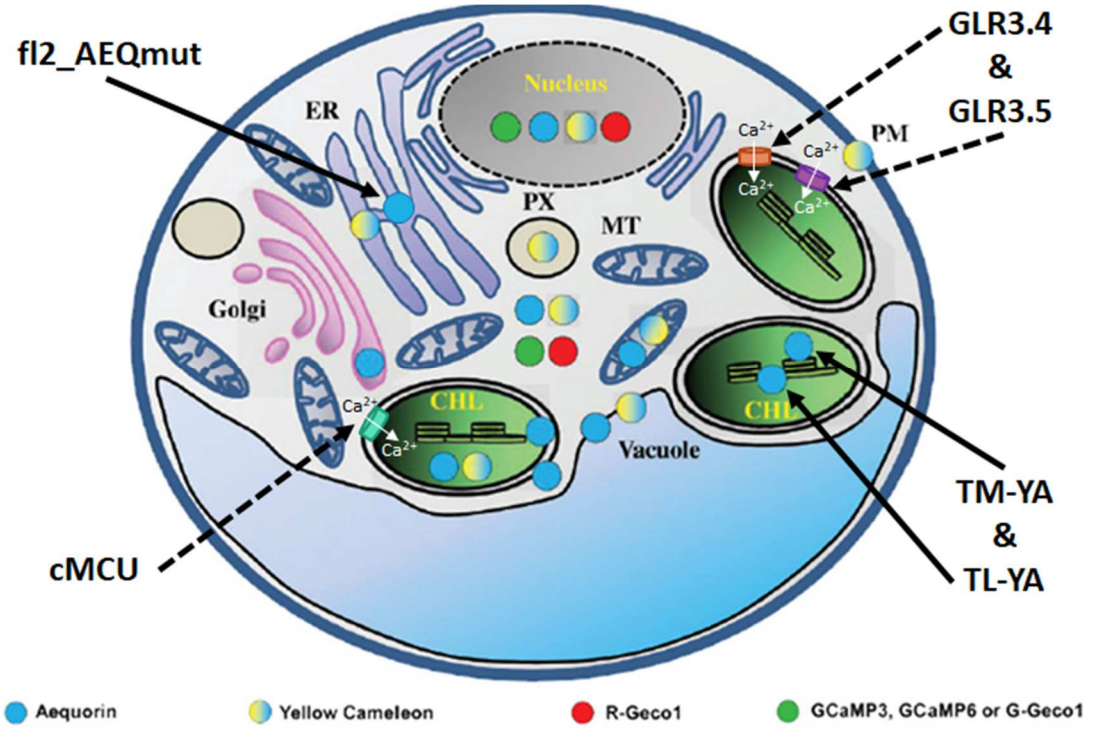

Fig. 1. The currently available toolkit of organelle-targeted genetically encoded Ca^{2+} indicators in the plant cell. Solid arrows indicate the novel aequorin-based Ca^{2+} reporters generated in this thesis: TL-YA and TM-YA, targeted to the thylakoid lumen and thylakoid membrane, respectively, and fl2_AEQmut, targeted to the ER. Dashed arrows indicate the chloroplast-located Ca^{2+}-permeable channels (cMCU and GLR3.4/3.5) that were investigated in this thesis (modified from Costa *et al.,* 2018).

REFERENCES

Brini M (2008) Calcium-sensitive photoproteins. Methods **46:** 160-166

Costa A, Navazio L, Szabo I (2018) The contribution of organelles to plant intracellular calcium signalling. J Exp Bot **69:** 4175-4193

Marti MC, Stancombe MA, Webb AA (2013) Cell- and stimulus type-specific intracellular free Ca^{2+} signals in *Arabidopsis*. Plant Physiol **163:** 625-634

Ottolini D, Cali T, Brini M (2014) Methods to measure intracellular Ca^{2+} fluxes with organelle-targeted aequorin-based probes. Methods Enzymol **543:** 21-45

Sello S, Perotto J, Carraretto L, Szabo I, Vothknecht UC, Navazio L (2016) Dissecting stimulus-specific Ca^{2+} signals in amyloplasts and chloroplasts of *Arabidopsis thaliana* cell suspension cultures. J Exp Bot **67:** 3965-3974

Ph.D. ACTIVITIES (2016-2019)

Seminars

During my Ph.D. I attended a total of 37 seminars and courses specifically organized for Ph.D. students by the Ph.D. Program in Biosciences (University of Padova). The seminars were chosen according to my research interests as well as in order to widen my perspectives, and ranged from plant cell biology and physiology to molecular biology, ecology and bioinformatics.

Attended courses

- Participation to the "XXII International School of Pure and Applied Biophysics: Intracellular ion channels and transporters in plant and animal cells" organized by the Italian Society for Pure and Applied Biophysics (SIBPA) and by “Istituto Veneto di Scienze, Lettere ed Arti” (IVSLA). Venice (Italy), 15-19 Jan. 2018.
- Participation to the “Summer School in Plant Phenotyping” organized by the Working Groups in “Cell and Molecular Biology” and “Biotechnology and Differentiation” of the Italian Botanical Society (SBI). Metaponto (MT, Italy), 3-5 July 2019.

Publications

- Sello S, Moscatiello R, Mehlmer N, Leonardelli M, Carraretto L, **Cortese E**, Zanella FG, Baldan B, Szabo I, Vothknecht UC, Navazio L (2018). Chloroplast Ca^{2+} fluxes into and across thylakoids revealed by thylakoid-targeted aequorin probes. *Plant Physiol* 177: 38-51. *[IF 6.305]*
- Moscatiello R, Sello S, Ruocco M, Barbulova A, **Cortese E**, Nigris S, Baldan B, Chiurazzi M, Mariani P, Lorito M, Navazio L (2018). The hydrophobin HYTLO1 secreted by the biocontrol fungus *Trichoderma longibrachiatum*

triggers a NAADP-mediated calcium signalling pathway in *Lotus japonicus*. *Int J Mol Sci* 19: 2596. *[IF 4.183]*

- Teardo E, Carraretto L, Moscatiello R, **Cortese E**, Vicario M, Festa M, Maso L, De Bortoli S, Calì T, Vothknecht UC, Formentin E, Cendron L, Navazio L, Szabo I (2019). A chloroplast-localized mitochondrial calcium uniporter transduces osmotic stress in *Arabidopsis*. *Nat Plants* 5: 581-588. *[IF 13.297]*

- **Cortese E**, Carraretto L, Baldan B, Navazio L (2019). Photosynthetic and heterotrophic cell suspension cultures. In: Arabidopsis Protocols, Fourth Edition. Sanchez-Serrano JJ, Salinas J eds. Springer, Berlin (DE). *Meth Mol Biol* series *(invited Chapter, in revision, September 2019)*.

International congresses

- Moschin S, Nigris S, Ezquer I, Masiero S, Cagnin S, **Cortese E**, Colombo L, Casadoro G, Baldan B. In the basal Angiosperm *Nymphaea caerulea* the complexity of the reproductive structures is underlined by the MADS-box genes expressed during their development. Workshop on Molecular Mechanisms Controlling Flower Development. Padova (Italy), 3-7 Sept. 2017 *[selected for an oral communication]*.

- Sello S, Moscatiello R, Mehlmer N, Leonardelli M, Carraretto L, Zanella F, **Cortese E**, Baldan B, Szabo I, Vothknecht UC, Navazio L. Thylakoid-targeted aequorin probes reveal an integrated role for thylakoids in Ca^{2+} homeostasis and modulation of chloroplast Ca^{2+} signals. 2017 Plant Calcium Signalling Conference. Norwich (UK), 5-7 Sept. 2017 *[selected for an oral communication]*.

- Szabo I, Teardo E, Moscatiello R, Carraretto L, Vicario M, **Cortese E**, Festa M, De Bortoli S, Calì T, Vothknecht UC, Formentin E, Cendron L, Navazio L. A chloroplast-localized mitochondrial calcium uniporter homolog mediates stress-specific response in Arabidopsis plants. 20th European Bioenergetics Conference. Budapest (Hungary), 25-30 Aug. 2018 *[selected for an oral communication]*.

- **Cortese E**, Moscatiello R, Carraretto L, Brini M, Navazio L. Measurements of calcium dynamics in the plant endoplasmic reticulum: an aequorin-based approach. V International Plant Science Conference (IPSC) (113° Congresso della Società Botanica Italiana). Fisciano (SA, Italy), 12-15 Sept. 2018 *[selected for an oral communication]*.

- **Cortese E**, Pettiti F, Giletta A, Genre A, De Stefani D, Negro A, Navazio L. Establishment and evaluation of novel fluorescent reporters for the analysis of calcium-mediated communication in the arbuscular mycorrhizal symbiosis. VI International Plant Science Conference (IPSC) (114° Congresso della Società Botanica Italiana). Padova (Italy), 4-7 Sept. 2019 *[poster]*.

- Carraretto L, Teardo E, Moscatiello R, **Cortese E**, Vicario M, Festa M, Maso L, De Bortoli S, Calì T, Vothknecht UC, Formentin E, Cendron L, Navazio L, Szabo I. A chloroplast-localized mitochondrial calcium uniporter transduces osmotic stress in *Arabidopsis*. 11th Congress of the Italian Society of Plant Biology. Padova (Italy), 4-6 Sept. 2019 *[poster]*.

National congresses

- Moschin S, Nigris S, **Cortese E**, Cagnin S, Masiero S, Ezquer I, Baldan B. MADS-box genes involved in the development of the reproductive structures of *Nymphaea caerulea*. Fascination of Plants Day@UniPD. Padova (Italy), 16 May 2017 *[oral communication]*.

- Nigris S, Moschin S, **Cortese E**, Cagnin S, Masiero S, Ezquer I, Casadoro G, Baldan B. MADS-box genes involved in the development of the reproductive structures of *Nymphaea caerulea*. Riunione dei Gruppi di Lavoro di Biologia Cellulare e Molecolare e Biotecnologie e Differenziamento. Milan (Italy), 14-16 June 2017 *[oral communication]*.

- Moschin S, Nigris S, Masiero S, Cagnin S, **Cortese E**, Colombo L, Casadoro G, Baldan B. The canonical ABC(D)E model is not suitable for the flower of the basal Angiosperm *Nymphaea caerulea*. Riunione dei Gruppi di Lavoro

di Biologia Cellulare e Molecolare e Biotecnologie e Differenziamento. Sanremo (IM, Italy), 13-15 June 2018 *[oral communication].*

- Nigris S, Moschin S, Ezquer I, Masiero S, Cagnin S, **Cortese E**, Colombo L, Casadoro G, Baldan B. Insights into the AGAMOUS subfamily genes of the water lily *Nymphaea caerulea*. Riunione dei Gruppi di Lavoro di Biologia Cellulare e Molecolare e Biotecnologie e Differenziamento. Sanremo (IM, Italy), 13-15 June 2018 *[oral communication].*

- **Cortese E**, Moscatiello R, Teardo E, Carraretto L, De Bortoli S, Vothknecht UC, Cendron L, Szabo I, Navazio L. The involvement of chloroplast Ca^{2+}-permeable channels in plant organellar Ca^{2+} signalling. Riunione dei Gruppi di Lavoro di Biologia Cellulare e Molecolare e Biotecnologie e Differenziamento. Sanremo (IM, Italy), 13-15 June 2018 *[oral communication]*.

- **Cortese E**, Moscatiello R, Sello S, Carraretto L, Teardo E, Pettiti F, Vothknecht UC, Cendron L, Brini M, Szabo I, Navazio L. Unlocking the contribution of chloroplasts and the endoplasmic reticulum to Ca^{2+} homeostasis and signalling in the plant cell. Riunione dei Gruppi di Lavoro di Biologia Cellulare e Molecolare e Biotecnologie e Differenziamento. Napoli (Italy), 12-14 June 2019 *[oral communication]*.

Grants and awards

- Jan. 2018: Bursary awarded by the European Biophysical Societies' Association (EBSA) to attend the "XXII International School of Pure and Applied Biophysics: Intracellular ion channels and transporters in plant and animal cells". Venice (Italy), 15-19 Jan. 2018.

- Sept. 2019: Bursary awarded by the Italian Botanical Society (SBI) to attend the “VI International Plant Science Conference (IPSC) (114° Congresso della Società Botanica Italiana)”. Padova (Italy), 4-7 Sept. 2019.

Tutored students

- Greta Battaggia, Curricular stage, Bachelor's degree in Biotechnologies, University of Padova (academic year 2016/2017).
- Nazifou Ouro-Gomma, Curricular stage, Bachelor's degree in Molecular Biology, University of Padova (academic year 2018/2019).
- Francesca Pettiti, Curricular stage, Master degree in Evolutionary Biology, University of Padova (academic year 2018/2019).